Sclerochronological and geochemical records from *Porites* spp. in Fiji: Assessing massive coral response to environmental changes

Ana Samperiz Vizcaino

School of Earth and Environmental Sciences

Cardiff University

Thesis submitted for the Degree of Doctor of Philosophy

December 2022

Summary

Coral reefs are one of the most biologically diverse systems on Earth and the ecosystem services they provide are of high importance for coastal communities and beyond. Yet, they are becoming increasingly threatened by global (climate change) and local stressors (e.g., land-derived pollution, overfishing). Many studies have focused on understanding how scleractinian (reef-building) corals in inshore reefs are responding to these environmental stressors and their potential compounding effects. However, this is complicated due to the lack of high-resolution records of both environmental parameters and coral growth. Records of coral growth and geochemistry from the aragonitic skeletons of massive scleractinian corals can be used as effective archives of modern and past changes in reef water quality, coral calcification rate and physiology, improving our understanding of reef-specific and species-specific responses of corals to multiple stressors.

In this thesis, I aim to disentangle the relationship between coral growth, skeletal deposition, geochemical composition, and environmental conditions in Fiji. I acquire sclerochronological and geochemical records from massive *Porites* spp. corals from four inshore reefs adjacent to different catchment environments in Viti Levu, Fiji, alongside remotely sensed environmental data. I reconstruct the sensitivity of *Porites* spp. to environmental changes, explore the fundamental physiological controls on the incorporation of SST proxies into skeletal aragonite, and explore site-specific environmental and hydrological controls on reef water quality and the use of proposed proxies for terrigenous input. Sclerochronological records of coral growth (linear extension, density, and calcification) are obtained from *Porites* spp. cores using Computed Tomography. Geochemical records include measurements of a suite of trace and minor elemental concentrations in the coral skeletons using Laser Ablation – Inductive Coupled Plasma Mass Spectroscopy to assess a range of SST proxies (Sr/Ca, Mg/Ca, Li/Ca, and U/Ca) and terrigenous input proxies (Ba/Ca, Mn/Ca, Y/Ca, La/Ca, and Ce/Ca).

Coral growth records from inshore reefs show that although water quality plays a significant role in driving mean linear extension and calcification rate between 1998 and 2016, persistent thermal stress has the capacity to reduce coral growth across all locations, regardless of local conditions. This is important because under a scenario of amplified global warming and persistent thermal stress local management might not be enough to palliate the effects of climate change.

Traditional coral-derived SST proxies in inshore reefs in Fiji reflect SST variability to some degree and are applicable for paleotemperature reconstructions. However, multiple core replicates across locations are needed to build a composite record that accurately reflects SST. Results show the existence of biological controls ('vital effects') on the elemental composition of the corals as a response to reef-specific environmental factors, complicating the extraction of an SST signal.

In addition, application of terrigenous input proxies, although successfully recorded by the corals of this study, need to be considered on a site-by-site basis. This is because variable environmental and hydrological mechanisms lead to reef-specific changes in water quality as a response to climatic events (e.g., rainfall seasonality, tropical cyclones). As such, future interpretations of terrigenous input proxies will require of a deep understanding of hydrological and climatic catchment-coastal linkages.

Overall, this work showcases the use of coupled sclerochronological and geochemical methods for providing robust growth and environmental records and a better understanding of how environmental conditions have affected coral growth in vulnerable inshore reefs in the past.

Acknowledgments

Phew! It really does take a village… to complete a PhD.

To the people of Fiji, for to them belong the reefs where the coral samples of this study were collected, and everything within them.

It would have been impossible for me to get to this point without my supervisors, Sindia Sosdian, Eleanor John, Erica Hendy, Ken Johnson, and Stacy Jupiter. Five supervisors steering one (sometimes very lost) PhD student might sound like a crowd, but that could not be further from the truth. I am very grateful for all the encouragement they provided me with, and the many and lengthy discussions from a wide range of expertise and point of views that enriched my own ideas. They always made sure I felt at home when working away from Cardiff and that I had all the support needed to carry out my research. Thanks for being such a great team to learn from!

I want to thank Sindia Sosdian, for being an extraordinary mentor. I cannot thank her enough, first for trusting me to carry out this project, but also for her constant encouragement, support, patience, and openness. Sindia is an amazing scientist, and I feel privileged to have learnt from her. In reality, Sindia has been much more than my main supervisor, she is an inspiring role model (for science and for life). At times, research was hard and the obstacles felt too big, but her humanity, understanding and perpetual reassurance got me through. It has been quite the ride, but we made it.

It would have not been possible for me to carry out my work without the help and support of research and technical staff members at the many institutions I was involved with.

At Cardiff University, Michael Nairn taught me all things LA-ICPMS and the ways of perseverance with the instruments. Furthermore, he showed a great deal of patience answering the multitude of questions I had while trying to understand how the instruments worked. Lindsey Owen was always available to help me in the lab when I was trying to get analyses done. Edward Inglis allowed me to be the sole LA-ICPMS user for nearly three months and until all the data needed to finish my thesis was collected. Greg Shaw for his help teaching me how to make pellets out of pulverised carbonate material.

At the Natural History Museum London, Brett Clark and Vincent Fernandez carried out numerous CT scans of the coral cores used here, through several days (weeks, really). Furthermore, they were always welcoming, from the very first time I was there, and especially during the first few days using AVIZO and learning how to work with 3-dimensional datasets. They were incredibly patient explaining every mistake I made, and software error I encountered.

At the University of Bristol, Tom Davies and Liz Martin-Silverstone provided great help finishing CT scanning of coral samples and ensuring I had complete access to the facilities in order to finish data acquisition. Charles Clapham showed infinite patience with me while we were trying to figure out how to cut the long coral cores and was always keen on trying some of my ideas. Hayley Goodes helped and explained the functioning of the wire saw.

At Wildlife Conservation Society Fiji, Miriam Bhurrah provided access to several environmental datasets and dealt with Governmental bodies in Fiji on my behalf, in order to gain access to these data. Yashika Nand was incredibly helpful when I was planning my fieldwork trip to Fiji, dealing with different Ministries and Departments so I could get permits to conduct research in Fiji. Sangeeta Mangubhai, for her help and support, and willingness to host me at WCS in Fiji.

The Fiji Ministry of Land and Mineral Resources – Land Use Division and Fiji Meteorological Service for providing access to data. Also, the Fiji Ministry of Environment and Ministry of Education for the support gaining a research permit.

To Eleanor John, Sindia Sosdian and Jennie Mallela, who collected the coral cores that I would later use for this project. Their coring expedition would not have been possible without the support of the Ministry of iTaukei Affairs (Government of Fiji). Also, the villagers and Turaga-ni-Koro of Votua Village for their support with the dive efforts at Votua Reef. The villages surrounding Rakiraki and the Roko Tui of Ra, as their support allowed the collection of the Nananu-i-Ra cores. Greg Buxton helped collect the core at Suva Reef. The villages within the Muaivuso peninsula, and Mr Hemo Marvela, Chair of the Committee in charge of management of the Navakavu LMMA, supported the collection of the cores at Namuka Reef (including the core within Navakavu LMMA). Finally, also Fiu Manueli, former Dive Manager of the University of the South Pacific.

Simon Albert provided unpublished data from core samples from Fiji. Also, Grace Frank and Janice Lough supplied core X-ray and white light images of the Fijian samples stored at the Australian Institute of Marine Science.

Sindia Sosdian and Christopher Pierce allowed me to tag along on a fieldwork trip to Fiji in the early days of my PhD. Little did we know at the time, but this would be my only chance to visit Fiji before I finished. This trip was the first time I travelled outside of Europe, the first time I dived, and the first time I saw a reef with my own eyes! It was both scientifically and personally enlightening, and for that I am very grateful. Also, Eleanor John, Sara Fowell, Urska Martinic and Socratis Loucaides for they were great fieldwork companions. I cherish sunset drinks at the Holiday Inn in Suva.

The MôR gang, always there for refreshing discussions and support. It is great being part of such a wonderful and supportive research group.

Erin Harvey, Sara De Caroli and Sophie Slater were kind enough to read through the last version of this thesis, making sure every sentence made sense. Furthermore, they all have been a very important support through my PhD journey. And all the friends and colleagues at Cardiff University: Erin, Sara, Manny, Sophie, Ellie, Ben, among others, who provided a great number of coffee breaks and moments to respire and refresh the mind. And also outside of the office, Carlos, Imanol, and Cara, who were always there, cheering and reminding me that there is more to life.

My family, their endless encouragement and blind confidence in me over the last…well over my entire life really, has driven me to this moment. LA FAMILIA SIEMPRE SERÁ LA FAMILIA. OS QUIERO. And especial mention to my mum, for the fantastic artwork illustrating this thesis.

And last, but not least, to Dan. I am not sure how I would have made it through the last four years without your unwavering support (and the packed freezer of nutritious meals you always left me). This is, also, your time to celebrate.

Table of Contents

List of Tables

Chapter 1 | Introduction

> *It's the job that's never started as takes longest to finish, as my old gaffer used to say*
>
> Samwise Gamgee

Coral series #3(MVL)

Chapter 1 | Introduction

1.1. Coral reefs in a changing world

Coral reefs encompass only 0.1% of the ocean's surface (284,300 km^2; Spalding et al. 2001), and yet they are considered one of the most diverse, dynamic and productive ecosystems on Earth (Birkeland 1997), harbouring about 25% of all marine species (Burke et al. 2011). They provide numerous services of importance, estimated to be $20.8 billion USD/year (Cesar et al. 2003), as they supply habitat for ecologically and economically valuable fish, and create jobs in the fishing, recreational and tourism industries. Coral reefs also protect the shoreline, absorbing energy from the wave activity during storm events, contributing another $9 billion USD/year indirectly by preventing erosion and property damage (Cesar et al. 2003). Beyond the measurable economical services of these ecosystems, coral reefs play an important role in the carbon cycle and carbonate system in the ocean. Coral reef carbon cycle processes, both organic and inorganic, lead to dynamic changes in seawater carbon chemistry on daily (Shaw et al. 2012) and seasonal (Bates et al. 2010) time scales within the reef ecosystem, and have been shown to accumulate carbonate at a mean rate of 3 – 6 kg/m^2·yr (Barnes and Devereux 1984). Changes in the diversity and/or structural complexity of corals can therefore have severe adverse environmental and social effects.

Coral reefs are also one of the most vulnerable ecosystems on Earth due to their high sensitivity to environmental changes in their habitats (Hoegh-Guldberg 1999). Reef-building corals show limited tolerance to changes in light availability, climate and current patterns, sedimentation, salinity, pH and temperature (Fabricius 2005; Graham et al. 2006; Doney 2010; Burke et al. 2011). These organisms face different threats as a result of changes in their environment, of which 60% are local and directly human-induced (Burke et al. 2011). Natural disturbances, such as those derived from climatic oscillations (e.g., El Niño Southern Oscillation, ENSO) and tropical storms are short-lasting and infrequent enough as to enable recovery of the reefs (Nyström et al. 2000). However, in the emerging era of the Anthropocene, many coastal reefs have been degraded by centuries of overfishing and pollution, and climate change is exerting further stress on these systems and on people who depend on them (Hughes et al. 2017a).

These pressures can affect coral growth, reduce defence mechanisms and weaken colony recruitment, potentially causing shifts from a coral-dominated reef towards an algae-dominated state (Bruno et al. 2009). World-wide coral cover has decreased in the last few decades at a rate of 2% loss per year (Bruno and Selig 2007), amounting to a total loss of 14% of all the corals the world, which equates to ~11,700 km^2 of coral area (Figure 1.1.; Souter et al. 2021). Yet, it is difficult to assess whether it is caused by global or local pressures (Gardner et al. 2003), or even more, whether there are potential synergetic effects between global and local stressors putting coral reefs under a prolonged stress that ultimately endanger the continuity of the ecosystem (Ban et al. 2014).

1.1.1. Global stressors – Climate change

Climate change and the processes associated with it are one of the main contributors to coral loss (Souter et al. 2021). Global mean atmospheric CO_2 concentrations have increased from 280 ppm in the pre-industrial era (Raupach et al. 2007) to 415 ppm by 2022 (Dlugokencky and Tans 2022), reaching levels not seen since the Pliocene (Martínez-Botí et al. 2015). The multiple effects derived from increased atmospheric CO_2 require urgent action. Under the Paris Agreement (COP21), celebrated in 2015, the signatory parties agreed to keep the global average temperature rise this century as close as possible to 1.5ºC. In 2022, the UN finds that there is no credible pathway to 1.5ºC in place, and in fact, with no further strengthening of the policies currently in place, we are likely still under a 2.8ºC increase scenario (Friedlingstein et al. 2022).

As a consequence, the rapid global warming experienced over the past few decades is increasing the ocean temperature (Johnson and Lyman 2020), raising the sea level (Nerem et al. 2018), melting the ice sheets and permafrost (Shepherd et al. 2012), altering the hydrological cycle (Durack et al., 2012), changing atmospheric and oceanic circulation (Rahmstorf et al. 2015; Caesar et al. 2018), as well as driving stronger tropical cyclones with more intense rainfall (Trenberth et al. 2018), amongst other effects. Here we focus on the two main global stressors derived from climate change for coral reefs: ocean warming and ocean acidification.

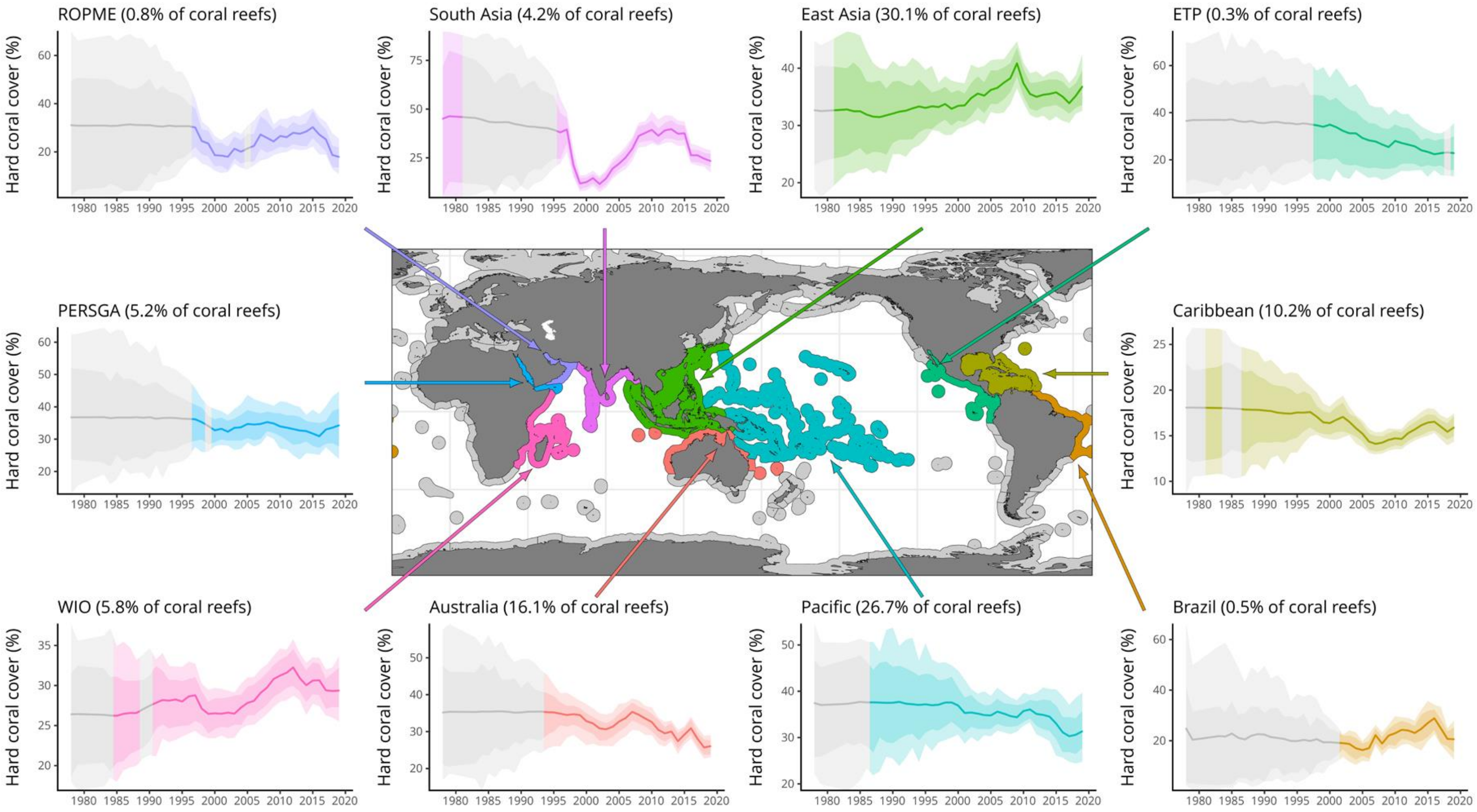

Figure 1.1. Long-term trends in the average cover of live hard coral in each of the ten Global Coral Reef Monitoring Network (GCRMN) regions. The solid line represents the estimated mean with 80% (darker shade) and 95% (lighter shade) credible intervals, which represent levels of uncertainty. Grey areas represent periods for which no observed data were available. Trends are coloured to match the GCRMN regions represented on the central map. The proportion of the world's coral reef area supported by each region is indicated by % of coral reefs. ETP is the Eastern Tropical Pacific. PERSGA is the Red Sea and Gulf of Aden. ROPME is the ROPME Sea Area. WIO is the Western Indian Ocean. (Taken from Souter et al. 2021).

1.1.1.1. Ocean warming

The geographical constraints on coral reef distribution are mainly limited by seawater temperature. Although corals are the most productive in a range of temperatures between 21 to 29ºC, they have been found to tolerate fluctuations from lows of 16-18ºC to highs of 30-33ºC (Hoegh-Guldberg 1999; Hume et al. 2013).

The global average seawater surface temperature (SST) shows a warming trend of 0.062ºC per decade between 1900 and 2019, but in the last decade (2010-2019) this rate has accelerated to 0.28ºC per decade (Garcia-Soto et al. 2021). Furthermore, this warming is amplified in the tropical regions, with an increase of 0.3-0.4ºC over the last three decades (Kleypas and Hoegh-Guldberg 2008). This tropical amplification occurs due to the fact that increased atmospheric temperatures limit the overturning circulation, resulting in decreased trade winds and a reduced sea level pressure gradient between the eastern and western Pacific. This reduces the amount of upwelling experienced in the eastern Pacific that aids to cool down the surface waters of the equatorial Pacific (Collins et al. 2010).

Despite tropical SSTs being generally within the range of tolerance for corals, several studies have found a decreasing trend in coral growth of *Porites* spp. across the Great Barrier Reef (GBR) (Cooper et al. 2008), Southeast Asia (Tanzil et al. 2013), the Red Sea (Cantin et al. 2010) and the South China Sea (Zhao et al. 2012; Chen et al. 2013), suggesting that, although corals are able to keep growing under warmer conditions, seawater temperatures at these regions might have surpassed a threshold for favourable environmental growth (Cooper et al. 2008; Lough and Cooper 2011).

Nevertheless, the principal impact of ocean warming on corals is coral bleaching, which primarily occurs during prolonged periods of thermal stress (and/or high light intensity). Coral bleaching is a process where the coral polyp expels its symbiotic zooxanthellae (Lewis et al. 2016), causing the coral tissue to lose its colour (photosynthetic pigments of symbionts). During a bleaching event, corals usually lose between 60% and 90% of their symbionts, and the remaining symbionts can lose between 50% and 80% of the photosynthetic pigments (Glynn 1996). The photosynthesis carried out by the zooxanthellae provides up to the 95% of the coral's total energy (Edmunds and Davies 1986; Muscatine 1990), thus coral calcification and reproduction rates tend to decrease during bleaching (Goreau and Macfarlane 1990; Leder et al. 1991), as these are energycostly processes. If normal SST conditions return promptly, the bleached corals can recover the zooxanthellae and resume their symbiotic relationship. However, if bleaching conditions are prolonged, corals will be susceptible to disease, starvation. and may finally die (Baird and Marshall 2002). As SSTs continue to increase, massive bleaching events are predicted to increase in frequency and intensity (Van Hooidonk et al. 2013), not allowing enough time for corals to recover and risking the collapse of entire reef systems (Graham et al. 2015).

1.1.1.2. Ocean acidification

In addition to ocean warming, between 25 and 30% of the atmospheric CO_2 emitted since 1850 is being absorbed by the ocean (Le Quéré et al. 2010). An increase in dissolved CO_2 in the seawater promotes the formation of carbonic acid (H_2CO_3), releasing hydrogen ions (H^+), thus decreasing the seawater pH and effectively acidifying the ocean.

Seawater pH changes seasonally and regionally due to biogeochemical processes such as spring phytoplankton blooms (Takahashi et al. 2014). Coral reefs show diel and seasonal variability in pH (Manzello 2010; Bates et al. 2010; Shaw et al. 2012) that can range between 7.65 to 8.40. However, absorption of anthropogenic CO_2 has caused a decrease in the global ocean surface pH from 8.2 to 8.1 since the Industrial Era (Doney et al. 2009), with pH reducing at a rate of 0.08 pH units per decade (Takahashi et al. 2014).The decreasing ocean pH also causes a reduction of the aragonite saturation state (Ω_{arag}), as a result of the limited availability of carbonate ions available for mineral precipitation which can potentially inhibit calcification.

Some studies suggest that increases in atmospheric CO_2 and associated declines in [CO_3^{2-}] and Ω_{arag} of the ocean's surface waters will reduce rates of calcification in coral reefs (Gattuso et al. 1999; Langdon et al. 2003; Anthony et al. 2008) while simultaneously increasing rates of bioerosion (Decarlo et al. 2015a; Enochs et al. 2016) and dissolution (van Woesik et al. 2013). On the other hand, other studies did not detect effects on coral calcification rates (e.g., Reynaud et al. 2003; Schoepf et al. 2013; Comeau et al. 2014, 2018). Variability of results suggest that response to ocean acidification is highly variable between species and sites. This is potentially due to different population traits linked to their capacity to upregulate the pH of the calcifying fluid to make more favourable conditions for calcification (Pandolfi et al. 2011).

1.1.2. Local stressors

While the primary stressor driving the coral decline at global scale is seawater warming (Cooper et al. 2012; Hughes et al. 2017b), the localised effects of overfishing and increased coastal runoff are considered the primary drivers influencing system shifts from coral to algal-dominated inshore reefs (Burkepile and Hay 2006; Duran et al. 2016). Furthermore, studies have shown that these chronic anthropogenic local stressors have the potential to act in synergy with seawater warming (Nyström et al. 2000; Bellwood et al. 2004; Pandolfi et al. 2005; Knowlton and Jackson 2008; Mora 2008; Carilli et al. 2010) diminishing the resilience of the corals to recover and propagate after an abrupt climatic event (such as tropical cyclones or bleaching events), and potentially aggravate coral-cover loss (Hughes et al. 2018a).

1.1.2.1. Land-use activities, runoff pollutants and water quality

One of the direct causes of decreasing water quality in coastal areas is the anthropogenic activities being carried out inland. The alteration of watersheds for human activities causes the degradation of inshore reefs through increases in freshwater discharge and sediments and nutrients input, often beyond natural levels, in coastal systems (Smith et al. 2001). Models estimate that 22% of the coral reefs in the world are threatened by inland pollution and soil erosion (Bryant et al. 1998), and on local scales it can be the most important pressure on inshore reefs (Fabricius 2005). Demographic changes, population increases, human migration towards coastal urban areas, and land clearance for food and/or housing or industrial activity tend to increase the pressure on reefs adjacent to these areas (Zak et al. 2004) by increasing the sediment load, nutrients and sewage waters reaching these inshore reefs.

An increase in sediment runoff can reduce light availability (which limits symbiont photosynthesis) and cause abrupt smothering of corals (Dodge and Vaisnys 1977; Rogers 1990; Fabricius and Wolanski 2000). In addition, the input of inorganic nutrients (NO_3^- and PO_4^-) dissolved in river water and/or adsorbed onto suspended particulate matter can trigger algal blooms and crown of thorns starfish predation (Hughes 1994; Lapointe 1997; McCook 1999; McCook et al. 2001; McClanahan et al. 2003; Weil et al. 2006), increasing skeletal loss due to bioerosion by grazers and borers as a result (Chazottes et al. 2002).

The increased input of nutrients sourced by agricultural and urban waters can also lead to imbalances in the internal nutrient cycling of reefs and negatively affect reef productivity and coral health (Rogers 1990; Druffel 1997; Szmant 2002). In addition, the ratio between nutrients (N:P) have been shown to also impact the photosynthetic productivity of the zooxanthellae symbionts (D'Angelo and Wiedenmann 2014).

1.1.2.2. Overfishing

Coral reefs, and the biomass productivity associated with them, play a key role for coastal communities, for both subsistence and commercial fishing (Robinson et al. 2019). However, excessive exploitation of fisheries resources, especially in highly populated areas, and poor management in general can cause a collapse of the ecosystem, altering the food web relationships and risking food security (e.g., Kinch et al. 2010).

This is especially the case with overfishing of herbivorous fishes (known as reef gardeners). These species feed on macro-algae, and on doing so they can greatly reduce their cover (Mumby 2009), and prevent reef shifts to algal-dominated systems. It is estimated that around 55% of the world's reef are affected by overfishing (Burke et al. 2011). In addition, destructive fishing (such as the use of explosives) is a widespread fishing technique in some regions, which can exert further physical damage to corals (Cesar et al. 2003).

In summary, anthropogenic activity is affecting corals through both global and local-acting stressors. Efforts to limit the impact of localised stressors might not be enough to counteract the effect of global events derived from climate change, like increased thermal stress and coral bleaching (Selig and Bruno 2010; Hughes et al. 2017a). Yet, several studies point that local actions (e.g. good coastal water quality) may support more thermally resistant corals (Fabricius 2005; Humanes et al. 2017) and facilitate recovery and diminish coral disease after disturbances (McClanahan et al. 2012; Vega Thurber et al. 2014).

1.1.3. Reef management and conservation

The history of marine conservation and the expected outcomes from the instauration of Marine Protected Areas (MPA) go hand by hand with the trends in land conservation. As described by Humphreys and Clark (2020), up until the 1960s, conservation was highly anthropocentric and focused in preserving the natural spaces for "education, inspiration, recreation and enjoyment". Between 1970s and 1980s, conservation efforts were focused primarily on single emblematic species, critical habitats and biodiversity. It was not until the 1980s when a broader management sense was acquired, favoured by the concept of 'sustainable development', when also the economic and social actors were starting to be considered.

Over the last four decades marine managers have moved from simple MPAs to integrated coastal management and ecosystem-based management (EBM), and later to resilience based management (RBM) (McLeod et al. 2019). While traditional MPAs have focused on managing fishing and preventing overfishing (for example by implementing no-take zones and defining species-specific fishing seasons), they have little power mitigating and reducing the land-based pollutants (e.g., sediment, nutrients and pesticides in terrestrial runoff), whose source are outside of the MPA designated areas.

Coupling land and sea management (known as "Ridge to Reef" management) can be complicated due to the lack of understanding of how these pollutants are originated and transported towards the reefs, and how they affect the corals, all of which are required for a successful implementation of management strategies (Bainbridge et al. 2018). Yet, this "Ridge to Reef" methodology is being successfully implemented and advanced in several locations (e.g., Beger et al. 2010; Álvarez-Romero et al. 2015; Jupiter et al. 2017).

Nowadays, conventional management is being substituted by a management focused on supporting the resilience of corals reefs, as well as the people and the economies supported by them, as a fully coupled socio-ecological system (Bellwood et al. 2004; McLeod et al. 2019). As defined by McLeod et al. (2019), RBM uses the acquired knowledge of current and future drivers influencing ecosystem functions to prioritize, implement, and adapt management actions that sustain ecosystems and human wellbeing. In this sense, acquiring full understanding of an ecosystem requires vast amounts of information, data and ecological surveys. Ecological models can help to understand the connections between land-use, water quality and reef resilience (e.g., Álvarez-Romero et al. 2014; Brown et al. 2017a) but a gap remains in the knowledge of what environmental conditions characterised coral reefs in the past and how reef-building corals responded to changes.

1.2. Coral calcification in scleractinian corals

1.2.1. Physical deposition of coral skeleton

Shallow reef-building scleractinian corals (Order: Scleractinia), commonly known as stony corals, build a calcareous exoskeleton ($CaCO_3$) in the form of aragonite in a process labelled coral calcification (also biomineralization). The living tissue (i.e., the coral animal) thinly covers the aragonitic skeleton (up to 2 cm thickness; DeCarlo and Cohen 2017) and is in fact in charge of skeletal formation. The control that living tissue exerts over skeletogenesis is patent due to the diversity of skeletal morphologies, which form the basis of taxonomical classification of scleractinian corals (Veron et al. 1996), with more or less success (Garland Jr and Kelly 2006). Ultimately, skeletal formation and coral growth result from the budding and extension of new polyps. However, the precise details under which biomineralization occur are still under debate.

Coral calcification models suggest that skeletal accretion occurs in two different stages (Figure 1.2.; Barnes and Lough 1993; Mollica et al. 2018): i) upwards skeletal extension (creating new skeletal elements) conforming (and formed by) the centres of calcification (COC), and ii) thickening of the skeleton along the areas in contact with living tissue. This thickening is carried out by the growth and stacking of bundles of aragonite fibres (Cohen and McConnaughey 2003).

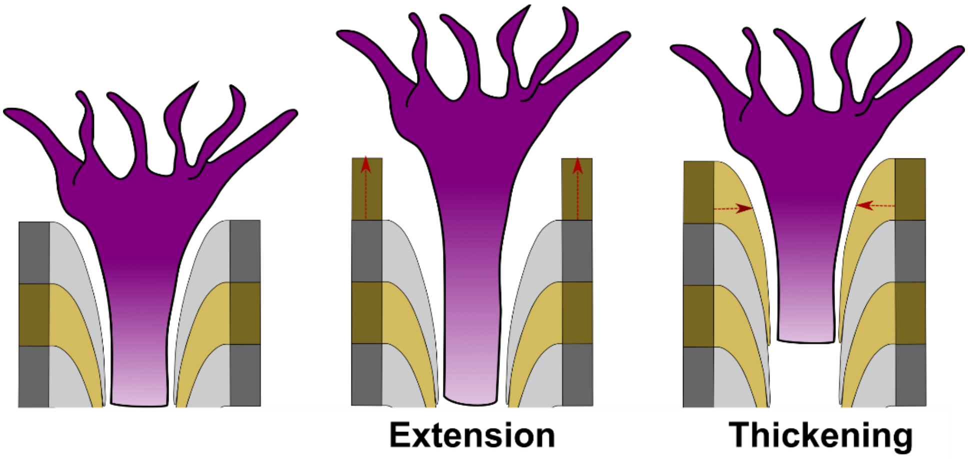

Figure 1.2. Schematic representation of coral skeletal growth (Modified from Mollica et al. 2018).

Coral skeleton growth is mediated by the living tissue. The calicodermis, formed by calicoblastic cells, is the layer of tissue in contact with the coral skeleton. The interface in between the calicoblastic cells and the skeletons is known as the extracellular calcifying fluid (ECF), considered to be semi-isolated from seawater (Figure 1.3).

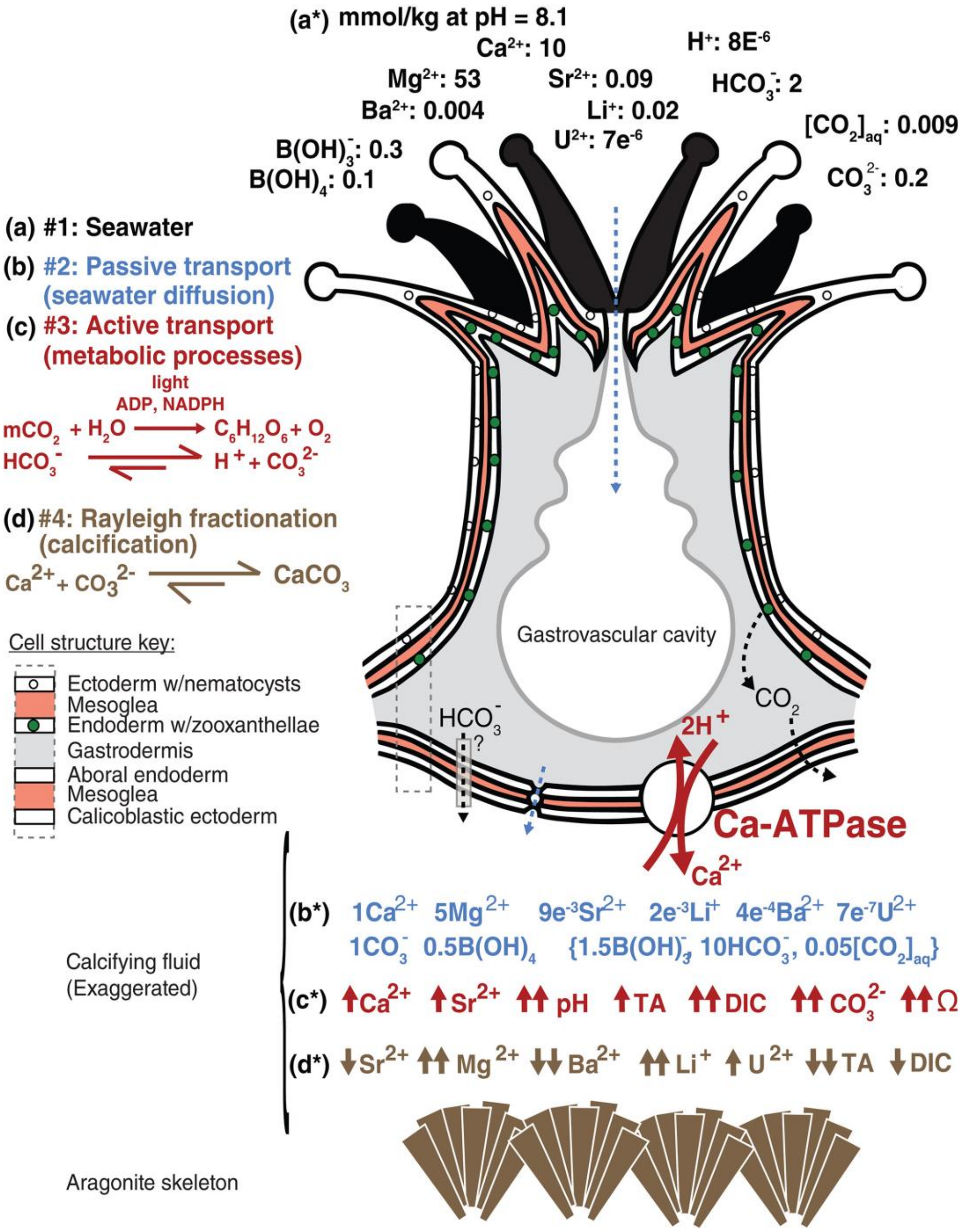

Figure 1.3. Overview of the main factors controlling the chemistry of the coral extracellular calcifying fluid (ECF): (a) seawater chemistry (black); (b) passive transport of ions via paracellular transport (blue); (c) active transport via transcellular pathways such as the Ca-ATPase pump, linked to metabolic DIC (mCO2) and ATP production by respiration and zooxanthellae photosynthesis, respectively (red); and (d) Rayleigh fractionation during calcification (tan). Taken from (Thompson 2022).

It is in this matrix (the ECF) where extracellular $CaCO_3$ is mineralised by precipitating dissolved calcium (Ca^{2+}), carbonate (CO_3^{2-}) and bicarbonate ions (HCO_3^-) (Eq. 1 to 3) from seawater. The pathways through which dissolved ions reach the ECF from the seawater and what regulates their presence are discussed in the section below:

$$Ca^{2+} + CO_3^{2-} \Leftrightarrow CaCO_3 \qquad \text{Eq. 1}$$

$$Ca^{2+} + HCO_3^- \Leftrightarrow CaCO_3 + H^+ \qquad \text{Eq. 2}$$

$$CO_2 + H_2O + Ca^{2+} \Leftrightarrow CaCO_3 + 2H^+ \qquad \text{Eq. 3}$$

It has been shown how environmental factors can exert control over coral calcification. In *Porites* spp. corals, growth variability is dependent not only on species and genetic traits (Weber et al. 1975) but also water depth, seasonality (light availability, seawater temperature) and water quality. This premise is key for the use of sclerochronological parameters derived from coral growth as paleoenvironmental indicators.

The mechanistic processes behind the environmental control over coral calcification are not clear, although some studies suggest that the rate at which aragonite is precipitated and secreted into the structural skeleton is dependent on holobiont sensitivity (photosynthetic rate by zooxanthellae, metabolic productivity, energy availability) to environmental changes (as reviewed by Tambutté et al., 2011 and Drake et al. 2020).

Shallow water scleractinian corals are commonly associated with photosynthetic symbionts, which are intracellular algae (Symbiodiniaceae) known as zooxanthellae (Kirk and Weis 2016). This symbiotic association benefits hosting corals by providing a readily-available source of nutrients, fixed carbon, and energy (autotrophy) (Falkowski et al. 1984) that favours calcification (i.e., light-enhanced calcification) (Moya et al. 2006). In addition, corals feed themselves by capturing planktonic prey (heterotrophy). Some studies have shown that differing sources of nutrients and energy play an important role in the biomineralization processes (Cuif et al. 1999; Allemand et al. 2011). However, this effect seems to be species-specific and cannot be generalised into all Scleractinia genera (including *Porites*). Nevertheless, changing environmental conditions that potentially alter the balance between autotrophy and heterotrophy will impact coral metabolism, availability of energy for skeletogenesis and ultimately the rates at which aragonitic material is deposited by the polyp.

1.2.2. Geochemistry of the coral skeleton

The biogenic aragonite that forms the coral skeleton is precipitated from the ECF, and as such the chemical composition of this interface is recorded in the skeletal geochemistry. Understanding the physiological and environmental controls affecting the ECF chemistry and the incorporation of elements into the biogenic aragonite improves the fidelity of the geochemical proxies and their use for environmental and climatic reconstructions.

Although the mechanisms underpinning calcification in the ECF are still under debate, it is suggested that there are three different pathways through which ions dissolved in seawater reach the ECF (as reviewed by Thomson 2020), and these three processes are biologically mediated by coral physiology: i) paracellular diffusion (passive transport) of dissolved ions (e.g., CO_3^{2-}, HCO_3^-, $[CO_2]_{aq}$, Sr^{2+}, Ca^{2+}, Ba^{2+}, Mg^{2+}, U^{2+}). This process does not exert chemical changes, and it reflects the chemical signature of local seawater. It is carried out through diffusion in between cells, but it might be also caused by leakage of seawater and/or passive transport through calicoblastic vacuoles (Allemand et al. 2011); ii) transcellular transport, a selective process that actively transport ions (e.g., Ca^{2+}, Sr^{2+}; Marchitto et al. 2018) against the electrochemical gradient increasing the concentration of said ions in the ECF relative to local seawater (McCulloch et al. 2017); iii) precipitation of biogenic aragonite (skeletal calcification), which exerts changes in the ECF chemistry through Rayleigh-like fractionation processes (See section 1.3.2.2). This occurs as different ions present very different partition coefficients (K_D) between the solution (ECF) and the solid (aragonitic skeleton) phases (Holcomb et al. 2014; DeCarlo et al. 2015b; Marchitto et al. 2018). For example, Sr^{2+} and Ba^{2+} ($K_D \sim 1$) are preferentially incorporated into the aragonite lattice over Mg^{2+} or Li^+ ($K_D << 1$).

Corals exert a tight regulation of the ECF chemical signature to favour $CaCO_3$ precipitation (known as *pH up-regulation*). Skeletal calcification from bicarbonate ions (Eq. 2 and Eq. 3) produces hydrogen ions (H^+) in the ECF, decreasing the pH and making conditions for precipitation less favourable. However, active transcellular transport of ions (e.g., via the Ca-ATPase pump) removes $2H^+$ for each Ca^{2+} ion transported into the ECF (Cohen et al. 2009; Allemand et al. 2011). The $2H^+$ ions are then transported to the site of photosynthesis in the coelenteron tissue layer. During this process, not only does the concentration of Ca^{2+} (key for $CaCO_3$ precipitation) increase, but the pH of the ECF also increases, shifting the DIC balance and the saturation state at this site of calcification, further enhancing precipitation.

This active up-regulation, however, has an energetic cost. Studies have found coral use energy from metabolic processes to carry out this process (Al-Horani et al. 2003) and that its ion exchange rates increase when high energy is available (Cohen and McConnaughey 2003). Changing environmental conditions and an increasing number of climatic events that impact coral physiology (e.g., thermal stress) can therefore significantly alter the geochemical composition of the deposited coral skeleton due to changes in metabolic energy and active transport of ions (e.g., Clarke et al. 2017, 2019; DeCarlo and Cohen 2017; D'Olivo and McCulloch 2017). This complicates the relationship between geochemical proxies and environmental signals and therefore the applicability of coral-derived paleoreconstructions.

1.3. Paleoenvironmental records from Porites spp.

As detailed above, coral reefs are facing an increasing intensity and number of impacts on a global and local scale. The ocean is warming, especially in the tropical regions, with thermal stress thresholds (leading to bleaching) being reached more frequently (van Hooidonk et al. 2016; Hughes et al. 2018a; Smale et al. 2019) and seawater becoming more acidic. These changes are likely to continue as the result of increasing atmospheric greenhouses gasses emissions. Furthermore, terrigenous input from catchment into inshore reefs and hydrological changes are also likely to increase due to more extreme rainfall and river flood events, as well as increased intensity of tropical cyclones (Fabricius 2005; Berkelmans et al. 2012; De'ath et al. 2012).

Several studies have shown how coral reefs are sensitive to these environmental changes (e.g., Cooper et al. 2008; Carricart-Ganivet et al. 2012; Humanes et al. 2017; Carballo-Bolaños et al. 2019; McClanahan et al. 2020) and that this occurs because of holobiont susceptibility and response (DeCarlo and Cohen 2017). A wealth of work is focusing on building an understanding on how further change will shape corals reefs in the future, and how this will affect human societies (Williams and Graham 2019). This knowledge is built upon current observations of the ecological, environmental, and climatic systems. These instrumental observations, however, are limited by both the low temporal and spatial coverage of data for variables such as seawater temperature, salinity, pH, sediment, nutrients, and pollutant inputs into coastal regions, especially before the 1970s when satellite monitoring of meteorologic and climatic variables started being implemented.

In this framework, the skeletons of massive scleractinian corals have been widely exploited as environmental and climatic paleo-archives capable of expanding the instrumental record of several variables, spatially and temporally, and on sub-seasonal to multi-decadal scales, going back several centuries (Felis and Pätzold 2003). Not only that, but they also provide information on how coral growth changed alongside environmental change (Lough and Barnes 2000; DeCarlo and Cohen 2017). Accurate assessments of what environmental changes reefs have been exposed to in the past and how coral calcification responded is vital for improving management and conservation efforts as well as predicting how will they respond to future climate change.

For this purposes, two main types of chronological records are now obtained from massive corals: i) sclerochronological records related to growth parameters and their variability, and ii) geochemical records from the dated coral skeleton. While traditionally there has been little methodological overlap between these two types of proxies, in recent years emphasis has been placed on the use of both types of proxies in tandem for obtaining reliable records with limited biases (e.g., Reed et al. 2021).

1.3.1. Sclerochronological records

The use of massive corals as environmental archives was unlocked after discovering their “rhythmic skeleton pattern” (DeCarlo and Cohen 2017): that is, it was observed that aragonite with different skeletal densities is accreted in winter and summer producing annual couplets (i.e., a pair of high/low density bands per year) (Knutson et al. 1972; Buddemeier et al. 1974). The appearance of high-density and low-density bands are the result of changes in skeletal thickening and allow us to build chronological models and date growth records accurately. Yet, there is uncertainty regarding the precise mechanisms behind these annual variations in skeletal density (Tanzil et al. 2016).

The nature of coupled density bands has been widely studied, and although it is generally accepted that the dual high- and low-density bands correspond to annual seasonality (Barnes and Lough 1993; Lough and Barnes 2000), a range of environmental factors have been related to density band formation. These include environmental variables such as sea temperature (Buddemeier et al. 1974; Weber et al. 1975; Lough and Barnes 1990, 1992; Klein et al. 1993), cloud cover/light level (Highsmith 1979; Klein and Loya 1991), salinity/freshwater runoff (Barnes and Taylor 2001), rainfall (Supriharyono 2004) and wave energy (Scoffin et al. 1992), as well as biological parameters/processes such as tissue thickness (Barnes and Lough 1993). It could be that formation of banding patterns at different geographical locations is driven by different factors dependent on the specific set of conditions to which the corals are acclimatized (Tanzil et al. 2016).

The discovery of density bands enabled the retrospective measurement of coral growth and the assessment of how this growth had changes across time. Coral growth is described by three different variables: i) annual linear extension rates (cm/yr); ii) average skeletal density (g/cm^3); and iii) calcification rate (g/cm^2 yr), which is a product of the former two and provides the mass of skeletal $CaCO_3$ deposited per year (Lough and Cooper 2011). These three growth variables are inter-related, and there is evidence that the precise relationship amongst them varies with species (Lough and Cooper 2011), although other factors can influence coral growth.

In the Indo-Pacific, massive *Porites* spp. are one of the most commonly used archives, as they are long lived (lifespan of centuries) and they form large reef-building colonies. This facilitates the generation of long records, which aids in the reconstruction of climatic and environmental events. In this coral genus, there is usually a negative relationship between linear extension and density, with a strong positive relationship between linear extension and calcification and only a weak negative relationship between density and calcification (Lough 2008).

Environmental conditions are strong drivers of growth variability within species, including *Porites* spp. (Lough and Barnes 2000). Extensive work has shown that seawater temperature exerts a strong control over *Porites* spp. linear extension and calcification rates, with calcification rates increasing ~ 0.3 g/cm^2·yr and linear extension increasing by 0.3 cm/yr per 1°C increase of seawater temperature (Lough 2008; Lough and Cantin 2014). This tight relationship enhances the use of growth proxies as temperature records and coral response to changes. Unsurprisingly, temperature anomalies, like those instigated by periodic climate events (e.g., ENSO, Pacific Decadal Oscillation (PDO)) can produce growth anomalies that have been used to study the recurrence of climate events (see for example work by Hendy et al. 2003). Similarly, events of severe thermal stress and bleaching tend to be characterised by high density bands in sclerochronological records, also informing us about the recurrence and intensity of these events over the years (Cantin and Lough 2014; Barkley and Cohen 2016) (Figure 1.4). Sediment and nutrient runoff have also been shown to affect coral growth. For example, it has been observed how *Porites* spp. within reefs near coastal development areas, and/or high sedimentation rates show a significantly decrease in linear extension (e.g., Crabbe and Smith 2005). Also, while nutrient input into reefs might initially favour linear extension, it eventually decreases once a certain exposure threshold has been exceeded (Marubini and Davies 1996; Marubini and Atkinson 1999). As such, sclerochronological records can also aid in the dating of certain events that temporarily changed the reef conditions.

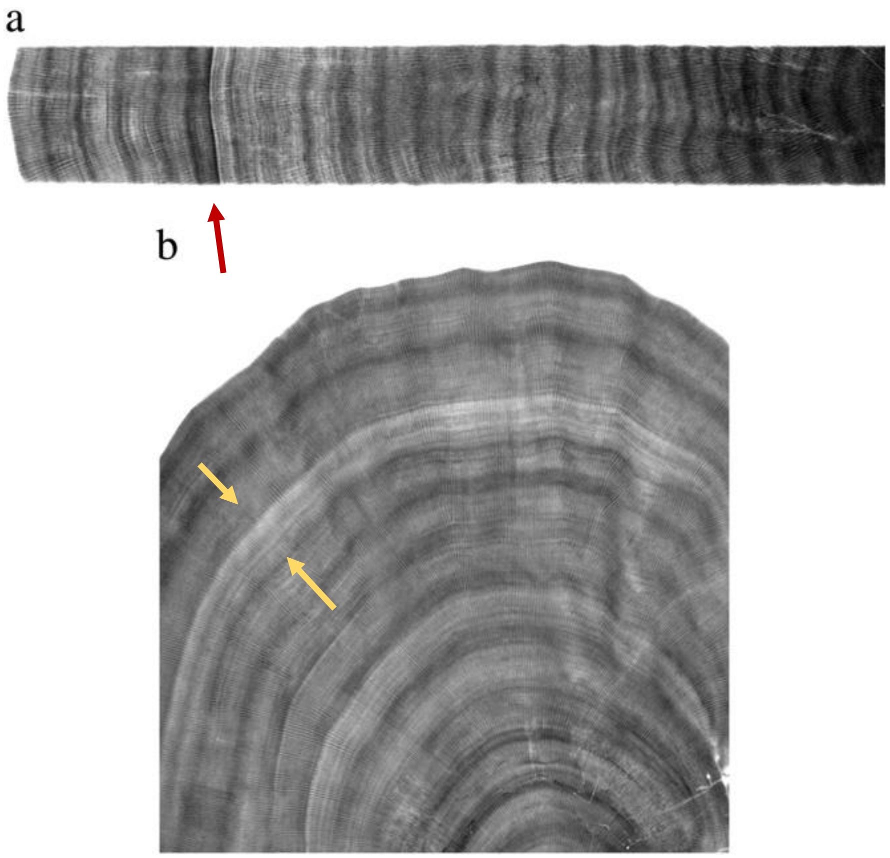

Figure 1.4. Examples of X-ray imaging of coral growth band. Image show X-ray positives from Porites spp. specimens from a) the Great Barrier Reef and b) Papua New Guinea. The dark band (high density; red arrow) in a) was dated to 1998 and shows slowed growth as a result of thermal stress. The light band (low density; yellow arrow) in b) was dated to 1997 and indicates reduced growth as a result of unusually cool water stress. Taken from (Lough and Cooper 2011).

1.3.1.1. Acquisition of sclerochronological proxies

X-radiographic imagery from massive coral skeletons enables the visualization of the seasonal density bands (Knutson et al. 1972) and is the basis for the measuring coral growth parameters. These measurements are usually obtained perpendicular to the major growth axis of a given coral sample to avoid biases (DeLong et al. 2013).

As reviewed by Lough and Cooper (2011), linear extension can be simply obtained by measuring the distance between equivalent points on annual bands from X-ray images (Carricart-Ganivet et al. 2000). Furthermore, the acquisition of continuous density measurements allowed to obtain annual linear extension by measuring the distance between annual density maxima and/or minima (Lough and Cooper 2011). Other non-radiometric techniques (UV luminescence and geochemical measurements) can be used to measure annual linear extension rates in some cases, but no other growth parameters.

Density measurements nowadays are usually obtained from X-ray densitometry (e.g., Helmle and Dodge 2011), gamma densitometry (e.g., Zoppe et al. 2022) or Computed Tomography (CT) techniques (e.g., DeCarlo et al. 2015a). While X-ray and gamma densitometry have been widely applied and reproduced (e.g., Tanzil et al. 2013) they are limited by the fact that measurements are 2-dimensional and have to be measured on an already cut and sliced coral (typically 5 – 7mm thick (Lough and Cantin 2014). Because corals present a convoluted pattern of 3-dimensional growth, it can be difficult to obtain slabs exposing the optimal path for measurements, especially when working with long cores, before any growth visualization is obtained. This problem is resolved with the use of computed tomography (CT), which allows for the acquisition of 3-dimensionals X-ray images of intact coral samples. This facilitates the identification of the path of the major growth axis and the acquisition of both annual extension and density measurements along this optimal transect, regardless of its orientation (e.g., Cantin et al. 2010; Carilli et al. 2012; DeCarlo et al. 2015a; Barkley et al. 2018).

1.3.2. Geochemical proxies

During skeletal formation, minor and trace elements that were originally dissolved in seawater are introduced in the ECF through different pathways and from there, they can be incorporated into the aragonite lattice (Druffel 1997). Usually, they are reported as a ratio to calcium (El/Ca: the amount of certain element per unit of Ca). Ultimately, the content of minor elements within the coral skeleton is determined by the chemical composition of the ECF, and although this is strongly influenced by coral physiology, minor elements in coral aragonite can retain the local seawater chemical signature at the time of its deposition (e.g., Gagan et al. 2000; Grottoli and Eakin 2007).

The measurement of geochemical proxies enables continuous quantification of a range of environmental variables across the timespan when the coral aragonite was precipitated. Even more, due to the banded nature of massive corals, and their rapid linear extensions (up to 2 cm/yr in *Porites* spp.), these proxies can be relatively easily dated through sclerochronological and/or radiometric (e.g., U-Th, radiocarbon, U/Pb) techniques, and are able to provide environmental and climate records from sub-monthly (e.g., Wyndham et al. 2004; Grottoli et al. 2013) to centennial resolution (e.g., Linsley et al. 2000; Tudhope et al. 2001) back to several hundred years ago (Gagan et al. 2000; Felis et al. 2003).

Coral geochemical proxy records from the Pacific Ocean have proven to be reliable for reconstructing past environmental change, including SST, salinity, rainfall (e.g., Dunbar and Wellington 1981; Le Bec et al. 2000; Hendy et al. 2002), nutrient availability (e.g., Lea et al. 1989; Shen et al. 1992a) and river input (e.g., Lough 1991; Klein et al. 2012).

However, the changing environmental conditions influencing coral growth (and coral physiology) might also influence the incorporation of elements into the skeleton (and biasing the El/Ca signature) (e.g., Goodkin et al. 2005; Clarke et al. 2017, 2019; D'Olivo and McCulloch 2017). For this reason, coupling sclerochronological and geochemical proxies can increase the fidelity and reproducibility of coral paleoreconstructions.

1.3.2.1. Incorporation of trace elements in the coral skeleton

As new skeleton ($CaCO_3$) is secreted from dissolved ions in the ECF (Ca^{2+} + CO_3^{2-}), various trace elements (e.g., Sr^{2+}, Ba^{2+}, Mn^{2+}, Mg^{2+}, Li^+ or UO_2^{2+}) are incorporated into the aragonite lattice. These trace elements are preferentially incorporated or excluded from the skeletal material depending on their partition coefficient (K_D), which is defined as the El/Ca ratio in the coral relative to that the ECF. Next, I describe the mechanisms of incorporation in the coral aragonite of the trace and minor elements investigated in this thesis.

It is well established that some elements, such as Sr^{2+}, substitute for Ca^{2+} (Sr^{2+} + CO_3^{2-}) (Allison et al. 2001; Finch et al. 2003), which is facilitated due to both ions (Sr^{2+} and

Ca^{2+}) being doubly positive and of similar size (1.26 Å and 1.18 Å respectively; Shannon 1976). Furthermore, Sr^{2+} has a partition coefficient of ~1 (de Villiers et al. 1994), meaning that this element is preferentially included into the aragonite lattice.

In the case of Mg^{2+} and Li^{+} it is not clear whether they substitute for Ca^{2+} or are trapped in structural defects of the mineral lattice that facilitate ionic adsorption (known as kinetic effects) (Rollion-Bard and Blamart 2015). Because their ionic radii (0.89 Å and 0.92 Å respectively; Shannon 1976) are much smaller than that of Ca^{2+}, it is argued that they are too small to directly substitute for this ion in the mineral lattice (Finch and Allison 2008; Montagna et al. 2014). In addition, both Mg^{2+} and Li^{+} have low partition coefficients (K_D <<1) which prevents them from being readily precipitated in the coral aragonite. The similarities between both these ions in terms of their size and partition coefficient suggests that their incorporation in the coral skeleton is controlled by a similar mechanism (Hathorne et al. 2013; Montagna et al. 2014).

Mechanisms of U (UO_2^{2+}) incorporation into coral aragonite are ambiguous (Sinclair et al. 1998; Fallon et al. 2003; Anagnostou et al. 2011; DeCarlo et al. 2015b; Chen et al. 2021). However, studies point towards U being incorporated into the aragonite lattice primarily as a cation-balanced complex (Endrizzi and Rao 2014), more specifically as $CaUO_2(CO_3)_3^{2-}$, as it is the dominant species found in seawater (Chen et al. 2021). Its partition coefficient is 0.93, making it readily incorporated into the aragonite (Amiel et al. 1973).

Ba^{2+}, similar to Sr^{2+}, has a ionic radii (1.42 Å; Shannon 1976) that facilitates its incorporation into coral aragonite by substitution of Ca^{2+} (Lea et al. 1989). Its partition coefficient is 1.11, thus exerting little fractionation and reflecting the ECF environment at the time of precipitation (Alibert et al. 2003; Akagi et al. 2004; Sinclair and McCulloch 2004; Lewis et al. 2007; LaVigne et al. 2016).

Reduced Mn^{2+}, when present in the water column, seems to be readily incorporated into the aragonite lattice in exchange for Ca^{2+} (Gagnon et al. 2012), despite the differences in ionic radii with calcium (0.96 Å Shannon 1976). Mn^{2+} has a partition coefficient into coral aragonite of 0.10 (Bruland and Franks 1983; Shen and Boyle 1988), not suffering a strong discrimination during precipitation and being incorporated in close proportion to its ECF ratio.

Finally, rare earth elements (REE), are incorporated into the coral aragonite by lattice substitution of Ca^{2+} due to similarities in ionic size (REE = 0.97 – 1.16 Å; Shannon 1976). Their partition coefficients with coral aragonite differ between elements but are generally close to unity (K_D ~0.70 - 2.41), and as such their El/Ca ratios in the skeleton reflect that of the ECF (Sholkovitz and Shen 1995; Akagi et al. 2004).

Coral geochemical proxies are established based on the assumption that the variability of El/Ca in the coral's skeleton reflects the El/Ca ratio of the ECF, which is influenced by the local seawater composition. Furthermore, changes in temperature can drive changes in the partition coefficient of the elements (thermodynamic effects), which will also be reflected in the skeletal El/Ca. In order to transform the El/Ca quantification into environmental information, the skeletal El/Ca signature must be calibrated against known environmental data (e.g., seawater temperature, turbidity, salinity). The resulting calibration can then be applied to historical "down-core" El/Ca records, with the aim of filling in spatial and temporal gaps in our instrumental environmental observations. Nevertheless, this method has some caveats, such as observed differences in El/Ca-environment calibrations across regions, reefs and even colonies (e.g., Corrège 2006) that emphasise the need for site and species-specific calibrations. Furthermore, both modern and fossil coral samples can suffer diagenesis that alters the original El/Ca signal leading to erroneous reconstructions (e.g., Hendy et al. 2007).

1.3.2.2. Rayleigh fractionation

Rayleigh fractionation is a complicating factor for reconstructing environmental and climatic signal from coral aragonite. As stated above, the coral skeletal El/Ca reflects the chemical composition of the ECF. Simultaneously, the chemistry of the ECF is controlled by the rate of seawater diffusion (both passive and active) and calcification rate. The different partition coefficients between trace elements (e.g., Sr^{2+} v. Li^{+} and Mg^{2+}) dictates that some elements will be preferentially incorporated into the coral aragonite (e.g., Sr^{2+}) relative to Ca^{2+}, while others will be preferentially excluded (e.g., Li^{+} and Mg^{2+}). As a result of this process, early aragonite precipitated from a "fresh batch" of ECF will have depleted Li/Ca and Mg/Ca values and higher Sr/Ca levels. As calcification progresses, Sr^{2+} and Ca^{2+} will become depleted, while Mg^{2+} and Li^{+} concentrations will remain the same. This mechanism, in a closed system such as the ECF, causes a progressive increase in the Li/Ca and Mg/Ca ratios in a process dictated by Rayleigh fractionation. As a result, subsequent precipitated aragonite will record this change in ECF composition by showing depleted Sr/Ca and increased Mg/Ca and Li/Ca until the ECF is renewed again. As such, the degree of Rayleigh fractionation represented by the composition of the coral skeleton is dependent on the rate at which ECF is renewed and on the mass fraction of aragonite precipitated from each ECF batch (Gaetani and Cohen 2006; Gagnon et al. 2007).

Thus, and as mentioned above, the El/Ca ratios in the corals' aragonite skeleton can change depending on ECF and local seawater chemical composition, thermodynamic effects over the partition coefficient of the elements, and also depending on the amount of mineral ($CaCO_3$) that is precipitated from a single batch of ECF. This last factor is influenced by the rates of seawater diffusion activity (coral physiology) and defines Rayleigh fractionation. These processes can mask the environmental control on element partitioning, and are known as "vital effects" and kinetic processes (Allison and Finch 2004; Sinclair 2005a; Gaetani and Cohen 2006; Cohen and Gaetani 2010).

1.3.2.3. SST proxies

One of the most commonly used SST proxies in *Porites* spp. corals are the El/Ca of various trace elements (Sr^{2+} (Beck et al. 1992); Mg^{2+} (Mitsuguchi et al. 1996); Li^{+} (Marriott et al. 2004); UO_2^{2+} (Shen and Dunbar 1995) in the coral skeleton, where changes in coral El/Ca have been found to strongly correlate with SST and climate variability across time.

Traditionally, Sr/Ca has been the most widely used coral proxy for SST reconstructions (Smith et al. 1979; Beck et al. 1992; Alibert and McCulloch 1997; McCulloch et al. 1999), based on a negative correlation with SST, which has been observed in numerous regions across Indo-Pacific and Atlantic reefs (as reviewed by Corrège 2006). Although it was initially thought that the Sr/Ca-SST correlation was due to inorganic controls of SST over K_{DSr} (Corrège 2006), empirical calibrations have shown differences in Sr/Ca sensitivity to SST (different slopes of linear regressions) and differences in mean Sr/Ca values among colonies (DeLong et al. 2007; Grove et al. 2013; Wu et al. 2014; Alpert et al. 2016; Sayani et al. 2019). This complicates the use of this SST proxy in fossil archives where calibration of modern coral Sr/Ca values and SST measurements is not possible. Although there is still uncertainty surrounding the observed variability in the Sr/Ca-SST relationship, Cohen et al. (2002) found that high rates of photosynthetic activity caused skeletal Sr/Ca values to decrease. Importantly, this hints at an indirect relationship between Sr/Ca and SST, whereby other environmental parameters (e.g., light irradiance) affect calcification processes and are then reflected in the Sr/Ca signal. Therefore, careful examination of the proxy must be carried out before using it to reconstruct SSTs.

Part of the varying sensitivity of the Sr/Ca-SST proxy can potentially be attributed to interlaboratory differences and/or measuring Sr/Ca along a suboptimal growth track (that is, not perpendicular to the maximum growth axis; Alibert and McCulloch 1997; DeLong et al. 2013). However, a number of studies have shown how physiological processes ("vital effects", i.e., Ca^{2+} pumping rate) can alter the Sr/Ca in the coral skeleton (e.g., Cohen et al. 2002; Allison and Finch 2004; Goodkin et al. 2005; Gaetani and Cohen 2006; Reed et al. 2021), therefore impacting the fidelity of the Sr/Ca-SST relationship. Discerning between SST, "vital effects" and Rayleigh fractionation signals in the coral Sr/Ca has proven difficult (Alibert and McCulloch 1997; Corrège 2006) and other SST proxies have been developed trying to improve SST reconstructions.

One of the newly explored coral-based SST proxies is Li/Mg (Casey et al. 2010; Montagna et al. 2014), which is based on the fact that Li^+ and Mg^{2+} concentrations in the ECF remain relatively constant throughout precipitation (Montagna et al. 2014). Li/Ca was found to have a negative correlation with SST (Hathorne et al. 2013), while Mg/Ca has a positive correlation with SST (Montagna et al. 2014), but these El/Ca ratios are heavily impacted by Rayleigh fractionation as calcification progresses, due to their low K_D values and changing $[Ca^{2+}]$. However, Rayleigh fractionation should have a weak influence over skeletal Li/Mg due to their similar K_D values and their variability in the coral aragonite being, in theory, exclusively reliant on the SST-sensitive partition coefficients of Li and Mg (Felis et al. 2003; Montagna et al. 2014; Marchitto et al. 2018). However, Fowell et al. (2016) showed that the use of Li/Mg records may still require species- and site-specific calibrations, and Rollion-Bard et al. (2015) suggested that this proxy might still present kinetic variability not caused by SST.

Another newly implemented SST proxy is Sr-U (DeCarlo et al. 2016), which combines Sr/Ca and U/Ca measurements. This proxy was developed following observations of inorganic aragonite precipitation where Sr/Ca values is sensitive to SST and Rayleigh fractionation, while U/Ca is sensitive to $[CO_3^{2-}]$ and Rayleigh fractionation, but not SST (DeCarlo et al. 2015b). As U-carbonate complexes co-vary with $[CO_3^{2-}]$, the observed correlation of U/Ca with SST (e.g., Hendy et al. 2002) could be indirectly governed by changes in [CO_3^{2-}] (Cheung et al. 2021). The Sr-U proxy works by isolating the temperature component from the determined Sr/Ca-U/Ca relationship and it was successfully applied to *Porites* spp. on interannual to decadal timescales (DeCarlo et al. 2016). This proxy was also used to reconstruct SST from Atlantic corals (*Pocillopora*, *Diploria*, *Orbicella*, *Diploria*) on similar timescales (Alpert et al. 2017) and at sub annual resolution in several genera (*Acropora*, *Pocillopora*, *Stylophora* and *Turbinaria*) from the Indian Ocean (Ross et al. 2019).

1.3.2.4. Terrigenous runoff proxies

Quantification and reconstruction of past coastal water quality (e.g., fresh water and sediment input, industrial and urban pollutants) is important for assessing how past conditions affected reef-building corals, identifying the sources of said elements (e.g., soil erosion from agricultural practices, or waste waters) and implementing appropriate management strategies. Trace element to calcium ratios of Ba/Ca, Mn/Ca and REEs in coral skeletons have been used extensively to understand long term anthropogenic impacts on water quality in shallow-water tropical regions (e.g., Fallon et al. 2002; Alibert et al. 2003; McCulloch et al. 2003; Lewis et al. 2007; Jupiter et al. 2008; Carilli et al. 2009; Carriquiry and Horta-Puga 2010; Prouty et al. 2010; Brodie et al. 2012; Maina et al. 2012; Inoue et al. 2014).

Ba^{2+} reaches the coastal zone adsorbed onto suspended fluvial sediment particles. In the estuarine mixing zone, Ba^{2+} is released into the seawater by ion-exchange with Mg^{2+} and Ca^{2+} where it is transported to coastal ecosystems and open ocean with the river flood plume (McCulloch et al. 2003; Sinclair and McCulloch 2004). As such, Ba/Ca records from inshore corals have been widely used as a proxy for river discharge, precipitation and flood events in the GBR (e.g., Alibert et al. 2003; McCulloch et al. 2003; Lewis et al. 2007; Jupiter et al. 2008; Prouty et al. 2010; Grove et al. 2013), North Pacific (e.g., Prouty et al., 2010) and Indian Ocean (e.g., Grove et al. 2012). However, some studies found Ba/Ca peaks that either lagged flood events (Moyer et al. 2012) or were completely decoupled from river discharge (Lewis et al. 2007, 2012; Saha et al. 2018; Tanzil et al. 2019). The biogeochemical cycle of Ba in coastal regions is not fully understood and certain processes have been proposed to explain why the Ba/Ca proxy for river discharge does not always work, such as coastal upwelling (Tudhope et al.

1996), barite formation associated with algal blooms and barite ingestion (Sinclair 2005a), SST influence (Grove et al. 2012), and Ba released from sediment fluxes and groundwater seeps (Prouty et al. 2010). Overall, and despite observations of inconsistent Ba/Ca content in coral skeletons, this proxy can be applied to reconstruct past surface biogeochemical processes and terrestrial discharge given that a detailed examination of the Ba/Ca signal is carried out to confirm it is effectively influenced by terrigenous input.

Similar to Ba^{2+}, Mn^{2+} in coastal seawater is mainly sourced through particulate matter in river discharge (Shen et al. 1991). The low salinity in the estuarine mixing zone causes Mn desorption from suspended sediments and this trace metal is transported within the river flood plume (Shen et al. 1991), where it seems to be incorporated into the coral aragonite in proportion to its concentration in seawater by substitution of Ca^{2+} (Alibert et al. 2003; Lewis et al. 2007). However, the mechanisms controlling the biogeochemical cycle of Mn in coastal environments are intricate. The availability of dissolved Mn^{2+}, the form in which it is incorporated in the aragonite lattice, depends not only on salinity and the amount of riverine sediment input, but also photo-reductive dissolution and a complex oxidation-reduction cycle (Shen et al. 1992b; Alibert et al. 2003; Wyndham et al. 2004; Lewis et al. 2012). Although Mn/Ca variability has been found to be influenced by primary productivity (Wyndham et al. 2004) and seasonal upwelling (Shen et al. 1991), inshore coral Mn/Ca variability is likely to reflect river discharge. A number of studies found variability of mean coral Mn/Ca corresponded with distance to the source of terrigenous input in the GBR (Wyndham et al. 2004; Jupiter et al. 2008) and Japan (Inoue et al. 2014). In the South West Pacific it was also found to be correlated with increased sedimentation as a result of mining operations (Fallon et al. 2002) and with wind patterns (Sayani et al. 2021; Chapman et al. 2022). In addition, studies have shown a link between coral Mn/Ca and variability in river runoff during large episodic climatic events (e.g. tropical cyclones) and decadal oscillation (e.g., PDO) in the Atlantic Caribbean (Moyer et al. 2012) and the South China Sea (Chen et al. 2015).

As with other trace elements used as proxies for terrigenous influence, REEs (Y, La, Ce, Pr, Nd, Sm, Eu, Gd, Tb, Dy, Ho, Er, Tm, Yb, Lu) are sourced to coastal environments through river discharge, where they experience desorption from particulate matter in the estuarine mixing zone, similar to Ba and Mn (as reviewed by Saha et al. 2016). It is theorised that REEs have a more conservative behaviour upon entering coastal regions than Ba and Mn and they are not influenced by primary productivity unlike these elements (Lewis et al. 2007). When REEs are incorporated into the coral aragonite lattice, they suffer minimal fractionation (Akagi et al. 2004; Leonard et al. 2019). These properties should make REEs excellent terrestrial sediment proxies. Very few studies have deepened in the application of other REEs beyond Y/Ca as a proxy for sub-annual events, but they have been applied to reconstruct long-term changes in sediment input and riverine influence in inshore reefs in the GBR (Wyndham et al. 2004; Jupiter et al. 2008; Leonard et al. 2019), South West Pacific (Fallon et al. 2002), South China Sea (Nguyen et al. 2013) and Japan (Akagi et al. 2004).

1.3.2.5. Complications of geochemical reconstructions: Diagenesis

Coral geochemical proxies enable the reconstruction of environmental and climatic events at high temporal resolution. However, diagenesis is a potential caveat that can complicate the correct interpretation of coral records.

The original aragonite deposited by the coral (primary aragonite) is susceptible to diagenetic alterations that can result in dissolution of the primary mineral, precipitation of secondary cements and/or recrystallization of coral aragonite to calcite. These modifications of the primary aragonite have the potential to alter not only the original skeletal density, but also the geochemical signature of the coral. For example, deposition of secondary cements have been found to show higher Sr/Ca than primary skeletal material (Cohen and Hart 2004), and secondary Mg-calcite shows lower Sr/Ca (Allison et al. 2007) than primary coral aragonite. Furthermore, dissolution of primary material has also been observed to lead to higher Sr/Ca, U/Ca and lower Mg/Ca than pristine coral aragonite (Hendy et al. 2007), potentially biasing the Sr/Ca-SST calibrations.

Importantly, diagenetic alteration of the coral geochemistry is not only found in fossil material (e.g., McGregor and Gagan 2003; Allison et al. 2007), studies have shown that diagenesis can also be present in modern corals (Hendy et al. 2007; Sayani et al. 2011). These findings warrant the need to screen corals for diagenesis before using them for paleoreconstructions to detect and avoid potential biases of the records. Different methods can be used to detect coral diagenesis: thin sections and transmitted light microscopy, scanning electron microscopy, and X-ray diffraction are among the most common.

1.3.2.6. Acquisition of geochemical proxies

Nowadays, the most common technique for measuring trace elements in biogenic aragonite is Inductively Coupled Mass Spectrometry (ICPMS), as it can measure the concentration of multiple elements simultaneously. Fundamentally, during ICPMS the sample analyte is introduced into the instrument, where is transferred to Ar-plasma. During this process, the high-temperature plasma ionises the sample. The generated ions are then transferred through the electrostatic lenses towards the quadrupole mass analyser. The quadrupole separates ions depending on their mass-charge ratio (m/z) and are then quantified by an ion detector. For coral aragonite, sample introduction for trace element analysis can be made in either solution (solution ICPMS) or solid phases (laser ablation ICPMS).

Solution ICPMS has been applied to analyse trace element content in corals for decades (e.g., Lea et al. 1989; Shen and Dunbar 1995; Lewis et al. 2007; Nagtegaal et al. 2012; D'Olivo et al. 2018; Leonard et al. 2019; Sayani et al. 2021). Solution analysis has the advantage of inferring high-sensitivity, enabling measurement of very low concentrations of elements (and isotopes). However, solution ICPMS coral records are usually obtained at low time resolution, being monthly or higher (see references above). This is due to mechanical limitations during drilling and sampling the coral skeleton coupled to the large amounts of sample needed. Furthermore, this methodology is time-consuming, particularly with respect to sample preparation before introduction in the ICPMS (e.g., chemical cleaning, dissolution, spiking).

The application of Laser Ablation (LA) to ICPMS permits the introduction of a "freshly" ablated solid analyte directly into the ICPMS. The use of a laser beam enables subsampling a solid without any intermediary steps at very high resolution (current LA instruments are capable of creating a uniform ablation beam as small as 2 µm in diameter). Sample preparation for LA-ICPMS is minimal and virtually non-destructive. It has been widely used for trace element analysis of corals (e.g., Sinclair et al. 1998; Fallon et al. 2002; Wyndham et al. 2004; Prouty et al. 2009; Grove et al. 2010, 2012; Maina et al. 2012; Moyer et al. 2012; LaVigne et al. 2016; Lewis et al. 2018; Tanzil et al. 2019) at very high resolutions (near daily), that facilitates the study of short-lived events (e.g., floods, tropical cyclones, upwelling) and their effects on corals.

1.4. Coral reefs in Fiji

Fiji has one of the largest and most diverse reef systems in the South West Pacific, covering an area of 4550 km^2 (Figure 1.5) (Mangubhai et al. 2019) and supporting a wealth of marine and reef biodiversity with nearly 350 different species of scleractinian corals present (Lovell and McLardy 2008). Yet, progressive loss of coastal biodiversity and habitat has been recorded (Jupiter and Egli 2011; Lawson et al. 2021; Singh et al. 2021) as a result of anthropogenically driven global and local threats.

Localised impacts include destructive fishing, overexploitation of fisheries resources and increased sedimentation and pollution in coastal reefs because of poor coastal development and land management (Dadhich and Nadaoka 2012; Ram and Terry 2016). The increasing population of Fiji coupled to population movements towards urban coastal areas are increasing the pressure on coral reefs. It has been recorded how poor agricultural practices and land clearing have increased land erosion and subsequently, increased nutrient levels in inshore reefs leading to growth of seagrass and macroalgae (Dutra et al. 2018). Some studies have found high levels of nitrates and phosphates in the inshore reefs along the Coral Coast (South-West Viti Levu) and the Yasawa and Mamanuca islands (Mosley and Aalbersberg 2003; Sykes and Morris 2007; Tamata 2007), sometimes at levels exceeding the threshold of coral tolerance. Along the Coral Coast river runoff is the main source of sediments and nutrients (Ram and Terry 2016). In the northern areas of Viti Levu and Vanua Levu, extensive cultivated areas of sugarcane (“Fiji’s sugarcane belt") favour increased soil erosion during intense rainfall events, leading to increased suspended particulate matter, nutrients and chemical phytosanitary products runoff in the waterways (Sykes and Morris 2007). Raw sewage from urban and highly populated areas is severely impacting water quality in the inshore reefs contiguous to these areas, especially in the Suva area (Suva Lagoon and Suva Harbour), Nadi Bay, Lautoka and Levuka harbours (Zann 1994). Furthermore, several studies have confirmed the presence of heavy metal and chlorinated compounds in coastal waters around Suva (Stewart and De Mora 1992; Maata and Singh 2008; Chand et al. 2011), leaching from urban and industrial sewage into the lagoon.

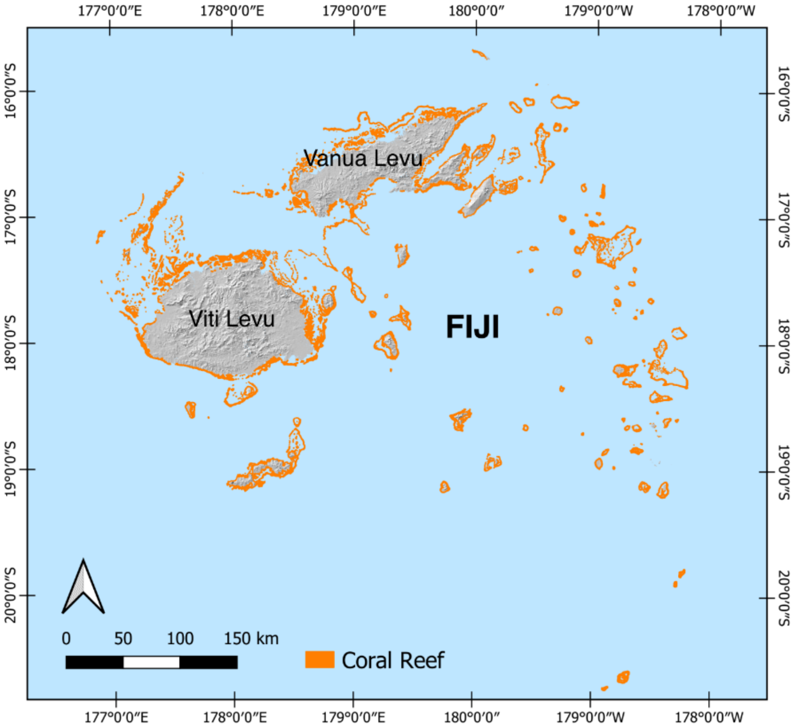

Figure 1.5. Map of Fiji. Orange regions are coral reefs.

In addition, climate change has placed an ever-increasing pressure on Fijian coral communities. Increasing seawater temperature and a number of thermal stress events have led to several bleaching events observed in Fijian reefs in 1989, 1998, and 1999 (Cumming et al. 2002), with widespread bleaching being recorded in 2000 for the first time (Cumming et al. 2002; Lovell and Sykes 2007). Widespread bleaching, although not to the extent of the 2000 event, was also recorded in 2002 and 2005 (Sykes and Morris 2007). During the El Niño event of 2016, despite high thermal stress being reported for the Fiji region, widespread bleaching was not observed. Furthermore, reef surveys and observations showed that the existing bleaching was reversed with the arrival of Cyclone Winston (Mangubhai 2016). Although monitoring efforts have shown that corals reefs in Fiji were generally able to recover from intense bleaching within ~5 to 10 years (Mangubhai et al. 2019), the predicted increase in intense bleaching frequency (van Hooidonk et al. 2016; Hughes et al. 2018a; Smale et al. 2019) coupled to diminished resilience to recover due to local impacts (Woolridge and Done, 2009) can severely risk the future of inshore reefs in Fiji.

Importantly, the Fiji economy is heavily dependent on coral reefs with an emphasis on tourism and fisheries. Therefore, the potential collapse of coastal reefs and the fisheries associated with them puts at risk coastal populations whose livelihood, economy and food source depends, ultimately, on healthy reefs (Kinch et al. 2010).

Reef managers use diverse strategies to mitigate the impact of local stressors to buffer the damaging effect of climatic events and ocean warming on coral reefs (McLeod et al. 2021). While some of the extensive coral reef systems in Fiji have been identified as potential climate refuges, where future climate impact is expected to be less severe (Beyer et al. 2018), portions of these same reefs are experiencing considerable threats and impact from local stressors, in particular sediment and nutrient runoff (Brown et al. 2017a, 2017b; Andrello et al. 2022).

1.4.1. Reef management in Fiji

Marine Protected Areas (MPA) are the cornerstone of most marine conservation strategies as they are effective at reducing one of the most prevalent threats to marine ecosystems: overfishing (Lester et al. 2009). However, traditional MPAs may not be able to protect marine ecosystems in places where land-based activities negatively impact these ecosystems (Brown et al. 2017a). A “ridge-to-reef” approach emphasising integrated coastal zone and resilience-based management are essential to establish a well-planned and effective conservation in these areas.

In the Fiji Islands, as a response to the decline in coastal biodiversity, there has been an increase in the amount of areas in the ocean under some sort of protection (O’Leary et al. 2017) and the abundance and biomass of targeted species have increased in result (Lester et al. 2009). Initiatives for conserving Fiji’s marine and terrestrial ecosystems have been supported by communities, NGOs, and the Fijian government. This is reflected in the increasing number of MPAs being established in Fijian waters, mostly in the form of Locally Managed Marine Areas (LMMAs).

Fiji’s nearshore waters are divided into 410 traditional fishing grounds (called *qoliqoli*), where the coastal villages implement a community-based resource management (Kitolelei and Kakuma 2022). The LMMAs were created in 1997 as a network-based reef management, to limit and control the increasing fishing pressure suffered by these inshore reefs. Fiji’s LMMAs cover over 10,000 km^2 and over 22% of all inshore areas (Robertson et al. 2020), they typically include management plans such as closures, size limits, catch limits, gear bans/restrictions, seasonal bans, or licensing controls, and have reported increased biodiversity, increased fish biomass and restored habitat (Clements et al. 2012; Bonaldo et al. 2017).

The primary tool applied for the management of coastal marine resources within LMMAs is the use of traditional temporary closures (called *tabu* areas), where the local community chooses the location, size, and management regime for their closed area (Govan et al. 2009). Despite the success of LMMAs for the recovering of fisheries, currently they do not include management strategies to mitigate poor water quality, which have been found to be one of the main stressors in inshore reefs in Fiji (Atherton et al. 2005). There is no doubt that management of protected areas cannot occur in isolation of potential disturbance from outside the protected reef ground. Efforts are being implemented by both the government, non-governmental organisations and the coastal communities who are working to establish a management placed in the context of a broader ecosystem framework in order to reduce local threats to reef systems and therefore improve resilience (Lester et al. 2009). In this framework, the Fiji National Biodiversity Strategy and Action Plan is aiming to protect 30% of its marine territory by 2025 (Department of Environment, Government of Fiji 2020), acknowledging the importance of good catchment and forest management to limit the threat to aquatic ecosystems (Jupiter et al. 2012).

However, coral reef condition, and how environmental change influences it, is poorly understood (Klein et al. 2012; Brown et al. 2017a, 2017b). The success of distinct management strategies is challenging to asses and/or model, especially across a large area like Fiji, due to the complex nature of ecological processes operating across multiple scales on coral reefs (Done et al. 2010). Modelling processes have been shown to be successful to establish coastal areas with poor water quality and how they are connected to catchment soil erosion and sediment input (Brown et al. 2017a). Yet, the limited data available to represent these processes (Klein et al. 2012) and the lack of long-term reconstructions of nearshore water quality represent a limitation towards the integration of land and sea management as a single system.

It is for this reason that coral growth and environmental records have a great potential to help understand how water quality has changed across time. Ultimately, the results of this study could contribute to the efforts being carried out to link land processes and coastal water quality, which are necessary to implement an integral watershed management that protects inshore reefs and the services they provide for the coastal communities.

1.5. This thesis: Understanding the response of inshore massive *Porites* spp. corals to environmental changes over time

As stated above, coral reefs are complex ecosystems that support the livelihoods of the human communities established around them. Climate change severely affects coral reefs, and, globally, seawater warming represents the main threat to these systems. In addition, inshore coral reefs are also being impacted by anthropogenic activities (e.g., land clearing, urban expansion, industrial and agricultural growth) that lead to an increase in sedimentation, dissolved inorganic nutrients and pollutants in reef waters.

Both climate change-induced environmental changes and decreased coastal water quality are already having negative effects on average growth rates of reef-building corals globally and have the potential to fully collapse the ecosystems. In this framework, integrated land-coast management efforts have the potential to reduce local impacts and maintain the resilience of coral reefs to limit the effects of climate change. Yet, carrying out this management successfully is complicated by a number of limitations due to the complexities in the catchment system and the conditions that lead to increased sedimentation in the inshore reefs, coupled to the understanding of how corals are affected by them. As such, there are only a few studies in the world addressing the relationship between watershed status and the state of the marine habitat.

In Fiji, coral bleaching, although not massive, has now become an annual event and the increasing population settling in the main islands (Viti Levu and Vanua Levu) coupled to the economic activity derived from these demographic changes have the potential to decrease the resilience of these inshore reefs towards global impacts. However, there is a lack of long-term records of coastal water quality, limiting the correct implementation of a management strategy. While various local organizations routinely monitor coral reef condition in Fiji through direct in situ observations, these provide only a limited snapshot of the current ecosystem state. Coral growth reconstructions from massive reef-building corals can provide unique insight to understand how past environmental conditions have affected present day state and inform reef managers.

The overarching goal of this thesis is to disentangle the relationships between coral growth, water quality and climatic events in Fijian inshore reefs, and reconstruct the sensitivity of reef-building corals to environmental changes. The specific aims are:

1. Determine the variability of coral growth across different inshore reefs with different catchments, land-use and coastal water quality and across time (1998 – 2017). This will allow to investigate what environmental variables influence and drive coral growth in Fiji and to further understand whether local management can improve the impact of seawater warming.
2. Investigate the potential of *Porites* spp. corals from inshore reefs in Fiji as SST archives. Furthermore, this work will also highlight environmental controls and events that alter coral physiology and the geochemical signal with it.
3. Explore records of terrigenous influence from *Porites* spp. in Fiji, examine the environmental conditions and climatic events that control their input into inshore reefs and determine whether they can be used as records of past inshore water quality.

1.5.1. Thesis outline

In this thesis I address each of the aims listed above in detail, including the methods followed for the acquisition of data and a synthesis of the results and direction for future work.

Chapter 2: Methods

Chapter 2 comprises a detailed description of the techniques and processes executed during the duration of this project. They include information on coral collection, sample processing and analytical methods used to obtain data (i.e., CT scanning and LA-ICPMS). This chapter also includes information on the environmental data used along this thesis, both remotely sensed and in-situ, as well as its sources.

Chapter 3: What if "acting locally" is not enough? Coastal turbidity and heat stress control coral growth in Fiji

In this chapter I examine the annual growth variability experienced by *Porites* spp. on four different inshore reefs from Viti Levu, showing high variability in linear extension (~2 cm/yr to ~ 0.7 cm/yr) across locations. Although SST seasonality and magnitude is similar on all sites, catchment extension, land-use and population present great differences, which is reflected in the mean turbidity gradient observed from nearly crystalline to turbid waters as well as its seasonality. By coupling environmental and growth data, it can be observed that mean differences in growth are driven by water quality in absence of SST differences. Furthermore, growth data also show how thermal stress exerts a negative control over coral growth. This is evidenced by the generalised decline observed from 2014 onwards following the intense 2014 – 2016 marine heatwave period in the Indo Pacific, and this decline was observed regardless of water quality parameters.

Chapter 4: Overcoming growth effects in Fijian corals for the application of trace element paleothermometry

This chapter includes monthly resolved geochemical trace elemental ratios (i.e., Sr/Ca, Mg/Ca, Li/Ca, U/Ca) from *Porites* spp. skeletons and explores their robustness as SST proxies in Fiji. Coupling of geochemical and growth data showed that skeletal calcification and growth rates exert some control over the skeletal geochemistry well beyond Rayleigh fractionation. On examination of these results, data shows how this growth control over the skeletal El/Ca is influenced by seawater turbidity, which complicates the acquisition of robust El/Ca-SST calibrations by masking the SST signal. Nevertheless, by colony replication and standardization of the El/Ca signal across several colonies it is possible to constrain the SST signal from the other local environmental variables, creating a more robust calibration.

Chapter 5: Coral Ba/Ca, Mn/Ca and REE records from Fiji *Porites* spp. and their potential as inshore reef water quality archives

In chapter 5, I focus on known proxies for terrigenous input (i.e., Ba/Ca, Mn/Ca, Y/Ca, La/Ca, and Ce/Ca) obtained from *Porites* spp. samples. Monthly resolved coral El/Ca and environmental data are used to explore whether inshore *Porites* spp. in Fiji can aid in reconstructing past coastal water quality. The data show different seasonal variability across El/Ca within each location, and also differences in the signal across locations. In this chapter I dive into the environmental and climatic variables that might be influencing different signals within and across sites and results show that the response of different catchments to similar climatic events (seasonal rainfall, tropical cyclones, …) is very complex. Although coral proxies are promising water quality archives in Fijian inshore reefs, a deep knowledge of the catchment-inshore system must be acquired before interpreting the driver of El/Ca.

Chapter 6: Conclusions and future work

Finally, Chapter 6 summarises the major findings of this thesis and builds the final conclusions from each individual chapter before providing an outlook into the potential future work needed to reinforce the key findings and work towards the main goal of the thesis.

Chapter 2 | Methods

What you will see, if you leave the Mirror free to work,
I cannot tell. For it shows things that were, and things
that are, and things that yet may be. But which is it
that he sees, even the wisest cannot always tell.
Do you wish to look?

Galadriel

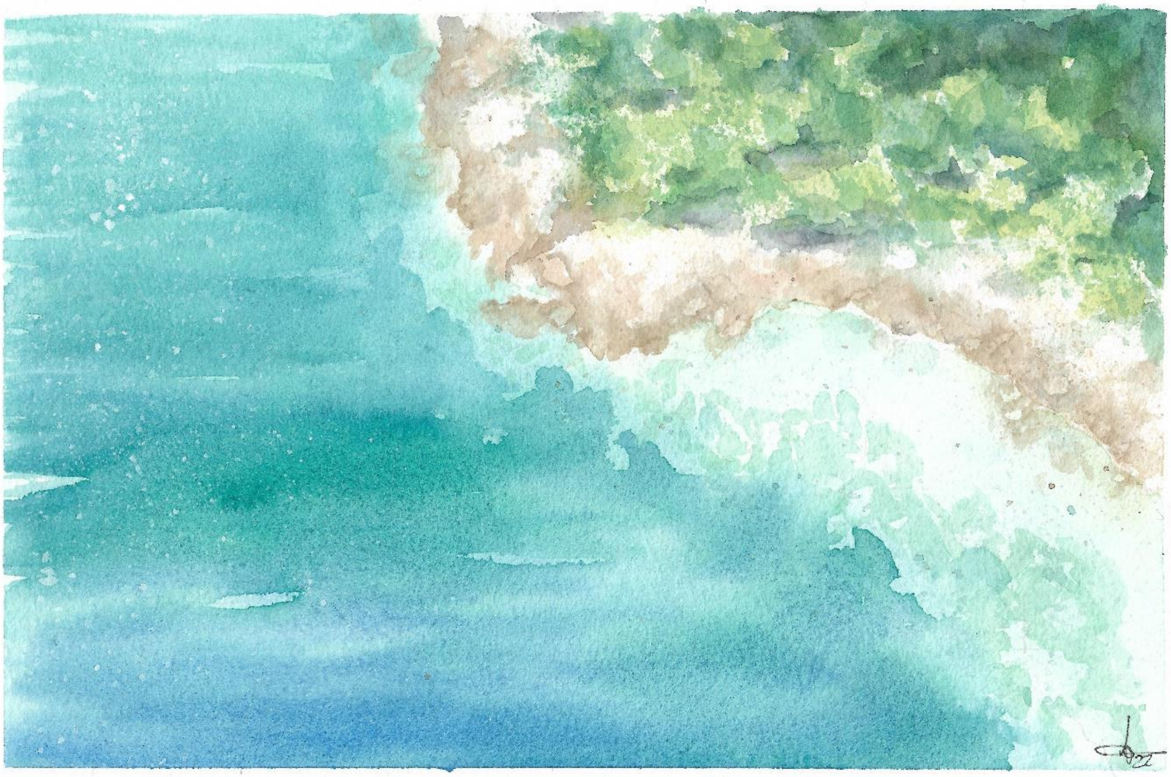

Coral series #6 (MVL)

Chapter 2 | Methods

2.1. The Fiji Islands

The Fiji Islands are located in the South West Pacific Ocean, between the 15°S – 22°S latitude and 177°E – 179°W longitude, encompassing an area of 650,000 km^2, of which less than 3% (~18,300 km^2) is dry land (Fiji Meteorological Service 2006).

The Fijian archipelago consists of about 330 islands and more than 500 islets and cays (Printemps 2008). The largest island and population centre is Viti Levu, which has an area of 10,489 km^2 (Macfarlene et al. 2009), and contains Suva, the capital of the country. The locations of this study are all inshore reefs around Viti Levu (Sections 2.2. and 2.3.). The second largest island of the country is Vanua Levu, which has an area of 5,556 km^2 (Macfarlene et al. 2009), and together with Viti Levu represents 87% of the total land area of Fiji (Leslie 1997). After the last governmental census in 2017, the population of Fiji included 884,887 people, 55.9% of which were urban dwellers and 44.1% inhabited rural areas. Despite the population of Fiji having kept growing in the last decades, the rate at which it has done so has been decreasing down to a current 0.6% per year (FBoS 2017). The proportion of Fiji's urban population has been also increasing in every decade, but it was not until 2007 that it constituted 50% of the population (FBoS 2017). Over 75% of the total population live within 5 km of coastal areas (Andrew et al. 2019) where most of the services and infrastructure are located (Agrawala et al. 2003).

This increasing density of population in urban coastal areas, coupled with the need for the sea and inshore reefs for subsistence and monetary needs by a portion of the people, results in an increasing level of stress on the marine ecosystems (Tamata 2007) especially in the peri-urban settlements around the main cities (Vuki et al. 2000). Fiji's economy is mostly sustained by agricultural, logging and fishing activities, manufacturing of products obtained by these industries and tourism, the latter of which has grown significantly over the years (FBoS 2017).

2.1.1. Climate

The Fiji archipelago experiences a typical tropical marine climate characterised by relatively constant air temperatures throughout the year (22 – 30°C), occasionally reaching up to 32°C and down to 18°C (Fiji Meteorological Service 2006). There are two differentiated seasons: from November to April (wet/summer) and May to October (dry/winter). Fiji is located in the south eastern edge of the South Pacific Convergence Zone (SPCZ) (Figure 2.1), which is one of the main controllers on Fiji’s climate. During the austral winter the SPCZ shifts north (away from Fiji), causing lower rainfall, incursion of colder seawater temperatures and higher seawater salinity. During the summer the SPCZ is located close to Fiji, and the opposite conditions (warmer seawater temperatures and lower salinities) become apparent (Wu et al. 2013).

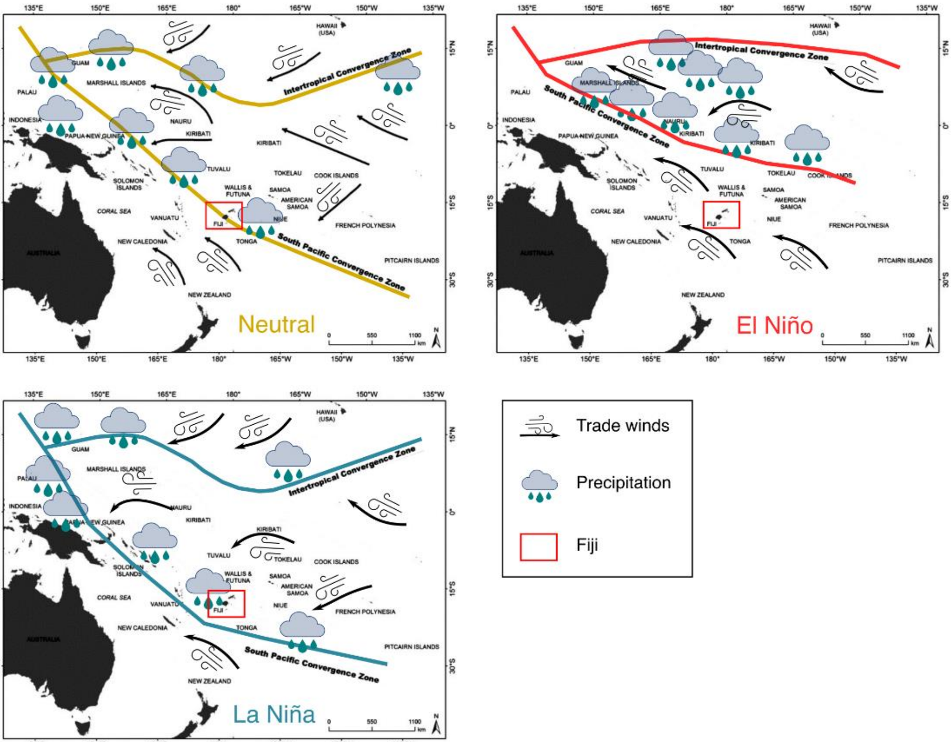

Figure 2.1. Movements of the IPCZ and SPCZ, trade winds and convergence precipitation areas in the South West Pacific. (Modified from Bell et al. 2011; Mangubhai et al. 2019).

Sea surface currents predominantly flow from the south towards the west and are strongly influenced by the south eastern trade winds. Coastal waters remain above 20°C with summer maxima around 30°C. Tides are semi-diurnal with neap tides having a mean range of 0.90 m and spring tides 1.30 m (Ryland 1981).

South easterly trade winds are the predominant winds in Fiji, which also present a seasonal pattern influenced by the SPCZ movements. During summer (November to April), winds are generally light, and the weakening of the south eastern winds facilitates temporary incursions of north-west winds (Mataki et al. 2006). During winter (May to October) the wind component changes, with strong and persistent south eastern winds (Mataki et al. 2006).

The rainfall regime is also influenced both by seasonality in the SPCZ and the prevailing south eastern trade winds, and by island orography. This is especially evident in the largest islands, where annual rainfall parameters and relative humidity are consistently higher in the wind-ward side of the islands, in comparison to the lee-ward (Fiji Meteorological Service 2006). Furthermore, any high land mass in the islands lying in the path of south-east trade winds receive much of the precipitation where rainfall increases fairly consistently with altitude (Fiji Meteorological Service 2006). The mountains of Viti Levu create regional climatic differentiation, with wet zones on the windward side (southeast of the island) and dry climatic zones on their leeward sides (northwest side).

The climatic differentiation and different rainfall regimes across Viti Levu are more evident during winter. Annual rainfall in the dry zone averages ~2000 mm, whereas in the wet zones, it ranges from ~3000 mm around the coast to ~6000 mm on the high lands. During winter (dry season), the dry zones receive generally less than 100 mm/month, while wet zones receive ~150 mm/month. During summer (wet season), the variation in the monthly totals between the two zones is little, being the rainfall received of ~400 mm/month in both locations (Fiji Meteorological Service 2006).

Daily and seasonal atmospheric temperature variability in Fiji is relatively small (Fiji Meteorological Service 2021). In general, the dry season experiences cooler average temperatures than the rainy season. Temperatures during the coldest and the warmest months vary by about 2 to 4°C (Fiji Meteorological Service 2021). Furthermore, an increasing trend in atmospheric temperature (both minimum and maximum) from 1989 has been detected (Kumar et al. 2014) and various climatic models have predicted that atmospheric temperatures will continue to increase over the course of the 21st century with very high confidence (Australian Bureau of Meteorology and CSIRO 2011).

Year-to-year climate variations are mostly influenced by ENSO. ENSO phases exacerbate the movements of the SPCZ and the effects on climatic variables (Figure 2.1.), with El Niño phases being characterised by low rainfall and colder temperatures than normal, and La Niña presenting higher rainfall than usual and warmer temperatures (both atmospheric and of seawater). However, no evidence has been found of the Pacific Decadal Oscillation (PDO) modulating the correlation between rainfall and ENSO phases in this region (Kumar et al. 2014).

Droughts in Fiji are linked to El Niño phases of ENSO. The SPCZ migration towards the equator experienced during El Niño results in below average rainfall (Fiji Meteorological Service 2021). Severe droughts in recent times occurred in 1987, 1992, 1997/98, 2003, 2010, and 2015-2017 (Iese et al. 2021).

Fiji is occasionally traversed by tropical depressions and cyclones, typically between November and March, that tend to track from the northwest (Fiji Meteorological Service 2006). These weather systems result in extended heavy rainfall (Mataki et al. 2006) and can trigger flooding events (e.g. floods in southwest Viti Levu in 1931, 1993, 2003 and 2012) (Brown et al. 2017c). Furthermore, monsoon troughs can also trigger severe flooding (e.g., 2009 flood in Viti Levu) (Brown et al. 2017c).

2.1.2. Geology and soils in Viti Levu

The Fiji Islands sit above the Fiji Plateau, an ocean platform that reaches up to 2000 – 3000 m water depth. Viti Levu (together with Vanua Levu) comprises the oldest rocks of the archipelago (Kumar 2005). A core of Eocene igneous rocks (Wainamala Group) makes up the highest and central part of these islands, and these are surrounded by Quaternary sedimentary rock formations (Kumar 2005).

Both Viti Levu and Vanua Levu are dominated by steep, deeply incised rivers and streams (Morrison et al. 1990). Only the coastlines are flat and a few meters in altitude. Within the rest of the island altitude can vary from 200 m above sea level to the highest point in Fiji, Mount Tomanivi (1,324 masl), in Viti Levu (Limalevu 2008).

Soil characteristics in Viti Levu are strongly linked to topography and climatic conditions (Morrison et al. 1990) and can be generally divided into three groups: i) fertile soils in floodplain areas derived from river and marine deposition with highly organic parent material; ii) soils developed in low hills characterised by weathered volcanic materials, limestone and marls, and iii) soils developed on steep hills and mountains weathered from raw volcanic material (Leslie 1997). Soil erodibility is not only dependent on soil type, but also on vegetation cover, land use and parent material characteristics. The tropical soils of Viti Levu are characterised by a deep weathering profile, with a considerable higher permeability and porosity compared to the underlying parent rock (Ram et al. 2019); this favours saturation under wet conditions and leads to extensive sediment runoff (Ram et al. 2019).

2.1.3. Land cover in Viti Levu

Land use in Viti Levu is largely influenced by anthropogenic activities, where agriculture and forestry are the main industrial activities shaping land use (Avtar et al. 2022). Remote sensed data showed that between the years 2000 and 2020 forest cover in Viti Levu decreased 334.6 km^2 (forest cover in 2020 is 6855 km^2 – 4.65% decrease), being substituted mostly by shrub and grassland (1000 km^2 in 2020 – 35.40% decrease), agricultural land (2361 km^2 in 2022 – 75% increase) and developed land (328 km^2 in 2020 – 131% increase) (Ram, 2022).

One of the main economic exports of Fiji is sugarcane (Printemps 2008). This agricultural activity is usually located in the northwest of Viti Levu (and Vanua Levu), where the climate is characterised by long and dry winters that favour the crops (Singh 2020). The area of land dedicated to sugarcane, however, has reduced from 650 km^2 (in 1999) to 370 km^2 (in 2020) due to urban development occupying flat and fertile land previously occupied by crops (Fiji Sugar Corporation 2020; Singh 2020).

Land practices such as overgrazing, commercial forestry and sugarcane cultivation, especially when carried out in hilly areas with high slopes, have caused an increase in catchment erosion and sediment delivery to flood plains under tropical storms (Terry et al. 2008), contributing towards catchment degradation (Atherton et al. 2005).

2.2. Study locations

2.2.1. Votua Reef – Coral Coast

The Votua reef is located in a stretch of coastline known as the Coral Coast, which is on the south coast of Viti Levu (Figures 2.2. and 2.6.). The coral reefs in the Coral Coast are directly adjacent to the shoreline, and these fringing reefs are particularly susceptible to land-based pollution (Mosley and Aalbersberg 2003).

The Votua Reef is enclosed within a marine protected area (MPA), that constitutes a no-take zone, designated in 2002 but is only 300 m away from a heavily fished zone. Nevertheless, a study shows that the reef within the MPA had dominance of hard-coral cover (57%) with low macroalgal presence (3%), whereas the non-protected zone displays a very different community structure, with minimal coral cover (3%) and macroalgae dominance (47%) (Rasher and Hay 2010). In 2014, a temporary no-take zone was established 1 km west of the previous permanent MPA no-take zone. Mosley and Aalbersberg (2003) measured nutrient levels along the Coral Coast. In their study, one of the sampling sites was in the Votua reef, ~50 m away from where the Votua cores were collected for this study (See section 2.3.), and water samples were also collected at the mouth of the Votua Creek. The mean levels of nitrates measured at the reef were 0.72 µM, and 0.32 µM for phosphates. The mean N:P ratio was 6 indicating that seawaters in the Votua reef are enriched in phosphates relative to unpolluted seawater. Nitrate and phosphate levels measured at the Votua Creek were 6.9 µM and 0.53 µM respectively, which gives a N:P ratio of 13. It could be that the Votua Creek is a major source of nutrients to the coast, as nutrient concentrations are somewhat higher here than in the seawater samples, which are typically originated from human waste and chemicals (e.g., detergents, fertilisers).

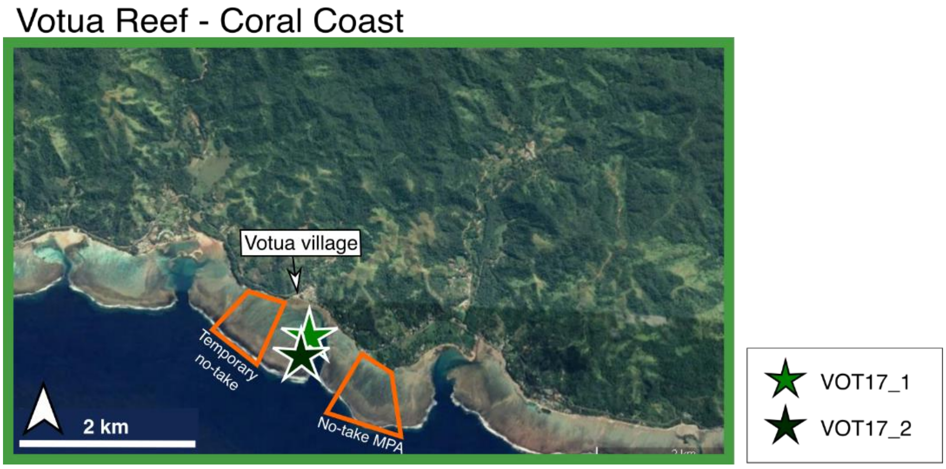

Figure 2.2. Satellite image of the Votua Reef in the Coral Coast. Star symbols represent the coring locations of each sample. Orange areas are protected no-take areas.

The Votua catchment is a well-documented catchment in Fiji, and hence the information available is more abundant than in the other catchments considered for this study. The Votua watershed has an area of 12.21 km^2, of which 10.11 (83%) is forested. It is quite steep, with a slope of 17.54° (Atherton et al. 2005b). The main water stream in the area is the Votua Creek, with a length of ~9 km, whose mouth is ~500 m away from the core collection site. Human activities, where present, are restricted to the lower watershed close to the main highway and the coast, where the Votua village is situated. Close to the village there are small (< 0.01 km^2) subsistence farms that are mostly located in the floodplain areas and comprise of dalo, cassava, banana, plantain and pawpaw plantations (Ram and Terry 2014). A study on potential soil loss found that only 4.2% of the area had potential erosion rates greater than the tolerance limit for tropical soil (Ram and Terry 2014). This is due to the role that vegetation cover and slopes play in determining erosion in the Votua catchment. This study also collected hydrological data to study short-term sediment dynamics between October 2009 and May 2010 determining that most of the rainfall in the Votua watershed was produced by a small number of high intensity events, and that only the highest rainfall events (high intensity or high accumulated rainfall) increased turbidity in the creek.

2.2.2. Nananu-i-Ra

Nananu-i-Ra is an island located around 3 km off the north coast of Viti Levu, near the town of Rakiraki in the Ra province (Figures 2.3. and 2.6.). It has an area of 2.75 km^2, of which only 0.41 km^2 (15%) are forested. The maximum elevation of the island is 180 m. Nananu-i-Ra is a privately owned island and is mainly residential (Atherton et al. 2005).

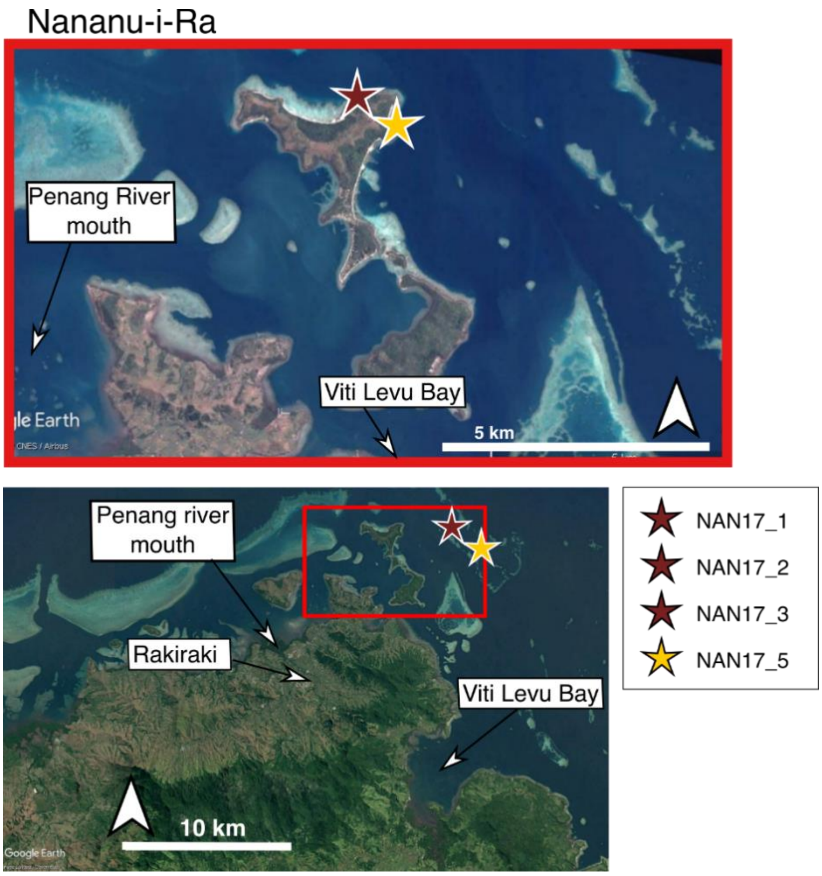

Figure 2.3. Satellite images of the Ra region and close-up of Nananu-i-Ra island. Star symbols represent the coring locations of each sample.

The Nananu-i-Ra Island catchment is small with a minimal slope with no large river or creek inputs (Atherton et al. 2005). The island sits off the shore of the so-called “sugarcane belt” which is found along the coastal parts of Rakiraki and Saivou districts (northeast Viti Levu), where a high portion of Fiji’s sugarcane crops and production are found. In this context, the catchments of the Penang River and the several small catchments surrounding Viti Levu Bay (Figure 2.3.) have an important role controlling coastal water quality parameters. The Penang River is one of the most important rivers in the islands. Its catchment has an area of 102.20 km^2, of which only 18.24 (18%) are forested, with the remaining 83.96 km^2 (82%) being mostly dedicated to agricultural and farming activities (Atherton et al. 2005). In 1878 a sugar mill was built in the city of Rakiraki, next to the river, the Penang sugar mill. The mill closed in 1922 and reopened activity in 1926. From then, it operated uninterrupted until 2016, when the Tropical Cyclone Winston caused severe and irreparable damage and it was permanently closed.

No studies have been carried out measuring pollutants in the coastal waters nearby the Ra province. Despite this, we must consider the potential impact of the sugarcane crops for the nutrient input into the coastal reefs, as well as the extended fluvial system, carrying other pollutants and sediments. During the collection of the coral cores, freshwater lenses were detected in the area, indicating a persistent land influence in the reef.

2.2.3. Suva Reef – Fish Patch

Fish Patch is located in the Suva Reef, an urban reef surrounding the city of Suva at the entrance of the Suva Harbour (Figures 2.4. and 2.6.). In Fiji, southeast trade winds are an important component in the distribution of seawater parameters (e.g., salinity, temperature, turbidity). Nevertheless, the Suva Harbour is protected from the trade winds by the hilly Suva peninsula (Singh and Aung 2008). It has an average depth of 15 m, with depths of 80-100 m in the Suva Passage (Penn 1983).

Suva Harbour is influenced by three rivers, the Tamavua, Lami and Veisari Rivers, being the first two the most important tributaries. The Tamavua catchment covers 29.06 km^2, of which 19.88 (65%) is forested. The Lami catchment has an area of 21.54 km^2 with 16.18 km^2 (75%) forested. The Veisari river has an area of 28.14 km^2, with 21.71 km^2 (77%) being forested (Atherton et al. 2005). Freshwater discharge into the Suva Harbour affects the surface salinity near the head of the harbour (Singh and Aung 2008). Surface salinity and turbidity in the Suva passage, where Fish Patch is, can also been influenced by sediment runoff and freshwater discharge from the Rewa River in the Laucala Bay (east of the Suva Peninsula) (Figure 2.3.). Southeast trade winds are able to mobilise the water mass within the Suva Lagoon (Laucala Bay) into the Fish Patch area through the Nasese channel, where seawater turbidity and flow are high (Singh and Aung 2008).

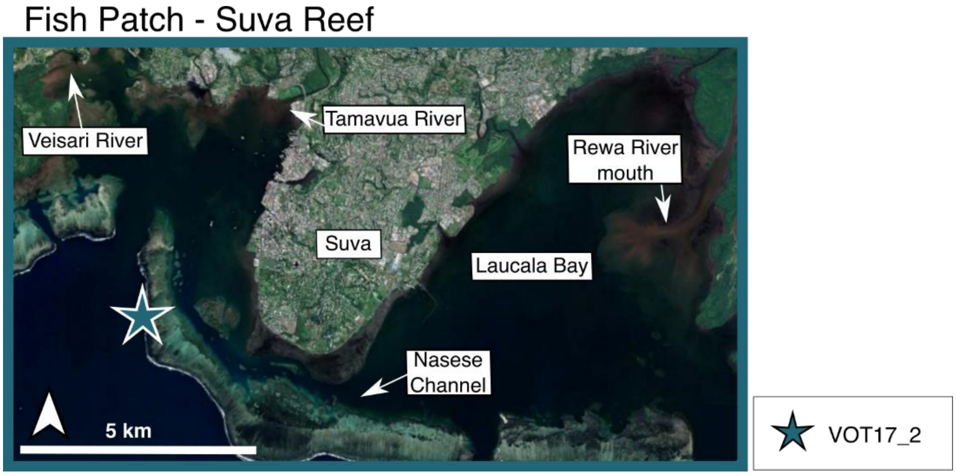

Figure 2.4. Satellite image of the Suva Reef and Suva peninsula showing the coring location (Fish Patch), Laucala Bay and Suva Harbour. Star symbols represent the sample collection location.

Around Suva Harbour there are various major industrial zones, which contain shipyards, a paint manufacturing plant, a battery recycling facility and zinc galvanising factories. A municipal rubbish dump, closed in 2005, was also located on the coast near Lami. This dump leached into the aquatic environment, polluting the Suva Harbour as well as the Lami and Tamavua Rivers, which flush fresh water into the harbour (Maata and Koshy 2001). High levels of Cu, Fe and Zn were recorded in sediment samples around the Suva industrial area and the Lami dump (Maata and Koshy 2001). Elevated levels of Pb were also evident in sites nearby the battery factories (Naidu and Morrison 1994; Gangaiya et al. 2018). Furthermore, high levels of Sn were also found across the Suva harbour, which could be sourced by marine paints from ships, as tin-based paints are still used in Fiji (Maata and Koshy 2001).

2.2.4. Namuka Reef

The Namuka Reef is a broad fringing reef located west of the Suva Harbour (Figures 2.5. and 2.6.), although influence of seawater from the Suva Harbour seems to be limited (Collen et al. 2011). The eastern area of the Namuka reef is protected by the Navakavu

Locally Managed Marine Area (LMMA), which in 2002 implemented a no-take zone in the area. The LMMA is next to the Muaivuso peninsula (Figure 2.5.) with presence of small villages (Muaivuso and Waiwanaki) and farming land. The peninsula is surrounded by a fringing coral reef, mangroves, and remnants of coastal littoral forest (IUCN 2009). A small island called Namuka Island can be found to the west of the LMAA, but it remains outside the boundaries of the LMMA mentioned above. Namuka Island had some anthropogenic development in the recent past (Ghazanfar et al. 2001) and is currently a privately owned island with a small touristic resort established in it in 2015. There are no rivers or creeks directly discharging into the reef, and some grass lands and mangroves are found in the coastal area in Viti Levu. Furthermore, both surface runoff and wastewater from Muaivuso and Waiwanaki villages are likely to be directed towards the reef (Atkinson and Collen 2000).

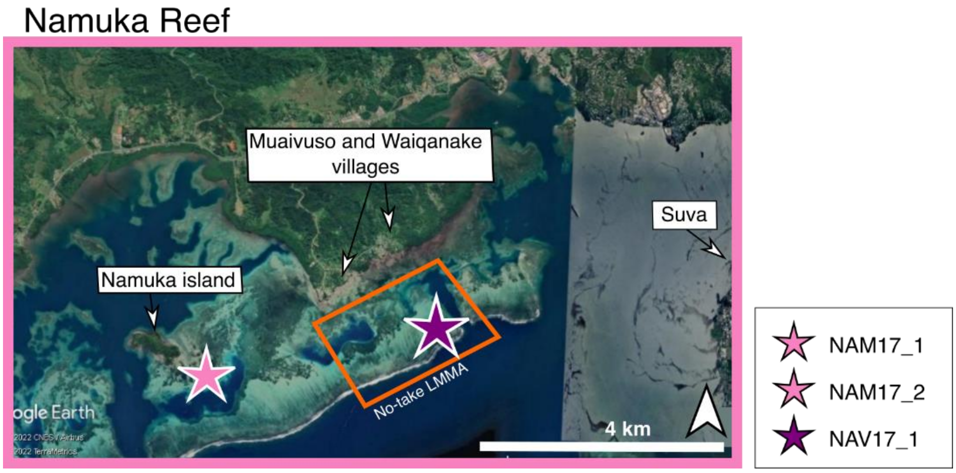

Figure 2.5. Satellite image of Namuka Reef and Muaivuso Peninsula. Star symbols represent the coring locations of each sample. Orange areas are protected no-take areas.

2.3. Study samples

2.3.1. Coring locations

For this study, ten coral cores were drilled in May 2017 from live *Porites* spp. colonies from inshore reefs in these four different study locations around the coast of Viti Levu (Fiji) (Figure 2.6.; Table 2.1.). In the Votua Reef two cores were collected on the reef flat near the channel (Figure 2.2.). Coral colonies were within ~50 m of distance from each other. Four cores were collected on a fringing reef off Nananu-i-Ra Island (Figure 2.3.), three of which were within ~50m of each other, sheltered from the common south-east surface currents. The fourth core was collected ~2 km away, on the other side of the reef, and exposed to the surface currents. One core was collected in the west Suva Reef, in the Fish Patch area (Figure 2.4.). Lastly, three cores were collected along the Namuka Reef (Figure 2.5.): one of these cores was collected within the Navakavu LMMA and two were extracted within ~2.5 m of each other, just south of Namuka Island.

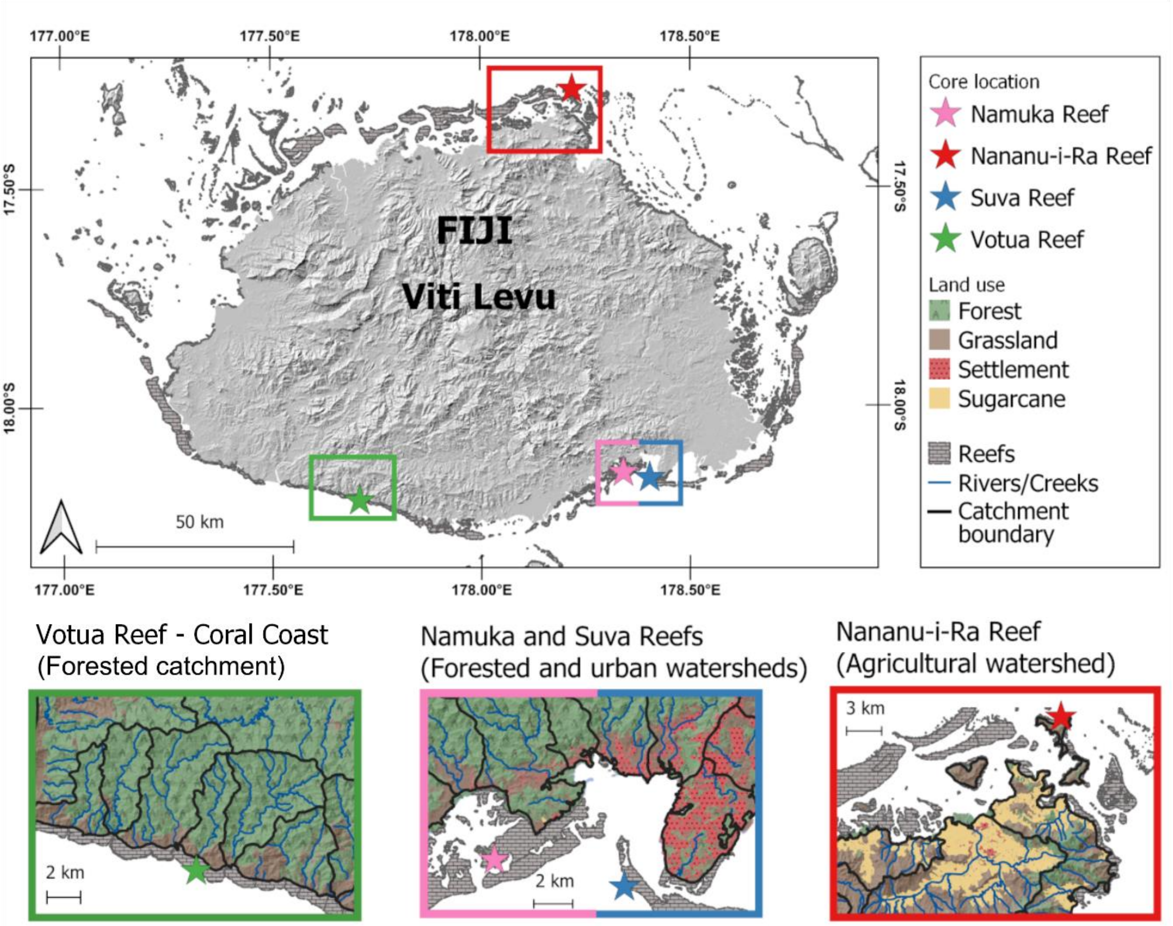

Figure 2.6. Map of Viti Levu (Fiji). Start symbols represent the coring locations of the samples of this study. Cores VOT17_1 and VOT17_2 were extracted from the Votua Reef in the western Coral Coast. NAM17_1 was extracted from Namuka Reef. FP17_1 was extracted from the Suva Reef. NAN17_2 and NAN17_5 were extracted from the shores of Nananu-i-Ra.

Sampled colonies were located at a depth of 2 – 3 m, except the colony at Fish Patch, which was at 8 – 10 m deep. Core drilling was carried out between 18th and 28th of May 2017 by Dr Sindia Sosdian, Dr Eleanor John and Dr Jennie Mallela (Figure 2.7.). Coral heads sampled were approximately 2 m in diameter and coral cores were extracted from the top of the colonies using a pneumatic drill fitted with a 6 cm diameter drill barrel. Finally, coral core cavities were filled with resin plugs to minimize impact to coral colonies. All the coral cores were immersed in fresh water for 24 h and consequently air dried for several days.

Figure 2.7. Dr Jennie Mallela coring a *Porites* spp. using a pneumatic drill with a diamond coated coring barrel. Photo: Dr Sindia Sosdian and Dr Eleanor John.

2.3.2. Cutting and cleaning procedure

Following CT scanning and identification of major growth axis within each core (See Section 2.4.2.), samples were cut open parallel to the growth axis. Subsequent slabs of 6 mm up to 1 cm thickness were cut parallel to the first cut surface. Cutting was carried out at the sample preparation facilities of the School of Earth Sciences, University of Bristol. For samples of length shorter than 25 cm (Table 2.1.) a diamond wire saw was used; this saw allowed for highly precise sectioning with minimal sample loss ("kerf" ~1mm) and we obtained up to 6 slabs from each coral sample (Figure 2.8.). Samples longer than 25 cm were cut with a rock saw using a diamond coated disc, allowing us to obtain a total of four slabs from each core. Only fresh water was used as lubricant on both saws. The cut slabs were immersed in DI water and cleaned using a Cole-Parmer Ultrasonic Processor Probe. Both surfaces of the slabs were cleaned 3 – 4 times, changing the water after every pass and until the water remained clear (Figure 2.8.). Coral slabs were then air dried.

Table 2.1. Core ID, locations, and span of coral samples of this study and included coral data from Fiji available in the literature.

Location	Core ID	Section	Species	Date collection	Latitude (Dec.°)	Longitude (Dec.°)	Depth (m)	Core length (cm)	Core span (Years)	Reference
Coral Coast (Votua Reef)	VOT17_1	1	*Porites* spp.	18/05/2017	-18.213823	177.710655	2-3	13	1965 - 2017	This study
		2	*Porites* spp.	18/05/2017	-18.213823	177.710655	2-3	25	1965 - 2017	This study
		3	*Porites* spp.	18/05/2017	-18.213823	177.710655	2-3	47	1965 - 2017	This study
	VOT17_2	1	*Porites* spp.	18/05/2017	-18.213823	177.710655	2-3	14	1990 - 2017	This study
		2	*Porites* spp.	18/05/2017	-18.213823	177.710655	2-3	39	1990 - 2017	This study
Nananu-i-Ra	NAN17_1	1	*Porites* spp.	22/05/2017	-17.298108	178.230095	2-3	10	1979 - 2017	This study
		2	*Porites* spp.	22/05/2017	-17.298108	178.230095	2-3	8	1979 - 2017	This study
		3	*Porites* spp.	22/05/2017	-17.298108	178.230095	2-3	23	1979 - 2017	This study
	NAN17_2	1	*Porites* spp.	22/05/2017	-17.298108	178.230095	2-3	15	2003 - 2017	This study
	NAN17_3	1	*Porites* spp.	22/05/2017	-17.298108	178.230095	2-3	33	1990 - 2017	This study
	NAN17_5	1	*Porites* spp.	23/05/2017	-17.279467	178.227683	2-3	12	1983 - 2017	This study
		2	*Porites* spp.	23/05/2017	-17.279467	178.227683	2-3	31	1983 - 2017	This study
Suva Reef (Fish Patch)	FP17_1	1	*Porites* spp.	28/05/2017	-18.143753	178.401692	8-10	52	1931 - 2017	This study
		2	*Porites* spp.	28/05/2017	-18.143753	178.401692	8-10	32	1931 - 2017	This study
Namuka reef	NAV17_1	1	*Porites* spp.	20/05/2017	-18.1458	178.37736	2-3	48	1981 - 2017	This study
	NAM17_1	1	*Porites* spp.	20/05/2017	-18.151255	178.347347	2-3	12	2008 - 2017	This study
	NAM17_2	1	*Porites* spp.	25/05/2017	-18.151255	178.347347	2-3	55	1931 - 2017	This study
		2	*Porites* spp.	25/05/2017	-18.151255	178.347347	2-3	43	1931 - 2017	This study
Dennis Patch	DP1	-	*Porites* spp.	24/05/2005	-18.15451	178.4157	NA	45	1977 - 2005	S. Albert (*Pers. Comm.)*
	DP2	-	*Porites* spp.	24/05/2005	-18.15451	178.4157	NA	60	1968 - 2005	S. Albert (*Pers. Comm.)*
Namuka Reef (Muaivuso)	MV1	-	*Porites* spp.	22/05/2005	-18.14828	178.37376	NA	50	1974 - 2005	S. Albert (*Pers. Comm.)*
	MV2	-	*Porites* spp.	22/05/2005	-18.14828	178.37376	NA	40	1971 - 2005	S. Albert (*Pers. Comm.)*

Location	**Core ID**	**Section**	**Species**	**Date collection**	**Latitude (Dec.º)**	**Longitude (Dec.º)**	**Depth (m)**	**Core length (cm)**	**Core span (Years)**	**Reference**
Coral Coast (Namada)	NM3	-	*Porites* spp.	23/05/2005	-18.19082	177.62128	NA	60	1958 - 2005	S. Albert (*Pers. Comm.)*
	NM4	-	*Porites* spp.	23/05/2005	-18.19082	177.62128	NA	60	1972 - 2005	S. Albert (*Pers. Comm.)*
Vuda Point	VP1	-	*Porites* spp.	25/05/2005	-17.69068	177.40759	NA	95	? - 2005	S. Albert (*Pers. Comm.)*
	VP2	-	*Porites* spp.	25/05/2005	-17.69068	177.40759	NA	40	1969 - 2005	S. Albert (*Pers. Comm.)*
Great Astrolabe Reef (Dravuni)	DR1	-	*Porites* spp.	19/05/2005	-18.72469	178.5462	NA	130	1903 - 2005	S. Albert (*Pers. Comm.)*
	DR2	-	*Porites* spp.	19/05/2005	-18.64589	178.55164	NA	60	1940 - 2005	S. Albert (*Pers. Comm.)*
Kubulau	S2S1	-	*Porites* spp.	01/01/2007	-16.934275	178.984483	NA	30	1988 - 2006	(Jupiter et al. 2010)
	S3S3	-	*Porites* spp.	01/01/2007	-16.852207	179.049234	NA	45	1977 - 2006	(Jupiter et al. 2010)
Coral Coast	CC	-	*Porites* spp.	21/11/2018	-18.2019	177.6656	2	33	2003 - 2018	(Goberdhan and Kininmonth 2021)
Suva Reef (Dennis Patch)	DP	-	*Porites* spp.	20/09/2018	-18.1672	178.4206	3	51	1981 - 2018	(Goberdhan and Kininmonth 2021)
Namuka reef	NV	-	*Porites* spp.	31/05/2018	-18.1472	178.3631	4	49	1975 - 2018	(Goberdhan and Kininmonth 2021)
Savusavu Bay	AB	-	*Porites* lutea	01/12/2001	-16.81667	179.2333	8	389	1617 - 2001	(Linsley et al. 2006)
Vanua Balavu	FVB1-H4	-	*Porites* spp.	01/11/2004	-17.335	-178.945	6	236	1841 - 2000	(Dassié et al. 2014)
	FVB2-H1	-	*Porites* spp.	01/11/2004	-17.34167	-178.9283	1	294	1847 - 2000	(Dassié et al. 2014)

Continuation **Table 2.1.** Core ID, locations and span of coral samples of this study and included coral data from Fiji available in the literature.

2.3.3. Other cores

To increase the number samples from Fiji and validate the growth rates observed in Chapter 3 I also included data from other coral records from Fiji available in the literature (Table 2.1.; Figure 3.1.). These were ten cores from five locations around Viti Levu (S. Albert., *Pers. Comm.*), three cores from three inshore reefs in Viti Levu (Goberdhan and Kininmonth 2021), two cores from two areas in Kubulau Reef (Vanua Levu; Jupiter et al. 2010), one core from Savusavu Bay (Vanua Levu; Linsley et al. 2006) and two cores from Vanua Balavu (Dassié et al. 2014)

.

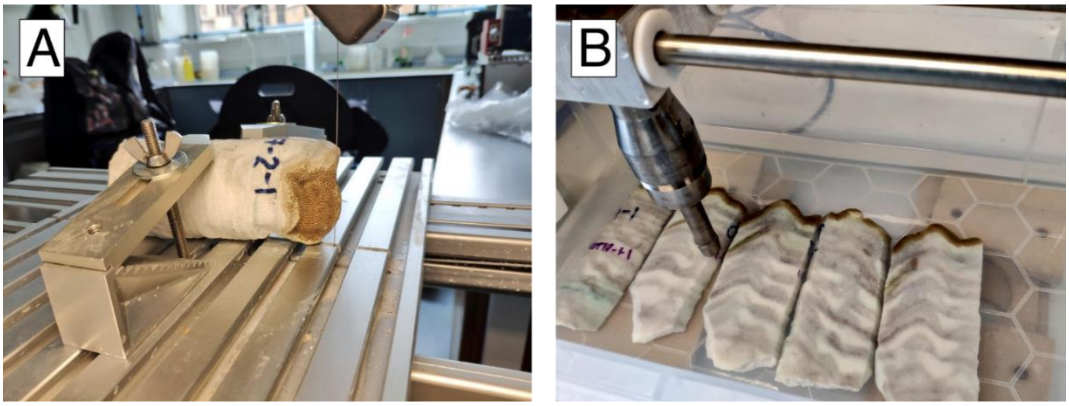

Figure 2.8. A) Diamond wire saw used to cut coral cores < 30 cm in length. B) Ultrasonic probe used to clean the slabs from cutting debris and dust.

2.4. Analytical methods

2.4.1. Laser Ablation – Inductively Coupled Plasma Mass Spectrometer

Laser Ablation - Inductively Coupled Plasma Mass Spectrometry (LA-ICPMS) is an analytical technique that allows for in-situ analysis of solid coral samples by a microbeam (laser ablation (LA)). This rapid technique requires minimal sample preparation and produces records with high spatial resolution. ICPMS allows the analysis of an extensive suite of elements simultaneously with high sensitivity. This system has been widely used in coral studies, measuring both “major” (e.g., Sinclair et al. 1998; Fallon et al. 1999; Alibert et al. 2003; LaVigne et al. 2016; Wu et al. 2021) and “minor” trace elements, including rare earth elements (REE) (e.g., Fallon et al. 2002; Wyndham et al. 2004; Prouty et al. 2009).

LA-ICPMS analyses were carried out at the CELTIC facilities, in the School of Earth and Environmental Sciences at Cardiff University between December 2021 and February 2022. In LA, The amount of ablated material is controlled by the fluence (J/cm^2), a measurement of energy density depending on beam energy (mJ) and area of the beam (cm^2). The frequency at which the material is ablated (and fed into the ICPMS) is controlled by shot frequency (Hz), the number of laser shots per second. The LA system used was an ASI RESOlution-SE ArF excimer (193 nm) fitted with S155 dual-volume sample cell. This system produces a beam of up to 100 μm diameter, which is masked and focused onto the sample with an on-sample fluence of >15 J/cm^2 and a frequency of up to 14 shots per seconds (Hz). Critically for coral analysis due to skeletal heterogeneities, the laser beam can be expanded up to 280 μm diameter (at the expense of reduced sample fluence). A large beam size during coral LA-ICPMS analysis provides higher ablation rates (more material ablated), which allows for a higher sensitivity necessary for the measurements of REE (Fallon et al. 2002; Wyndham et al. 2004) and averages the ablation area over different skeletal structures (i.e., thecal wall, septa, pali, columella) that can potentially drive elemental heterogeneity (Allison and Finch 2009). The dual-volume cell improves signal stability and uniformity and allows for very rapid washout times (<1 s), improving time resolved acquisition of the geochemical signal by the ICPMS. The movement range of the stage accepts samples of up to 15x10 cm to be analysed, limiting the number of cuts and disruptions needed in long core slabs.

The RESOlution-SE laser is coupled to an Agilent 8900 triple quadrupole ICPMS. To guarantee a stable signal over the duration of the analysis at high enough sensitivity, the amount of ablated material entering the ICPMS is carefully controlled. This is achieved by ensuring a constant on-sample fluence (J/cm^2) and shot frequency (Hz) with further adjustments to gas flows (N_2, He) entering the ablation cell can improve signal.

2.4.1.1. Method summary

In this section I present a summary of the LA-ICPMS methodology and instrument configurations (Table 2.2.) applied on the coral samples analysed in this study.

A laser beam was masked with a rectangular slit (Sinclair et al. 1998) to obtain a 200x50 μm beam of 200 μm width perpendicular to the direction of the laser path and 50 μm length parallel to the laser path (and coral growth). The size and shape of this beam maintains a high spatial resolution (i.e. ~weekly resolution in *Porites* spp.) in the laser path, while maximising ablated material (higher sensitivity), ensuring enough material is entering the ICPMS for analysis (Sinclair et al. 1998). The laser was fired with a pulse of 12 Hz, and a fluence of ~2.5mJ/cm^2.

Table 2.2. Laser and ICPMS configuration during coral analysis.

Laser settings	
Slit size	200 x 50 um
Fluence	2.5 - 3 J/cm2
Shot frequency	12 Hz
Scan speed	40 -50 um/s
He flow	350 ml/min
N2 flow	3.5 ml/mil
U+/Th+	~1
Oxide formation (%ThO$^+$/Th$^+$)	<0.5%

ICPMS settings	
RF Power	~1350 W
Cones	Nickel
Acquisition Mode	Time resolved
Time slice	1.19 s

The ablation transect followed by the laser beam was parallel to the exposed major growth axis of each coral slab, and thus perpendicular to growth bands. This path was identified through exploration of CT scan images (See Section 2.4.2.). The length of the transect ablated in each coral sample differed between the long cores (~14 cm) and replicate cores (~6 cm) depending on desired temporal length of the geochemical record (~17 years and ~5 years respectively).

Each transect was ablated four times, of which three were analysed following ablation by ICPMS. The first pass acts as "pre-ablation" cleaning, with rapid laser shots and scan speeds (i.e., 8 Hz and 200 μm/s), to clear the surface in the beam path of any potential solid debris, dust, etc. The second pass, "cleaning transect", removed the outer ~0.50 μm of the coral surface, exposing fresh skeletal surface for subsequent analysis. This ablation was carried out at a scan speed of 150 μm/s and introduced into the ICPMS for conditioning. The two subsequent transects (analysis transects), run at the optimised scan speed of 50 μm/s, were completed in ~80 minutes for the long cores, and ~35 minutes for the replicate cores. Each entire transect was split into 1 cm sub-transects (~6 minutes of ablation + ICPMS measurement time). At least 20 seconds of background were measured before and after each sub-transect to allow for long-term drift-correction. The first analysis transect was used to assess variations in major elements (e.g., Li, Mg, Mn, Sr, Ba, U) and the second analysis transect was used to assess variations in minor elements (e.g., REEs). This method developed from previous approaches used in LA-ICPMS coral geochemical analysis, where a series of 'cleaning' passes are used followed by analysis for minor and major elemental ratios (e.g., Fallon et al. 2002; Wyndham et al. 2004).

A range of major and minor element isotopes were analysed by the ICPMS. These were ^{7}Li, ^{11}B, ^{25}Mg, ^{27}Al, ^{31}P, ^{43}Ca, ^{47}Ti, ^{55}Mn, ^{86}Sr, ^{89}Y, ^{137}Ba, ^{138}Ba, ^{139}La, ^{140}Ce, ^{143}Nd, ^{147}Sm, ^{153}Eu, ^{157}Gd, ^{166}Er, ^{172}Yb, ^{175}Lu, ^{208}Pb and ^{238}U. However, not all elements were detectable with most minor elements (e.g., Yb, Lu) below limits of detection (See section 2.4.1.3.). The ablated condensed vapor of analyte was carried to the ICPMS by He and N_2 gas and elements were measured as counts per second (cps) in "time-resolved" mode with a 1.19 seconds resolution, meaning the ICPMS scanned through the mass spectrum recording individual datapoints for each element every ~1.19 s.

The effective resolution of each data point in this study was 77 μm. This value is dependent on ICPMS acquisition time, laser beam width, shot frequency and scan speed. The acquisition time from the ICPMS was ~1.19 s (as seen above), the laser beam used had a width of 50 μm, and the sample stage was moved at 50 μm/s. Thus, effectively every 1 El/Ca datapoint (at ~1.19 s) produced by the ICPMS corresponded to measurements averaged across ~119 μm. Average coral growth of samples in this study ranges from ~6 mm/yr to ~20 mm/yr, hence temporal resolution of geochemical analysis was highly dependent on sample growth. This means the number of datapoints per year across samples varied from ~51 to ~168 on average, translating to weekly to 2.2-days temporal resolution.

The standards NIST610, NIST612, NIST614 and JCp-1 were measured at the beginning and end of each coral transect. Furthermore, alternating NIST612 + NIST610, NIST612 + NIST614 and NIST612 + JCp-1 were measured every five coral sub-transects. The reference values for elemental concentrations in both silicate glass standards are taken from the GEOREM website (http://georem.mpch-mainz.gwdg.de/sample_query_pref.asp), updated from Jochum et al. (2011) and Inoue et al. (2004). Data reduction was processed using the Python package LAtools (Branson et al. 2019) following an established protocol. Each transect was background corrected, despiked, normalised to ^{43}Ca and calibrated against NIST612, NIST614, or JCp-1 (See section 2.4.1.4.).

2.4.1.2. Laser optimisation and stability assessment

This study constitutes the first set of analyses carried out at the CELTIC facilities using the RESOlution-SE system plus the beam expander (to gain a beam size of 200 µm in diameter). Previous LA-ICPMS analyses at CELTIC utilized a narrow slit size (5x50 µm) and a rotating slit with emphasis on analysis of giant clams at daily resolution, for which the beam expander was not necessary. As such, I investigated the ideal range of laser operating parameters to produce a reproducible, accurate and precise ICPMS signal given the beam size required.

As stated above, in the LA-ICPMS analysis, the sensitivity and stability of the ICPMS signal depends primarily on laser settings (i.e., spot size, laser beam energy, fluence and shot frequency). The use of a beam expander involves a significative loss of fluence of up to 40 – 60%. For example, in December 2021 a laser energy of 10 mJ (max. laser energy) resulted in a fluence of ~6 J/cm^2 without a beam expander, and a fluence of < 3 J/cm^2 with a 200 µm beam expander. Previous work has shown that optimal fluence values for LA-ICPMS analysis of marine carbonates, and specifically coral samples, range from 4 – 12 J/cm^2 depending on the laser ICPMS setup (Table 2.3.). With the CELTIC laser setup, I identified the ideal laser operating conditions to achieve high sensitivity and stability whilst using a large beam size and considering the reduced fluence.

For this work, I assessed the optimal operating parameters for the laser with a beam size of 200x50 µm, by exploring a range of fluences (3 to 6 J/cm^2) and shot frequencies (6 to 14 Hz) on the standard reference material NIST612 to obtain the combination of parameters that derived a sensitive and stable ICPMS signal with minimal elemental fractionation. I analysed NIST612 across from linear ablation paths (200x50 µm) for a total of 70 seconds at a scan speed of 20 µm/s to pinpoint the ideal settings. Ideally a carbonate standard material would have also been used to corroborate that the optimal laser parameters did not produce matrix-specific fractionation. However, availability of this material is scarce (See Section 2.4.1.4.).

Table 2.3. Summary of some LA-ICPMS studies analysing a suite of elements in *Porites* spp. corals and the standardization associated with the analytical method. Isotope specified when available in the literature

Reference	Elements	Slit Size (µm)	Fluence (J/cm^2)	Frequency (Hz)	Standard material
Sinclair et al. 1998	B, Mg, Sr, Ba, and U	600 x 20	5 - 10	10	Inhouse $CaSiO_3$
Fallon et al. 1999	B, Mg, Sr, Ba and U	500 x 50	100mJ	5	Inhouse $CaSiO_3$. coral powder
Fallon et al. 2002	^{10}B, ^{46}Ca, ^{55}Mn, ^{66}Zn, ^{89}Y, ^{137}Ba, ^{139}La, ^{140}Ce, ^{208}Pb, and ^{238}U, ^{139}La, ^{140}Ce, ^{141}Pr, ^{146}Nd, ^{147}Sm, ^{153}Eu, ^{157}Gd, ^{159}Tb, ^{163}Dy, ^{165}Ho, ^{166}Er, ^{169}Tm, ^{172}Yb, and ^{175}Lu	500 x 100	(100 mJ)	10	NIST614, NIST612
Alibert et al. 2003	^{43}Ca, ^{84}Sr, ^{25}Mg, ^{11}B, ^{238}U, and ^{138}Ba, ^{137}Ba, ^{31}P, ^{55}Mn, ^{89}Y, ^{111}Cd, ^{238}U, and ^{46}Ca	500 x 50	NA	5 /20	NIST614, NIST612
Wyndham et al. 2004	^{10}B, ^{25}Mg, ^{43}Ca, ^{55}Mn, ^{84}Sr, ^{137}Ba, and ^{238}U and ^{46}Ca, ^{137}Ba, ^{139}La, ^{140}Ce, ^{143}Nd, ^{147}Sm, ^{151}Eu, ^{157}Gd, ^{166}Er, ^{172}Yb	500 x 50 / 500 x 100	(50/100 mJ)	5 / 10	NIST614, NIST612
LaVigne et al. 2008	^{11}B, ^{25}Mg, ^{31}P, ^{48}Ca, ^{55}Mn, ^{56}Fe, ^{59}Co, ^{60}Ni, ^{63}Cu, ^{64}Zn, ^{87}Sr, ^{138}Ba, ^{238}U	500 x 50	4	10	NIST612
Jupiter et al. 2008	^{43}Ca, ^{84}Sr, ^{138}Ba	400 x 40	5 - 10	5 Hz	In-house coral powder, NIST614
Hathorne et al. 2011	B, Mg, Ca, S, Sr, U	100 (spot)	5	5	JCp-1, NIST612
Grove et al. 2012	Ca, Ba	400 x 40	5 - 10	5 Hz	In-house coral powder, NIST614
Moyer et al. 2012	^{25}Mg, ^{43}Ca, ^{55}Mn, ^{86}Sr, ^{89}Y, ^{138}Ba	385 x 40	12 - 15	10	NIST610, NIST612
Mallela et al. 2013	P, Ba, Ca	400 x 40	5	5	In-house coral powder, NIST614
Lewis et al. 2018	Ba, Mn, Y, Sr, U, B Ca.	500 x 50	5 - 10	5	NIST614
Tanzil et al. 2019	^{138}Ba, ^{43}Ca	150 x 150	NA	10	NIST610, NIST612

Element cps were internally standardised to ^{43}Ca cps, and the El/Ca normalised to the mean to facilitate comparison across all El/Ca. (Figure 2.9.). Lowest %RSD were established at 5 J/cm^2 and 12 Hz, as evidenced by B/Ca and Sr/Ca and U/Ca (1.29%, 1.61% and 1.54% respectively). However, due to laser energy decline over time and delay of optics maintenance due to COVID-19 (there were six months in between laser optimisation and coral analysis), a fluence of 2.5 J/cm^2 was the highest achievable on a routine basis whilst maintaining stability during the duration of the analyses every day. I applied a fluence of 2.5 J/cm^2 and a shot frequency of 12 Hz, as all %RSD values at any combination of fluence and shot frequency are below 5% (Table 2.4.), which is suitable for coral geochemical analysis. Optics array maintenance occurred in spring 2022 following data collection. After maintenance, fluence values greater than 3 J/cm^2 were obtainable again, so future analyses will be able to use 5 J/cm^2 and 12 Hz. Regardless, data collected is reproducible and of good quality based on standard reproducibility, signal stability and background within each and across all analysis days.

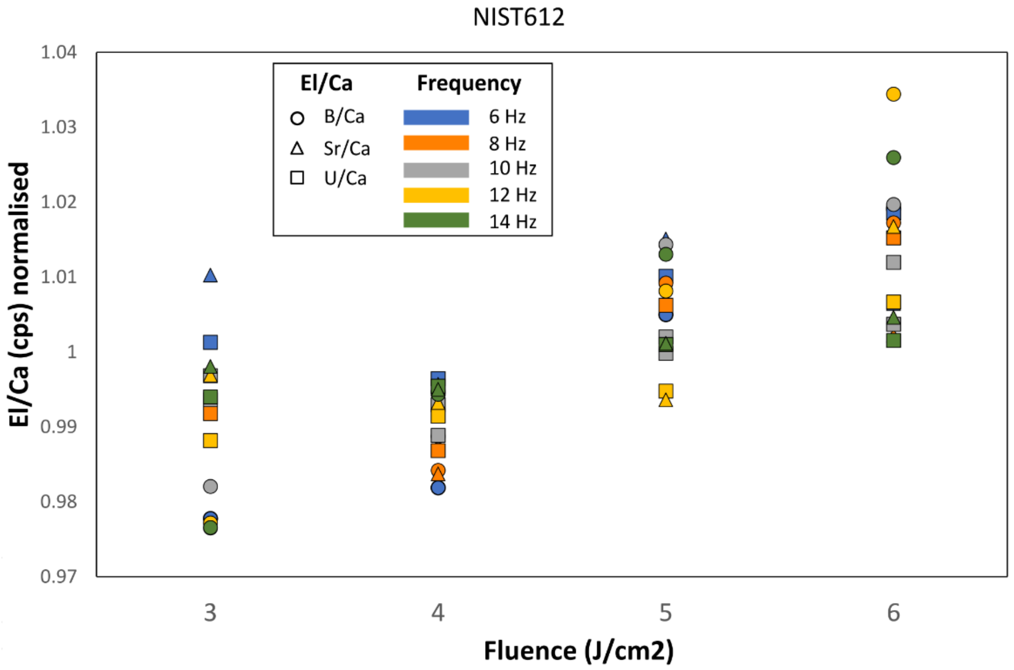

Figure 2.9. Optimization of laser fluence and shot frequency: El/Ca ratios (normalised to mean ratio for all fluences) on NIST612. Elemental ratios shown represent light, medium, and heavy isotopes.

Light, medium and heavy elements used in this study were monitored to observe whether different fractionation occurred across the mass spectrum. The relative standard deviations (%RSD) of each El/Ca ratio were calculated (Table 2.4.) and we observed that for all elements investigated here, low shot frequencies (6 Hz and 8 Hz) gave higher %RSD values, and this is consistent across fluence values of 3 to 6 J/cm^2. In all cases, %RSD values are below 5%, which is an acceptable signal stability. Interestingly, Mg/Ca shows a considerably higher variability than any other element, although %RSD values were still <5%. This can be due to heterogeneities found in Mg in NIST612 (Evans and Müller 2018).

Table 2.4. Relative Standard Deviations (% RSDs) for a range of minor and major elemental ration measured in NIST612 for all tested combinations of laser conditions, with fluence ranging 3 – 6 J/cm2 and frequency 6 – 12 Hz.

	J/cm^2	6 HZ	8 Hz	10 Hz	12 Hz	14 Hz
B/Ca	**3**	2.29	1.87	1.85	1.70	1.45
	4	1.70	1.71	1.89	1.29	1.24
	5	1.56	1.41	1.24	1.14	1.20
	6	1.67	1.54	1.36	1.40	1.23
Mg/Ca	**3**	4.73	3.79	2.89	3.84	2.85
	4	4.77	4.06	3.53	3.73	2.40
	5	4.11	3.43	2.96	2.71	3.02
	6	4.06	4.17	3.32	3.33	2.60
Mn/Ca	**3**	2.14	1.99	1.71	1.54	1.21
	4	1.96	1.58	1.60	1.38	1.22
	5	1.66	1.53	1.20	1.37	1.22
	6	1.67	1.67	1.62	1.04	1.16
Sr/Ca	**3**	2.69	2.17	2.23	2.10	1.81
	4	2.23	2.09	2.15	2.04	1.62
	5	2.40	1.83	1.51	1.61	1.31
	6	2.44	1.71	2.34	1.94	1.55
Y/Ca	**3**	1.35	1.31	1.37	0.99	0.97
	4	1.25	1.25	1.30	1.00	1.03
	5	1.31	1.35	1.19	1.04	0.91
	6	1.46	1.38	1.34	0.96	0.86
Ba/Ca	**3**	1.61	1.30	1.69	1.04	1.14
	4	1.42	1.43	1.23	1.22	1.13
	5	1.34	1.58	1.31	1.12	1.00
	6	2.00	1.43	1.29	1.08	1.05
La/Ca	**3**	1.53	1.39	1.65	1.28	1.22
	4	1.77	1.52	1.74	1.21	1.12
	5	1.53	1.68	1.45	1.15	0.94
	6	1.60	1.31	1.54	1.23	1.08
U/Ca	**3**	2.93	2.41	1.95	1.78	1.91
	4	2.11	2.23	2.32	1.77	1.48
	5	1.80	1.87	2.00	1.54	1.65
	6	1.98	2.41	2.05	1.50	1.25

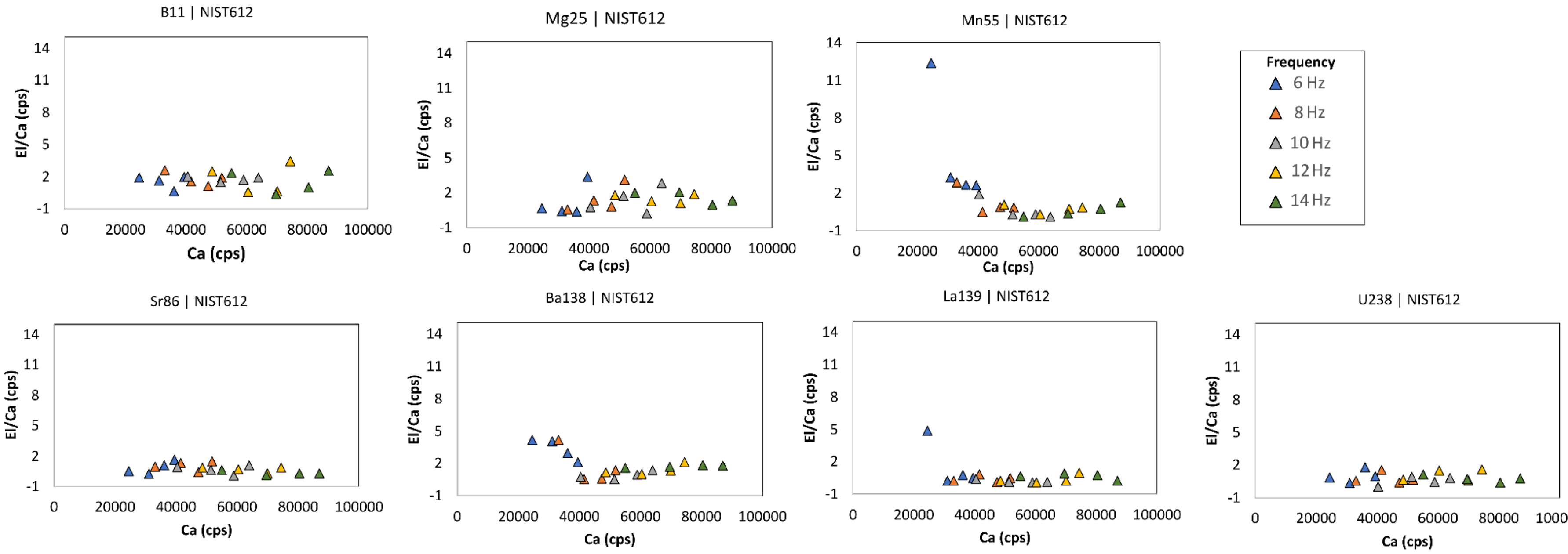

Figure 2.10. Plasma loading effect on El/Ca. Varying fluences and shot frequency in NIST612 represented by mean/El/Ca at each configuration setting versus amount of material ablated (^{43}Ca cps). El/Ca ratios were normalised to their respective means.

Table 2.5. Mean elemental values for coral samples analysed and LOD based on the background signal. Data highlighted in red shows mean values below LOD. Data highlighted in bold shows values close to LOD.

Core	**VOT17_2_1**		**VOT17_1_1_1**		**VOT17_1_1_2**		**NAN17_5_1**		**NAN17_2_1**		**FP17_1_1**		**NAM17_1_1**	
	Sample mean	*LOD*	Sample mean	*LOD*	Sample mean	*LOD*	Sample mean	*LOD*	Sample mean	*LOD*	Sample mean	*LOD*	Sample mean	*LOD*
^{7}Li	624.85	*34.59*	546.28	*38.27*	349.29	*37.87*	816.75	*45.50*	991.17	*69.58*	513.05	*28.89*	639.98	*32.32*
^{11}B	13047.53	*33.24*	17276.55	*13.96*	8310.75	*12.71*	14703.59	*24.47*	22002.30	*13.54*	6480.96	*8.37*	12523.44	*23.44*
^{25}Mg	14338.28	*0.00*	18446.89	*0.00*	9175.05	*0.00*	31231.88	*1.12*	28194.31	*0.00*	7627.15	*0.00*	15166.77	*0.00*
^{27}Al	356.87	*20.59*	2631.87	*12.29*	431.09	*14.69*	3674.68	*17.57*	3501.55	*16.25*	323.89	*15.83*	235.53	*18.73*
^{31}P	6053.51	*3482.73*	4344.74	*1858.94*	**1515.88**	*1329.18*	16094.39	*3787.97*	**2971.97**	*2071.35*	2457.07	*1033.35*	6884.25	*3028.63*
^{43}Ca	194541.62	*37.57*	268625.84	*29.73*	146807.98	*21.40*	215961.28	*35.78*	305271.48	*33.00*	112622.56	*22.49*	197816.63	*36.43*
^{47}Ti	**2.55**	*4.69*	2.88	*1.70*	3.19	*1.55*	**3.04**	*3.24*	16.19	*2.99*	160.03	*0.00*	**3.39**	*4.33*
^{55}Mn	**3945.56**	*3821.31*	**3363.49**	*2801.33*	**2235.04**	*1980.65*	**4862.89**	*3929.95*	**3754.42**	*3533.59*	**1877.36**	*1615.86*	**3758.19**	*3643.12*
^{86}Sr	406059.49	*71.35*	549280.15	*49.09*	372022.60	*42.47*	444900.14	*64.41*	616551.84	*56.69*	276644.26	*30.46*	409734.58	*65.78*
^{88}Sr	695195.20	*0.00*	949643.30	*0.00*	642997.10	*0.00*	763620.70	*0.00*	1063821.00	*1.12*	481736.80	*0.00*	700478.70	*0.00*
^{89}Y	403.38	*0.00*	282.36	*0.00*	190.97	*0.00*	327.92	*0.00*	140.18	*0.00*	284.07	*0.00*	286.12	*0.00*
^{137}Ba	5347.72	*0.00*	15171.46	*0.00*	3244.59	*0.00*	3668.69	*0.00*	8206.09	*0.00*	6417.72	*0.00*	14569.56	*0.00*
^{138}Ba	16361.32	*0.00*	50173.92	*0.00*	10221.39	*0.00*	11608.47	*0.00*	25647.46	*0.00*	20224.20	*0.00*	49833.72	*0.00*
^{139}La	30.88	*0.00*	35.68	*0.00*	24.67	*0.00*	36.72	*0.00*	22.29	*0.00*	171.60	*0.00*	22.06	*0.00*
^{140}Ce	32.73	*0.00*	31.54	*0.00*	23.91	*0.00*	30.61	*0.00*	17.52	*0.00*	169.66	*0.00*	21.77	*0.00*
^{143}Nd	**8.29**	*0.00*	**9.22**	*0.00*	**7.19**	*0.00*	**9.31**	*0.00*	**4.05**	*0.00*	161.35	*0.00*	**4.38**	*0.00*
^{146}Nd	23.87	*0.00*	26.05	*0.00*	18.84	*0.00*	26.58	*0.00*	11.59	*0.00*	166.27	*0.00*	12.38	*0.00*
^{147}Sm	**3.21**	*0.00*	**3.44**	*0.00*	**3.25**	*0.00*	**3.28**	*0.00*	**1.38**	*0.00*	159.68	*0.00*	**1.62**	*0.00*
^{153}Eu	**3.90**	*0.00*	**4.26**	*0.00*	**3.66**	*0.00*	**4.07**	*0.00*	**2.02**	*0.00*	160.22	*0.00*	**2.92**	*0.00*
^{157}Gd	**5.10**	*0.00*	**5.15**	*0.00*	**4.53**	*0.00*	**4.56**	*0.00*	**2.19**	*0.00*	160.40	*0.00*	**2.59**	*0.00*
^{166}Er	**9.45**	*0.00*	**7.06**	*0.00*	**6.35**	*0.00*	**7.71**	*0.00*	**2.81**	*0.00*	162.15	*0.00*	**5.89**	*0.00*
^{172}Yb	**7.47**	*0.00*	**4.12**	*0.00*	**4.24**	*0.00*	**7.28**	*0.00*	**1.64**	*0.00*	161.30	*0.00*	**4.45**	*0.00*
^{175}Lu	**5.71**	*0.00*	**2.88**	*0.00*	**3.33**	*0.00*	**6.12**	*0.00*	**1.32**	*0.00*	160.87	*0.00*	**3.75**	*0.00*
^{208}Pb	312.53	*2.34*	378.90	*3.15*	367.12	*2.34*	353.53	*5.38*	2205.50	*1.55*	9715.70	*3.45*	677.84	*1.70*
^{235}U	87.86	*0.00*	123.84	*0.00*	105.30	*0.00*	94.40	*0.00*	121.69	*0.00*	243.36	*0.00*	97.44	*0.00*
^{238}U	6007.00	*0.00*	8472.81	*0.00*	7179.20	*0.00*	6453.64	*0.00*	8335.77	*0.00*	6011.26	*0.00*	6626.80	*0.00*

I also explored how El/Ca varied across the range of fluences and frequencies depending on plasma loading (measured as ^{43}Ca cps) (Figure 2.10.). Variations in plasma loading (variations in amount of material transferred to the ICPMS), can potentially introduce matrix effects in the ICPMS, causing a short-term signal drift. This data consistently shows that for NIST612, below 40000 Ca cps, there are some fractionation (~30% difference) on certain elements (Mg, Mn, Ba). However, < 40000 cps of ^{43}Ca is only achieved at low fluences and shot frequencies.

Maintaining a careful balance so that material input is optimised to maximise instrument sensitivity and stability without triggering elemental fractionation is key. We determined that a fluence of 2.5 J/cm^2 and a shot frequency of 12Hz was ideal to obtain a stable El/Ca signal through each analysis session, as it keeps %RSD of all elements explored below 2.5% (Table 2.4.).

Here, shot frequencies have a large influence on sensitivity. For example, for a given fluence, a change in shot frequency from 6 Hz to 14 Hz produces a ~3% change in Sr/Ca. If fluence values change from 3 J/cm^2 to 6 J/cm^2 but shot frequency remains the same, there is a < 1% change in Sr/Ca. This importance of frequency rates v. fluence was observed previously in a study carried out with this same laser system, although connected to a Thermo Element XR magnetic sector field HR-ICP-MS (Nairn 2018).

2.4.1.3. Background signal and limits of detection

The limit of detection (LOD) of each isotope was calculated using the Longerich et al. (1996) method, where LOD is background signal + 3.3SD of background signal. Mean element (cps) signal for each coral sample and LOD for corresponding elements are represented in Table 2.5. Mean ^{47}Ti is below LOD for all samples. Further, mean ^{55}Mn is close to LOD for every sample. This is due to interferences between carrier gases ^{40}Ar and ^{15}N elevating background counts of mass 55. Because Mn is an element of crucial importance for land use and water quality reconstruction (See Chapter 5), we examine closely the Mn signal for each sample below. Furthermore, most REE show consistently less than 20 cps, with exception of ^{89}Y, ^{139}La, and^{140}Ce.

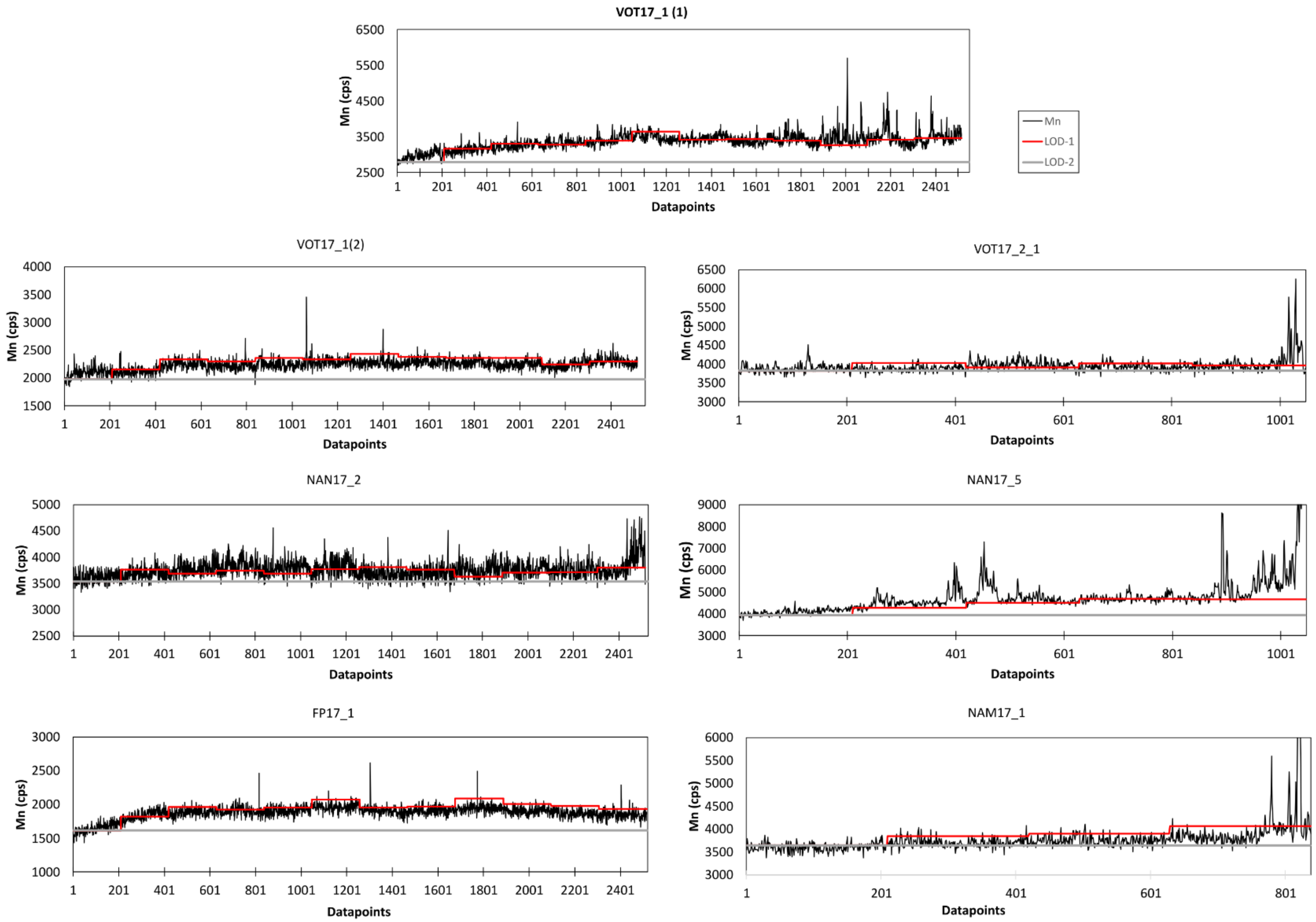

Figure 2.11. Raw Mn signal (cps) of each sample. Red line (LOD-1) represents background measurements before each sub-track. Grey line (LOD-2) is background measured before starting the coral path. Usual methods include background measurement only before starting coral ablation (LOD-2).

Analysis of raw ^{55}Mn data for each sample (Figure 2.11.) shows how a number of measurements fall below LOD. Previous work has shown that background m/z = 55 can be reduced by adding H_2 to the analyte gas prior to ionization on the ICPMS. Unfortunately, this system was not available for RESOlution_SE at CELTIC at the time of the analysis. Here, I tried adding H_2 gas in the collision cell (post-ionization) which proved to be not useful in reducing mass 55 background. Nevertheless, all the temporal events assessed in Chapter 5 showing elevated Mn/Ca were always above LOD and therefore I investigate the drivers of coral Mn. For the purposes of Chapter 5, when exploring potential environmental signal of Mn/Ca, I focus solely on elevated events, and not in minima values and oscillations.

2.4.1.4. Standardization

Analytical reproducibility for each element was monitored through all the standards used on every day of analysis. Here, I report internal reproducibility as mean and %RSD of El/Ca of every day of analysis, and external accuracy (measured value/reported value) and precision (2x SD of accuracy) for all the four standards used in this study (Table 2.6.). Calcium (^{43}Ca) is used as the internal standard throughout.

Ideally, this optimisation experiment would have also been carried out using a carbonate material to limit matrix effects. However, due to coral heterogeneity across both skeletal features and temporal space (environmentally driven variability), analysis of a coral piece for these purposes would not have been straightforward to assess and consider for laser optimization. Previous work has explored carbonate standards to assess this issue, using JCp-1 (*Porites* spp. pellet), MACS-3, and in house pressed *Porites* spp. standard (Sinclair, 1998; Fallon, 1999). The carbonate standard "JCp-1" was only made available to CELTIC in December 2021 by a donation from collaborators (this standard is no longer in production) after the laser optimisation experiment had already been executed. Regardless, previous work has shown that silicate-based standards such as NIST provide reproducible data on coral samples (Table 2.3.). Here, based on my optimization study, I use the NIST glass standards primarily but assess JCp-1 during coral geochemical analysis to identify the ideal suite of standards to use for the coral samples here, matching the closest El/Ca ratios of the coral samples to each available standard (Table 2.7.).

Table 2.6. Mean internal accuracy and long-term reproducibility (external accuracy and precision) of the secondary standards used in this study. Data in red indicate reproducibility error >5%. Internal reproducibility is reported as mean and %RSD of El/Ca of every day of analysis. External accuracy is calculated as measured value/reported value. Precision is calculated as 2x SD of accuracy.

Std	**610**					**612**				
Value	Mean	%RSD	*Rep. value*	Acc.	Prec.	Mean	%RSD	*Rep. value*	Acc.	Prec.
Li/Ca	3.41E-02	1.59%	*3.32E-02*	2.76%	1.19%	2.66E-03	2.11%	*2.73E-03*	2.42%	3.10%
B/Ca	1.57E-02	1.43%	*1.59E-02*	1.66%	2.03%	1.70E-03	2.15%	*1.49E-03*	13.72%	24.29%
Mg/Ca	1.06E-02	1.77%	*9.40E-03*	12.43%	4.23%	1.28E-03	4.15%	*1.32E-03*	3.18%	14.22%
Al/Ca	1.86E-01	3.20%	*1.88E-01*	1.06%	2.27%	3.77E-01	2.09%	*1.88E-01*	101.10%	5.35%
P/Ca	7.91E-03	1.66%	*6.54E-03*	20.97%	2.81%	1.75E-03	6.91%	*7.07E-04*	147.28%	896.81%
Ti/Ca	5.32E-03	1.81%	*4.64E-03*	14.66%	7.71%	4.26E-04	4.28%	*4.33E-04*	1.61%	15.98%
Mn/Ca	3.83E-03	1.41%	*3.97E-03*	3.71%	1.09%	3.45E-04	1.97%	*3.32E-04*	3.99%	5.18%
Sr/Ca	3.03E-03	1.32%	*2.90E-03*	4.53%	0.88%	4.13E-04	2.31%	*4.22E-04*	2.06%	5.80%
Y/Ca	2.51E-03	1.52%	*2.56E-03*	2.05%	0.97%	2.09E-04	1.57%	*2.03E-04*	3.09%	2.52%
Ba/Ca	1.60E-03	1.51%	*1.62E-03*	1.32%	1.80%	1.36E-04	1.94%	*1.35E-04*	0.57%	3.08%
La/Ca	1.53E-03	1.91%	*1.56E-03*	2.05%	1.41%	1.25E-04	2.35%	*1.22E-04*	2.55%	2.91%
Ce/Ca	1.56E-03	2.00%	*1.59E-03*	1.77%	1.44%	1.35E-04	2.57%	*1.29E-04*	4.23%	5.98%
Pb/Ca	9.21E-04	2.44%	*1.01E-03*	9.11%	2.33%	9.15E-05	3.40%	*8.77E-05*	4.45%	10.83%
U/Ca	9.32E-04	2.83%	*9.54E-04*	2.34%	2.61%	7.52E-05	3.61%	*7.40E-05*	1.76%	7.95%

Std	**614**					**JCp-1**				
Value	Mean	%RSD	*Rep. value*	Acc.	Prec.	Mean	%RSD	*Rep. value*	Acc.	Prec.
Li/Ca	1.15E-04	3.56%	*1.15E-04*	0.16%	3.91%	7.76E-06	20.17%	*5.68E-06*	36.64%	19.01%
B/Ca	6.18E-05	4.85%	*6.50E-05*	4.97%	5.07%	5.41E-04	5.01%	*4.54E-04*	19.08%	5.05%
Mg/Ca	6.31E-04	5.71%	*6.55E-04*	3.67%	1.03%	4.58E-03	5.86%	*4.07E-03*	12.51%	3.75%
Al/Ca	3.80E-01	2.25%	*1.89E-01*	101.54%	5.39%	1.15E-03	66.01%	*1.86E-03*	38.45%	28.79%
P/Ca	5.21E-05	45.24%	*1.73E-04*	69.94%	33.53%	1.98E-05	78.27%			
Ti/Ca	3.22E-05	13.37%	*3.55E-05*	9.35%	11.98%	9.86E-05	99.49%			
Mn/Ca	1.17E-05	2.86%	*1.22E-05*	3.77%	4.95%	1.83E-06	38.92%	*1.90E-06*	3.97%	26.22%
Sr/Ca	2.40E-04	2.76%	*2.46E-04*	2.82%	5.24%	8.85E-03	4.34%	*8.81E-03*	0.46%	2.81%
Y/Ca	4.11E-06	2.73%	*4.19E-06*	1.96%	3.48%	3.19E-07	39.84%			
Ba/Ca	1.11E-05	3.28%	*1.10E-05*	1.06%	2.24%	6.08E-06	20.98%	*7.87E-06*	22.69%	13.42%
La/Ca	2.39E-06	3.38%	*2.44E-06*	1.95%	2.86%	5.24E-08	43.29%			
Ce/Ca	2.58E-06	3.80%	*2.73E-06*	5.45%	2.85%	1.79E-06	96.61%			
Pb/Ca	5.58E-06	4.40%	*5.28E-06*	5.67%	9.68%	1.42E-07	33.56%	*9.06E-08*	56.63%	23.75%
U/Ca	1.70E-06	4.75%	*1.63E-06*	4.13%	4.76%	3.55E-06	10.32%			

Table 2.7. Standard material chosen for standardisation of elements examined in this study.

Standard Material	Elements standardised
NIST612	^{7}Li, ^{43}Ca
NIST614	^{11}B, ^{25}Mg, ^{43}Ca, ^{55}Mn, ^{89}Y, ^{137}Ba, ^{138}Ba, ^{139}La, ^{140}Ce, ^{238}U
JCp-1	^{43}Ca, ^{86}Sr, ^{88}Sr

Analytical reproducibility of each El/Ca differs across different standards. For example, B/Ca accuracy is > 15% in both NIST612 and JCp-1, but lower (<5%) in NIST610 and NIST614. In this study I have standardised each element against the closest standard value that showed good reproducibility (Tables 2.6. and 2.7.). For example, the mean Sr/Ca of samples in this study is ~9.20 mmol/mol, and the closest standard Sr/Ca value is found in standard JCp-1 (Sr/Ca = 8.81 mmol/mol), while Sr/Ca values in NIST standards range from 0.24 to 2.90 mmol/mol. For Sr/Ca, JCp-1 shows high reproducibility (accuracy error < 5%) and a ratio close to that of the coral samples and hence it is selected to standardise Sr/Ca. By matching standard El/Ca values to mean coral values we minimise any fractionation derived from matrix effects and ensure we obtain the best reproducibility possible. Even though the majority of El/Ca values are standardised against glass standards (NIST612 and NIST 614; Table 2.7.), matrix effects and mass fractionation have been shown to be minimal (e.g., Fallon et al. 2002; Wyndham et al. 2004; LaVigne et al. 2016) as mentioned above.

2.4.2. Computerised Tomography

2.4.2.1. Sample scanning

All coral cores were scanned using X-Ray computed tomography (CT). CT measurements were carried out using a Nikon Metrology HMX ST 225 with a voxel resolution of 50 µm at the Natural History Museum of London and XTM facilities at the University of Bristol. Scan parameters were 360° at 180 kV, 0.22 mA and 708 ms of exposure time with a 1.00 mm copper filter. A Micro-CT HA Phantom hydroxyapatite density standard was scanned with each coral sample for density calibration and acquisition of absolute density values. The standard has five cylindrical inserts each with different densities ranging from 1.13 g/cm^3 (the base cylinder) up to 1.90 g/cm^3. The scans were reconstructed as 1400 x 1400 16-bit TIFF files.

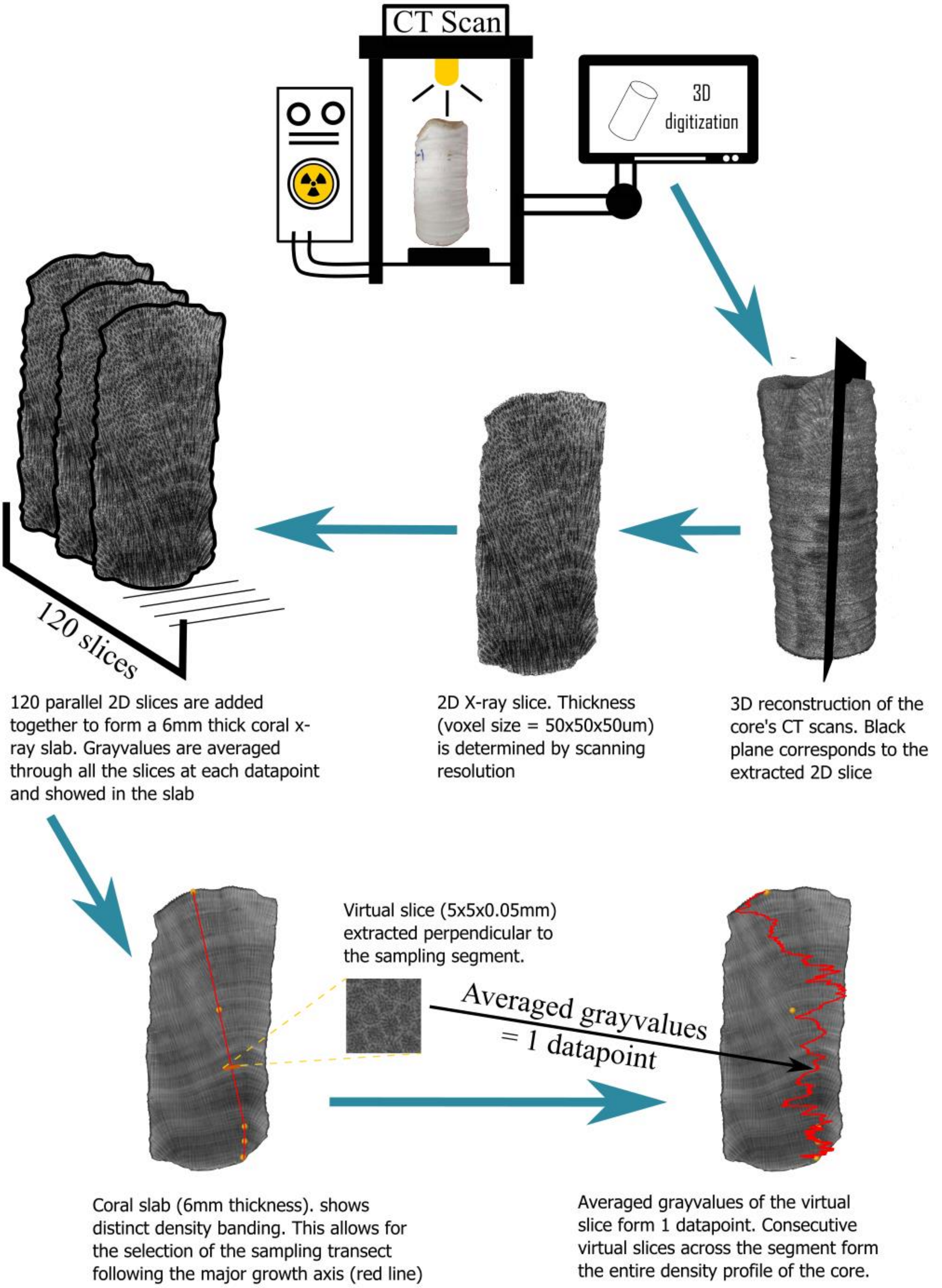

120 parallel 2D slices are added together to form a 6mm thick coral x-ray slab. Grayvalues are averaged through all the slices at each datapoint and showed in the slab

2D X-ray slice. Thickness (voxel size = 50x50x50um) is determined by scanning resolution

3D reconstruction of the core's CT scans. Black plane corresponds to the extracted 2D slice

Virtual slice (5x5x0.05mm) extracted perpendicular to the sampling segment.

Coral slab (6mm thickness). shows distinct density banding. This allows for the selection of the sampling transect following the major growth axis (red line)

Averaged grayvalues of the virtual slice form 1 datapoint. Consecutive virtual slices across the segment form the entire density profile of the core.

Figure 2.12. Diagram of work-flow from CT scanning to data processing and density acquisition.

2.4.2.2. Density calibration and data acquisition

Scan reconstruction was conducted using AVIZO LITE (v. 9.7.0) (Figure 2.12.). The single slices (2D, x and y axis) were stacked (z axis) to build a 3-dimensional reconstruction of each core sample. Cross-sectional slices (along the z axis) were used to explore corallite growth direction and find the major growth axis. The criteria followed for identifying the major growth axis were: i) ensuring that the corallite walls were as parallel as possible to the slice throughout the length of the core, from top to bottom; and ii) avoiding areas of distorted growth (e.g., growth scars, bioerosion, growth valleys).

Each slice has a thickness of 50 μm (i.e., it averages grey-values across 50 μm of material). In order to observe seasonal banding in *Porites* spp. corals, X-rays/grey-values need to be averaged across slabs of 6 – 7 mm thickness. Here, I created a virtual X-ray slab of 6 mm by adding together 120 2-D slices (120 x 50 μm = 6000 μm) in AVIZO LITE and averaging each voxel's grey-values perpendicularly (Figure 2.12.). This procedure allows us to visualise seasonal density banding and confirm that the path of the major growth axis chosen is, indeed, perpendicular to the growth bands. Ensuring that the growth axis is perpendicular to the growth bands is key to avoid errors in measuring linear extension, where an oblique growth axis across an annual pair of band would result in a longer extension than it actually is (DeLong et al. 2013).

Density measurements were carried out by averaging grey-values on a 5 x 5 mm area centred around the growth axis on each individual slice (Figure 2.12.). The area of this square was chosen to be able to obtain a density value averaged across at least 20 corallites, but without extending towards a skeletal area secreted at a different period due to the bumpy growth of most cores. The coordinates of the starting and finishing points of the growth axis were extracted from the 3-D stack using AVIZO LITE. Both, axis coordinates and sample slices, were input into a Python script. The script identifies the voxel location of the growth axis vector at each single slice in between the starting and finishing coordinates, then it selects voxels on an area of 5 x 5 mm centred across the growth vector and computes the average grey-value of the volume (1.25 mm^3). This operation is repeated across every slice between starting and finishing points of the growth axis. The output is a timeseries dataset of grey-values along the growth axis. Average grey-values were also obtained from each cylinder of the hydroxyapatite density standard on each scan.

Scan quality was explored by calibrating the density standard grey-values to each known density, where they are expected to follow a linear fit ($R^2 > 0.95$). Furthermore, validity of the density calibration is only possible for those values encompassed by the standard (i.e., 1.13-1.90 g/cm^3), and as such I inspected density values of each coral sample to ensure they were always within calibration values. Conversion of grey-values to density along the growth axis of each coral sample was carried out using the core-specific density calibrations.

2.4.3. UV luminescence

Coral slabs were photographed under ultraviolet (UV) light to obtain potential images of seasonal fluorescent banding. The corals were illuminated using a handheld Crime-lite 82S UV light source, positioned as close as possible to the coral slab. Photographs were taking directly from overhead using an anti-glare orange camera filter.

In theory, under UV light, the fluorescent lines can be distinguished from the aragonite background due to differences in their brightness and yellow/green colour. Yet, UV fluorescence did not show any remarkable event (e.g., intense rainfall, flooding, etc.) in the coral samples of this study (See Appendix A for images of cores under UV and white light). A potential explanation of this behaviour might be due to the presence of seasonal grey bands through many of the coral samples, hindering the presence of UV lines. However, even in coral cores showing pristine white aragonite, pronounced fluorescence was lacking. The sample NAM17_1_1 was the only sample showing annual fluorescence, and these observations aid in establishing a chronology in this sample.

2.5. Core age models

The age models of the coral samples were calculated in two steps by using data derived from both CT scans and geochemical analysis.

First, annual linear extension rates for each core were extracted from both density profiles and X-ray images of virtual slabs (6 mm thickness). Measurements between density maxima (as standard procedure; e.g., Felis et al. 2009) were made on the density profiles of each core. In some cases, density profiles showed a clear seasonal pattern, but some samples did show a more complicated seasonal variability that did not allow for recognition of annual density minima and maxima. In these cases, X-rays of virtual slabs, where clear seasonal growth bands were visualised (See section 2.4.2.2.), were used to identify annual density maxima and measure distance between them.

This annual timescale, derived from measurements between density maxima exclusively, assumes a constant linear growth through the year independently of the season. To refine the age models, the annual core chronologies were processed by aligning seasonal variability in Sr/Ca (See Section 2.4.1.1.) (minima and maxima) with seasonal variability in SST (maxima and minima) assuming an inverse correlation between Sr/Ca-SST (as seen elsewhere, e.g., DeLong et al., 2014). We used Sr/Ca (instead of other SST proxies) since it is the El/Ca ratio that best correlates with SST for all cores (See Chapter 4). Because age model refinement is based on geochemical signals, it can only be performed on the samples analysed using LA-ICPMS. As such, refined coral age models are used for Chapters 4 and 5. For the purposes of Chapter 3, where growth parameters of all samples available are analysed, we use the initial age model built with density and X-ray images to ensure consistency across samples. Comparison of Sr/Ca time-series before and after refinement (Figure 2.13.; Table 2.8) show how age models were only modified around 65 (± 3) days on average by applying the Sr/Ca-SST refinement method. Hence, I am confident that the age models built on the first phase and used in Chapter 3 are valid.

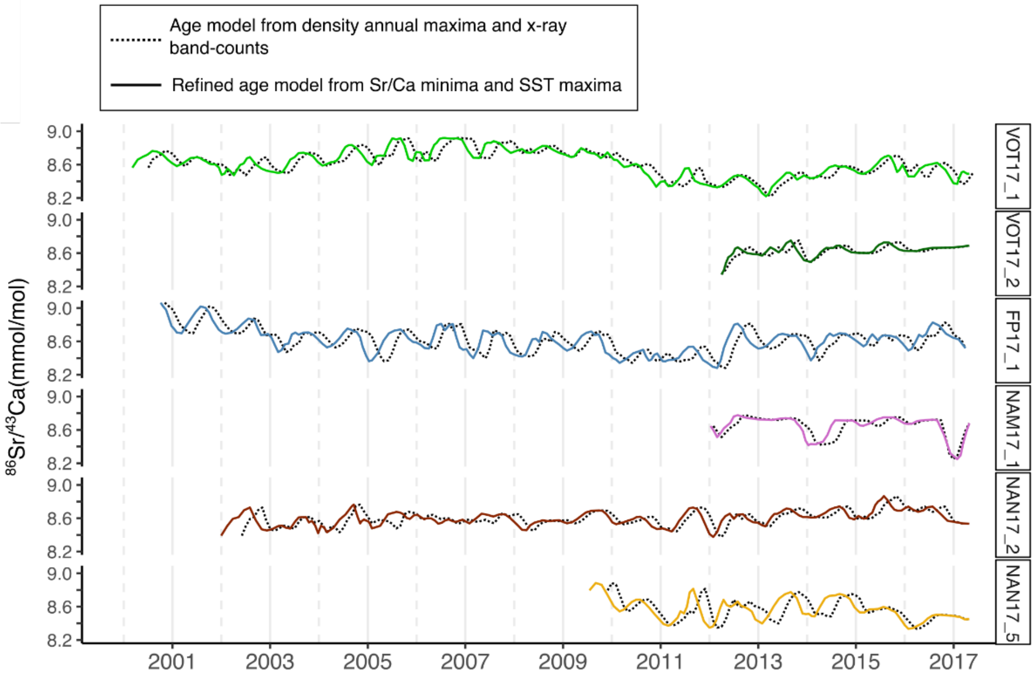

Figure 2.13. Monthly Sr/Ca (Chapter 4) for coral samples showing change in the age model from the annual chronology obtained from density maxima and counting (dotted lines) and refined data with Sr/Ca minima and maxima datapoints.

Table 2.8. Mean days of difference in Sr/Ca age models of each sample between the initial core chronologies (obtained from density maxima and density banding) and the refined Chronologies (from Sr/Ca seasonal minima and maxima).

Core	Mean difference (Days)	2SE
VOT17_1	71.9	2.76
VOT17_2	44.1	6.64
FP17_1	75.94	2.76
NAM17_1	50.15	10.26
NAN17_2	79.24	5.92
NAN17_5	70.22	6.5

2.6. Environmental data

Below I detail the sources and datasets used to collate the environmental data analysed in this thesis. Mean environmental values for each location are described in Table 2.9 and monthly data from 1998 until 2017, including climatological monthly mean for the same period, at each location are presented in Figure 2.14.

Table 2.9. Mean environmental data at each location of this study for the period 1998 – 2017.

		Votua Reef		Nananu-i-Ra		Namuka Reef		Suva Reef	
		Mean	SD	Mean	SD	Mean	SD	Mean	SD
SST	°C	26.83	1.40	26.85	1.46	26.73	1.45	26.69	1.49
Rainfall	mm/month	246.24	149.01	193.49	198.32	246.24	149.01	246.24	149.01
SSS	gl/L	35.21	0.57	35.06	0.34	35.17	1.10	35.17	1.10
K_d490	m^{-1}	0.03	0.01	0.07	0.02	0.05	0.02	0.06	0.04
Chl-a	mg/m^3	0.17	0.15	0.52	0.34	0.33	0.22	0.39	0.70
Wind speed	m/s	2.03	1.07	6.25	2.74	3.82	1.65	5.34	2.25

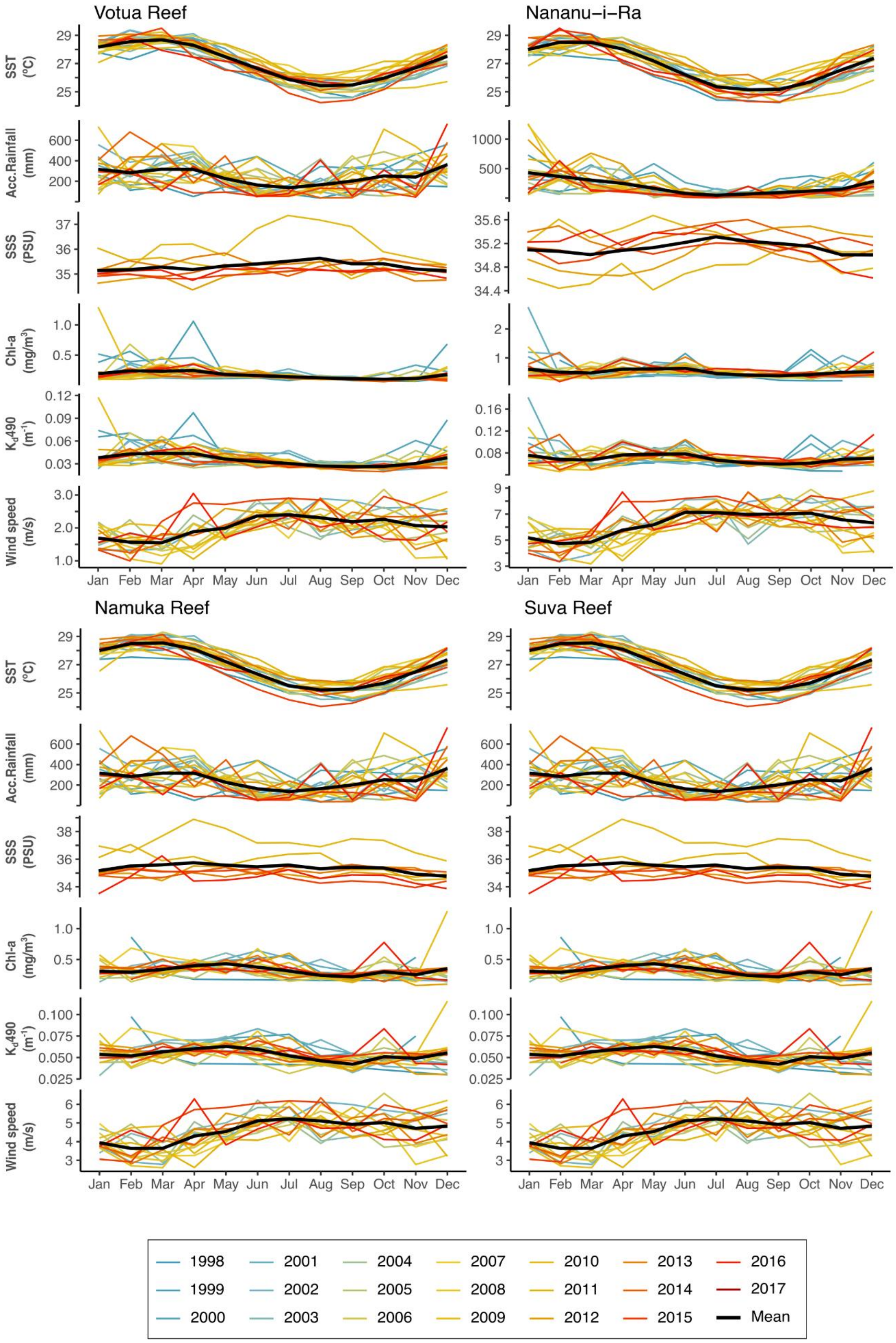

Figure 2.14. 1998 – 2017 monthly average data for environmental variables at Votua Reef, Nananu-i-Ra, Namuka Reef and Suva Reef. Black line is climatological average data for each month.

2.6.1. Seawater temperature

Local seawater temperature was obtained from the ReefTEMPS network dataset (Varillon et al. 2018). ReefTEMPS encompasses a network of seawater sensors in the South and West Pacific Ocean. Of these networks, a total of 11 coastal sensors are anchored in Fijian marine territory, of which three are located in reefs around Viti Levu. Temperature data from the closest available logger to each location of this study is used (Figure 2.15.; Table 2.10.). Temporal resolution of raw data is 10 minutes, covering from ~2013 to May 2017 (date of core collection). Data reduction was carried out to obtain a daily resolved dataset.

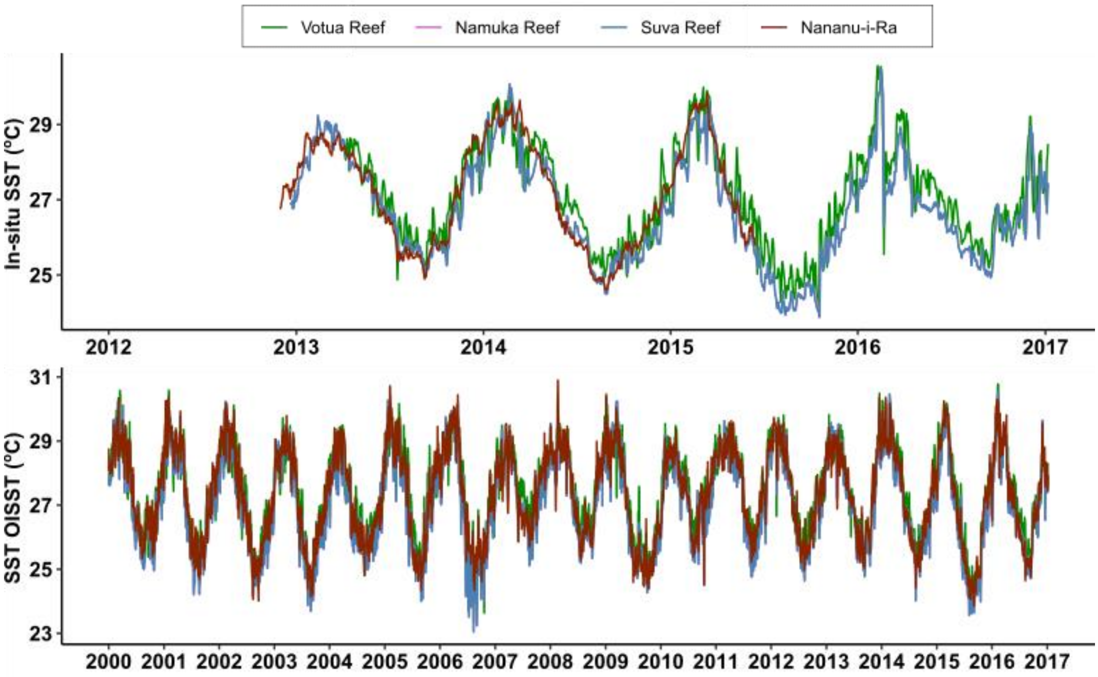

Figure 2.15. Local and OISST (remote sensed) daily seawater temperature data at each location. Each colour represents the inshore reefs of this study.

Due to the short span of the seawater temperature dataset available from in-situ data loggers, gridded satellite-derived seawater surface temperature (SST) was obtained for each location to obtain a complete dataset covering at least the same period as coral data studied here (1998 – 2017) (Figure 2.15.). The are several satellite-derived SST products available with a range of spatial and temporal resolution. I extracted SST data from 3 different satellite products: i) Advanced Very High Resolution Radiometer (AVHRR) Pathfinder v 5.3 (Saha et al. 2018), ii) Coral Reef Watch (CRW) *CoralTemp* 5km SST v.3.1 (Liu et al. 2014) and iii) Daily Optimum Interpolation SST (OISST) (Reynolds et al. 2007; Banzon et al. 2016). In all cases, SST data was extracted from the single pixel (of varying resolution depending on SST dataset) containing the core location, or the closest available (Table 2.10.).

Pathfinder SST is available twice-daily (day and night) from 1981 onwards, with a resolution of 4 km. This SST product is derived from the AVHRR sensors onboard several NOAA's polar-orbiting satellites. I obtained nighttime-only data in order to minimize the effects of solar heating (Casey et al. 2010). In this study only the highest quality data available for each pixel (levels 4 and 5) were selected.

CRW *CoralTemp* dataset has a resolution of 5 km and is available daily, *gap-free*, from 1985 onwards. *CoralTemp* is derived from three nighttime-only different satellite products (NOAA's near real-time Geo-Polar Blended SST product, NOAA's Geo-Polar Blended SST reanalysis and the UK Meteorological Office's (Met Office) Operational SST and Sea Ice Analysis (OSTIA) reanalysis).

Finally, OISST dataset is available daily (nighttime) with a resolution of ~25 km. This dataset combines satellite product derived from AVHRR sensors and in-situ observations (from buoys and ships).

Different SST gridded products have been used in coral research (e.g., DeLong et al. 2014; DeCarlo and Harrison 2019; Reed et al. 2021). The different algorithms applied to obtain SST from satellite data, and the different spatial resolution and coverage can result in potential regional biases in the different products, making some datasets more accurate in certain locations and timeframes. Here, I examined differences and correlation between the three satellite datasets to determine whether there were deviations in the data between them and decide whether one was more adequate for Fiji (See Section 2.6.7.).

Thermal stress was evaluated as Degree Heating Weeks (DHW). DHW were obtained from the CRW *CoralTemp*'s daily global 5 km satellite coral bleaching DHW (method shown in Liu et al. 2017). This product measures the accumulation of heat stress that coral reefs experienced over the prior 12 weeks. It is a cumulative measurement of both intensity and duration of heat stress, and it is expressed in the unit °C-weeks. DHWs over 4 °C-weeks have been shown to cause significant coral bleaching; values over 8 °C-weeks have caused severe bleaching and significant mortality.

Table 2.10. Coral coring coordinates for each location of this study and location coordinates of paired environmental data in this study.

Location		Votua	Nananu-i-Ra	Suva	Namuka
Core	Latitude	-18.213823	-17.298108/ -17.279467	-18.143753	-18.1458/ -18.151255
	Longitude	177.710655	178.230095/ 178.227683	178.401692	178.37736/ 178.347347
Seawater temperature (in-situ)	Resolution	--			
	Latitude	-18.21	-17.522033	-18.15975	-18.15975
	Longitude	177.673167	178.51405	178.39995	178.39995
SST (Pathfinder)	Resolution	~4km			
	Latitude	-18.27083	-17.3125	-18.14583	-18.14583
	Longitude	177.7292	178.2292	178.3958	178.3542
SST(CRW)	Resolution	~5 km			
	Latitude	-18.225	-18.325	-18.125	-18.175
	Longitude	177.725	178.275	178.425	178.375
SST (OISST)	Resolution	~25 km			
	Latitude	-18.375	-17.375	-18.125	-18.125
	Longitude	177.625	178.375	178.375	178.375
Rainfall	Resolution	--			
	Latitude	-18.12	-17.37	-18.12	-18.12
	Longitude	178.47	178.16	178.47	178.47
Ocean Colour (SeaWiFs)	Resolution	~9 km			
	Latitude	-18.29167	-17.29167	-18.20833	-18.20833
	Longitude	177.625	178.29167	178.375	178.375
Ocean Colour (MODIS-Aqua)	Resolution	~4 km			
	Latitude	-18.22917	-17.3125	-18.14583	-18.14583
	Longitude	177.7292	178.2292	178.3958	178.3958
Wind (in-situ)	Resolution	--			
	Latitude	-18.12	-17.37	-18.12	-18.12
	Longitude	178.47	178.16	178.47	178.47
Wind (CCMP)	Resolution	~25 km			
	Latitude	-18.24885	-17.24906	-18.14997	-18.14997
	Longitude	177.7477	178.2476	178.3465	-17.84784
SSS (SMOS)	Resolution	~25 km			
	Latitude	-18.24807	-17.42482	-18.04191	-18.04191
	Longitude	177.7954	178.3141	178.3141	178.3141

2.6.2. Rainfall

Rainfall is routinely recorded by the Fiji Meteorological Service through a network of weather stations located across the country. Rainfall data for this study was provided by the Fiji Meteorological Service. The closest weather stations to each location with a dataset covering at least the 1998 – 2017 period were selected (Figure 2.16.; Table 2.10.). For Votua, despite being the Nacocolevu station the closest (~30 km) available weather station, I selected data from Laucala Bay instead. This is justified because Votua is located wind-ward and Nacocolevu, although nearby, it is on the lee-ward of the mountains. Because topography exerts a great impact over Viti Levu's climatology I considered Laucala Bay data to be more representative of the rainfall events experienced in Votua.

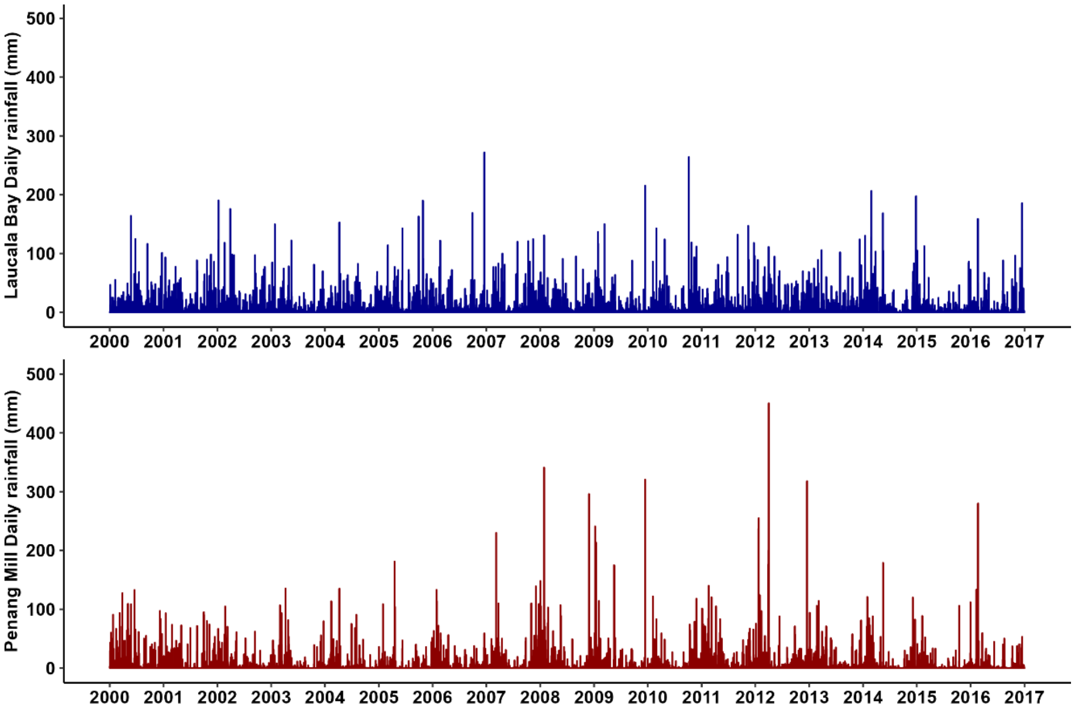

Figure 2.16. Daily rainfall data at the two weather stations from where precipitation data was extracted in this study. Data from Laucala Bay weather station (Blue) was paired to samples from the Votua reef (Coral Coast), Fish Path (Suva reef) and Namuka reef. Data from Penang Mill weather station was paired to coral samples from Nananu-i-Ra.

2.6.3. Wind

Daily wind direction and speed was also provided by the Fiji Meteorological Service. The availability of wind data differed across stations. As with rainfall, wind data was selected from the closest station to each locations covering the longest period possible (starting between 2011 – 2015 until May 2017) (Figure 2.17.; Table 2.10.).

Satellite wind data was obtained from the Cross-Calibrated Multi-Platform (CCMP), a gap-free gridded product produced using satellite and buoy wind measurements. The available resolution of data is 6-hourly at ~25 km. CCMP v 2.0 data was retrieved from 1x1 pixel encompassing each coral location from January 2002 until December 2016 (end of dataset) (Figure 2.17.).

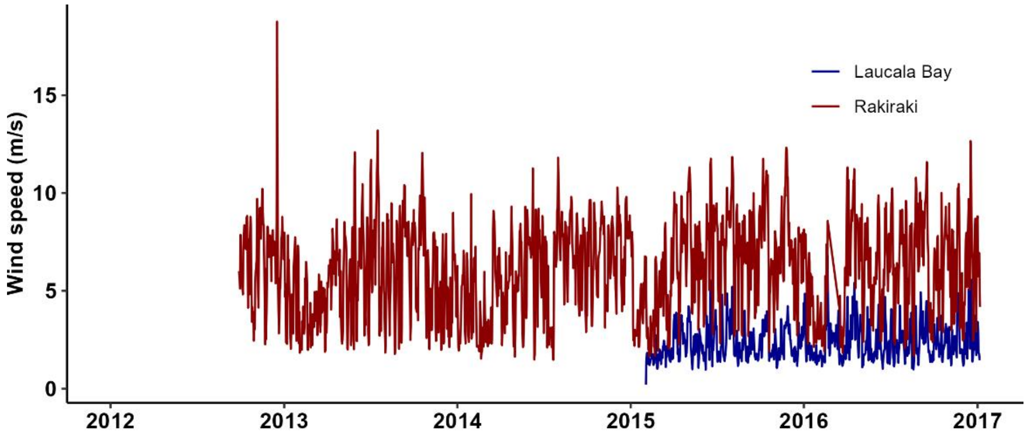

Figure 2.17. Daily wind speed data from weather stations in Laucala Bay and Rakiraki. In-situ win data is used to validate remote sensing wind speed (See section below).

2.6.4. Ocean colour

To characterise water quality at each location, the diffuse attenuation coefficient at a wavelength of 490 nm ($K_d490(m^{-1})$) and the chlorophyll-a concentration (mg/m^3) were derived from satellite ocean colour (OC) data (Shi and Wang 2010). Level-3 data (gridded) were obtained from both SeaWiFS and MODIS-Aqua products. SeaWiFS product is available with a resolution of 9 km, and daily data was obtained between September 1997 and July 2002. The MODIS-Aqua product has a resolution of 4 km, and daily data were obtained between July 2002 until May 2017. Similar to SST, an area of 1x1 pixel enclosing each core location was selected (Figure 2.18.; Table 2.10.).

Across all four locations of this study K_d490 and chlorophyll-a values show a high degree of correlation ($R^2 = 0.93$, $p < 0.0001$) (Figure 2.19). This observation is not surprising, as a turbid water can be associated with biological processes such as phytoplankton blooms (e.g., Platt et al. 1988) and/or river runoff and associated sediment plumes (Nezlin and

DiGiacomo 2005), and sediment resuspension and transportation (Acker et al. 2002; Shi and Wang 2008). Supporting this observation, Shi and Wang (2010) found that moderate increases in seawater turbidity ($K_d490 < 0.3$ m^{-1}), like those observed across all locations here, tended to be associated with an elevation of chlorophyll-a concentration. Considering this, and the close correlation between the two variables in this thesis, I use K_d490 in the figures and representations as a more comprehensive variable, although both variables were tested at all times.

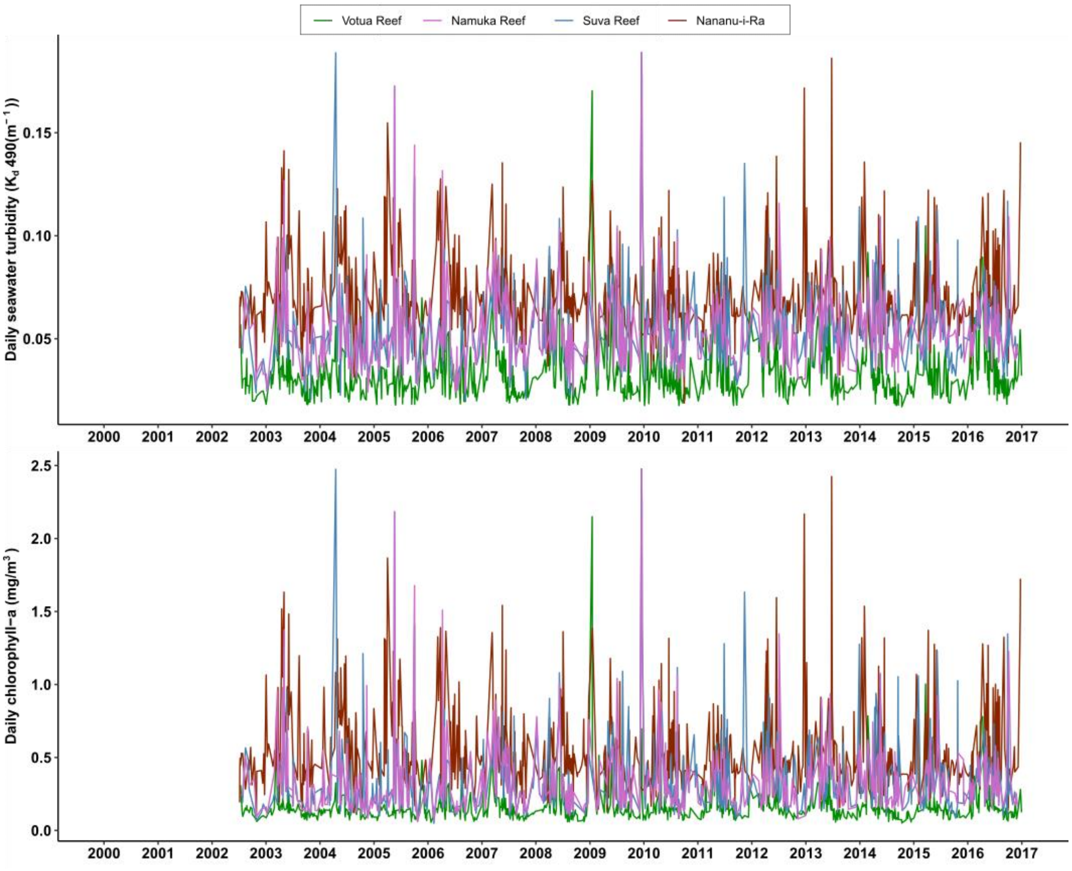

Figure 2.18. Daily Ocean Colour Data from MODIS Aqua. Panel A show seawater turbidity measured as K_d490. Panel B shows Chlorophyll-a concentration. Colours represent each inshore location in this study.

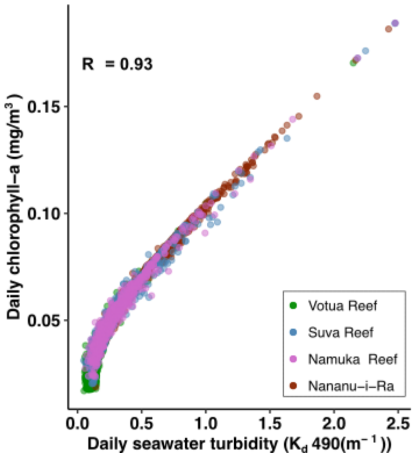

Figure 2.19. Linear correlation between daily Ocean Colour Data from MODIS Aqua at each location of this study.

2.6.5. Sea surface salinity

Sea surface salinity (SSS) data was obtained from level-3 CATDS Ocean Salinity (Figure 2.20.). This satellite product is obtained from ESA's Soil Moisture and Ocean Salinity (SMOS) mission. Daily-resolved data with a ~25 km resolution was obtained from the closest pixel to each location from January 2010 until May 2017 (Table 2.10.).

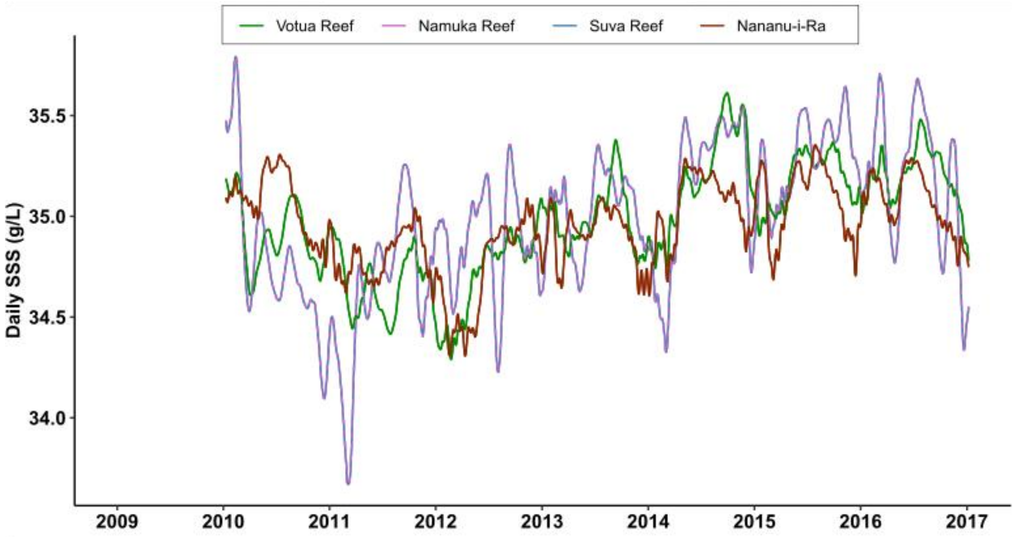

Figure 2.20. Monthly Sea Surface Salinity (SSS) from SMOS satellite product. Colour represents each location in this study.

2.6.6. ENSO and tropical storms

El Niño Southern Oscillation (ENSO) phases were extracted from the Oceanic Nino Index (ONI), which is calculated through a 3-month running average of SST anomalies

(SST obtained as product of ERSST.v5) in the Nino 3.4 region (5°N–5°S, 120°–170°W). SST anomalies are calculated based on a 30-yr period and are updated every 5 years (SST anomalies in this study were calculated using the 1986 – 2020 mean). ONI data between 1998 and 2017 was obtained from NCEP NOAA.

Trajectory and characteristics of tropical storms and cyclones occurred over Fiji from 1970 until 2017 were obtained from the NOAA Office for Coastal Management (Table 2.11.).

Table 2.11. List of Tropical Storms (TS) and Cyclones reaching Fiji (within 100 km distance) from 1998 until May 2017

Date	Cat.	Name	Date	Cat.	Name
21/12/1998	2	Cora	02/01/2009	TS	Lin
06/01/2000	TS	Iris	11/12/2009	1	Mick
13/06/2000	TS	Neil	29/01/2010	TS	Oli
28/02/2001	3	Paula	10/03/2010	4	Tomas
23/02/2002	TS	Unnamed	20/01/2011	2	Wilma
11/12/2002	TS	Yolande	28/01/2011	TS	Yasi
25/12/2002	1	Zoe	22/03/2011	TS	Bune
10/01/2003	3	Ami	05/02/2012	TS	Cyril
25/01/2003	TS	Cilla	01/04/2012	TS	Daphne
10/03/2002	1	Eseta	10/12/2012	4	Evan
01/01/2004	TS	Heta	18/01/2013	TS	Garry
08/04/2004	TS	Unnamed	25/02/2014	TS	Kofi
27/01/2005	TS	Lola	08/03/2014	1	Lusi
20/03/2005	TS	Sheila	19/03/2015	TS	Reuben
06/01/2006	TS	Tam	13/10/2015	TS	Unnamed
09/02/2006	1	Vaianu	29/12/2015	4	Ula
01/02/2007	TS	Unnamed	16/02/2016	5	Winston
01/04/2007	TS	Cliff	04/04/2016	4	Zena
03/12/2007	3	Daman	17/04/2016	TS	Amos
15/01/2008	3	Funa	21/04/2017	TS	Unnamed
26/01/2008	1	Gene	11/12/2009	1	Mick
25/01/2009	TS	Hettie	29/01/2010	TS	Oli

2.6.7. Land use

Geospatial vector datasets of land use data in Fiji (corresponding to 2015) were provided by the Land Resource Planning and Development, Department of Agriculture, Government of Fiji.

2.6.8. Remote sense data validation

To validate the satellite product, we compared satellite environmental data with the equivalent in-situ data. This was only possible for seawater temperature and wind, as these were the only variables with both in-situ and remotely sensed data.

We compared the different satellite SST datasets (Pathfinder, CRW and OISST) between themselves to detect potential regional biases. They were also compared with in-situ seawater temperature data. We compared mean values for the entire datasets and explored linear correlations of daily data. Note that for SST measurements, Namuka Reef and Fish Patch fall within the same pixel due to resolution of remotely sensed data. For wind data, we compared mean values between the remote sensed (CCMP) and the in-situ data. Linear correlations were also explored for the daily resolved data.

2.6.8.1. SST

Mean remotely sensed SST showed no clear differences between satellite products or with in-situ data (Table 2.12.). In addition, paired correlations of remotely sensed and in-situ data show high degrees of correlations at all locations ($R^2 > 0.80$) (Figure 2.21.). This indicates that remotely sensed SST can represent in-situ seawater temperature well in all inshore reefs of this study. Nevertheless, it is important to note that there is a relatively large scatter of the datapoints and that at low temperatures (< 26°C) satellite data shows a cold-bias (data below 1:1 line, especially in the Votua Reef) and warm-bias (above 1:1 line), especially evident in Nananu-i-Ra and Fish Patch (Suva Reef) for both Pathfinder and CRW products. These small differences could indicate that a well-defined small scale temperature stratification is present in the first few meters (Pan et al. 2017), and this might be important during stress events, when only a few degrees can change the response of corals (Cooper et al. 2012). Although satellite data is similar across all three datasets, for this study we choose to work with OISST (Figure 2.22.) data due to it being a gap-free dataset completed with both satellite and in-situ measurements and show the best correlation with our in-situ data, although just marginally.

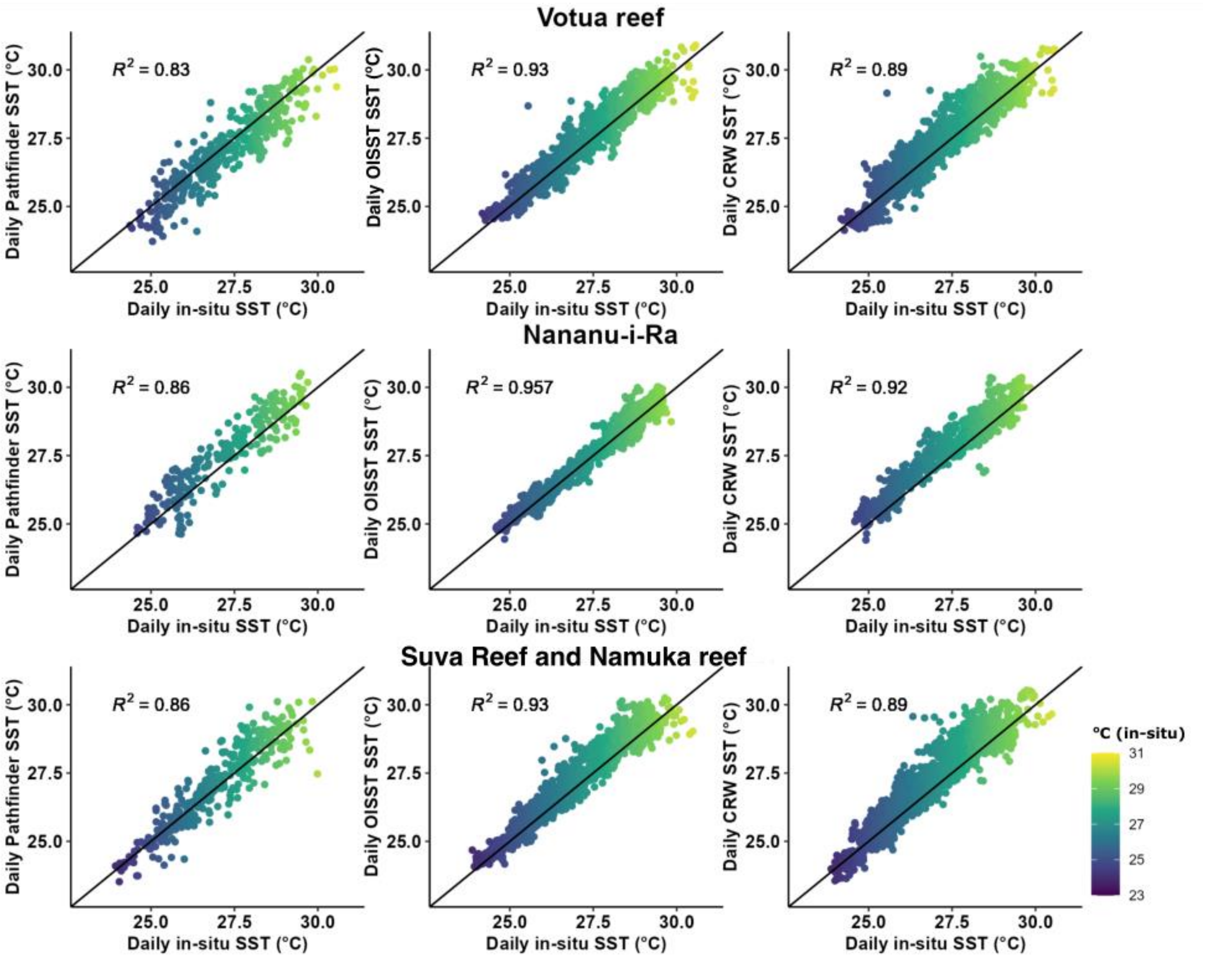

Figure 2.21. Scatterplot of seawater temperature data from in-situ loggers and remotely sensed SST data from Pathfinder, OISST and CRW product. Black line represents the 1:1 correlation line.

Table 2.12. Mean (and 2SE) SST and wind speed data from in-situ measurements and remote sensed data at each location.

	Votua reef		Nananu-i-Ra		Fish Patch		Namuka reef	
	Mean	2SE	Mean	2SE	Mean	2SE	Mean	2SE
SST in-situ	27.2	0.06	27.2	0.08	26.9	0.06	26.9	0.06
SST Pathfinder	27.1	0.06	27.1	0.06	27	0.07	27	0.07
SST CRW	27.3	0.03	27	0.03	27	0.03	27	0.03
SST OISST	27.4	0.03	27.4	0.03	27.1	0.03	27.1	0.03
Wind in situ	2.33	0.06	6.07	0.10	2.33	0.06	2.33	0.06
Wind satellite	2.03	0.02	6.25	0.07	5.34	0.05	3.82	0.11

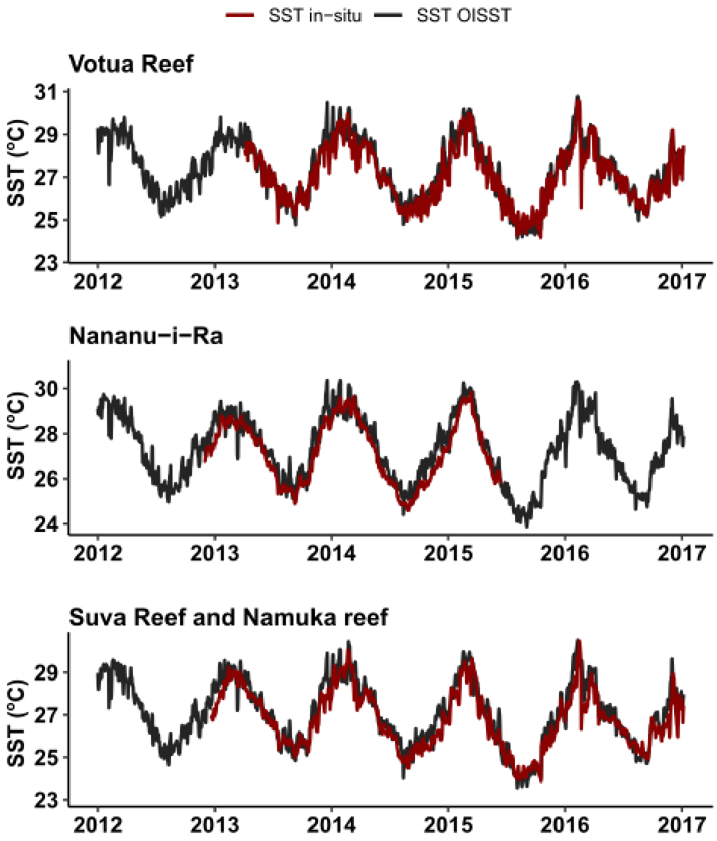

Figure 2.22. Daily SST data at each location from in-situ loggers (Red line) and OISST product (Grey line).

2.6.8.2. Wind

Mean wind data is similar between remotely sensed data and in-situ data in both the Votua reef and Nananu-i-Ra (Table 2.12.). However, notable differences are seen for the Namuka reef data (Δ = 1.49 m/s) and Fish Patch (Δ = 3.01 m/s). Paired correlations show high correlation of data (Figure 2.23.); however, data shows large scatter around the 1:1 line across the entire range of wind speeds, as well as a positive bias for remote sensed data in both Namuka and Suva Reef, where satellite product show higher wind speeds than in-situ data from Laucala Bay (Figures 2.23. and 2.24.). Wind speed conditions tend to be highly localised and can vary greatly across short distances, especially due to orographic effects on flow dynamics. In-situ values are measured in-land, while satellite values are taking from pixel data above the coast/inshore reefs, and therefore a difference in winds are to be expected. These results indicate that remotely sensed wind data can be representative of general conditions in the study locations, but absolute values should be interpreted with caution.

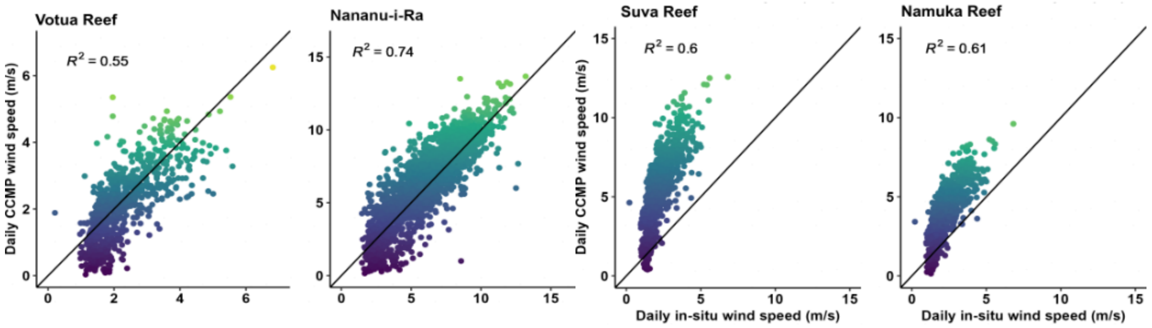

Figure 2.23. Scatterplot of wind speed data from in-situ loggers and remotely sensed data from CCMP product. Black line represents the 1:1 correlation line.

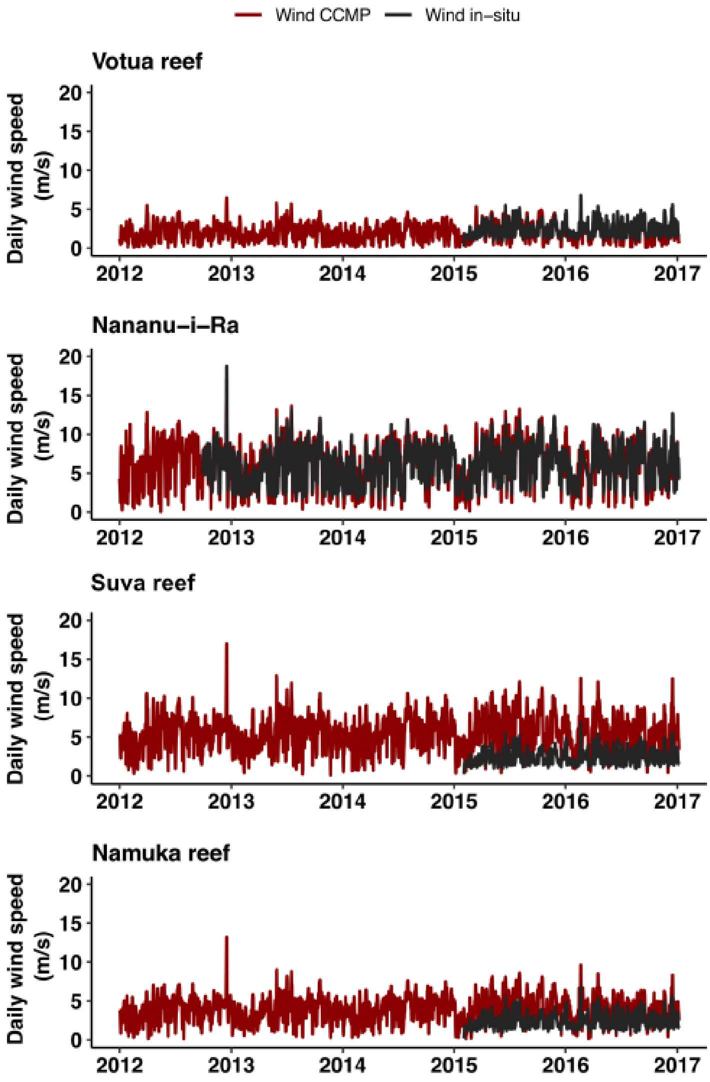

Figure 2.24. Daily wind speed data at each location from in-situ loggers (Red line) and CCMP satellite product (Grey line).

Chapter 3 | What if “acting locally” is not enough? Coastal turbidity and heat stress control coral growth in Fiji

> *There are many things in the deep waters; and seas and lands may change. And it is not our part here to take thought only for a season, or for a few lives of Men, or for a passing age of the world. We should seek a final end of this menace, even if we do not hope to make one.*
>
> Gandalf

Coral series #5 (MVL)

Chapter 3 | What if “acting locally” is not enough? Coastal turbidity and heat stress control coral growth in Fiji

Abstract

In this study we explore how coral growth in Fiji is linked to both local and global stressors. Twenty-eight *Porites* spp. cores from nine diferent regions across Fiji were analysed in this chapter. I explored the main environmental drivers of coral growth in these locations over the 1998 – 2016 interval. A linear relationship was found between annual linear extension and seawater turbidity (as K_d490 product), as well as annual calcification and seawater turbidity (GLM; $R^2 = 0.38$, $p < 0.001$ and $R^2 = 0.26$, $p < 0.001$ respectively).

Absolute and relative growth rates from cores of this project (ten cores collected in May 2017) were binned into five-year intervals. All locations show a significant decrease in linear extension and calcification rate (decreases of 12.50 – 19.40%) during the 2013 – 2016 period relative to the previous years (repeated-measurements ANOVA, $p < 0.01$). This decrease is triggered by elevated thermal stress (measured as DHW and SST during the summer months) experienced across all sites during the 2013 – 2016 period. Coral growth for each core was statistically modelled. Both seawater turbidity and average summer SSTs explained the observed absolute extension rates across the Fiji locations over the studied period (GAMM, pseudo-$R^2 = 0.76$, $p < 0.05$). These results suggest that the observed linear extension gradient across Fiji is controlled by seawater turbidity, but that heat stress plays an important role in driving interannual variability. Despite heat stress causing similar relative decreases in growth in most sites, it is important to note that the absolute values of coral growth differ across reef locations. We emphasise the importance of local land management in potentially reducing river runoff and coastal pollution in Fiji, but question whether the extent of this “local approach” to preserve positive net coral (and reef) growth can overcome the climate change driven conditions in the long term.

3.1. Introduction

Coral reefs play an important role in social, ecological, and chemical processes in marine and coastal ecosystems (Hoegh-Guldberg 1999; Cesar et al. 2003; Bates et al. 2010; Shaw et al. 2012). Reef-building corals are fundamental in sustaining reef structural complexity and diversity (Pratchett et al. 2008) and are therefore key in preserving the services these ecosystems provide. However, coral reefs are particularly vulnerable to disturbance (Hoegh-Guldberg 1999; Graham et al. 2006). An intensifying number of local and global threats, from overfishing and coastal pollution to climate change, are making reefs increasingly susceptible to damage and degradation (Burke et al. 2011).

In order to improve coral reef management, it is imperative to understand how reefs are responding to global change. Model predictions point towards an increase in seawater surface temperature (SST) in the tropics between 2 and 4°C over the next 100 years (IPCC 2021), and it is expected that worldwide reefs will experience severe thermal stress by 2050 (Meissner et al. 2012). By the end of the 21st century, nearly a third of the coral reefs around the world are likely to disappear due to both global and local stressors (Eyre et al. 2018). In a framework where at least 500 million people worldwide depend, to certain extent, on reef ecosystem services (Burke et al. 2011; Souter et al. 2021), there is a need to investigate the consequences of coral exposure to both acute and chronic environmental stressors. Maintenance of these ecosystems depends on the reef framework and reef accretion rates, which is determined by net coral growth of reef-building specimens.

Coral growth in reef-building massive corals (like *Porites* spp.) is dependent on several factors such as species, water depth, light availability, SST and water quality. *Porites* spp. corals mineralise their skeleton as aragonite, and most of them host dinoflagellate algae (*Symbiodinium*) within the polyps forming a symbiotic relationship (as reviewed by West and Salm 2003). Coral growth in massive corals results from the budding and extension of new polyps. The skeletal aragonite is then secreted by the epidermis of the lower part of the polyp (as reviewed by Drake et al. 2020), and the rate at which it is secreted is dependent on the sensitivity of the coral symbiont to environmental variability (DeCarlo and Cohen 2017). As a result, it has been observed that coral growth response to changing environmental conditions is both site and species-specific. Determining drivers of skeletal growth from coral records enables examinations of tolerance thresholds and helps predict the consequences of future climate and environmental change.

Coral growth is described by linear extension (cm/yr), average skeletal density (g/cm^3) and calcification rate (g/cm^2·yr) (Lough and Cooper 2011). Extensive work has shown that SST is one of the main drivers of coral growth (as reviewed by Lough and Cantin, 2014); however, other environmental variables can play an important control over growth rates beyond SST. Several studies have reported a declining trend in calcification rates of *Porites* spp. within inshore reefs in areas with strong anthropogenic impacts, and correlated with increasing SSTs across the Indo-Pacific from the ~1900s onwards (Cooper et al. 2008; Tanzil et al. 2013; D'Olivo et al. 2013; Su et al. 2016; Carilli et al. 2017). However, studies adressing long term trends in growth and calcification rates in both offshore reefs and inshore reefs with minimal human impact in the GBR, Western Australia and South West Pacific have not identified such declines with increasing SST (Cooper et al. 2012; D'Olivo et al. 2013; Carilli et al. 2017; Razak et al. 2019). This suggests that, although SST might generally drive coral calcification rates, local anthropogenic stressors (such as increased levels of sediments and nutrients) and poor coastal water quality might have a key role in diminishing resilience to current SST warming (Mora 2008; Carilli et al. 2009; Razak et al. 2019).

Reef managers use strategies aiming to mitigate local stressors (i.e., overfishing and diminished water quality) to buffer the damaging effect of climatic events and ocean warming on coral reefs (McLeod et al. 2019). While some of the extensive coral reef systems in Fiji have been identified as potential climate refuges, where future climate impact is expected to be less severe (Beyer et al. 2018), portions of these same reefs are experiencing considerable threats and impact from local stressors, in particular sediment and nutrient runoff, which are strongly linked to catchment land-use (Brown et al. 2017a, 2017b; Andrello et al. 2022). Identification of places where environmental conditions are favourable for coral growth will be critical for prioritizing locations for management action, for example through marine protected areas, to support the Fiji Government's national commitment to protect 30% of its waters by 2030 (Department of Environment, Government of Fiji 2020). However, the lack of understanding of environmental drivers of coral growth in Fijian reefs, where multiple environmental stressors interact, complicates adequate implementation of an integrated coastal management.

Here, I resolve this gap by identifying the environmental variables that have controlled coral growth in inshore reefs of Fiji between 1998 and 2016. I compile coral growth records from 28 *Porites* spp. cores collected from 9 different locations across Fiji. These include the ten *Porites* spp. cores collected for this project along with growth data from 18 other *Porites* spp. cores from Fiji available in the literature. The cores include those from inshore reefs adjacent to different catchments (different catchment size, land-use and cover) and offshore reefs with low terrestrial influence. I determine how coral linear extension rates have evolved over the past 19 years across space and time and relate changes to shifting environmental conditions experienced by reefs. Analysis of the data showed that both seawater turbidity and heat-stress act as drivers of coral growth across Fiji. Seawater turbidity controls growth rates across different locations whereas heat-stress plays an important role driving interannual variability.

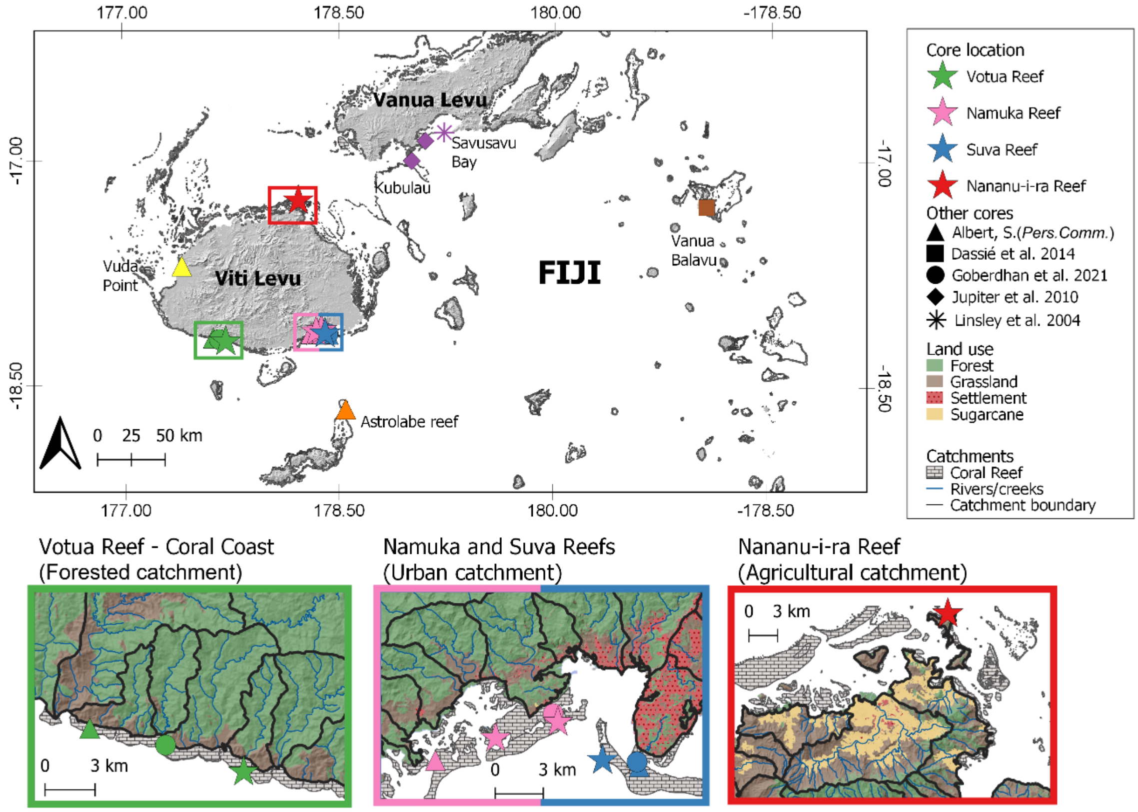

Figure 3.1. Map of Fiji and locations of cores in this study. Star symbols are locations of cores collected in this study. Other shapes are location of other cores with available data. Land colours correspond to land-use. Black demarcations are catchment areas.

3.2. Methods Summary

3.2.1. Reef locations and coral samples

In this study, I analyse coral growth records from 28 *Porites* spp. cores collected in nine different locations across Fiji (Figure 3.1.). These include the ten coral cores drilled in May 2017 from four different inshore reefs around Viti Levu for this project. Two of the cores were collected in the Votua Reef, along the Coral Coast (South Viti Levu); three cores were collected along the Namuka Reef (South East Viti Levu); one core was collected in Fish Patch, in the Suva Reef (South East Viti Levu); and four cores were collected on a reef in Nananu-i-Ra island (North East Viti Levu). To increase the amount of coral growth data from Fiji and validate our observed growth rates we also include data from other coral core records from Fiji available in the literature: i) eight *Porites* spp. cores collected in November 2005 from four inshore reefs in Viti Levu (two cores from Vuda Point, West Viti Levu; two cores from the Namada Reef, on the Coral Coast, South Viti Levu; two cores from the Muaivuiso Reef, South East Viti Levu; and two cores from Dennis Patch in the Suva Reef, South East Viti Levu), and two cores from a fringing reef in Dravuni island (Great Astrolabe Reef) (S. Albert, *Pers. Comm.*); ii) three *Porites* spp. cores from three inshore reefs in Viti Levu (Namolevu Beach Bures in the Coral Coast, Namuka, and Dennis Patch reefs) collected in 2018 (Goberdhan and Kininmonth 2021); iii) two *Porites* spp. cores retrieved from two different reefs near Kubulau (Vanua Levu) in 2006 (Jupiter et al. 2010); iv) one *Porites* spp. cores from an inshore reef in Savusavu Bay (Vanua Levu) collected in 2001 (Linsley et al. 2006); v) and two *Porites* spp. cores from Vanua Balavu Island (Dassié et al. 2014) collected in 2000 and 2004. More information on these samples can be found in Chapter 2 – Section 2.3.3.; Table 2.1. In this chapter we use ‘Coral Coast’ when referring to all samples available from this region (VOT17_1, VOT17_2, NM3, NM4 and CC; Table 3.1.), and ‘Votua Reef’ when we are only referring to the cores collected for this project in May 2017 (VOT17_1, VOT17_2).

Table 3.13. Average growth parameters and environmental variables for each coral core included in this chapter References for each coral core: [1] This study; [2] S. Albert (*Pers. Comm.*); [3] Goberdhan et al. 2021; [4] Jupiter et al. 2010; [5] Linsley et al. 2006; [6] Dassié et al. 2014.

Location	Core ID	Linear Extension (cm/yr)	Density (g/cm^3)	Calcification (g/cm^2 · yr)	Time span	Distance to coast (km)	Catch. area (km^2)	Forest cover (%)	SST (^{o}C)	SST summer (^{o}C)	K_d490 (m^{-1})	Chl-a (mg/l)	Rainfall (mm)	Wind speed (m/s)
Coral Coast (Votua Reef)	VOT17_1 [1]	1.42	1.47	2.08	1998 - 2016	0.9	10 - 35	80	27.06	28.67	0.03	0.17	2981.45	2.03
	VOT17_2 [1]	1.60	1.43	2.29	1998 - 2016	0.9	10 - 35	80	27.06	28.67	0.03	0.17	2981.45	2.03
Coral Coast (Other)	NM3 [2]	1.30	1.21	1.53	1998 - 2004	0.5	10 - 35	80	26.92	28.63	0.04	0.18	2939.30	2.03
	NM4 [2]	1.59	1.22	1.94	1998 - 2004	0.5	10 - 35	80	26.92	28.63	0.04	0.19	2939.30	2.03
	CC [3]	1.37	--	--	2003 - 2016	0.4	10 - 35	80	27.10	28.65	0.03	0.16	2951.86	2.03
Nananu-i-Ra	NAN17_1 [1]	0.75	1.59	1.24	1998 - 2016	0.3	20 - 100	13	27.07	28.50	0.07	0.54	2368.36	6.25
	NAN17_2 [1]	0.90	1.74	1.55	1998 - 2016	0.3	20 - 100	13	27.12	28.53	0.07	0.54	2389.01	6.25
	NAN17_3 [1]	0.81	1.86	1.49	1998 - 2016	0.3	20 - 100	13	27.07	28.50	0.07	0.54	2368.36	6.25
	NAN17_5 [1]	0.71	1.61	1.14	1998 - 2016	0.4	20 - 100	13	27.07	28.50	0.07	0.54	2368.36	6.25
Namuka Reef	NAV17_1 [1]	1.04	1.76	1.82	1998 - 2016	1.3	6.5 - 30	70	26.94	28.48	0.05	0.33	2981.45	3.82
	NAM17_1 [1]	1.12	1.48	1.66	1998 - 2016	2.8	6.5 - 30	70	26.95	28.51	0.05	0.34	2990.43	3.82
	NAM17_2 [1]	1.08	1.51	1.63	1998 - 2016	2.8	6.5 - 30	70	26.94	28.48	0.05	0.33	2981.45	3.82
	MV1 [2]	1.45	1.30	1.88	1998 - 2004	1.8	6.5 - 30	70	26.84	28.42	0.05	0.30	2939.30	3.82
	MV2 [2]	1.32	1.22	1.61	1998 - 2004	1.8	6.5 - 30	70	26.84	28.42	0.05	0.30	2939.30	3.82
	NV [3]	1.15	--	--	1998 - 2016	0.8	6.5 - 30	70	26.95	28.50	0.05	0.33	2992.84	3.82
Suva Reef (Fish Patch)	FP17_1 [1]	0.77	1.56	1.23	1998 - 2016	2.4	10 - 20	5	26.94	28.48	0.06	0.05	2981.45	5.34
Suva Reef (Dennis Patch)	DP1 [2]	1.13	1.11	1.24	1998 - 2004	0.8	10 - 20	5	26.84	28.42	0.06	0.40	2939.30	5.34
	DP2 [2]	0.75	1.41	1.06	1998 - 2004	0.8	10 - 20	5	26.84	28.42	0.06	0.40	2939.30	5.34
	DP [3]	0.97	--	--	1998 - 2016	1.0	10 - 20	5	26.92	28.44	0.06	0.44	2888.86	5.34
Vuda Point	VP1 [2]	1.29	1.06	1.37	1998 - 2004	2.3	30 - 200	30	27.00	28.76	0.06	0.38	2939.30	2.69
	VP2 [2]	1.00	1.22	1.22	1998 - 2004	2.3	30 - 200	30	27.00	28.76	0.06	0.38	2939.30	2.69

Location	Core ID	Linear Extension (cm/yr)	Density (g/cm^3)	Calcification ($g/cm^2 \cdot yr$)	Time span	Distance to coast (km)	Catch. area (km^2)	Forest cover (%)	SST (°C)	SST summer (°C)	K_d490 (m^{-1})	Chl-a (mg/l)	Rainfall (mm)	Wind speed (m/s)
Great Astrolabe Reef (Dravuni)	DR1 [2]	1.29	1.22	1.57	1998 - 2004	>10	0.8	35	26.34	28.23	0.05	0.39	2157.60	--
	DR2 [2]	1.36	1.14	1.54	1998 - 2004	>10	0.8	35	26.34	28.23	0.05	0.39	2157.60	--
Kubulau	S2S1 [4]	1.08	--	--	1998 - 2005	3.5	50	70	26.75	28.37	0.06	0.40	1982.91	5.75
	S3S3 [4]	0.65	--	--	1998 - 2005	10.4	50	70	26.75	28.37	0.06	0.47	1982.91	5.75
Savusavu Bay	AB [5]	1.20	1.86	2.23	1998 - 2001	7.3	15 - 200	10-70	26.75	28.37	0.05	0.21	2363.50	5.75
Vanua Balavu	FVB1-H4 [6]	1.69	--	--	1998 - 1999	5.4	50	35	26.98	28.49	0.04	0.19	2157.60	--
	FVB2-H1 [6]	0.73	--	--	1998 - 1999	5.4	50	35	26.98	28.49	0.04	0.21	2491.00	--

Continuation **Table 3.1.** Average growth parameters and environmental variables for each coral core included in this chapter References for each coral core: [1] This study; [2] S. Albert (*Pers. Comm.*); [3] Goberdhan et al. 2021; [4] Jupiter et al. 2010; [5] Linsley et al. 2006; [6] Dassié et al. 2014.

3.2.2. Quantification of coral growth parameters

Growth parameters from coral cores collected in May 2017 were extracted from X-ray CT scans. A detailed description of the methods is found in Chapter 2 – Section 2.4.2. In summary, annual linear extension values (cm/yr) were obtained from X-ray images, by measuring distance between visible high-density bands. This was aided by developing a density profile (g/cm^3) along the major growth axis and measuring the distance between density maxima. The calcification rate (g $CaCO_3$/cm^2·yr) was also obtained as a product of the previous two growth parameters.

The methods used to obtain growth parameters from the other Fijian *Porites* spp. cores available in the literature are detailed as follows. The coral cores collected by Dr S. Albert in November 2005 were sliced lengthwise using a diamond-tipped circular saw into 7 mm thick ‘slabs’ at the Australian Institute of Marine Science (AIMS) and X-rayed at the Wesley Hospital (Townsville, Australia). Density measurements along the major growth axis were obtained from a combined X-ray densitometer/luminometer. Annual linear extension was obtained measuring distance density maxima by using Coral XDS software.

Only linear extension data was available from the cores collected in Kubulau (Vanua Levu) (Jupiter et al. 2010). These cores were cut into ~7 mm thick slabs and X-rayed at Australian National University (ANU) and the core chronologies were established by measuring distance between high-density bands.

Linear extension data from *Porites* spp. samples in Goberdhan and Kininmonth (2021) were obtained by first slicing the coral cores in ~7 mm slabs and then taking X-rays of the slabs at the College of Medicine, Nursing and Health Sciences Department of Medical Imaging Science in Suva (Fiji). Annual extension was measured as the distance between consecutive high-density bands. Importantly, in this study, I do not use the linear extension rates published by (Goberdhan and Kininmonth 2021). Instead, I reinterpreted their X-ray images and re-measured distance between seasonal high-density bands due to a discrepancy of methods. I argue that in some locations (Coral Coast and Namuka), Goberdhan and Kininmonth’s (2021) measurements of linear extensions are based on sub-seasonal density variability (e.g., monthly bands and/or dissepiments), which are clearly visible in these cores due to the high extension rates (see an example of the new chronologies in Appendix B).

For the *Porites* spp. sample from Savusavu Bay (Vanua Levu) (Linsley et al. 2006, 2019), annual linear extension rates were obtained from $\delta^{18}O$ and Sr/Ca data, by measuring the distance between signal minima and maxima and tying points with SST data (Linsley et al. 2006). Density measurements were carried out by CT scanning the coral slabs at the Albany Advanced Imaging Center, New York. Average density was measured at five-year intervals over an area approximately covering 2 years of growth (Linsley et al. 2019).

Finally, only linear extension rate data are available from the coral cores from Vanua Balavu. These were obtained from $\delta^{18}O$ measurements along the major growth axis, by linking the lightest $\delta^{18}O$ in each seasonal cycle to the warmest month of the year and measuring the distance between these points (Dassié et al. 2014).

One of the aims of this study is to pair and compare growth across all Fijian sites for which growth data is available. For our compilation, we use annual linear extension rates as a measurement of coral growth rather than coral calcification. While coral calcification can be considered a more comprehensive measurement of coral growth (as it is calculated from both linear extension and density), *Porites* spp. data shows a strong correlation between calcification and linear extension ($R^2 > 0.90$; Figure 3.3.), indicating that linear extension can represent growth in this genus. In addition, we encounter two complications. First, not all available *Porites* spp. cores have density measurements, but for all of them it was possible to obtain annual extension data. Second, where density data is available, different methods were used to obtain the densities (CT scans + hydroxyapatite standard, CT scans + coral standards, X-ray densitometry) and previous work has found the existence of an offset between density measurements obtained by different methods. Due to a lack of inter-method and inter-laboratory calibrations for density quantification, comparison of absolute density and calcification rates between studies is difficult. DeCarlo et al. (2015a) successfully obtained absolute density values from *Porites* spp. cores by using coral standards of known density during the CT-scanning. Carilli et al. (2017), on the other hand, while calibrating using a hydroxyapatite standard, noted an overestimation of CT-derived density of 12% relative to buoyant weights from the same samples. Corallite size and microporosity seem to play a key role when determining bulk skeletal density (Carilli et al. 2017) and could be the source of these differences. However, resolving methodological differences in density quantification are beyond the scope of this study.

Absolute calcification data is also collected here but exclusively for cores in this study (i.e., cores collected in May 2017). Relative linear extension and calcification rates are calculated for the coral cores of this study by normalising single annual records to the mean over the 1998 – 2016 period (reported as % change). Relative growth changes per location are calculated by obtaining the arithmetic mean of relative growth from all cores from a given location. Composite relative growth for Fiji is obtained by applying the arithmetic mean to the annual relative growth of all the cores. Five-year binned data is calculated as the arithmetic mean of annual relative growth in intervals of five years.

3.2.3. Environmental data

Instrumental environmental data available for the study period 1998 – 2016 and land cover data for the year 2015 were also included in this study. Full details on the sources of environmental data can be found in Chapter 2 – Section 2.6.

In summary, I used daily SST data derived from OISST for every location. Annual average SSTs were calculated as the arithmetic mean of daily data. Summer average SSTs were calculated as the arithmetic mean of daily SSTs during the climatologically warmest months of the year (i.e., January, February, March, April). SST anomalies were obtained by calculating the difference between composite SSTs (annual or summer averages) and SST climatology for the studied period (1998 – 2016) for either annual or summer-month intervals. Five-year binned data are calculated as the arithmetic mean of annual SSTs in intervals of 5 years. Cumulative thermal stress at each location was obtained as daily DHW from the CRW database. For analysis of data in yearly intervals (annual data) I use the maximum DHW recorded for said year. Five-year binned data are calculated as the maximum DHW recorded for each five-year interval. Water quality at each location was characterised from Level-3 daily satellite ocean colour (OC) data (SeaWiFS and MODIS) and included the diffuse attenuation coefficient at a wavelength of 490 nm (K_d490, m^{-1}) and chlorophyll-a concentration (mg/m^3). Annual averages of both parameters were calculated as the arithmetic mean of the daily data from each year. Five-year binned data were calculated by averaging annual means in five-year intervals. Although in the results we report average values of both K_d490 and chlorophyll-a concentration we use only K_d490 for building statistical models due to the close correlation between these two parameters ($R^2 = 0.93$) across all locations of this study (See Methods Chapter – Section 2.6.4.).

3.2.4. Statistical modelling

ANOVA tests were used to test whether annual growth rates within reefs were statistically different. Average absolute annual growth was then calculated at each location by averaging across cores. Generalised Linear Models (GLM) were used to examine the relationship of SST, DHW and seawater turbidity with annual growth data. Annual growth data from each coral core was standardised before applying GLM to assess trends over time at each location. Five-year binned data were calculated to allow for high interannual variability in growth rates. A repeated measurements ANOVA test was used to identify reef-specific significant changes in growth during each time period. A Generalised Additive Mixed Model (GAMM) was used to examine the relationship between each coral growth and the local environmental variables during the period 1998 – 2016. All statistical analyses were performed in R.

3.3. Results

Annually resolved coral growth data (linear extension, calcification) were compared with different key environmental variables (seawater turbidity, SST, thermal stress) to investigate the main drivers of coral growth during the interval 1998 – 2016, both between locations and across time. The 1998 – 2016 interval is chosen as it is the maximum common period to all coral cores of this study.

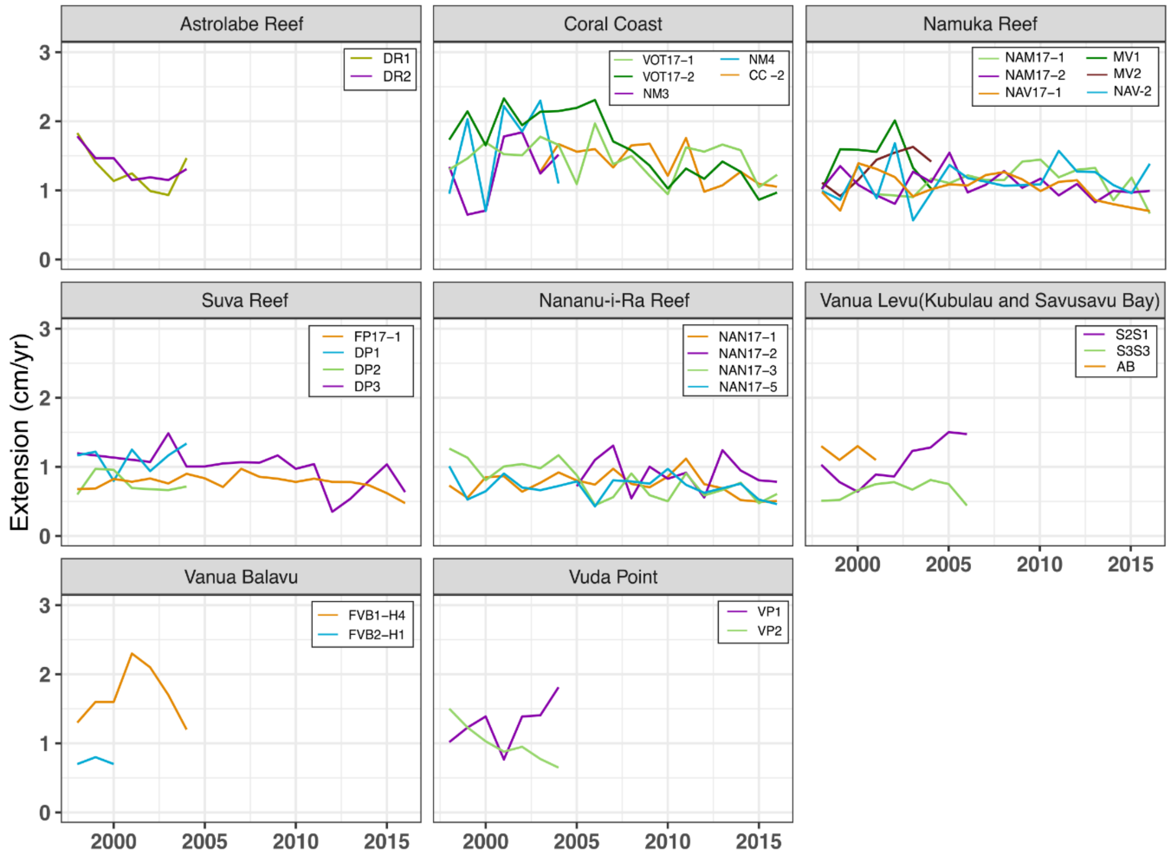

Figure 3.2. Annual linear extension data from all the cores used in this study for the period 1998-2016.

3.3.1. Spatial gradients of environmental variables and coral growth

For the 1998 – 2016 period, a gradient in the average annual linear extension is observed, with the Votua Reef experiencing the highest extension rates, and Nananu-i-Ra the lowest (Table 3.1.; Figure 3.2.). Average linear extension rate is 1.49 cm/yr (SD = 0.53) in the cores from Votua Reef, 1.48 cm/yr (SD = 0.54) in those from Vanua Balavu, 1.30 cm/yr (SD = 0.11) in the Great Astrolabe Reef corals, and 1.13 cm/yr (SD = 0.30) in cores from Vuda Point. For corals in the Namuka Reef and Suva Reef, the average linear extension rates are 1.10 cm/yr (SD = 0.33), and 0.82 cm/yr (SD = 0.21), respectively. In Savusavu Bay, the average linear extension rate is 0.87 cm/yr (SD = 0.34) and in the Nananu-i-Ra Reef, the corresponding value is 0.75 cm/yr (SD = 0.17). Annual average densities are 1.50 g/cm^3 (SD = 0.10) in the Votua Reef cores and 1.57 g/cm^3 (SD = 0.08) in the cores from the Namuka Reef. The Suva reef recorded an average density of 1.68 g/cm^3 (SD = 0.08). Average skeletal density in the Nananu-i-Ra cores was found to be 1.75 g/cm^3 (SD = 0.11). Calcification rates are 2.23 g/cm^2 yr (SD

= 0.78) in the Votua Reef, 1.72g/cm^2 yr (SD = 0.71) in the Namuka reef, 1.37 g/cm^2 yr (SD = 0.36) in the Suva reef, and 1.31 g/cm^2 yr (SD = 0.63) in the Nananu-i-Ra reef.

Based on the corals of this study (annual growth from 1998 – 2016) and other corals with both available linear extension and density data (data from 1998 until collection year), we found that linear extension was significantly correlated with calcification rate (R^2 = 0.89, $p < 0.0001$), and, to some extent, inversely correlated with density (R^2 = 0.10, $p < 0.0001$). No correlation was found between density and calcification rates (R^2 = 0.00, $p > 0.1$) (Figure 3.3.).

To be able to compare growth rates of corals collected for this study with those calculated from published data from other cores (with only annual linear extension rates available), we focus solely on linear extension. A linear relationship was observed between average extension at each location and seawater turbidity at both annual and five-year binned data (R^2 = 0.38, $p < 0.001$, R^2 = 0.65, $p < 0.001$; Figure 3.4.). No significant relationship was found between annual average linear extension and SST ($p > 0.1$; Figure 3.4.).

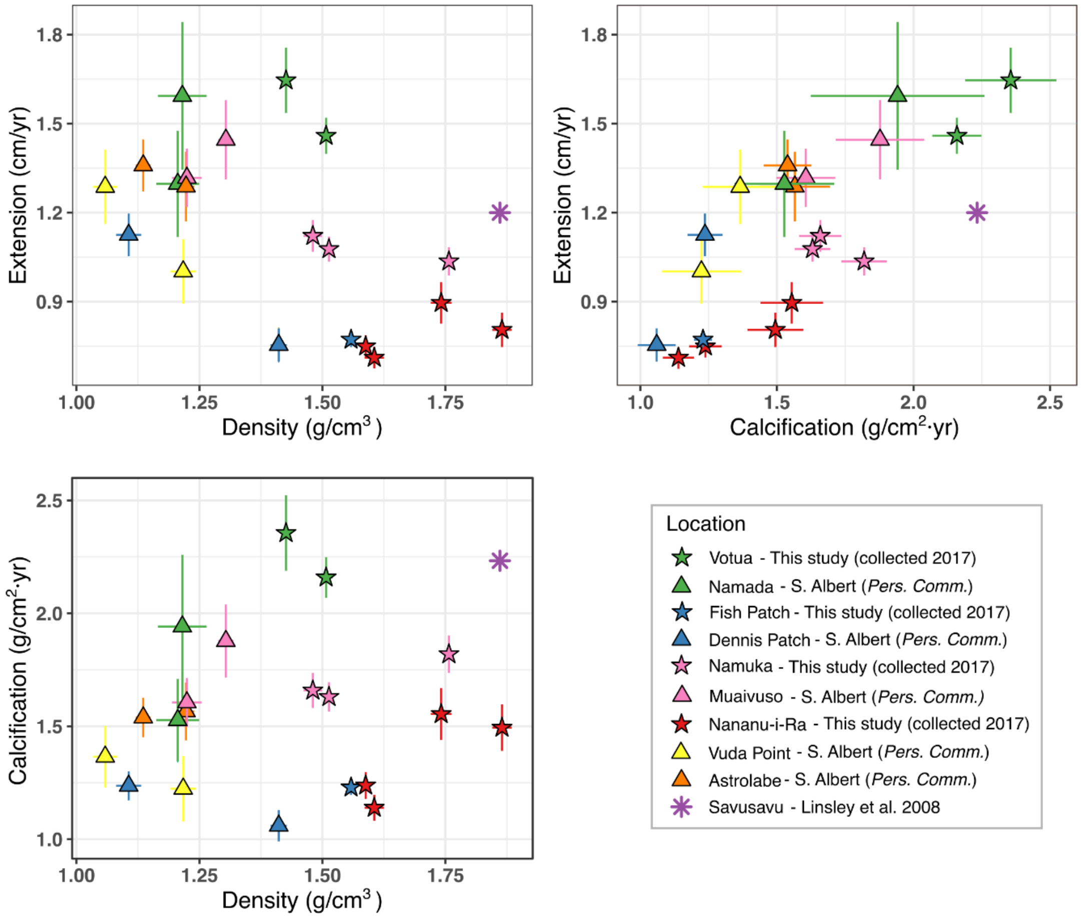

Figure 3.3. Average growth parameters for 21 cores for the period 1998-2016. Includes only cores with both linear extension and density data available. Triangles represents cores from this study collected in 2005, with density obtained via densitometer. Stars represents cores from this study collected in 2017 and density obtained via CT imaging.

Absolute SST and SST seasonality are similar across all locations. There is a warming trend between September and February reaching a maximum monthly mean of 28.5°C, and cooling SSTs between March and August, with a minimum monthly mean of 25.1°C. Mean annual SSTs were similar across sites, with a maximum difference of 0.3°C. Unlike SST, annual K_d490 and chlorophyll-a (chl-a) concentrations recorded at each location presented clear differences, with a gradient of turbidity linked to total catchment area and percentage of catchment covered by mature forest (Table 3.1.). In general, the reefs at Votua (small catchment, high forest cover, low population) and Vanua Balavu Island consistently show the lowest mean values for both K_d490 and chl-a (0.035 m^{-1}, 0.17 mg/m^3 and 0.034 m$^{-1,}$ and 0.17 mg/m^3 respectively). The Nananu-i-Ra Reef (large catchment area, high agricultural land cover and highly populated) registered the highest mean values for K_d490 (0.071 m^{-1}) and chl-a (0.54 mg/m^3). The seasonality pattern for both seawater turbidity and chl-a is also different across sites (See Methods Chapter – Section 2.6 and Figure 2.14). For example, the Votua Reef and Namuka Reef experience maximum and minimum annual turbidity during Dec-Jan and Jul-Aug respectively. Conversely, the Nananu-i-Ra Reef (and the Suva Reef to a lesser extent) experiences peak turbidity values during Dec-Jan, and again in May-Jun. Registered seasonal rainfall values at each location followed the expected climatological regimes (wetter on the windward side; drier on the leeward side). Average seasonal rainfall at the Laucala Bay rainfall station (this data is coupled to Votua, Namuka and Suva Reefs coral growth) was 2000 mm in the wet season and 1500 mm in the dry season. At the Penang Mill rainfall station (data coupled to Nananu-i-Ra coral data), average rainfall is 1800 mm and 500 mm in the wet and dry seasons, respectively. Rainfall for other locations were not available. Annual average wind speeds also differed between locations, with the lightest winds registered at the Votua Reef (2.24 m/s) and the strongest winds in Nananu-i-Ra (6.07 m/s). Seasonality in wind speed was similar across locations, with wind minima being observed between January and February, a sharp increase in April, and speeds remaining high until November. The watersheds that discharge in the vicinity of each studied reef have different land use and land cover, as well as different extension rates (Figure 3.1.; Table 3.1.). Watersheds discharging to the south coast of Viti Levu (Votua Reef, Namuka Reef and Suva Reef) are smaller (between 10 and 35 km^2 on average) and have smaller rivers/creeks than watersheds that drain to the north coast and discharge near the Nananu-i-Ra reef (90 km^2 on average).

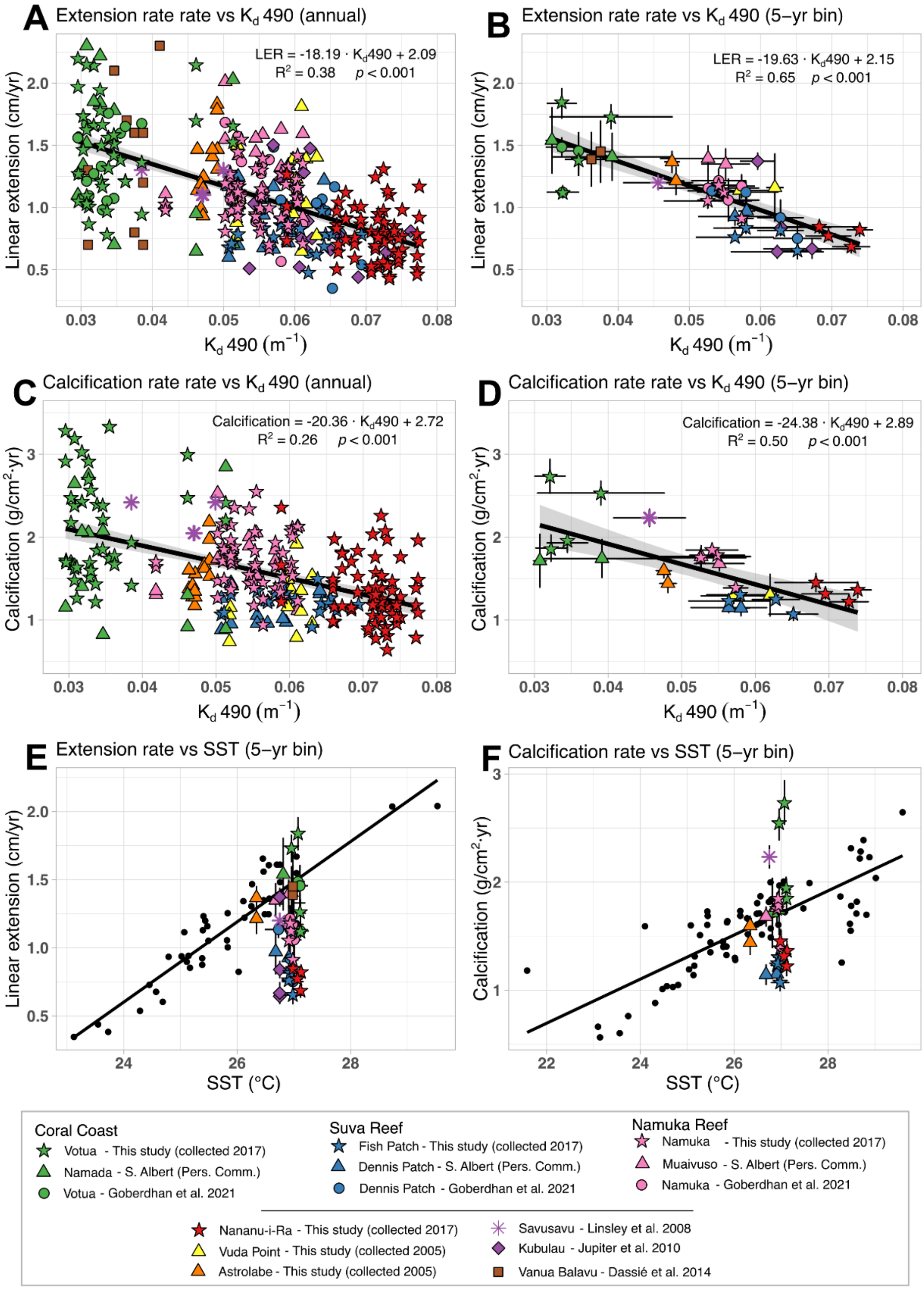

Figure 3.4. (A) Raw annual linear extension data from all cores. Linear extension v. seawater turbidity, (B) five-year bin of linear extension vs seawater turbidity from all cores, (C) Raw annual calcification from all cores v. seawater turbidity, (D) five-year bin of annual calcification v. seawater turbidity, (E) five-year r bin of linear extension rate v. SST and (F) five-year bin calcification rate v. SST. Only a significant relationship between linear extension and turbidity is observed. Black datapoints in (E) and (F) are from Lough et al. 2014 and represent annual average data from *Porites* spp. in the GBR. Annual extension and calcification of *Porites* spp. in the GBR follow a relationship with SST.

3.3.2. Temporal variability in environmental variables and coral growth

Over the period 1998 – 2016, daily SSTs across Fiji do not show any trend (See Chapter 2 – Section 2.6.1.). However, elevated heat stress (DHW > 5) is observed across all sites in 2000, 2002, 2009 and 2014 to 2016 (Figure 3.7). No significant trends are observed for daily seawater turbidity and chl-a concentrations over the same period at any of the locations (See Chapter 2 – Section 2.6.4; Figures 3.5. and 3.6.). Furthermore, no trends are observed for daily accumulated rainfall or wind speed during the 1998 – 2016 period (See Chapter 2 – Section 2.6.3.).

Temporal variability was assessed only for the coral cores of this study (covering the 1998 – 2016 period). A significant temporal decrease in extension rate was found at both the most (Nananu-i-Ra) and the least (Votua Reef) turbid reefs with respective changes of 23.9% and 54.9% (GLM, $p < 0.05$). No significant trend was found between annual extension (%) and time for the Suva and Namuka Reefs over the 1998 – 2016 period (GLM, $p > 0.1$). As high interannual variability between specimens can complicate the assessment of long-term trends, annual data was binned into five-year time intervals (1998 – 2002, 2003 – 2007, 2008 – 2012 and 2013 – 2016).

The five-year binned data across all sites showcase a significant decrease in linear extension rate during the 2013 – 16 interval relative to the previous five-year periods (repeated measurements ANOVA, $p < 0.01$) (Figures 3.5. and 3.6.). Coral linear extension rate decreased by 19.40% at Votua Reef, 17.60% at Namuka Reef, 12.50% at Suva Reef and 18.50% at Nananu-i-Ra Reef, relative to the average. Additionally, there was a decrease of 10% in the Votua Reef records during the interval 2008 – 2012 that is not reflected in any other location.

Using a Generalised Additive Mixed Model (GAMM) (Eq. 1), we demonstrate that observed records of coral growth in Fiji in five-year intervals are explained by both seawater turbidity and SST during the warmest months (Jan, Feb, Mar, Apr) over the studied time period (pseudo-$R^2 = 0.76$, $p < 0.05$) (Figure 3.7.):

$$\text{Linear extension} = K_d490 + \text{SST summer} + s(5yr),\ \text{random} = \sim 1|\text{Reef}$$

where the fixed components of the model were K_d490, SST summer and the five-year bin. K_d490 and SST summer variables represent annual average seawater turbidity and average SST between January and April. The variable 5yr is used to account for the time-series nature of the dataset. The random component of the model (i.e., "Reef") represents the location where each coral core was collected, and it is included to account for the non-independency measurements between these cores and limit auto-correlation.

These results suggest that the observed linear extension gradient across Fiji is controlled by seawater turbidity, but that heat stress plays an important role in driving interannual variability.

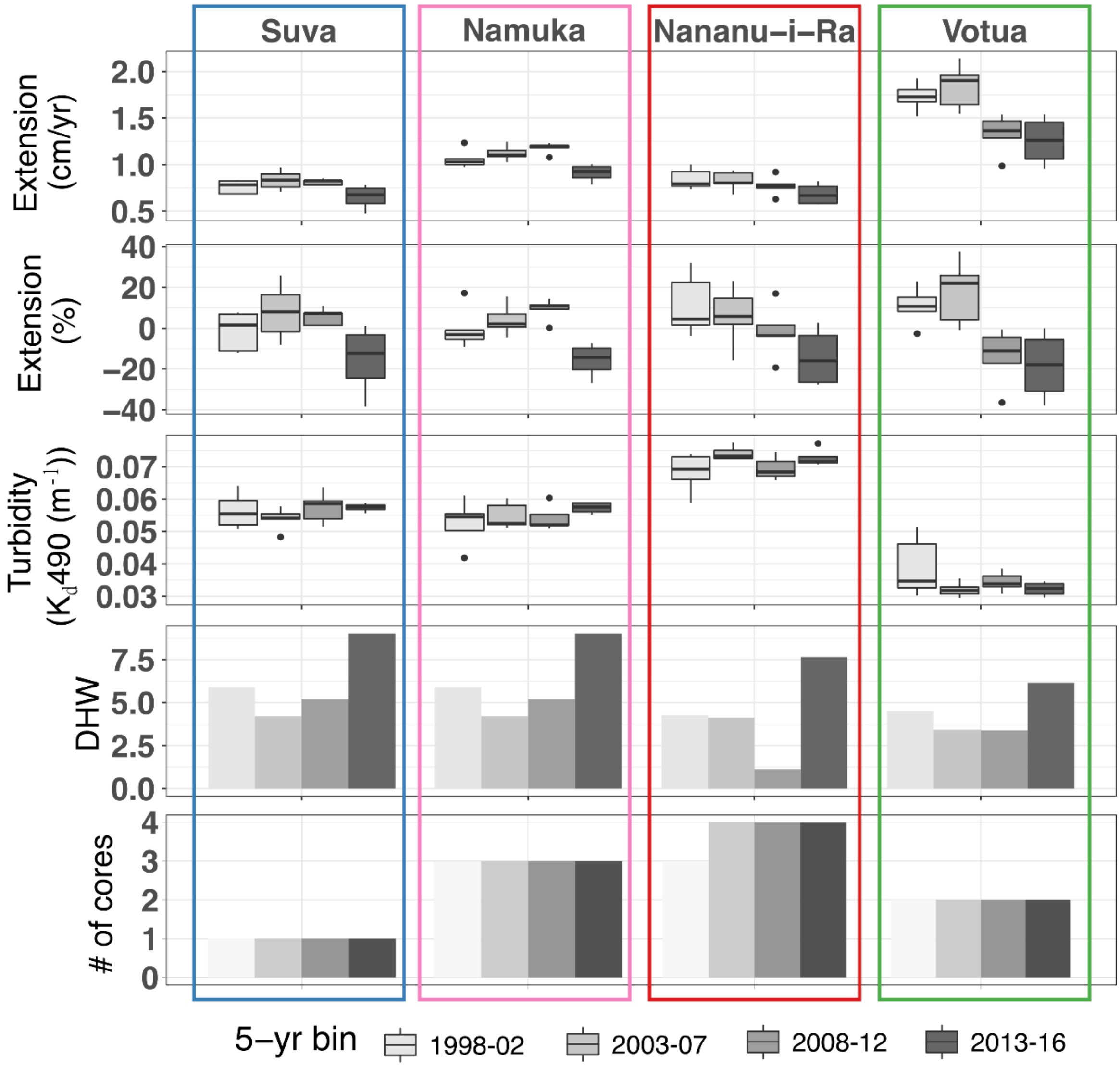

Figure 3.5. Five-year averaged data for observed absolute (cm/yr) and relative (%) extension rates, seawater turbidity and DHW at each location, also including number of cores within each data bin. This analysis includes only cores from this study collected in 2017.

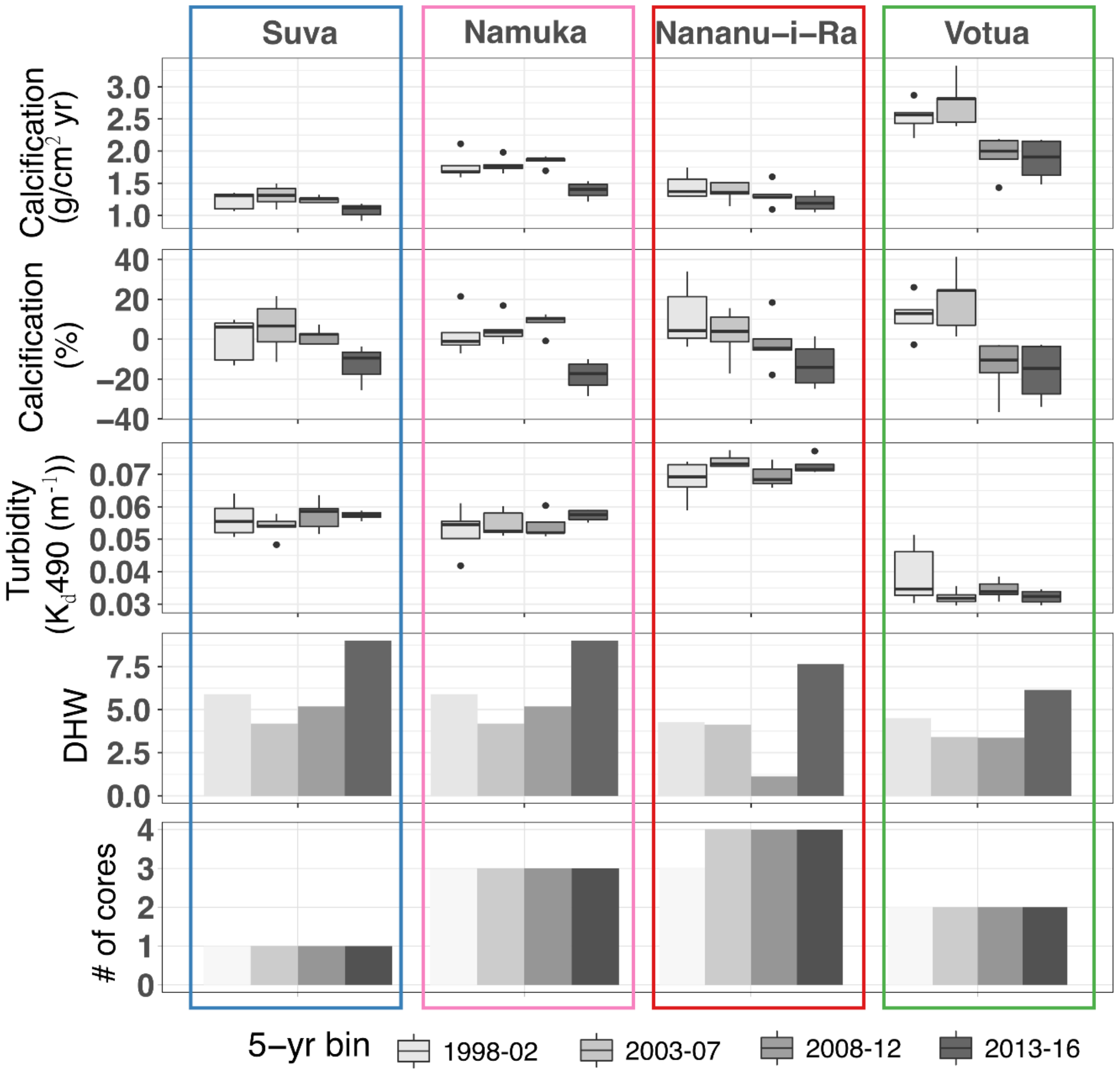

Figure 3.6. Five-year averaged data for observed absolute (g/cm^2 yr) and relative (%) calcification rates, seawater turbidity and DHW at each location, also including number of cores within each data bin. This analysis includes only cores from this study collected in 2017.

3.4. Discussion

This study shows that seawater turbidity and heat stress are the main drivers of coral growth at the surveyed sites in Fiji. In the framework of climate change, SSTs are predicted to keep increasing in Fiji and although this increase is likely to be <1°C by 2030 (relative to 1990), by the end of the century it is predicted to increase between 1.3 and 2.4°C (Australian Bureau of Meteorology and CSIRO 2011). Accumulated rainfall during the wet season is also projected to increase over the course of the 21st century, and extreme rainfall events are predicted to increase in intensity and frequency (Australian Bureau of Meteorology and CSIRO 2011); this is likely to cause increased sediment input to nearshore environments and therefore increased turbidity. Because of the link between turbidity and coral growth shown in the results of this study, reef growth is likely at risk as turbidity increases.

Here, I examine the relationship between seawater turbidity and the spatial growth gradient and then discuss the relationship between temporal growth variability and elevated heat-stress events. Importantly, we did not find significant interaction effects between seawater turbidity and heat-stress, and growth anomalies triggered by high heat-stress periods were found in all locations regardless of water quality. Yet, it is imperative to acknowledge that *Porites* spp. corals at the more turbid reefs are at higher risk of growth cessation due to an already low annual growth rate. For this reason, determining what controls seawater turbidity in Fijian inshore reefs is key to improve reef management strategies in the face of climate change and the expected projections for Fiji.

3.4.1. Spatial gradients in coral growth are linked to coastal turbidity

The observed relationships between growth parameters, with linear extension and calcification being strongly correlated, and no significant correlation between density and calcification, have been widely observed in *Porites* spp. corals (e.g., Scoffin et al. 1992; Lough and Barnes 2000; Elizalde-Rendón et al. 2010). Annual extension rate, as used in this study, is a reliable indicator for describing annual coral growth and it has been used as such in a number of studies on annual to centennial timescales (e.g., Tanzil et al. 2009; Cooper et al. 2012).

Environmental conditions have an important influence over annual growth parameters in *Porites* spp. corals (Barnes and Lough 1992; Lough and Cooper 2011). In particular, several studies have shown that linear extension and calcification rates in this genus tend to linearly increase with SST in the GBR (Lough and Barnes 1997; Lough 2008), French Polynesia (Bessat and Buigues 2001) and South China Sea (Nie et al. 1997). However, more recent evidence points towards a disruption of this increasing growth trend once a given SST threshold is reached (e.g., Tanzil et al. 2009), after which the coral experiences thermal stress causing reduced growth, bleaching and ultimately coral mortality (Lough and Cantin 2014). However, other variables also exert some degree of control over growth and extension rates (e.g., light intensity; as reviewed by Lough and Cooper 2011).

In Fiji, there is a clear gradient in the recorded annual extension rates across locations (Figure 3.4. A and B). Goberdhan and Kininmonth (2021) also observed a gradient in linear extension rate across different reefs in Fiji, and they attributed this to latitudinal changes. However, the rates originally provided by these authors (Coral Coast ~6 mm/yr, Namuka ~9 mm/yr, Suva Harbour ~5 mm/yr) do not agree with our average rates by location. This is especially true in the Coral Coast (Votua Reef) and Navakavu (Namuka Reef) where Goberdhan and Kininmonth (2021) report the lowest annual extension rates while the cores in this study from these approximate locations have among the highest annual linear extension rates of the entire dataset. Upon reinterpretation of their core chronologies, the new annual extension rates are 1.37 cm/yr in the core from the Coral Coast, 1.15 cm/yr in the Navakavu core (Namuka Reef), and 0.96 cm/yr in the Dennis Patch core; these values are much closer to those from cores in this study. These new values, however, do not show a decreasing trend in linear extension rate with increasing latitude and cannot possibly explain the gradient across all locations considered in this study.

SST alone cannot be the driver of our observed differences in coral growth, as SSTs across all the study locations are similar in terms of absolute values and seasonal profile. In fact, only the growth rates from the cores collected in the Votua Reef and Great Astrolabe Reef (locations with low turbidity and minimally impacted by catchment development) would fall within the expected growth rates based on the local SST relationship observed in the GBR (Figure 3.4.; Lough 2008). However, this observed deviation in the relationships between coral growth and local SST is not exclusive to Fiji; a number of studies have reported the same observations from *Porites* spp. corals in the Indo-Pacific (Anthony and Fabricius 2000; Edinger et al. 2000; Fabricius et al. 2011; Shi et al. 2012; Tanzil et al. 2013; Carilli et al. 2017; Bolouki Kourandeh et al. 2018), indicating that in these locations other environmental parameters (such as turbidity, nutrient concentration or light irradiance) are the dominant drivers of coral growth.

Across our sites, there are distinct differences in average seawater turbidity (and Chl-a concentration). Here, we observe that the variations in annual growth rate across all locations follow a significant linear relationship with average annual seawater turbidity, where lower seawater turbidity corresponds with higher annual linear extension rates (LM $R^2 = 0.65$, $p < 0.0001$) (Figure 3.4.). This relationship implies that seawater turbidity is the main control on the observed spatial variability in coral growth across Fiji. Seawater turbidity is a parameter of water quality that relates to light penetration and availability in the water column. As such, the role of seawater turbidity as a driver of differences in coral growth is not surprising. However, the processes that can drive to increased turbidity are diverse, and include biological processes and algal blooms (Platt et al. 1988), river runoff and associated sediment plumes (Nezlin and DiGiacomo 2005), and sediment resuspension and transportation (Acker et al. 2002; Shi and Wang 2008). Increased terrestrial sediment input into inshore reefs is usually linked to catchment land use and coastal development and is regarded as a major threat to coral health (Kleypas and Eakin 2007). Coastal turbidity has been observed to cause increased sedimentation, coral smothering, increased concentrations of nutrients and pollutants, limited light availability and bioerosion (Marubini and Atkinson 1999; Carricart-Ganivet and Merino 2001; Crabbe and Smith 2005; D'Olivo et al. 2013; Schönberg et al. 2017). In Fiji some studies have described how sediment and nutrient input into inshore reefs is altering ecological communities. Brown et al. (2017a) linked catchment land-use to remotely sensed coastal turbidity, and Brown et al. (2017b) showed how coastal turbidity is an important contributor to reduced coral cover and coral complexity, which resulted in impacts to reef fish communities. In addition, benthic cyanobacteria mats, which used to be present in reefs only during the warm months are now persisting through the year resulting in decreased fish herbivory (Ford et al. 2018, 2021). Thus, increasing seawater temperatures coupled with increased sedimentation and nutrient availability in coastal reefs can affect coral growth, reduce defence mechanisms, and weaken colony recruitment. Furthermore, they can potentially engage in negative feedback processes that accelerate ecosystem decline, ultimately causing loss of coral cover, biodiversity and reduced reef carbonate accretion, resulting in shifts from a coral-dominated reef towards an algae-dominated state (Fabricius 2005; Bruno et al. 2009).

Water quality measurements in coastal Fiji are sparse and in the majority of the cases refer to single measurements (Mosley and Aalbersberg 2003; Tamata 2007; Singh and Aung 2008) rather than long-term highly resolved datasets. This complicates assessments of how coastal turbidity is impacting different inshore reefs in Fiji. Nevertheless, the differences in catchment size and land use across the studied locations have an obvious impact on coastal water quality (Brown et al. 2017a), with reefs near smaller, highly forested catchments (Votua Reef) presenting low K_d490. Sediment and nutrient load are considered the major pollutants of coastal waters in Fiji around the main islands (Atherton et al. 2005; Brown et al. 2017a) and they have led to reduced coral cover, and increased turf and macro-algae (Sykes and Morris 2007; Brown et al. 2017b), contributing to long-term ecological sifts and degraded coral reef conditions. This is likely a consequence of large-scale sugarcane agriculture and deforestation resulting in soil erosion and fertilizers washing into waterways during high rainfall events (Barbour and Terry 1998; Dadhich and Nadaoka 2012; Ram and Terry 2016).

As part of Fiji's strategy to adopt an integrated coastal management, different monitoring programs have been in place since 2007 to evaluate reef status in Fiji (Sykes and Morris 2007; Ellison and Fiu 2010) and inform management and protection decisions. Yet, a gap in the understanding of coastal processes and reef accretion across different areas in Fiji remains open. Here, we confirm that reef-specific seawater turbidity has a major role in driving average coral growth and add to the existing studies showing that coastal turbidity not only is a major driver of coral cover, but also of coral growth. This has important consequences favouring shifts from coral to algal-dominated reefs, changing reef ecology and altering coral and reef-associated species abundances, because under diminished calcification, reef accretion can become negative, leading to reef structural collapse (Eakin 1996).

3.4.2. Heat-stress affects temporal variability of coral growth

Despite annual SST having only a minor role in coral growth control across sites, there are indications that heat-stress does impact inter-annual variability of coral growth in Fiji. The five-year bin data analysis of core samples of this study (1998 – 2016) demonstrates a generalised decrease in coral growth across all sites during the 2013 – 2016 period (Figures 3.5. and 3.6.). Growth decreased by 20% in the Votua Reef, by 17% in the Namuka Reef, by 12% in the Suva Reef and by 18% in the Nananu-i-Ra Reef. This coral growth decline is coeval with exceptionally high heat-stress levels (DHW > 6 across all sites), and both the diminished coral growth and thermal stress are unprecedented in our environmental records for the last two decades.

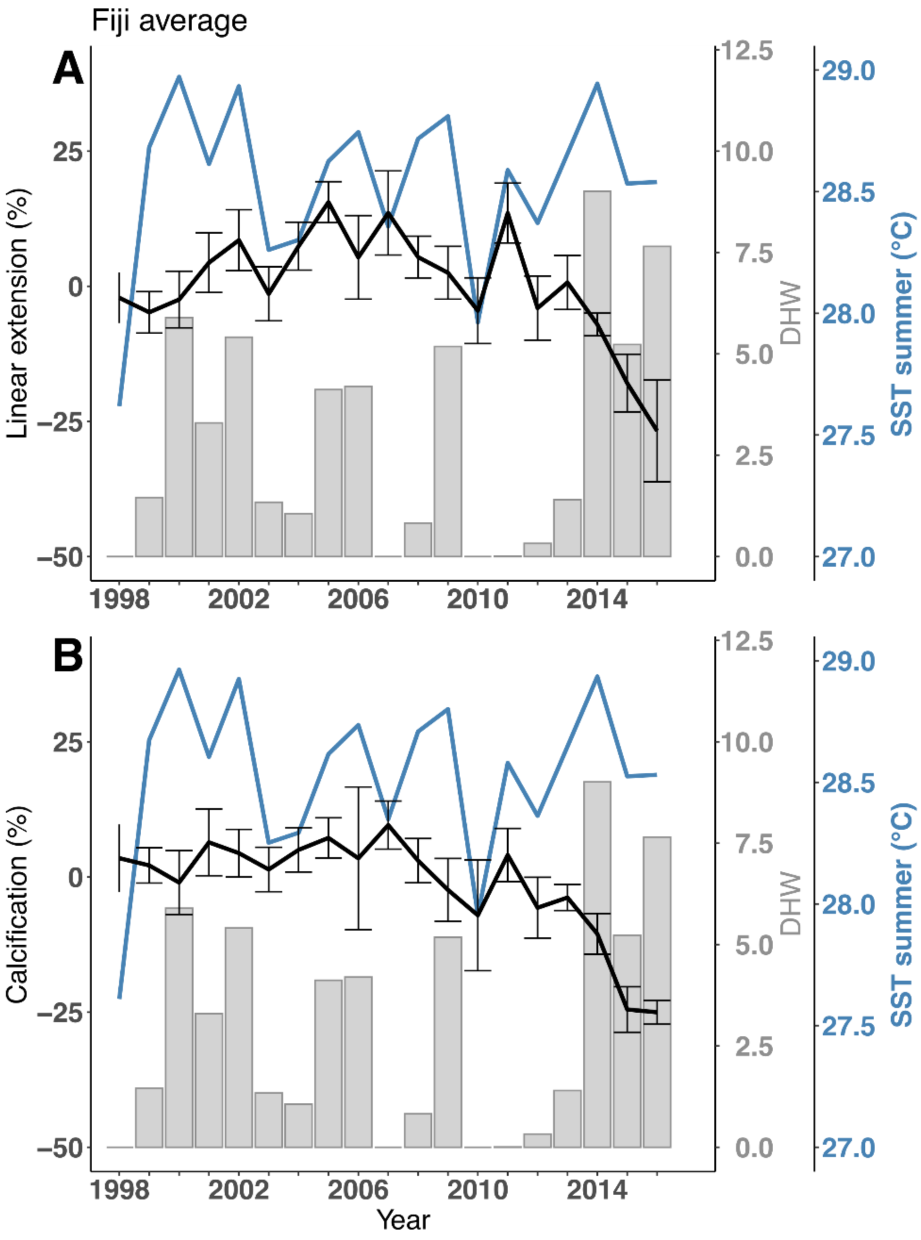

Figure 3.7. Time-series data for a Fiji average for the period 1998 - 2016. (A) Linear extension and (B) Calcification. Black line is annual change rate calculated as percent difference with long-term anomalies. Error bars represent SE. Grey columns are max. annual observed DHW at all locations. Blue line represents average SST recorded during the climatologically warmest months (Jan, Feb, Mar, Apr).

The Fiji average annual coral growth (linear extension and calcification), as shown in Figure 3.7., shows how average summer (January – April) SST has remained elevated since 2012, with consecutive high heat-stress (measured as DHW) events in 2014, 2015 and 2016. This increase in the duration and intensity of heat stress events corresponds with the decline in coral growth observed across all sites from 2013 onwards. Negative growth anomalies were also observed in the intervals 1998 – 2000 and 2007 – 2010, which correspond to elevated heat-stress events (DHW > 4), with a return to positive coral growth anomalies during the following year. Widespread bleaching events were recorded in Fiji during 2000, 2002, and 2005 (Sykes and Morris 2007). However, widespread bleaching was not observed during the increased thermal-stress period between 2014 and 2016 (Mangubhai 2016). Interestingly, no decrease in coral growth was observed during 2002, but data shows a clear link between decreased coral growth and accumulated heat-stress during the studied period. A similar influence of water quality and SST over coral growth was modelled in Fiji by Goberdhan and Kininmonth (2021); despite the different growth records, their statistical modelled aligns with the findings of this study regarding the influence of site-specific water quality and annual SST on growth rates, including the importance of distance to shore, Chl-a concentration, tropical cyclones and ENSO events.

Many studies have shown a link between DHW, accumulated heat-stress, bleaching and impacts on coral growth; and thermal stress is linked with reduced calcification (De'ath et al. 2009; Cantin et al. 2010; Donovan et al. 2021; van Woesik and Cacciapaglia 2021), even before bleaching is evident. In Fiji, corals live within 2°C of their upper thermal tolerance limit during the summer months (Ellison and Fiu 2010), which implies that during the warm season corals occupy waters above the optimum temperature for calcification (Cooper et al. 2008), and as SST follows the projected increasing trends (Australian Bureau of Meteorology and CSIRO 2011) it would be expected for annual growth rates to keep decreasing accordingly. It is important to note that a decrease in coral growth is observed across all sites, regardless of seawater turbidity. The Votua Reef and Nananu-i-Ra (the least and most turbid locations, respectively) both experience a decrease of around 20% in respect to the average extension rate. Yet, no significant temporal trends (positive or negative) in seawater turbidity were found in any of the locations studied that could solely explain this decline over time. Furthermore, the parameters that might affect water quality (i.e., catchment land-use, rainfall events and seasonal winds) (Ram and Terry 2016; Brown et al. 2017a) have also not experienced significant increases over the studied period (Australian Bureau of Meteorology and CSIRO 2011; Ankita and Kazuo 2014; Kumar et al. 2014) supporting the observation in this study of seawater turbidity remaining stable between 1998 – 2016.

Based on coral growth records and environmental conditions it is difficult to establish to what extent coral heat tolerance is affected by local environmental conditions. None of the samples of this study show evidence of bleaching during the massive bleaching events recorded in Fiji (i.e., 2000, 2002, 2005), but this lack of bleaching records is not unusual. McClanahan et al. (2020) reported that Fijian coral reefs are among the most resistant to bleaching under heat stress in the Indo-Pacific. Furthermore, Hendy et al. (2003) shows how statistically unlikely it is to find bleaching scans in massive *Porites* spp. colonies. These observations led to the consideration that a lack of evidence for bleaching in the skeletal record cannot be interpreted as a lack of thermal stress experienced by the corals (Buddemeier et al. 2004), as it is possible that bleaching is just one of multiple stress responses, and these might not be as easily identifiable as bleaching (e.g., reduced growth and calcification) (McClanahan et al. 2020). However, all our cores show a skeletal feature (i.e., partial mortality and/or high-density band) during 2016. This is more evident in the Nananu-i-Ra, Namuka and Suva reefs, than in the Votua Reef (See core images in Appendix A). This 2016 feature is likely to be caused by altered environmental conditions during Tropical Cyclone (TC) Winston in February 2016, rather than by cumulated thermal stress. Winston was a category 5 TC, and the strongest on record for Fiji and the South West Pacific, recording sustained winds of up to 280 km/h and gusts of 306 km/h, causing damages to infrastructure, agricultural and coastal ecosystems (Mangubhai et al. 2019; Asia-Pacific Data Research Center). Impacts on nearshore environments due to elevated sedimentation, abrasion and physical damage to corals were likely during this episodic event, and as such are recorded in the coral skeleton. Other TCs like Evan (Cat. 4, 2012) and Zoe (Cat. 5, 2002) during the period of this study also led to damage in Fiji but are not evident in the skeletal records. Interestingly, only the cores from the Votua Reef (the ones that show limited skeletal alteration in 2016) show partial mortality in 2015. Although I suspect this might be caused by a combination of thermal stress and higher light irradiance due to the occurrence of a strong El Niño (causing lower than usual rainfall and therefore less coastal turbidity), this cannot be answered with the current available data.

In Fiji, there is no indication that growth decline caused by thermal stress is enhanced nor diminished by local seawater turbidity. There is abundant evidence that local anthropogenic stressors (overfishing, eutrophication, increased sedimentation) can diminish the thermal threshold of corals, potentially leading to bleaching, and compromised annual calcification rates (Nyström et al. 2000; Bellwood et al. 2004; Castillo and Helmuth 2005; Pandolfi et al. 2005; Knowlton and Jackson 2008; Mora 2008; Carilli et al. 2009, 2010, 2012, 2017; Fabricius et al. 2013; Wooldridge 2017; Donovan et al. 2021). Yet, other studies have explored the role of turbid reefs as climate refugia, where suspended sediments limit light irradiance, thus alleviating thermal stress, limiting coral bleaching (Sully and Van Woesik 2020; van Woesik and Cacciapaglia 2021) and facilitate coral heterotrophy (Anthony and Fabricius 2000), moderating impacts. These studies explored the limitations of turbidity as a moderator of thermal stress, and found a genera-specific effect, with *Porites* spp. corals benefiting the least from turbidity in a warm ocean (van Woesik and Cacciapaglia 2021). Further, this benefit occurs in coastal reefs with a turbidity 'goldilocks' zone with K_d490 values between 0.08 and 0.127 m^{-1} (Sully and Van Woesik 2020) (our most turbid reef, Nananu-i-Ra, has an annual average value of 0.075 m^{-1}) and where turbidity is driven by tidal regime (van Woesik and Cacciapaglia 2021), as opposed to locations with ephemeral turbidity events driven by accumulated rainfall and/or winds (as in the locations of this study). In any case, the existence of compounding effects between water quality and heat stress, and whether these are positive or negative, is highly reef-specific. While a similar relative decline is observed in all locations regardless of water quality, the absolute growth rates are very different between the Votua Reef (less turbid) to the Nananu-i-Ra Reef (most turbid). Coastal turbidity makes corals in these locations more vulnerable to increasing SSTs and thermal stress as it lowers the net calcification. This leaves these reefs at a higher risk of collapse and shift towards an algal-dominated regime, and this threshold is more likely to be reached by the more turbid reefs that are showing already limited growth.

An integrated management approach that enables a reduction in coastal turbidity has the potential to improve coral growth rates, maintaining coral cover and sustaining a healthy and productive reef. However, an extensive knowledge of coastal and land-processes are required in order to pinpoint the exact causes leading to increased turbidity (e.g., sediment load, nutrient concentration leading to algal blooms, sourced by river runoff, driven by wind-mixing). For this purpose, historical records of both coral growth and environmental variables are required.

3.4.3. Future changes in coral growth

Coral growth in Fiji is mainly driven by seawater turbidity and heat stress, and therefore we hypothesize that any change, direct or indirect, in these environmental parameters will have an impact on coral growth. Ongoing ocean warming is decreasing carbonate accretion rates in Fijian inshore reefs (Figure 3.7.). Despite the fact that our coral cores do not show signs of past bleaching (no abnormal density bands visible), the association between thermal stress and reduced linear extension and calcification rates is clear.

As global climate models forecast an increase in SST of between 2 and 4°C by the end of the century (IPCC, 2021), thermal stress is becoming more prevalent (Heron et al. 2013; McClanahan et al. 2020) coinciding with positive SST anomalies (DeCarlo et al. 2017a; Hughes et al. 2017b; Barkley et al. 2018). It is becoming evident that we are unlikely to be able to keep global warming to 1.5°C by the end of the century (Stammer et al. 2021; Friedlingstein et al. 2022) and annual coral growth rates are likely to continue decreasing, thus the continuity of these reefs will critically depend on our capability to manage local stressors (Hughes et al. 2018b). Seawater turbidity plays a role in limiting or exacerbating absolute growth rates under thermal stress; however, the potential for local strategies to reduce its impact might be limited. Our observations indicate that seawater turbidity in Fijian inshore reefs does not depend exclusively on local factors and land use management, but it is amplified by climatological components such as rainfall events and wind patterns. Different seasonal profiles are observed for seawater turbidity across locations of this study. These differences seem to be driven by changes in wind pattern, promoting turbulent mixing and/or upwelling events, as have been observed in Laucala Bay, near Suva (Viti Levu) (Singh and Aung 2008). Consequently, reefs exposed to strong seasonal winds are likely to experience enhanced turbidity. An intensification in the Pacific trade winds in the last three decades (England et al. 2014; Takahashi and Watanabe 2016) has been identified, a trend that could be having important repercussions on reef turbidity in Fiji, and subsequently on coral growth rates. Increased severity of tropical storms has been linked to climate change (Elsner et al. 2008; Knutson et al. 2010), and climate models predict further increases in the intensities of the strongest storms and increased rainfall rates in tropical regions (Walsh 2015).

Managing land use to limit river runoff and sedimentation in reefs might be a successful strategy in certain inshore reefs in Fiji to sustain coral growth rates.

3.5. Conclusion

In summary, coastal turbidity controls coral annual extension rates across Fiji. Simultaneously, thermal stress diminishes annual coral growth, and this is observed similarly at all sites, regardless of seawater quality levels. This suggests that resilience of reef-building *Porites* spp. corals in Fijian inshore reefs to thermal stress might not be increased by limiting local stressors. A 20% decrease in coral growth has been observed in Fijian inshore reefs since 2013 as a result of enhanced thermal stress in consecutive years. As 76% of the Fijian population live within 5 km from the coast (Andrew et al. 2019) and many of them rely directly on thriving coral reef ecosystems for jobs and provision of protein (Whippy-Morris 2009), assessing the trajectory of these ecosystems is key for preserving the services they provide to human communities. We demonstrate coral growth records in Fiji reflect the environmental conditions in which they grew, and furthermore they are being negatively impacted by SST warming, thermal-stress events, and poor coastal water quality. We need long-term reconstructions of coral growth, environmental conditions, and climatic events in these reefs over the last century to fully understand the consequences and predictions of coral growth in Fiji over the next decades.

Chapter 4 | Overcoming growth effects in Fijian corals for the application of trace element paleothermometry

> *There is nothing like looking, if you want to find something […]. You certainly usually find something, if you look, but it is not always quite the something you were after.*
>
> Thorin Oakenshield

Reef series #4 (MVL)

Chapter 4 | Overcoming growth effects in Fijian corals for the application of trace element paleothermometry

Abstract

Paleotemperature proxies can provide robust estimates of past temperature changes at high spatial and temporal resolution. In particular, geochemical proxies measured from coral skeletons offer an opportunity to resolve SSTs at sub-seasonal resolution. One of the most commonly used coral SST-proxies are measurements of the ratio of certain trace elements to Ca (El/Ca) in the coral skeleton; however, differences in mean composition and temperature sensitivity have been found in different regions and environments (e.g., Alpert et al. 2016; Sayani et al. 2019), attributed to "vital effects". These "vital effects" can be originated by coral physiological processes during biomineralization affecting the trace element partitioning beyond environmental controls. Therefore, the robustness and applicability of the El/Ca proxies for reconstructing SST depends on resolving the source of "vital effects".

In this study I investigate the robustness and potential of traditional (Sr/Ca, U/Ca, Mg/Ca, and Li/Ca) and newly developed (Li/Mg, Sr–U) SST proxies in the South-West Pacific. Six *Porites* spp. cores were collected at four different inshore locations at reefs around Viti Levu (Fiji). No instrumental differences in SST (mean or seasonality) are observed between the sample sites. However, a strong seawater turbidity gradient is observed across these locations. We generated monthly resolved El/Ca timeseries covering a period from 2001 to 2017 using LA-ICPMS.

Sr/Ca, Mg/Ca, Li/Mg and U/Ca generally exhibited the co-variability expected under different Rayleigh fractionation rates acting during skeletogenesis and across reefs. In addition, all mean El/Ca across sites showed to be correlated with density. Sensitivity to SST variability differed across El/Ca proxies, although Sr/Ca was consistently the most sensitive proxy for SST. Results showed that SST proxies in Fiji are influenced by an interplay between SST, Ca^{2+} pumping and Rayleigh fractionation, and skeletal density. Furthermore, we show how differences in density and aragonite precipitation across reefs is associated with local environmental conditions (i.e., seawater turbidity), and as

such this variable is impacting El/Ca in this region complicating the acquisition of SST records. I show that replicating several colonies across a region and creating a composite Sr/Ca record helps constrain the SST signal and creates a more robust reconstruction than single core records, enabling SST reconstruction in this region.

4.1. Introduction

Reconstructing the thermal history of the ocean (e.g., ocean circulation and heat content) is vital for understanding the key components of the climate system, and the sensitivity of marine ecosystems to such changes (Hughes et al. 2017a). For this purpose, continuous temperature records are key in understanding how climate change is affecting the ocean (Lough 2008). However, historical records of sea surface temperature (SST) prior to the period of modern instrumentation (1980s) are scarce and geographic coverage is limited (Trenberth et al. 2007). To fill in the gaps where instrumental data is not available (both spatial and temporal), several marine SST archives (e.g., molluscs, corals, foraminifera) have been explored and temperature proxies developed based on the geochemical variability (e.g., stable oxygen isotopes ($\delta^{18}O$), alkenones) within the archive. Tropical reef-building corals allow for monthly resolved geochemical records and, as such, they have been widely used to reconstruct SST and hydrological variability in tropical and sub-tropical regions on seasonal and centennial timescales (e.g., Beck et al. 1992; de Villiers et al. 1994; Alibert and McCulloch 1997; Linsley et al. 2008; Nurhati et al. 2009; DeLong et al. 2013; Tierney et al. 2015; Jimenez et al. 2018; Wu et al. 2021), and they provide a valuable insight into future climate variability and its impact on coastal ecosystems. Furthermore, by combining sclerochronological techniques in genera that show annual growth bands (e.g., *Porites, Diploastrea, Montastraea, Diploria*, etc.) with dating methods such as U-series (e.g., Clarke et al. 2017) and radiocarbon (e.g., Wu et al. 2021), fossil corals provide the means to reconstruct environmental changes in deep time (e.g., Last Glacial Maximum).

In the Indo Pacific, massive *Porites* spp. are one of the most commonly used geochemical archives (Lough and Cantin 2014). They can form large reef-building colonies, are long-lived (lifespan of centuries) and have a growth rate of 10-20 mm/yr. *Porites* spp. coral polyps are small (~1 mm) and deposit their aragonitic skeleton in concentric annual bands (Knutson et al. 1972) that can be visualised using X-ray techniques, like CT, (Cantin et al. 2010; DeCarlo et al. 2015a; Barkley et al. 2018), making this archive useful to explore changes in coral growth as well. Furthermore, *Porites* spp. corals show high resistance under unfavourable conditions such as thermal stress (Klepac and Barshis 2020) showcasing their usefulness to provide continuous climate records in the past. Overall, these characteristics allow for high-resolution (at sub-monthly resolved) multi-decadal to multi-century (Lough 2011) geochemical and growth records.

Measurements of El/Ca ratios (i.e., Sr/Ca, Mg/Ca, Li/Ca, and U/Ca) in *Porites* spp. skeletons have been widely used as SST-proxies. In the coral reef environment, these trace elements are transported as dissolved ions from the open seawater into the Extracellular Calcifying Fluid (ECF) (Sinclair et al. 2006; Gaetani et al. 2011; Tambutté et al. 2011; Gagnon et al. 2012) from where the coral polyp precipitates its aragonitic coral skeleton ($CaCO_3$). These elements are preferentially incorporated or excluded from the skeletal material depending on their partition coefficient (K_D), defined as the El/Ca ratio in the coral relative to that in seawater. SST proxies are established on the basis that variations in SST govern changes in the K_D of different elements. However, this is not the only factor controlling El/Ca in coral aragonite, and other co-occurring processes can influence the coral El/Ca signal beyond the influence exerted by SST.

As new skeleton ($CaCO_3$) is secreted from dissolved ions in the ECF (Ca^{2+} + CO_3^{2-}), various trace elements (e.g., Sr^{2+}, Mg^{2+}, Li^+ or UO_2^{2+}) are incorporated into the aragonite lattice at a ratio dictated by their partition coefficients. Due to differences in the partition coefficients of these elements (K_D Sr ~ 1.1, Beck et al. (1992); K_D Mg and K_D Li <<1, Montagna et al. (2014)) Rayleigh fractionation exerts some control over the skeletal El/Ca signal. In this process, aragonite precipitated at the beginning of a fresh batch of ECF will show elevated Sr/Ca and depleted Li/Ca and Mg/Ca levels. As skeletal formation continues, both [Sr^{2+}] and [Ca^{2+}] will become depleted much faster than [Mg^{2+}] and [Li^+]. This causes the Mg/Ca and Li/Ca ratios in the ECF to increase and as such these will also increase in the precipitated mineral. In addition to Rayleigh fractionation, biomineralization models have focused on the role of active modification that corals exert over the chemical composition of the ECF via a Ca-ATPase enzyme (Ferrier-Pagès et al. 2002; Tambutté et al. 2011; Marchitto et al. 2018). Marchitto et al. (2018) proposed a simple model to explain the range of El/Ca values recorded in marine calcifiers focusing on the corals' ability to pump Ca^{2+} ions into the ECF in exchange for H^+ (product of $CaCO_3$ precipitation). A fast Ca^{2+} pump will cause an increase in the pH and an increase in concentrations of Ca^{2+}, Sr^{2+}, and CO_3^{2-} in the ECF with respect to seawater; conversely, it will cause a decrease in the El/Ca ratio of other elements (Sinclair 2005b). Another model developed by DeCarlo et al. (2015b) to explain co-variability of Sr/Ca and U/Ca fits with the above model, defining that seawater exchange, Ca^{2+} pumping and aragonite precipitation modify the influence of U/Ca in the skeleton.

Thus, El/Ca in the coral aragonite are influenced by the partition coefficient of each element and the amount of $CaCO_3$ that is being mineralised by a single batch of ECF. The latter is manipulated by Ca^{2+} pumping activity and influences how much Rayleigh fractionation will occur. These processes, not directly influenced by SST variability, are known as "vital effects" and can complicate the use of El/Ca as SST proxies (Allison and Finch 2004; Sinclair 2005b; Gaetani and Cohen 2006; Cohen and Gaetani 2010). Further, as coral El/Ca ratios might not be a direct inorganic effect of SST over element partitioning but a biologically mediated process (Sinclair et al. 2006), multiple components, such as SST and local environmental variables (e.g., seawater turbidity, tidal effects, light availability, trophic level, etc.), could exert a control over coral calcification and coral El/Ca.

One of the strategies used to overcome "vital effect" anomalies and/or local environmental influences in single core El/Ca records is the use of replicated overlapping coral colonies to produce a single 'composite' record (Hendy et al. 2002; Sayani et al. 2019). A composite record constrains the mean climatic signal over the studied period and improves the accuracy of the El/Ca-SST reconstruction.

Although Sr/Ca is one of the most used coral SST proxies (see review by Corrège 2006), several studies have reported varying sensitivities of the proxy to SST changes and differences in mean Sr/Ca values among colonies that do not correspond to mean SST differences (e.g., Grove et al. 2013; Alpert et al. 2016; Sayani et al. 2019). Coral physiology and related "vital effects" have been shown to impact coral Sr/Ca (e.g., Allison and Finch 2004; Gaetani and Cohen 2006), altering the Sr/Ca-SST relationship. Disentangling the SST signal from the "vital effects" and the associated Rayleigh fractionation is complicated. Currently, the application of the Sr/Ca proxy requires the implementation of site and colony-specific calibrations with instrumental SST, however this protocol is time consuming and complicates its application to fossil corals.

The use of Li/Mg as an alternative SST-proxy (Case et al. 2010; Montagna et al. 2014) is based on the similar partition coefficient of Li^+ and Mg^{2+}. Both Li/Ca and Mg/Ca were found to be correlated with SST, although they both are heavily influenced by Rayleigh fractionation (Montagna et al. 2014), often completely masking the SST signal. However, by obtaining Li/Mg ratios the effect of Rayleigh fractionation is, in theory, removed, with the remaining signal being exclusively influenced by SST (Montagna et al. 2014; Marchitto et al. 2018). Nevertheless, work by Fowell et al. (2016) showed how species and site-specific calibrations might still be needed for the application of Li/Mg. Furthermore, Rollion-Bard et al. (2015) suggested that this proxy might still present variability not directly related to SST, and Mitsuguchi et al. (2001) suggested that Mg/Ca adsorption onto the aragonite skeletal material might present fine-scale heterogeneity that could also alter the Li/Mg signal beyond SST.

Recently, Sr–U (DeCarlo et al. 2016) was also proposed as a new SST proxy on the premise that it isolates the SST component from the Rayleigh fractionation in the established Sr/Ca-U/Ca relationship. However, the incorporation of U into the ECF and into the coral aragonite remain poorly understood (Anagnostou et al. 2011; DeCarlo et al. 2015b; Chen et al. 2021), which can complicate the full potential of Sr–U as an SST proxy in some cases. It has been successfully applied in *Porites* spp. to reconstruct SST at interannual timescales (DeCarlo et al. 2016), however its validity in this coral genus at sub-annual resolution is still unexplored.

Studies have shown how SST proxy application for paleo-SST reconstructions is not universal, as some proxies might work better in certain regions and still reef-specific calibrations might be required. For this reason, a multi-proxy approach can increase not only the accuracy of the climatic reconstructions but maximise the regional coverage of SST records from areas where the application of SST proxies has proven difficult, such as the South-West Pacific. The Fiji Islands are located in a privileged position to record the shifting activity of the South Pacific Convergence Zone (SPCZ), the El Niño Southern Oscillation (ENSO) (Bagnato et al. 2004) and the Interdecadal Pacific Oscillation (IPO) (Folland et al. 2002). Hence, multi-decadal climatic reconstructions obtained from corals in this region are particularly useful for evaluating how climate change is affecting the Pacific Ocean. To date, climate variability and SPCZ movements have been successfully reconstructed by measuring $\delta^{18}O$ in multiple Fijian *Porites* spp. cores (Le Bec 2001; Linsley et al. 2004, 2006, 2008; Dassié et al. 2014) and also

Diploastrea heliopora (Bagnato et al. 2004), concluding that SSS, rather than SST, is the primary driver of coral $\delta^{18}O$ in this region.

The Sr/Ca proxy has also been applied to Fijian *Porites* spp., with varying success. Linsley et al. (2004) measured Sr/Ca along a core collected in Savusavu bay (Vanua Levu) and found a significant correlation with SST at monthly timescales ($R^2 = 0.70$, slope = -0.055) during a time span of 27 years (1970-1997). A second *Porites* spp. core within the same reef was also analysed for Sr/Ca (Linsley et al. 2006). Correlation of these two Fijian cores over 1780-1997 at annual timescales was of 22% with a mean offset of 0.14 mmol/mol (Linsley et al. 2006). This suggest that the Sr/Ca-SST correlation is uncertain in interannually resolved data, and unknown factors might influence coral Sr/Ca. Juillet-Leclerc et al. (2006) used a neural network to calibrate geochemical data from a Fijian *Porites* spp. with instrumental SST and concluded that in this region climatic records in corals skeletons are more complex than initially supposed, and likely not linear. Furthermore, Sr/Ca was also tested in a single *Diploastrea heliopora* core from Savusavu Bay (Bagnato et al. 2004) and the results suggest a good agreement with SST at annual timescales ($R^2 = 0.84$, slope = -0.034), although monthly timescales were not explored in this study. Consequently, more work is needed in this region to refine SST proxy calibrations, apply alternative SST proxies, and further understand the dominant controlling factors over coral El/Ca and develop techniques that allow for accurate paleotemperature reconstructions.

In addition to exploring the relationship between El/Ca and SST, studies have explored the interaction between "vital effects" or physiological processes and coral El/Ca variations. For example, when linear extension rates of *Porites* spp. fall below 0.5 cm/yr, coral skeletons record positive Sr/Ca anomalies (Goodkin et al. 2005) biasing SST reconstruction towards cooler records (DeLong et al. 2013). Significant correlations have been observed between Sr/Ca and Mg/Ca and density in *Porites* spp. from Galapagos (Reed et al. 2021) consistent with Rayleigh fractionation effects. Furthermore, under thermal stress coral calcification can diminish or even cease and alter the incorporation of trace elements (Sr/Ca, Mg/Ca) into the coral aragonite (e.g., Marshall and McCulloch 2002; D'Olivo and McCulloch 2017; Ferrier-Pagès et al. 2018; D'Olivo et al. 2019). The use of CT scans, compared to traditional X-ray methods, offers the possibility of virtually exploring the 3-dimensional growth of each core, thus guiding where to cut each coral slab exposing the most favourable path for geochemical analysis (Cantin et al.

2010). This can limit the geochemical anomalies resulting as a product of sampling across suboptimal paths (DeLong et al. 2013) and allows further exploration of patterns in calcification and El/Ca.

In this chapter I use high-resolution El/Ca (Li/Ca, Mg/Ca, Sr/Ca, and U/Ca) analysis and coral growth measurements (density, linear extension, and calcification) from six *Porites* spp. coral cores from four Fijian inshore reefs during the interval 2001 – 2017. These records are coupled to remote sensed environmental variables (SST and seawater turbidity (K_d490)) to investigate the potential for SST reconstructions using established and alternative coral-based proxies in the South-West Pacific. Further, through examining the covariation between elements, I explore the effects of Rayleigh fractionation, Ca^{2+} pumping, and non-thermal environmental factors influencing El/Ca variability. I show that averaged Sr/Ca across replicates cores (composite record) seems to be the most suitable proxy for SST reconstruction in Fijian corals as it is the least influenced by other factors (i.e., coral growth). Furthermore, I also show that El/Ca variability across the *Porites* spp. corals in this study is influenced by Ca^{2+} pump activity and Rayleigh fractionation.

4.2. Methods Summary

4.2.1. Reef environmental data

Instrumental environmental data available between 2001 – 2017 (the period examined in this chapter) were included here. Full details on the sources of environmental data can be found in Chapter 2 – Section 2.6. Daily SSTs for each location were obtained from the OISST dataset. Monthly SSTs were calculated as the arithmetic mean of daily SSTs. DHW were obtained from the daily CRW product. Monthly DHW was obtained as the maximum DHW recorded at each location on every month. Daily water quality parameters at each location were characterised through seawater turbidity ($K_d490(m^{-1})$) and chlorophyll-a concentration (mg/m^3) and was derived from MODIS-Aqua between 2002 – 2017. In this chapter we solely use seawater turbidity due to its high correlation with chlorophyll-a ($R^2 = 0.93$, See chapter 2 – Section 2.6.4.). Also, for the purpose of this study (light availability for the corals) seawater turbidity is a more comprehensive parameter and thus more adequate. Monthly seawater turbidity (and chlorophyll- a) was obtained as the arithmetic mean of daily datapoints. Daily rainfall data from the closest available weather stations from each study site were provided by the Fiji Meteorological

Services. Votua, Suva and Namuka Reef cores were paired with Laucala Bay rainfall station (located at < 15 km distance for Suva and Namuka Reefs, and ~80 km for Votua Reef). Cores in Nananu-i-Ra were paired with Penang Mill weather station data (< 15 km). Monthly rainfall was calculated as the accumulated rainfall over the duration of each month (mm/month).

4.2.2. Coral samples

Coral cores from six massive *Porites* spp. colonies from four different locations were analysed to investigate SST-proxy trace element variability (Figure 4.1.). The four study locations included two inshore reefs adjacent to small and forested catchments (Votua Reef on the Coral Coast and Namuka Reef), one reef in the vicinity of a catchment with high presence of sugarcane crops and grasslands (Nananu-i-Ra) and one urban reef (Fish Patch in Suva Reef). More information on these locations is presented in Chapter 2 – Section 2.2. Included in this set were pairs of cores from each location with one long coral core, useful to explore longer temporal variability, and a short replicate core, to explore reproducibility between coral colonies. Cores from two colonies (long core: VOT17_1 and replicate core: VOT17_2) were collected from the Votua Reef along the Coral Coast (South Viti Levu). Cores from two colonies (long core: NAN17_2 and replicate core: NAN17_5) were collected at a fringing reef on Nananu-i-Ra Island, 3 km off the coast in the Ra province (North Viti Levu). One core (long core: FP17_1) was collected at the Suva reef, at the entrance of the Suva harbour, and a core from the Namuka Reef (NAM17_1) was selected as a replicate core (Figure 4.1.).

4.2.3. Growth parameters

Growth parameters from these coral cores were obtained from X-ray CT scans. A detailed description of the protocol is in Chapter 2 – Section 2.4.2. In summary, skeletal density (g/cm^3) was measured continuously along the major growth axis based on the CT imaging (following methods in Cantin et al. 2010). Annual linear extension rates (cm/yr) were obtained from both X-ray images visualising seasonal density bands, by measuring distance across the major growth axis from one high density band to the next, and from density profiles of each coral core measuring distance between density maxima (Lough and Cooper 2011). The calcification rate (g $CaCO_3$/cm^2·yr) was also obtained as a product of the previous two growth parameters. For the purposes of this chapter, we used density as a measurement of skeletal growth due to its availability at the same time resolution as El/Ca (monthly), in contrast to linear extension and calcification, which are obtained at annual resolution.

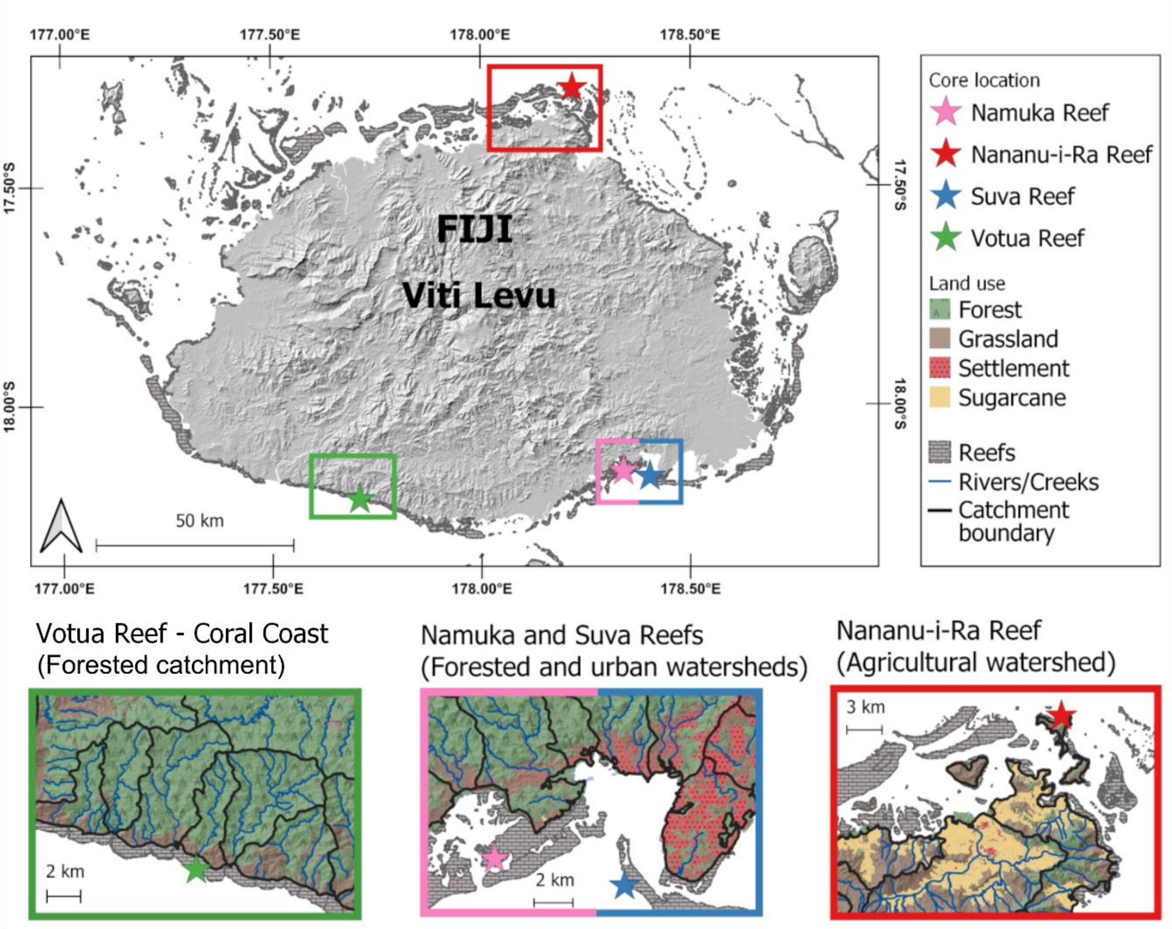

Figure 4.1. Map of Viti Levu (Fiji). Star symbols represent the coring locations of the samples of this study. Cores VOT17_1 and VOT17_2 were extracted from the Votua Reef in the western Coral Coast. NAM17_1 was extracted from Namuka Reef. FP17_1 was extracted from the Suva Reef. NAN17_2 and NAN17_5 were extracted from the shores of Nananu-i-Ra.

4.2.4. LA-ICPMS

Coral slabs were cut parallel to the major growth axis identified through CT scans and LA-ICPMS measurements were carried out following the same path where density had been measured. The laser beam used had a size of 200x50 µm. The optimised ablation parameters and analytical settings determined in Chapter 2 – Section 2.4.1.2. were used here, corresponding to a laser pulse of 12Hz and a Fluence of 2.5 J/cm^2. The ablation path was set following the major growth axis of the exposed slab. Each coral sample was ablated (and El/Ca measured) three times (three transects) on the exact same path. The first transect served as a cleaning ablation, removing the outer ~0.50 µm of the ablation path surface, and exposing a fresh surface for subsequent analysis. At least 20 seconds of background were measured before and after each sub-transect to allow for long-term drift-correction. The standards NIST610, NIST612, NIST614 and JCp–1 were measured at the beginning and end of each coral transect. Furthermore, alternating NIST612 + NIST610, NIST612 + NIST614 and NIST612 + JCp–1 were measured every five sub-transects.

4.2.5. Coral chronology

Annual age models obtained from CT scans (band counting and density minima and maxima) were refined following standard approaches (Felis et al. 2009). Monthly resolved chronologies were extrapolated using the annual chronology obtained from CT scans, the location of the sample at the time of its collection (May 2017) and subsequent alignment in peaks and troughs of Sr/Ca with SST assuming an inverse correlation between Sr/Ca–SST as seen elsewhere (e.g., DeLong et al. 2014). Despite all El/Ca being explored for chronology refinement, Sr/Ca was chosen for showing consistent significant correlations with SST (See Results 4.3.2.1.) and clear seasonality in each of the cores of this study.

4.2.6. Data processing

Each individual laser ablation transect was processed using the Python package LAtools (Branson et al. 2019) following an stablished protocol. Each transect was background corrected, despiked, normalised to ^{43}Ca and calibrated against NIST612, NIST614, or JCp-1. Analytical reproducibility of the standard material was monitored throughout every day of analysis. It is reported as internal reproducibility (mean El/Ca and %RSD), and external accuracy (measured value/reported value) and precision (2x SD of accuracy) (See details in Chapter 2 – Section 2.4.1.4). Accuracy and precision of Sr/Ca (0.46% and 2.81% respectively), Li/Ca (2.42% and 3.10%), Mg/Ca (3.76% and 1.03%), U/Ca (4.13% and 4.76%).

After refining the chronology of each coral transect, the resolution of the raw data was calculated to be nearly-weekly (based on the number of datapoints and skeletal extension of each sample). A low-pass filter of width 4 was applied to each transect to remove fine-scale signals corresponding to time-scales < 1 month (Sinclair 2005b) (as 1 month = 4 weeks, resolution of the raw data). Filtered data was then averaged at monthly time-scales (1 datapoint per month).

In the results and discussion of this chapter, I refer to single core data, all core data, and/or composite data. While single core geochemical data is simply a specific El/Ca timeseries for each single core (e.g., one timeseries of Sr/Ca from VOT17_1), all core data considers all data from all samples for a given El/Ca (e.g., six timeseries of Sr/Ca in total, from VOT17_1, VOT17_2, FP17_1, NAM17_1, NAN17_2 and NAN17_5), and composite data refers to one timeseries obtained through standardization and averaging across all core timeseries for a given El/Ca. To build the composite timeseries, single core data was standardised to each mean, and then this deviation was applied over the mean El/Ca of FP17_1 (e.g., one Sr/Ca timeseries obtained after standardization of Sr/Ca VOT17_1 and applying deviations to the FP17_1 mean. After following this process for every core, then a single timeseries is obtained after applying an arithmetic mean to the standardised Sr/Ca timeseries from each core).

All statistical analysis were performed in R. Pearson's correlation (r) was used to calculate correlations between El/Ca, with a significance of 95%. Ordinary Least Squares regression (OLS) were used to calculate the relationships between El/Ca, and environmental and growth data. Generalised Linear Models (GLM) were used to examine the relationship between SST residuals from Sr/Ca and Li/Mg, DHW and number of cores.

4.3. Results

Core statistics are presented in Table 4.1. Mean Mg/Ca ranged from 3.37 mmol/mol (FP17_1) to 5.12 mmol/mol (NAN17_5) and was consistently highest in Nananu-i-Ra samples and lowest in Suva Reefs. Mean Li/Ca ranged from 5.61 µmol/mol (FP17_1) to 7.14 µmol/mol (NAN17_2), with highest values found in Nananu-i-Ra and lowest in Suva Reefs. Cores from Votua Reef showed contrasting results, with a difference of ~1 µmol/mol between samples. Lowest mean Sr/Ca was measured in Suva with 8.60 mmol/mol (FP17_1) and highest in Votua Reef 9.26 mmol/mol (VOT17_2). Finally, mean U/Ca values showed the lowest at Nananu-i-Ra with 1.09 µmol/mol (NAN17_2), and highest in Votua Reef with 1.36 µmol/mol (VOT17_2).

Table 4.1. Mean El/Ca and relative SD of each SST proxy for each entire core.

Location	Core	Record span	Li/Ca (µmol/ mol)	RSD (%)	Mg/Ca (mmol/ mol)	RSD (%)	Sr/Ca (mmol/ mol)	RSD (%)	U/Ca (µmol/ mol)	RSD (%)	Li/Mg (mmol /mol)	RSD (%)	Sr-U	RSD (%)
Votua Reef	VOT17_1	2001-2017	6.97	7.64%	4.04	11.65%	8.81	1.82%	1.21	8.20%	1.76	9.83%	7.47	1.34%
	VOT17_2	2012-2017	6.03	4.03%	3.60	6.11%	9.26	0.76%	1.36	3.91%	1.69	5.83%	7.74	0.83%
Suva Reef	FP17_1	2001-2017	5.61	7.97%	3.37	15.32%	8.60	1.69%	1.10	11.39%	1.70	9.76%	7.37	1.01%
Namuka Reef	NAM17_1	2012-2017	6.11	8.68%	3.81	20.70%	9.20	1.35%	1.35	7.18%	1.67	13.35%	7.69	1.23%
Nananu-i-Ra	NAN17_2	2002-2017	7.14	6.79%	4.98	7.98%	8.65	1.04%	1.09	6.31%	1.44	9.65%	7.44	0.88%
	NAN17_5	2010-2017	7.02	6.48%	5.12	12.60%	8.79	1.48%	1.17	8.17%	1.40	10.50%	7.49	0.81%

4.3.1. Correlation between El/Ca

Co-variability of monthly (Figure 4.2.) and annually (Figure 4.3.) resolved geochemical El/Ca coral data is distinct (Table 4.2.). At both resolved timescales Li/Ca–Sr/Ca and Li/Ca–U/Ca show the weakest, if significant at all, relationships, and Sr/Ca–U/Ca show the strongest, with Mg/Ca–Li/Ca also showing a strong correlation. Furthermore, monthly Sr/Ca–Mg/Ca is significantly correlated in five of the six cores, but not when considering all data, due to the differences in mean El/Ca across samples.

On monthly timescales, Sr/Ca and Mg/Ca are significantly negatively correlated within each core, including all core data, ($r = -0.19 – -0.67$, $p < 0.05$) except for NAN17_2. Similarly, U/Ca and Mg/Ca are significantly negatively correlated in each core sample and including all data ($r = -0.39 – -0.78$, $p < 0.05$). Sr/Ca vs Li/Ca only shows a significant positive relationship in NAN17_2 ($r = 0.51$, $p < 0.05$) and VOT17_1 ($r = 0.20$, $p < 0.05$), and negatively in FP17_1 ($r = -0.19$, $p < 0.05$). U/Ca–Li/Ca shows a significant negative relationship within cores VOT17_2, FP17_1, NAM17_1 and NAN17_5 ($r = -0.17 – -0.73$, $p < 0.05$), and positive in NAN17_2 ($r = 0.33$, $p < 0.05$). Sr/Ca–U/Ca shows a strong positive correlation across all cores, including all data ($r = 0.70 – 0.86$, $p < 0.05$). Li/Ca–Mg/Ca shows a positive relationship in all cores, including all data ($r = 0.36 – 0.78$, $p < 0.05$), except in NAN17_2.

On annual timescales, Sr/Ca–Mg/Ca shows a negative correlation, but it is significant only in cores VOT17_1 ($r = -0.64$, $p < 0.05$) and NAM17_1 ($r = -0.84$, $p < 0.05$). U/Ca–Mg/Ca shows a significant negative correlation in FP17_1, NAN17_2 and NAN17_5 ($r = -0.57 – -0.83$, $p < 0.05$), and a positive correlation when considering all data ($r = 0.11$, $p < 0.05$). Sr/Ca–Li/Ca and U/Ca–Li/Ca are both only significant in NAN17_2 ($r = 0.57$ and $r = 0.54$ respectively), following a positive relationship. Sr/Ca–U/Ca has a strong positive correlation in VOT17_1, FP17_1, NAN17_2 and NAN17_5, and also when considering all data ($r = 0.56 – 0.93$, $p < 0.05$).

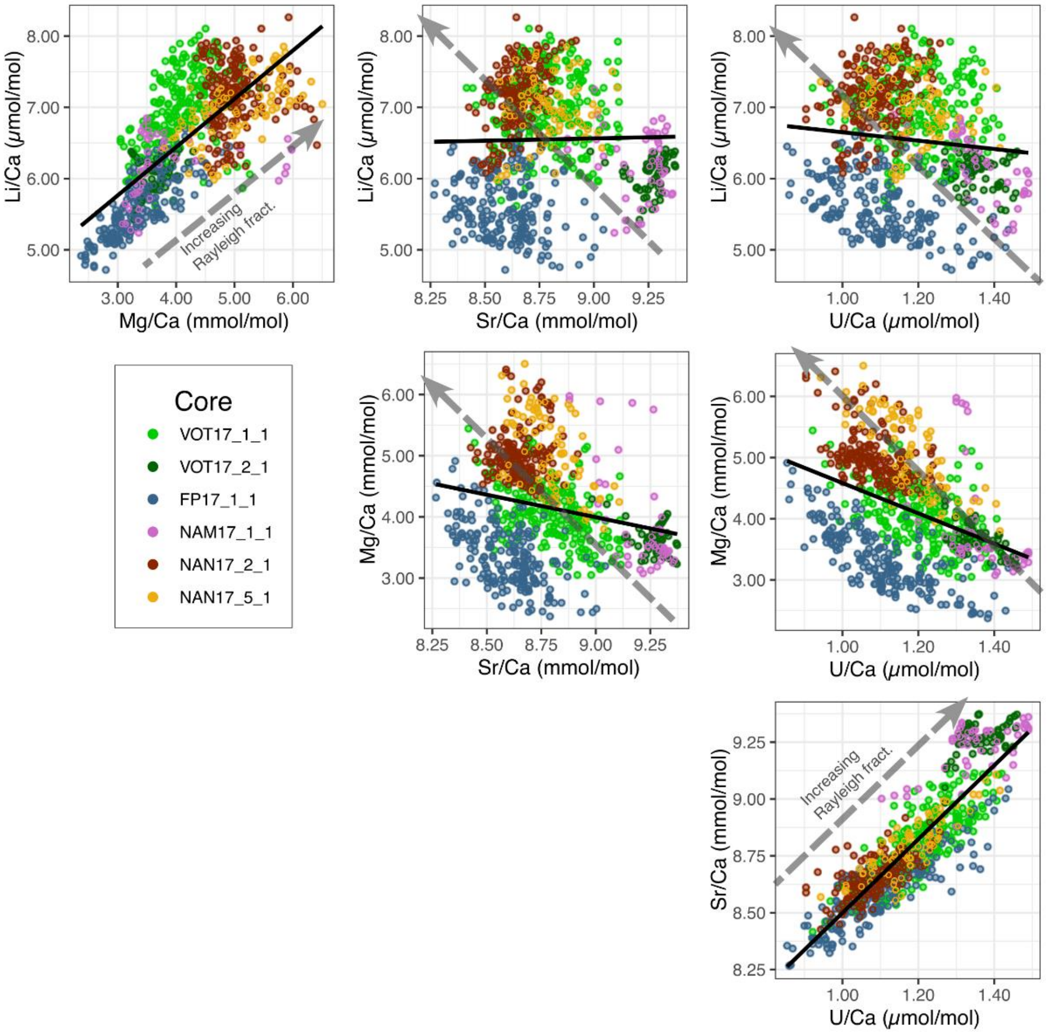

Figure 4.2. Cross-plots of monthly resolved El/Ca from all the samples of this study. Colour defines the core samples. Black lines indicate the best linear fit of the correlation. Grey arrows indicate expected movement of El/Ca under increasing Rayleigh fractionation effects in the ECF (as modelled by Sinclair, 2005; Marchitto et al., 2018; DeCarlo et al., 2016).

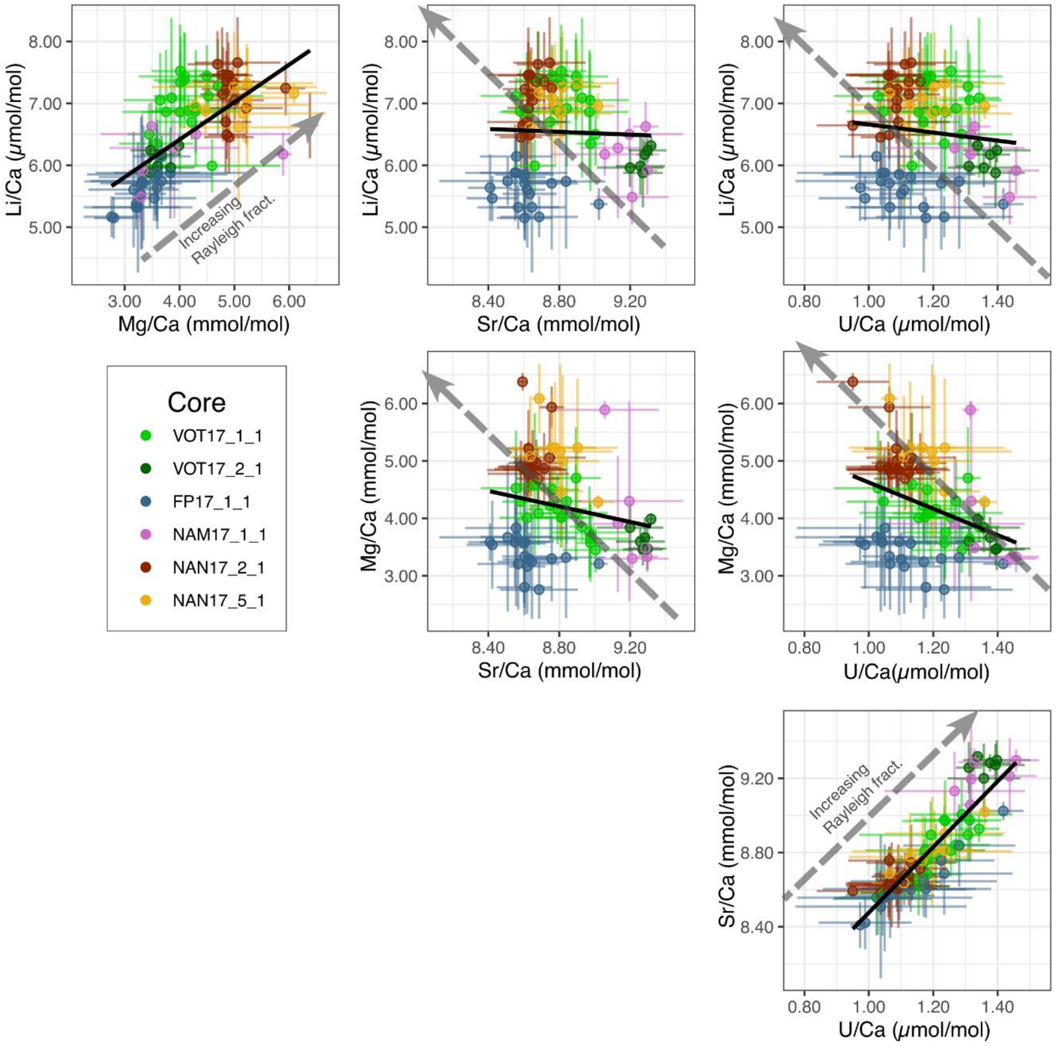

Figure 4.3. Cross-plots of annually resolved El/Ca from all the samples of this study. Colour defines the core samples. Black lines indicate the best linear fit of the correlation. Grey arrows indicate expected movement of El/Ca under increasing Rayleigh fractionation effects in the ECF (as modelled by Sinclair, 2005; Marchitto et al., 2018; DeCarlo et al., 2016).

Table 4.2. Pearson's r values of correlations between binned El/Ca at monthly and annual timescales for each core and all data. Bold values are statistically significant ($p < 0.05$).

Monthly	All	VOT17_1	VOT17_2	FP17_1	NAM17_1	NAN17_2	NAN17_5
Li/Ca-Mg/Ca	**0.73**	**0.47**	**0.36**	**0.78**	**0.49**	0.06	**0.62**
Li/Ca-Sr/Ca	**0.07**	0.03	**0.2**	**-0.19**	-0.13	**0.51**	0.01
Li/Ca-U/Ca	**-0.07**	-0.01	**-0.17**	**-0.51**	**-0.73**	**0.33**	**-0.18**
Li/Ca-Li/Mg	**-0.21**	**0.19**	**0.34**	**-0.44**	-0.1	**0.68**	**-0.19**
Mg/Ca-Sr/Ca	**-0.19**	**-0.45**	**-0.49**	**-0.56**	**-0.67**	0.06	**-0.57**
Mg/Ca-U/Ca	**-0.39**	**-0.49**	**-0.68**	**-0.78**	**-0.55**	**-0.39**	**-0.74**
Mg/Ca-Li/Mg	**-0.81**	**-0.75**	**-0.74**	**-0.88**	**-0.91**	**-0.66**	**-0.87**
Sr/Ca-U/Ca	**0.86**	**0.79**	**0.51**	**0.85**	**0.57**	**0.7**	**0.85**
Sr/Ca-Li/Mg	**0.38**	**0.59**	**0.66**	**0.68**	**0.75**	**0.38**	**0.77**
U/Ca-Li/Mg	**0.55**	**0.61**	**0.51**	**0.79**	**0.35**	**0.58**	**0.84**

Annual	All	VOT17_1	VOT17_2	FP17_1	NAM17_1	NAN17_2	NAN17_5
Li/Ca-Mg/Ca	**0.69**	0.16	0.4	**0.83**	0.25	-0.27	0.35
Li/Ca-Sr/Ca	-0.04	-0.02	0.73	-0.21	-0.01	**0.57**	0.33
Li/Ca-U/Ca	-0.11	0.09	0.01	-0.41	-0.74	**0.54**	0.09
Li/Ca-Li/Mg	-0.22	0.43	0.24	-0.45	0.02	**0.74**	0.04
Mg/Ca-Sr/Ca	-0.19	**-0.64**	-0.03	-0.41	**-0.84**	0.1	-0.63
Mg/Ca-U/Ca	**0.11**	-0.46	-0.52	**-0.57**	-0.51	**-0.65**	**-0.83**
Mg/Ca-Li/Mg	**-0.85**	**-0.81**	-0.78	**-0.86**	**-0.96**	**-0.84**	**-0.92**
Sr/Ca-U/Ca	**0.91**	**0.86**	0.15	**0.96**	0.58	**0.56**	**0.93**
Sr/Ca-Li/Mg	**0.28**	**0.62**	0.54	0.43	**0.89**	0.22	**0.84**
U/Ca-Li/Mg	**0.42**	**0.53**	0.5	**0.53**	0.34	**0.74**	**0.94**

4.3.2. Correlation of El/Ca with environmental variables

Monthly and annually resolved coral El/Ca data were regressed against environmental variables. In the case of SST two different approaches were followed: 1) Calibrations of each single core El/Ca with SST and 2) Regressions of all data against SST. For regressions with seawater turbidity, all data was considered together.

Table 4.3. El/Ca-SST linear regression for each core at monthly timescales and composite El/Ca-SST linear regression. Bold values are statistically significant ($p < 0.05$).

		Sr/Ca - SST			Mg/Ca - SST			Li/Ca - SST			U/Ca - SST			Li/Mg - SST			Sr-U - SST		
Location	**Core**	**Int.**	**Slope**	**R2**	**Int.**	**Slope**	**R2**	**Int.**	**Slope**	**R2**	**Int.**	**Slope**	**R2**	**Int.**	**Slope**	**R2**	**Int.**	**Slope**	**R2**
Votua Reef	VOT17_1	10.04	-0.045	**0.13**	2.40	0.060	**0.02**	9.61	-0.097	**0.05**	2.02	-0.029	**0.13**	3.03	-0.047	**0.11**	7.80	-0.012	**0.03**
	VOT17_2	10.07	-0.029	**0.31**	2.48	0.042	0.06	7.18	-0.040	0.04	1.80	-0.016	**0.16**	2.56	-0.032	**0.19**	8.06	-0.011	0.05
Suva Reef	FP17_1	10.33	-0.063	**0.29**	-1.09	0.162	**0.16**	4.96	0.023	0.00	2.27	-0.042	**0.19**	3.65	-0.071	**0.30**	7.82	-0.016	**0.08**
Namuka Reef	NAM17_1	10.75	-0.055	**0.28**	-2.39	0.228	**0.11**	6.87	-0.024	0.00	1.84	-0.018	0.07	3.91	-0.082	**0.15**	8.70	-0.036	**0.16**
Nananu-i-Ra	NAN17_2	9.60	-0.034	**0.25**	4.27	0.026	0.01	8.15	-0.035	0.01	1.52	-0.016	**0.08**	1.86	-0.015	0.02	7.91	-0.017	**0.10**
	NAN17_5	10.55	-0.064	**0.39**	-2.99	0.292	**0.31**	5.65	0.048	0.02	2.36	-0.043	**0.32**	3.43	-0.074	**0.37**	7.93	-0.016	**0.11**
	Composite	9.86	-0.047	**0.40**	1.10	0.084	**0.12**	7.32	-0.063	**0.11**	2.01	-0.034	**0.32**	3.95	-0.080	**0.34**	7.90	-0.018	**0.23**

4.3.2.1. Single core El/Ca-SST calibrations at monthly scale

OLS regressions (p < 0.05) reveal a varying degree of El/Ca variability that can be explained by SST, not only among SST proxies, but also among cores (Table 4.3.; Figures C.1. to C.6. in Appendix C), with Sr/Ca, U/Ca and Li/Mg showing the strongest correlations on average. The Sr/Ca ratio explained by SST ranges from 13% in VOT17_1 to 39% in NAN17_5, being significant for all cores, and with slopes ranging from -0.029 mmol/mol per °C to -0.064 mmol/mol per °C. The amount of U/Ca correlated with SST varies from 8% in NAN17_2 to 32% in NAN17_5, with slopes ranging from -0.016 to -0.043 μmol/mol per °C. However, this correlation was not significant in NAM17_1. Li/Ca only showed a significant correlation with SST at Votua Reef (VOT17_1) with 5% varibility explained, and slopes of -0.097 μmol/mol per °C respectively. Also, Mg/Ca was significantly correlated with SST in FP17_1, NAM17_1, and NAN17_5, with a correlation between 10 and 36% and slopes ranging from 0.162 to 0.292 mmol/mol per °C.

Other SST proxies were also explored. Li/Mg was negatively correlated with SST to varying degrees across all cores except NAN17_2, varying from 11% in VOT17_1 to 36% in NAN17_5, and slopes ranging from -0.032 to -0.082 mmol/mol per °C. Sr–U only showed a somewhat strong correlation with SST in NAM17_1, with a correlation of 15% and a slope of -0.036 μmol/mol per °C. This relationship, although weak, was also significant in VOT17_1, FP17_1, NAN17_2 and NAN17_5 with a correlation below 10% and slopes ranging from -0.012 to -0.036 mmol/mol per °C (Table 4.3.; Figures C.1. to C.6. in Appendix C).

4.3.2.2. All core El/Ca data and environmental variables (SST and seawater turbidity)

When considering all data from all cores at annual timescales, only Li/Mg showed a negative significant correlation with SST ($R^2 = 0.10$, $p < 0.05$; slope = -0.13 mmol/mol per °C) (Table 4.4.; Figure C.7. in Appendix C). On monthly averaged data, although the relationships were significant for all El/Ca except Li/Ca, they were all below 8% ($R^2 < 0.08$) (Table 4.4.; Figure C.7. in Appendix C).

When correlating all annual El/Ca data against seawater turbidity (Table 4.4.; Figure C.8. in Appendix C), a significant negative correlation was found for Sr/Ca ($R^2 = 0.10$,

$p < 0.05$; slope = -4.82 mmol/mol per °C), U/Ca ($R^2 = 0.16$, $p < 0.05$; slope = -3.03 μmol/mol per °C), followed by Mg/Ca ($R^2 = 0.35$, $p < 0.05$; slope = 29.81 mmol/mol per °C) and finally Li/Mg ($R^2 = 0.46$, $p < 0.05$; slope = -8.34 mmol/mol per °C). At monthly resolved data, only Mg/Ca ($R^2 = 0.20$) and Li/Mg ($R^2 = 0.27$) showed a significant correlation (Table 4.4.; Figure C.8. in Appendix C), with the rest of El/Ca showing significant but weak correlations ($R^2 < 0.09$).

Table 4.4. Data from all samples. El/Ca versus SST and seawater turbidity at monthly and annual timescales. Bold values are statistically significant (p < 0.05).

	Monthly			Annual		
	Slope	**Intercept**	**R2**	**Slope**	**Intercept**	**R2**
Sr/Ca - SST	-0.043	9.98	**0.05**	-0.038	9.84	0.01
Mg/Ca - SST	0.1	1.39	**0.02**	0.342	-5.21	0.05
Li/Ca - SST	-0.038	7.59	0	-0.172	11.28	0.02
U/Ca - SST	-0.027	1.91	**0.06**	-0.048	2.5	0.04
Li/Mg - SST	-0.047	2.92	**0.08**	-0.135	5.31	**0.12**
Sr-U - SST	-0.014	7.85	**0.02**	0.015	7.07	0.00
Sr/Ca - Kd490	-2.394	8.95	**0.07**	-4.828	9.05	**0.1**
Mg/Ca - Kd490	17.952	3.21	**0.2**	29.805	2.6	**0.36**
Li/Ca - Kd490	4.806	6.3	**0.01**	7.844	6.12	0.03
U/Ca - Kd490	-1.927	1.27	**0.09**	-3.035	1.34	**0.17**
Li/Mg - Kd490	-5.3	1.89	**0.27**	-8.341	2.04	**0.47**
Sr-U - Kd490	-1.153	7.54	**0.03**	-1.457	7.57	0.03

4.3.3. Correlation of El/Ca data with coral growth

Significant correlations at both annual and monthly timescales were found between El/Ca and coral density (Table 4.5.; Figure 4.4.). A positive, and strongest, correlation was found for Mg/Ca ($R^2 = 0.49$ and $R^2 = 0.37$ at annual and monthly averages, $p < 0.05$). A negative correlation was found for Li/Mg ($R^2 = 0.40$ and $R^2 = 0.27$, $p < 0.05$), U/Ca ($R^2 = 0.20$ and $R^2 = 0.11$, $p < 0.05$), Li/Ca ($R^2 = 0.19$ and $R^2 = 0.14$, $p < 0.05$) and finally Sr/Ca ($R^2 = 0.12$ and $R^2 = 0.10$, $p < 0.05$) with the weakest correlation. No significant correlation was found between Sr–U and density for either the annual or monthly averaged data.

Relationships were also considered between all coral El/Ca data and other growth parameters (i.e., annual linear extension and calcification). However, no significant correlations are found between El/Ca and both annual linear extension and calcification rate in either the monthly or annually resolved data (Table 4.5.; Figure C.9. in Appendix C).

Table 4.5. Data from all samples. El/Ca versus density, linear extension and calcification at monthly annual timescales. Bold values are statistically significant ($p < 0.05$).

	Monthly			Annual		
	Slope	Intercept	R2	Slope	Intercept	R2
Sr/Ca - Density	-0.608	9.73	**0.09**	-0.742	9.69	**0.13**
Mg/Ca - Density	4.205	-2.44	**0.38**	4.629	-3.08	**0.46**
Li/Ca - Density	2.677	2.34	**0.17**	2.484	2.64	**0.16**
U/Ca - Density	-0.364	1.74	**0.11**	-0.454	1.89	**0.18**
Li/Mg - Density	-0.9	3.01	**0.27**	-1.051	3.26	**0.40**
Sr-U - Density	-0.204	7.79	**0.03**	-0.218	7.82	0.02
Sr/Ca - Extension	-0.001	8.76	0.00	-0.001	8.78	0.00
Mg/Ca - Extension	-0.028	4.42	**0.02**	-0.05	4.67	**0.06**
Li/Ca - Extension	0.057	6.04	**0.07**	0.049	6.12	**0.07**
U/Ca - Extension	0.002	1.14	0.00	0.004	1.14	0.01
Li/Mg - Extension	0.02	1.42	**0.13**	0.025	1.37	**0.24**
Sr-U - Extension	-0.002	7.49	0.01	-0.004	7.52	0.02
Sr/Ca - Calcification	-0.003	8.8	0.00	-0.003	8.83	0.00
Mg/Ca - Calcification	-0.003	4.22	0.00	-0.02	4.5	0.02
Li/Ca - Calcification	0.051	5.84	**0.13**	0.044	5.94	**0.13**
U/Ca - Calcification	0.001	1.16	0.00	0.001	1.16	0.00
Li/Mg - Calcification	0.011	1.45	**0.08**	0.015	1.39	**0.17**
Sr-U - Calcification	-0.003	7.51	0.01	-0.004	7.54	0.03

Relationships between growth parameters and environmental variables (i.e., SST and seawater turbidity) are investigated in depth in Chapter 3. Briefly, annual linear extension and calcification are highly correlated in all samples ($R^2 > 0.85$, $p < 0.05$). Linear extension and density are somewhat correlated ($R^2 = 0.10$, $p < 0.05$), while no significant correlation was found between density and calcification. Investigating single core growth parameters at annual intervals, no relationship was found between them and SST (except density-SST in FP17_1). All three parameters, however, are significantly correlated with local seawater turbidity ($R^2 = 0.43$ for density, $R^2 = 0.38$ for annual extension and $R^2 = 0.52$ for calcification; $p < 0.05$).

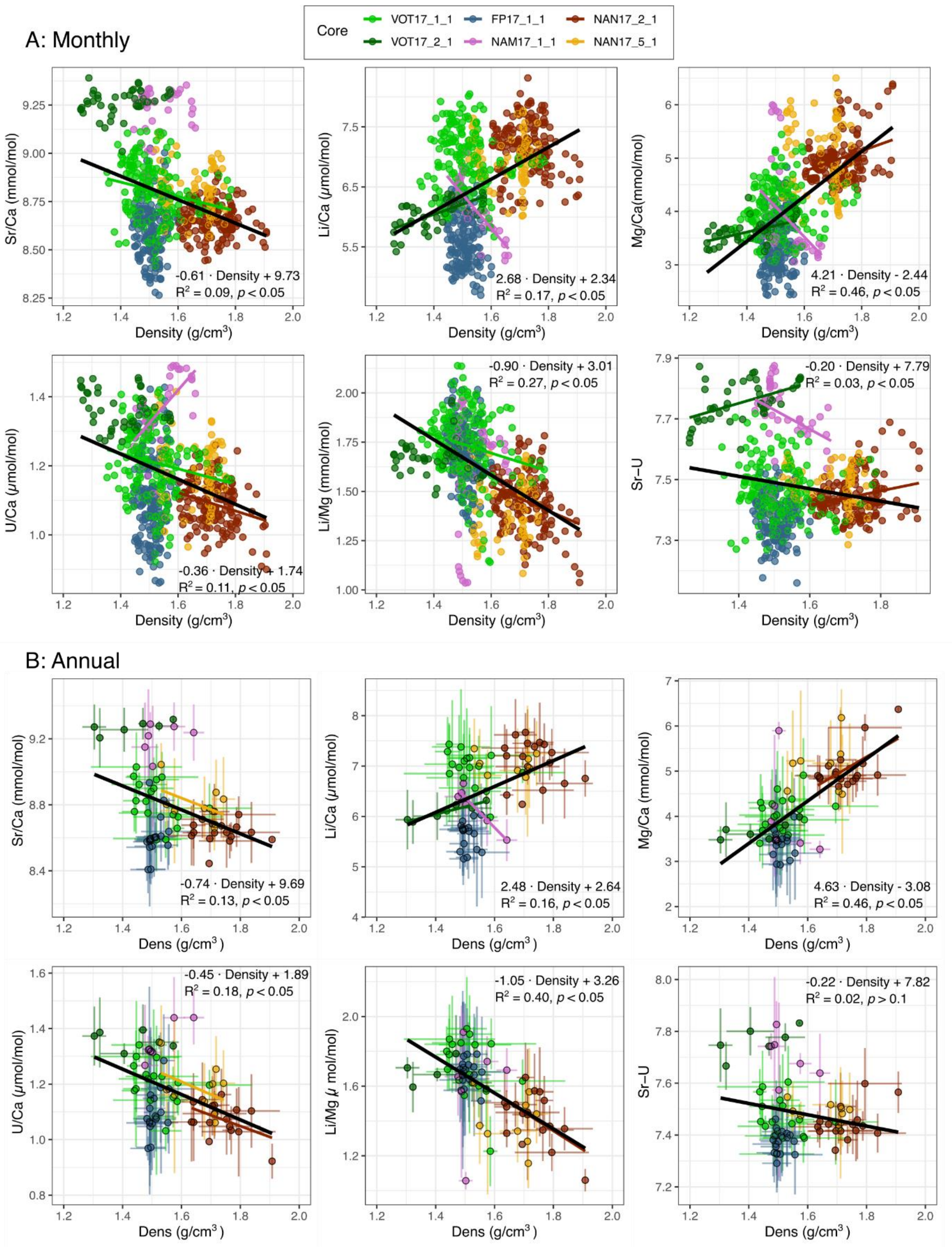

Figure 4.4. A) Monthly resolved El/Ca vs core density. B) Annually resolved El/Ca vs core density. Error bars are 2SD. Colour datapoints and linear regressions correspond to single core data. Only significant linear regressions (p < 0.05) are included. Black line is the best linear fit considering all data. Equation in each plot correspond to all data.

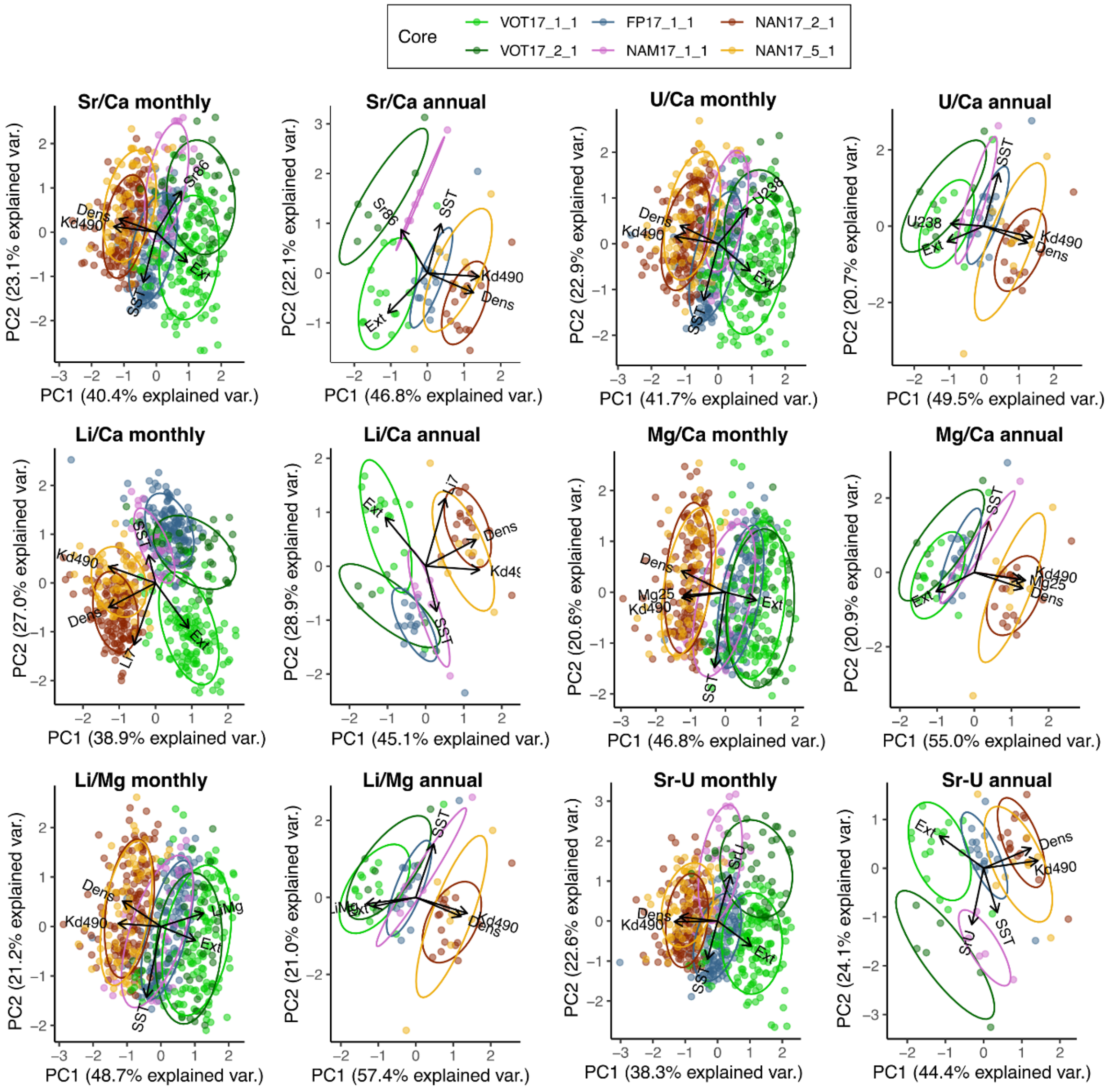

Figure 4.5. PCA biplots (data scores and loading vectors) of El/Ca from each core with SST, extension, density and seawater turbidity (K_d490) at monthly and annual timescales.

4.3.4. PCA analysis

Principal Component Analysis (PCA) was performed to identify the leading factors influencing coral El/Ca variability (Figure 4.5.) on both monthly and annually resolved El/Ca, growth, and environmental data. Growth data included density and extension, but not calcification (due to its high autocorrelation with extension). For each El/Ca, at either time scale, PC1 and PC2 were found to explain >70% of the variance. When PC3 was included, the explained variance was of > 90%. These results indicate that two independent processes control the coral El/Ca variability and that similar mechanisms are acting across cores. Loading vectors show how at monthly timescales El/Ca is correlated with SST (negative correlation in Sr/Ca, U/Ca, Li/Ca, Li/Mg and Sr–U; positive correlation in Mg/Ca). At annual timescales SST is a less dominant factor, with either density or seawater turbidity dominating the El/Ca signal (negative correlation in Sr/Ca, U/Ca, Li/Mg and Sr–U; positive correlation in Mg/Ca) except in Li/Ca, where SST dominates. Data scores shows consistently core grouping being dominated by two extremes: Votua cores versus Nananu-i-Ra cores, with Suva and Namuka samples falling in between. Data scores are mostly dictated by PC1 (Seawater turbidity and coral growth).

4.4. Discussion

4.4.1. Elemental ratio correlations and interplay of physiological processes

Coral aragonite El/Ca directly reflects the chemistry of the ECF (Cohen and Gaetani 2010). The chemistry of the ECF (and therefore coral El/Ca) is influenced by physiological processes controlling the diffusion of ions and seawater into the calcifying space (Tambutté et al. 2011), the rate at which new mineral is precipitated, and the Rayleigh fractionation occurring because of them (Cohen and Saenger 2006). Sometimes, these processes act to the point that they mask completely the SST influence over coral El/Ca, thus complicating the SST reconstruction from coral archives.

However, the assessment of elemental ratio variability can help understanding how biomineralization works, and the effects of environmental factors on biological processes. Consequently, the correlation and directionality of multiple trace elements have been used to decipher non-thermal controls over the coral El/Ca signal (Sinclair 2005b; Sinclair et al. 2006; Cohen and Gaetani 2010; DeCarlo et al. 2016; Marchitto et al. 2018). Here, I explore relationships between coral El/Ca to assess the influence of Rayleigh fractionation and Ca^{2+} pumping in the Fijian *Porites* spp. of this study.

Sr/Ca and Mg/Ca are negatively correlated in five out of six coral samples (r = -0.19 – -0.67; NAN17-2 shows a non-significant correlation; Table 4.2.; Figure 4.2. and Figure 4.3.). These results agree with what it would be expected under Rayleigh fractionation, with skeletal fractions showing high Sr/Ca and low Mg/Ca, and a progressive depletion in Sr/Ca mirrored by an incremental rise in Mg/Ca (Figure 4.2.; Figure 4.3.). However, when looking at all data from all coral samples, no correlation is observed due to mean differences in Sr/Ca and Mg/Ca across cores (Table 4.1.). The origin of mean differences of El/Ca across colonies (or even within colonies) such as that observed here has been attributed to differing physiological processes or rates that alter Ca^{2+} (and Sr^{2+} pumping; Marchitto et al. 2018). For example. small differences in Ca^{2+} pumping can cause some corals to precipitate aragonite more efficiently, or at a faster rate leading to different Rayleigh fractionation across samples and/or kinetic effects (e.g., crystal adsorption or elemental inclusion in crystal defects (Rollion-Bard and Blamart 2015), masking the SST signal. Under this same conceptual model, there is an expected negative correlation between Sr/Ca and Mg/Ca (Sinclair 2005b; Marchitto et al. 2018). Importantly, calcification physiology and environmental variables can both impact this process. This is further explored in Sections 4.4.2. and 4.4.3.

Li/Ca and Mg/Ca are positively correlated in five of our samples, which agrees with what has been observed in other studies (e.g., Montagna et al. 2014). The exception is again in NAN17_2 (Table 4.2.). This co-variability is expected under Rayleigh fractionation (Figure 4.2.; Figure 4.3.) and fits the biomineralization model presented by Marchitto et al. (2018). This biomineralization model illustrates that both Li^{+} and Mg^{2+} are incorporated into the ECF via paracellular diffusion, and therefore their initial composition remains similar to that of seawater. Due to their low precipitation coefficient (K_D Mg and K_D Li << 1) they are strongly discriminated against during aragonite precipitation which causes both ratios to increase due to Rayleigh fractionation. As a result, they will have a strong positive correlation with each other. Interestingly, in NAN17_2, Li/Mg changes across a range of 2 μmol/mol (6.00 – 8.20 μmol/mol) while Mg/Ca remains at ~5.00 mmol/mol, and there is no significant relationship between them. This implies that in this core some additional process at play controls Li/Ca changes while Mg/Ca remains stable. Furthermore, VOT17_1 shows an enrichment of Li/Ca with respect to Mg/Ca that deviates from the observed correlation (Figure 4.2.). In this core Li/Ca ranges between 6.00 and 8.00 μmol/mol, ~0.50 mmol/mol higher than the predicted correlation based on its Mg/Ca range (3.00 – 5.00 mmol/mol). It is unclear why the co-variability of Li/Ca-Mg/Ca, which is dependent on Rayleigh fractionation in the ECF, differs in these two samples, but it is not unprecedented. Hathorne et al. (2013) found negative correlation between Li/Ca and Mg/Ca ratios in *Porites* spp. and argued that, in this case, the mechanisms behind Li/Ca incorporation into the coral skeleton and the extent of variation depending on SST and/or Rayleigh fractionation are not clear. The presence of differing Li/Ca – Mg/Ca correlations from what is predicted under Rayleigh fractionation in our samples hints that other kinetic processes can be affecting Li/Ca and not Mg/Ca in these samples such as lattice defects that can trap these ions (Mitsuguchi et al. 2001; Watanabe et al. 2001; Rollion-Bard and Blamart 2015).

In the case of Li/Ca – Sr/Ca, and under biomineralization processes where Rayleigh fractionation was the main component controlling co-variability between El/Ca, Li/Ca would be expected to have a negative correlation with Sr/Ca (similar to that of Mg/Ca with Sr/Ca) (Montagna et al. 2014). However, in our samples only one coral (NAN17_2) out of the six follows this prediction (Table 4.2.) and, coupled with the lack of a relationship between Mg/Ca – Li/Ca indicates that an additional process is controlling incorporation of Li^+ into the coral aragonite in this colony. Possible controls could be environmental (such as SST in Hathorne et al. 2013) or kinetic (Rollion-Bard and Blamart 2015).

Finally, I explore the co-variability of U/Ca with other El/Ca. Data across all cores show a positive correlation between Sr/Ca and U/Ca (r = 0.70 – 0.86) (Figure 4.2.; Table 4.2.). This positive correlation has been observed in many studies (Cardinal et al. 2001; Fallon et al. 2002; Hendy et al. 2002; Quinn and Sampson 2002; Sinclair et al. 2006; Felis et al. 2009, 2012). DeCarlo et al. (2015b) developed a biomineralization model concluding that while Sr/Ca was dependent on SST, U/Ca was only controlled by $[CO_3^{2-}]$ of the ECF and that the observed strong correlations between coral Sr/Ca and U/Ca were derived from biomineralization processes indirectly mediated by SST. In this model, as with the observations by Sinclair (2005b) and the biomineralization model of Marchitto et al. (2018), an increase in Ca^{2+} pump would increase: i) the ECF pH and

[CO_3^{2-}] and enhance aragonite precipitation rate, and ii) increase Sr^{2+} in the ECF showing weak Rayleigh fractionation.

Co-occurring changes in [CO_3^{2-}] and Rayleigh fractionation controls U/Ca in the coral skeleton (DeCarlo et al. 2016), and negative correlations of U/Ca with Mg/Ca and Li/Ca are expected. While this is true for U/Ca – Mg/Ca across all core samples in this study (r = -0.39 – -0.78) (Table 4.2.; Figure 4.2.), U/Ca – Li/Ca negative correlations are only significant in samples VOT17_2, FP17_1, NAM17_1 and NAN17_5 (r = -0.17 – -0.73) (Table 4.2.; Figure 4.2.), again highlighting an additional control on Li^+ incorporation.

Overall, the correlation analysis between elemental ratios indicates that the El/Ca variability in the majority of the *Porites* spp. corals examined here can be explained with the current biomineralization models where Ca^{2+} pumping can alter the composition of the semi-isolated ECF, and subsequent mineral precipitation induces Rayleigh fraction. Partitioning of Sr/Ca (and U/Ca) into the coral aragonite is simply controlled by Ca^{2+} pumping, whereas Li/Ca and Mg/Ca is jointly controlled by Ca^{2+} pumping and strengthening Rayleigh fractionation. However, colony-specific processes establish the baseline El/Ca value, and potential causes are explored below.

4.4.2. Elemental variability and influence of growth

In section 4.4.1., I discussed the role of biomineralization, Ca^{2+} pumping and Rayleigh fractionation in modifying El/Ca in coral aragonite by examining the relationship between the elemental ratios. The rate at which these biogeochemical processes occur will additionally play a role controlling the elemental concentration in coral skeletons. Differences in skeletal growth rate (specifically linear extension and calcification) have been used to explain Sr/Ca (de Villiers et al. 1994; Ferrier-Pagès et al. 2002; Goodkin et al. 2005; Kuffner et al. 2012; Grove et al. 2013; Tanaka et al. 2015; Clarke et al. 2017) and Li/Mg variability (Fowell et al. 2016). Differences in Sr/Ca and Mg/Ca in colonies from similar reef environments (Reed et al. 2021) and in coeval transects within a single colony (Reed et al. 2021) have been linked to differences in skeletal density (DeLong et al. 2013). It is well established that environmental conditions including salinity, temperature, light, and *p*CO2 affect coral growth via calcification and physiological processes (Tambutté et al. 2011 and references therein), potentially changing the amount of energy available for Ca^{2+} pumping (Wu et al. 2021) and consequently modulating calcification (e.g., light-enhanced calcification via enhanced photosynthesis; Cohen et al. 2002) and coral El/Ca. In this section I investigate the co-variability between El/Ca and coral growth (using density extracted from CT scans), to investigate the influence of biomineralization rate on El/Ca.

Linear regression of El/Ca-density, considering all data from all cores, at both monthly and annual timescales (Figure 4.4.) show significant negative correlations for Sr/Ca, U/Ca and Li/Mg. Significant positive correlations were found for Mg/Ca and Li/Ca. And Sr–U did not show any correlation with density. The loading vectors of the PCA biplots (Figure 4.5.) show the same direction of these El/Ca-Density correlations. Reed et al. (2021) explored *Porites* spp. El/Ca (Sr/Ca, Mg/Ca and Ba/Ca) from Wolf Island (Galapagos) and their El/Ca variability with density and found the same directionality in the El/Ca correlations (negative for Sr/Ca and positive for Mg/Ca) at annual scales, although this observation was present within each core, but not when including all data from all cores as in this chapter. The contrasting results between Reed et al. (2021) and our study can be due to a combination of factors related to the length of the records and/or site-specific environmental factors. The coral cores in Reed et al. (2021) covered several decades (40 – 100 years, core dependent), while samples studied here encompass less than two decades (between 5 and 17 years, core dependent; Table 4.1.). The limited length of the coral data sets in this chapter and the exposure to continued thermal stress over the last ~4 years of the timeseries (2014-2017) and corresponding density variability could explain the lack of significant correlations within each core. Further, density variability within one core sample of Reed et al. (2021) is similar (or higher) than the density variability seen across all samples and sites of the Fijian *Porites* spp. of this study. Reed et al. (2021) density values vary by about ~1g/cm^3 across all core samples, with single core density values ranging from 0.50g/cm^3 to 0.90g/cm^3 whereas in these Fijian *Porites* spp. density across all cores vary by ~0.60g/cm^3, and single core densities show a smaller range, between 0.05g/cm^3 and 0.30g/cm^3. Additionally, the coral samples in Reed et al. (2021) were collected at two locations with similar environmental conditions, near Wolf Island (Galapagos), an inhabited and small island with no influence from nearby land and river run-off. This contrasts with the Fijian cores here, which are derived from reefs with diverse environments (e.g., across a seawater turbidity gradient). Overall, despite the differences in core length, environment, and exposure to thermal stress, both studies show an existing relationship between skeletal density and El/Ca.

As in section 4.4.1., examining the correlations between El/Ca and density can shed some light on biomineralization processes, deviations from expected Rayleigh fractionation and the potential for ECF modification via Ca^{2+} pumping. Corals with low density show elevated Sr/Ca and diminished Mg/Ca, opposite to corals with higher density (Figure 4.4.). Similar observations are made by Reed et al. (2021) where sections of their coral samples show a systematic increase of Mg/Ca and decrease of Sr/Ca as skeletal density increases. This is interpreted as a sign of Rayleigh fractionation, which agrees with our observations. Cores NAN17_2 and NAN17_5 (corals with highest density) shows a stronger Rayleigh fractionation than other corals of this study with lower density.

There are two potential mechanisms behind higher density being associated with stronger Rayleigh fractionation: i) Higher densities are due to an increased net calcification from a theoretical single unit of isolated ECF, therefore exerting stronger modification of the ECF composition, lowering Sr^{2+} and Ca^{2+} and increasing Mg/Ca and Li/Ca as coral skeleton is precipitated; ii) Higher densities occur as a result of limited calcification and low ECF renewal rate. Skeletal deposition, although diminished, continues from a slowly refreshed ECF, therefore strongly modifying its chemical composition and this being reflected as a strong Rayleigh fractionation (low Sr/Ca, high Mg/Ca and Li/Mg). In all cases, the primary driver of Rayleigh fractionation (and skeletal El/Ca) is not density in itself, but ECF renewal and mineral precipitation rate; with density being a function of this biological process.

Several questions remain on whether density is directly correlated to skeletogenesis and biomineralization, and to what extent. On the relationship of density with calcification and linear extension, I observed in Chapter 3 that coral samples from the Votua Reef (VOT17_1 and VOT17_2) show the highest calcification and linear extension rates of all samples and lowest density, and Nananu-i-Ra (NAN17_2 and NAN17_1) have the lowest calcification and linear extension rates and highest density. The link between density and linear extension is weak in the samples of this study ($R^2 < 0.10$), showing a negative correlation that was also observed in *Porites* spp. from the Great Barrier Reef (Lough 2008). Furthermore, previous studies on *Porites* spp. corals (Lough 2008) show how calcification (calculated as the product of linear extension and density) is influenced mostly by linear extension, and marginally by density. Thus, increased density is not necessarily directly caused by lowered linear extension. It is more likely, however, that biomineralization mechanisms determine extension and density independently, leaving these two variables only weakly correlated.

The cause of the lack of correlation between Sr/Ca, Mg/Ca, Li/Ca, U/Ca, and Sr–U with linear extension and calcification is not straightforward, although it was significantly correlated with Li/Mg (Table 4.5.; Figure C.9. in Appendix C). This poses the question: why would density be a better reflector of biological processes than linear extension or calcification in Fiji? Some studies have previously found significant correlations between Sr/Ca and linear extension in *Diploria* spp. (Goodkin et al. 2005) and calcification rate in *Montipora capitata* (Kuffner et al. 2012). Yet, similarly to this study, Reed et al. (2021) also found a lack of correlation between El/Ca and linear extension and calcification in *Porites* spp. Furthermore, DeLong et al. (2013) showed skeletal areas of *Porites* spp. where Sr/Ca and density changed despite linear extension remaining unchanged, which was also observed in Reed et al. (2021). Overall, this study and previous work suggests that relationship between growth parameters and El/Ca is species-specific. The inconsistency in relationships between geochemical data and growth parameters grants the need to carefully consider all parameters, as sensitivity to skeletogenesis mechanisms can be variable across regions, colonies and/or species (Lough and Cantin 2014).

Fijian *Porites* spp. with the highest calcification (lowest densities – VOT17_1 and VOT17_2) show the weakest Rayleigh fractionation and the samples with lowest calcification (highest densities – NAN17_2 and NAN17_5) show the strongest Rayleigh fractionation in their ECF. We hypothesise that in the case of Fijian corals, mean El/Ca is a combination of enhanced Ca^{2+} pumping resulting in a higher renewal rate of the ECF and a weak Rayleigh fractionation signature. Enhanced Ca^{2+} pump will also increase Sr^{2+}, pH, and $[CO_3^{2-}]$ in the ECF and will allow the coral to extend at a faster rate (showing low density). Limited Ca^{2+} pumping can result from limited energy available for the coral polyp (Wu et al. 2021) to promote calcification (resulting in high skeletal density), and ECF renewal rate is lower and/or reliant on paracellular passive seawater transport forcing a strong Rayleigh fractionation in the ECF (Cheung et al. 2021). These observations (i.e., biomineralization processes causing differences in El/Ca) fits the idea described in section 4.4.1. by exploring correlations between El/Ca. Biomineralization (being promoted by Ca^{2+} pumping into the ECF, increasing pH, $[CO_3^{2-}]$ and aragonite saturation state) affects El/Ca in a systematic way (increasing or decreasing the availability of Sr^{2+} and Ca^{2+}, and modifying Li/Ca and Mg/Ca in the ECF through Rayleigh fractionation).

4.4.3. Elemental variability and environmental parameters

PCA analysis shows that changes in reef environment, specifically turbidity (K_d490), also influences the SST-proxy coral El/Ca (Figure 4.5.). SST has a stronger influence on seasonal timescales, but on annual timescales El/Ca is controlled by SST, density, and turbidity (Figure C.7. and Figure C.8. in Appendix C). Remote-sensed environment data show a gradient in seawater turbidity and chlorophyll-a concentration between core sites which correlates with linear extension and calcification (negative correlation, $R^2 = 0.40$) and density (positive correlation, $R^2 = 0.25$). One pathway in which seawater turbidity can affect skeletal density and calcification is via photosynthesis rates, another is trophic differences associated with different turbidity regimes. Either could modify the amount of energy available for cellular activity (Marshall and McCulloch 2002; e.g., Ca^{2+} pumping via Ca-ATPase enzymes) and, coupled to SST seasonality influencing cellular activity (Sivaguru et al. 2021) would alter the energy balance of individual colonies.

Under clear water conditions, enhanced zooxanthellate photosynthesis allows corals to have surplus energy available for Ca^{2+} pumping and enhanced calcification (Cohen and McConnaughey 2003; Allemand et al. 2011). This translates into higher calcification rates but also a more regular supply of Ca^{2+} and Sr^{2+}, hence producing a weak Rayleigh fractionation in the coral aragonite. On the other hand, elevated annual turbidity supresses the availability of coral symbionts to photosynthesise, supplying less energy for biomineralization (Carricart-Ganivet and Merino 2001). This can directly lower the availability of the coral to modify the ECF by Ca^{2+} pumping, resulting in stronger Rayleigh fractionation (as observed). Furthermore, due to low photosynthesis levels, coral colonies under this regime might show higher heterotrophy and respiration levels, ultimately limiting their calcification (Tambutté et al. 2011). Increasing SST and light ability due to low seawater turbidity both allow for an increase of energy available to the coral for Ca^{2+} pumping, with enhanced Ca^{2+} pumping (and enhanced aragonite precipitation) being reflected as elevated Sr/Ca, elevated U/Ca and low Li/Ca and Mg/Ca (low Rayleigh fractionation), as in the cases of VOT17_1 and VOT17_2 (less turbid sites) (Figure 4.2. and Figure 4.3.). On the opposite side, in Nananu-i-Ra (more turbid sites) seasonal changes in SST change energy available for Ca^{2+}, but long-term elevated turbidity (with respect to other sites of this study) causes coral colonies to express lower Ca^{2+} pumping (and lower calcification), therefore low Sr/Ca and U/Ca, and elevated Li/Ca and Mg/Ca as a result of a strong Rayleigh fractionation (Figure 4.2. and Figure 4.3.). These findings align with previous work showing that the empirical relationship between El/Ca (Sr/Ca, Li/Mg, Sr–U) and SST was affected by local and reef-specific factors such as seawater carbonate chemistry, water depth, and runoff (Wei et al. 2000; Swart et al. 2002; Smith et al. 2006; Cole et al. 2016), light availability (Cohen et al. 2002; Reynaud et al. 2007) in addition to food availability and trophic level. The direction of the relationships between SST, density and seawater turbidity and each El/Ca is the same across variables (e.g., correlation of Sr/Ca-SST, Sr/Ca-density, and Sr/Ca-turbidity is negative in all cases), reinforcing the idea that this is caused by a physiological process being affected by different environmental variables in a similar way. This comparison shows that SST proxies in the Fijian *Porites* spp. of this study are influenced by an interplay between SST, Ca^{2+} pumping and Rayleigh fractionation. In addition, variability of skeletal density and aragonite precipitation rate are associated with the reef environment (i.e., seawater turbidity), which exerts an indirect control over the degree of Rayleigh fractionation shown in the coral skeleton. This can cause "vital effects" on the geochemical records, masking the influence of SST over coral El/Ca.

4.4.4. Overcoming confounding effects in SST reconstructions in South West Pacific

As shown in Section 4.4.3. confounding effects between SST and other environmental parameters can complicate temperature reconstructions at both seasonal and interannual scales. With our understanding of the influence that Rayleigh process, Ca^{2+} pumping, and growth/environment changes can have on El/Ca, we can investigate the potential of established (Sr/Ca) and alternative paleotemperature proxies (Li/Mg and Sr–U) in Fiji. In line with previous work (e.g., Sinclair et al. 1998; Fallon et al. 1999, 2003; Hathorne et al. 2011; Montagna et al. 2014; Fowell et al. 2016), El/Ca (Sr/Ca, Mg/Ca, Li/Ca, U/Ca) in coral samples of this study show a varying degree of relationships, although weak, with SST (Table 4.3.; Figures C.1. to C.6. in Appendix C). At monthly time-scales, Sr/Ca shows the strongest negative relationship with SST (sensitivity ranging between 0.029 and 0.064 mmol/mol per °C; $R^2 = 0.13 - 0.39$; Table 4.3.), wider than previous Sr/Ca-temperature sensitivities from other studies (Corrège 2006). Li/Mg shows negative correlations (sensitivity ranging between 0.036 and 0.081 mmol/mol per °C; $R^2 = 0.10 - 0.42$) among cores in agreement with previous studies (Montagna et al.

2014). Sr–U is weakly correlated ($R^2 = 0.04 – 0.15$) with SST, contrasting with work showing its application in *Porites* spp. at annual timescales (DeCarlo et al. 2016).

The range of correlations and sensitivities of Sr/Ca with SST across Fijian coral samples is not unprecedented. Previous attempts at SST reconstructions from Fijian corals have shown weak correlation between coral Sr/Ca from *Porites* spp. colonies both collected in the Savusavu Bay (Vanua Levu) over the 1780 – 1997 period ($R^2 = 0.20$; Linsley et al. 2006). Furthermore, when linearly regressing coral Sr/Ca with local SST of these two corals at Savusavu Bay, correlations were different ($R^2 = 0.74$, Linsley et al. 2004; $R^2 = 0.40$, Linsley et al. 2006). Sr/Ca from a *Porites* spp. colony at the Yasawa Islands (Fij, located ~40 km north-west of Viti Levu) revealed a significant, but not strong, correlation with SST ($R^2= 0.61$, Le Bec 2001). These observations led Juillet-Leclerc (2006) to conclude that Sr/Ca in Fijian *Porites* spp. is not always linearly related to SST and likely affected by other factors, either physiological or environmental. These studies, however, were limited to one elemental ratio (Sr/Ca) and their insights were solely regarding the proxy's potential to accurately reconstruct SST.

Further, the range of mean Sr/Ca among samples in this study (0.086 mmol/mol) would imply a mean SST difference among sites of 14.3°C (applying a sensitivity of 0.060mmol/mol per °C; Corrège 2006). In the case of Li/Mg, a range of 0.56 mmol/mol is observed across colonies, which would equivalate to a difference of 8.9°C across sites (applying Stewart et al. 2020). These differences not only are not coherent between themselves, but also not realistic as instrumental SST has shown how SST across all reef locations is virtually the same (t-test, $p < 0.05$; Chapter 2 – Section 2.6.1.). Differences in mean El/Ca and proxy sensitivity in El/Ca-SST correlation have been found not only between regions (South West Pacific v. Atlantic), but also within regions and even reefs. Similar calibration errors have been shown in the literature for Sr/Ca (e.g., Sayani et al. 2019) and Li/Mg (e.g., Fowell et al. 2016).

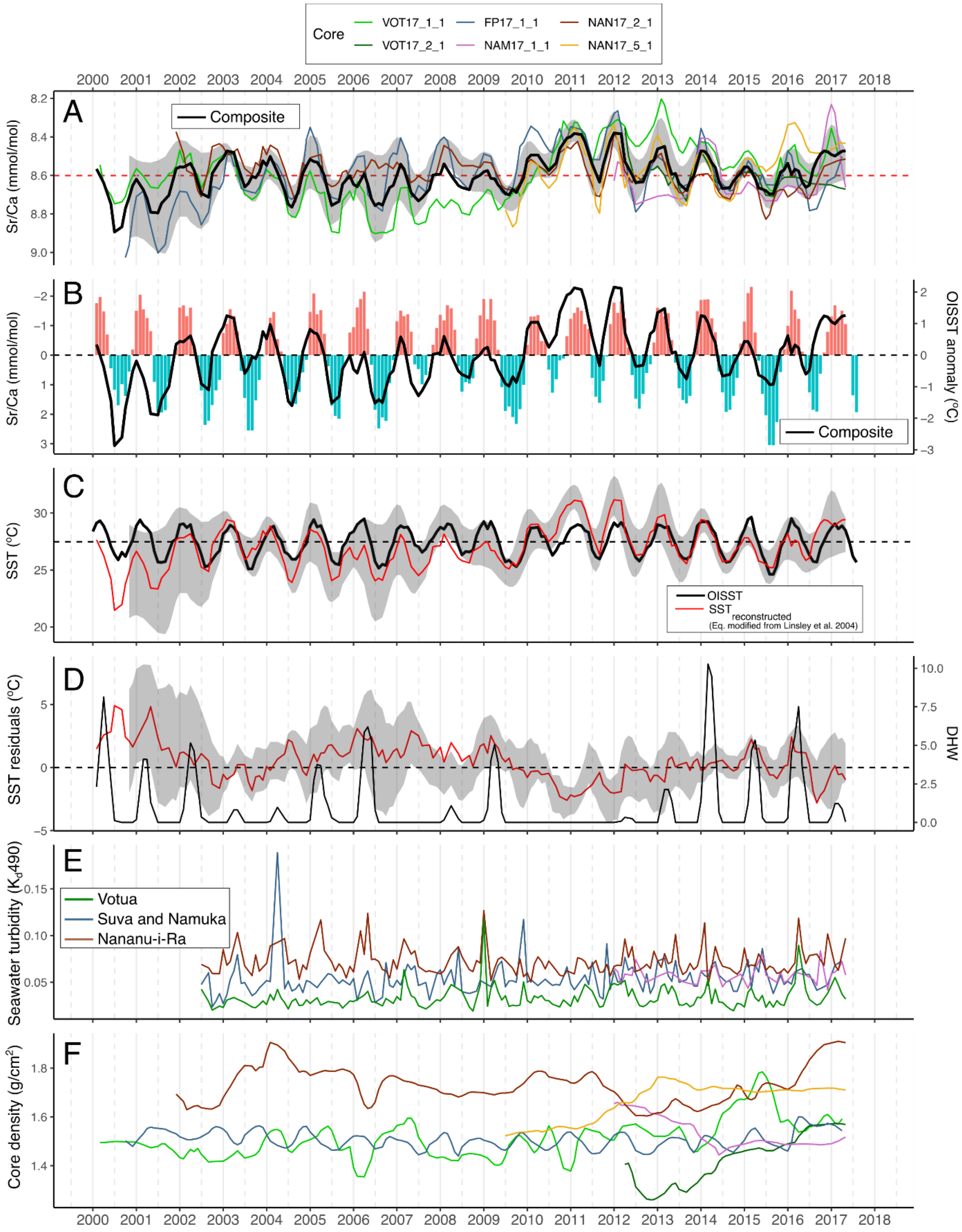

Figure 4.6. A) Normalised Sr/Ca of each core (colour lines) and averaged Sr/Ca from all cores (black line). Grey ribbon represents CI of the mean (95%). B) Averaged Sr/Ca (black line) and SST anomaly (computed for the 2000-2017 mean). C) Satellite SST (black line) and reconstructed SST from composite Sr/Ca using modified equation from Linsley et al. 2004 (red line), including 95% CI envelope (grey ribbon). D) SST residuals (SST satellite-SST reconstructed) (red line) + CI (95%) (Grey ribbon) and DHW (black line). E) Seawater turbidity at each reef of this study. F) Density of each core. All data is monthly resolved.

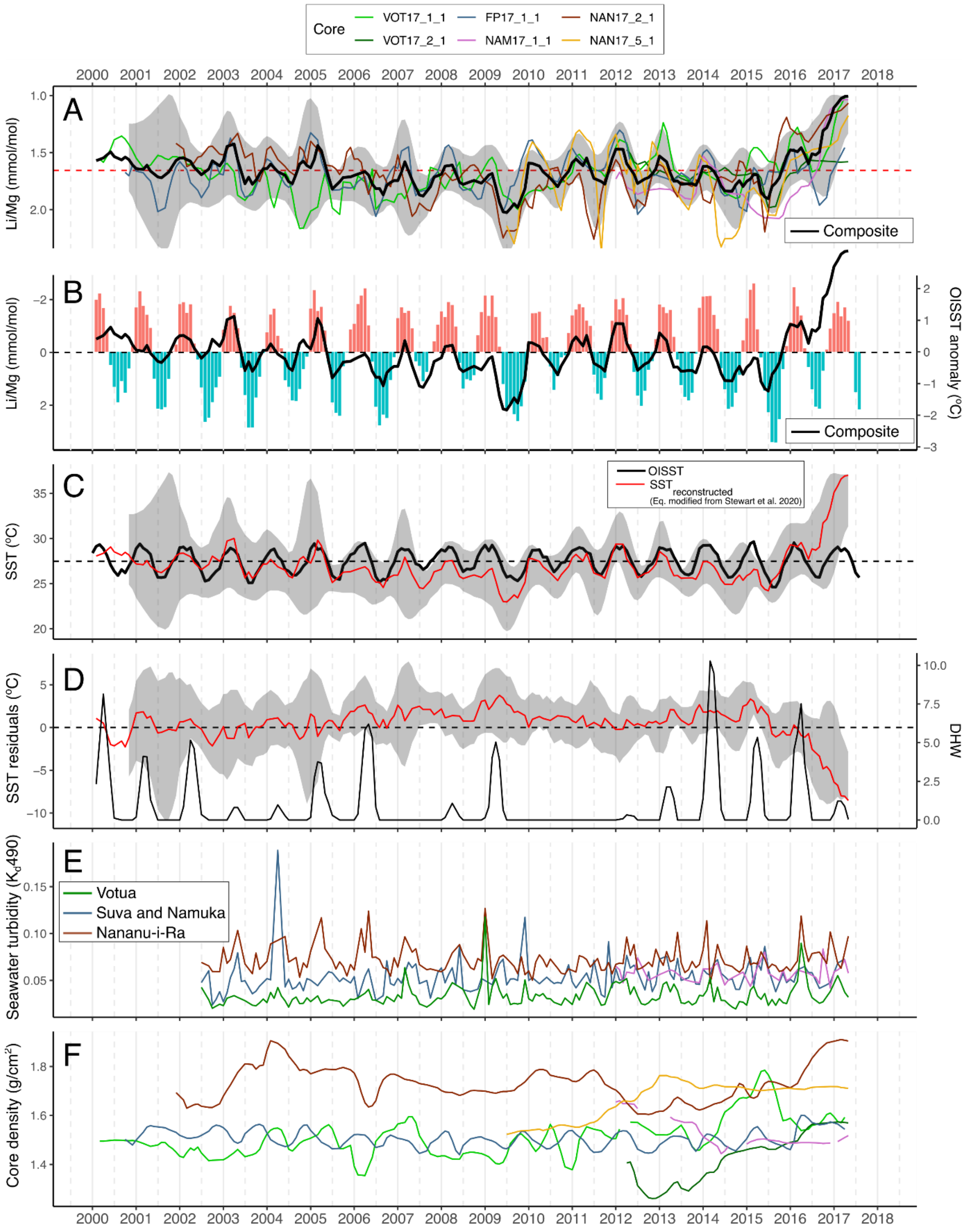

Figure 4.7. A) Normalised Li/Mg of each core (colour lines) and averaged Li/Mg from all cores (black line). Grey ribbon represents CI of the mean (95%). B) Averaged Li/Mg (black line) and SST anomaly (computed for the 2000-2017 mean). C) Satellite SST (black line) and reconstructed SST from composite Li/Mg using modified equation from Linsley et al. 2004 (red line), including 95% CI envelope (grey ribbon). D) SST residuals (SST satellite-SST reconstructed) (red line) + CI (95%) (Grey ribbon) and DHW (black line). E) Seawater turbidity at each reef of this study. F) Density of each core. All data is monthly resolved.

To overcome the interaction of SST, growth, and local environment in the El/Ca, I built Fiji Sr/Ca and Li/Mg composites by normalising the El/Ca signal of every sample and average into one averaged time-series (Figure 4.6.A and Figure 4.7.A). This approach, similar to the methodology applied in dendrochronology, has been successfully used before (Hendy et al. 2002; Lough 2004; Pfeiffer et al. 2009; Sayani et al. 2019) to constrain the common climatic signals (i.e., SST) and improve the robustness of the paleoreconstructions. In this study only Sr/Ca and Li/Mg composites are explored as they showed the best correlations with SST in every single core (Table 4.3.; Figures C.1. to C.6. in Appendix C). Sr–U is not further explored as the relationships with SST of each core were weak (<10%). The Sr–U proxy has been successfully used previously to reconstruct recent SST from several coral species in the South West Pacific (DeCarlo et al. 2016; Ross et al. 2019) and Atlantic (Alpert et al. 2017; Rodriguez et al. 2019). However, in Fijian *Porites* spp. in this study Sr–U fails to show a clear correlation with SST at both interannual and seasonal timescales. Further work is required before applying said proxy in Fiji, where both U/Ca and Sr/Ca show correlations with seawater turbidity and there are differences in mean Sr/Ca and U/Ca across reefs, thus "vital effects" seem to be still masking the SST signal in this region.

The data shows that averaging El/Ca across all replicated colonies improved the correlation with SST and smooths out colony specific variability to certain extent. For the averaged Sr/Ca, the correlation with SST is higher than any of the single core correlations ($R^2 = 0.40$; Table 4.3.), and it also is the strongest correlation with SST found. The averaged Li/Mg also shows a strongest correlation with SST than with any single core ($R^2 = 0.34$; Table 4.3.), but it is a weaker correlation than Sr/Ca.

To further explore the composite Sr/Ca and Li/Mg timeseries, their capacity to reconstruct SST at monthly timescales accurately and identify potential periods of time when the reconstruction deviates from the satellite SST, I converted Sr/Ca and Li/Mg datasets to reconstructed SST (Figure 4.6.C and Figure 4.7.C). The composite Sr/Ca has been transformed to SST using Sr/Ca-SST equation by Linsley et al. (2004) as it is the only available calibration for *Porites* spp. in Fiji. When applying this equation ($Sr/Ca = -0.053 \cdot SST + 10.65$; Linsley et al. 2004), we obtain a mean SST error of 11.67°C over the recorded SST (Figure C.10. in Appendix C). This deviation is attributed to the offset between the Linsley et al. (2004) mean Sr/Ca (9.22 mmol/mol) and the composite Sr/Ca mean in this study (8.60 mmol/mol). The need of site and colony-specific calibration for Sr/Ca has been observed previously in the South West Pacific (Corrège 2006), I therefore maintain the equation sensitivity of Linsley et al. (2004) but modify the intercept to adapt it to the Sr/Ca mean at 27°C (Fiji annual SST average) with the adapted equation being ($Sr/Ca = -0.053 \cdot SST + 10.03$). For Li/Mg, we used Stewart et al. (2020) equation for biogenic aragonite ($Li/Mg = 5.42e^{-0.05} \cdot SST$) as it is the most recent compilation of a universal Li/Mg calibration for aragonitic organisms. Using the Stewart et al. (2020) Li/Mg equation, at a given SST of 27°C (Fiji's annual average), the resulting mean Li/Mg of the equation is 1.41 mmol/mol. In contrast, mean Li/Mg of the coral samples in this study is 1.66 mmol/mol. This Li/Mg difference (0.25 mmol/mol) would reflect an SST error of 3.27°C. Fowell et al. (2016) found a similar divergence in Li/Mg based SST reconstruction with coral samples from different locations of a reef and expressed the need for site-specific calibrations. As such, we have adapted the universal Stewart et al. (2020) calibration to our averaged Li/Mg data (to $Li/Mg = 6.39e^{-0.050} \cdot SST$) and limit the deviation from satellite SST. This needed "standardization" between reconstructed SST and satellite SST might indicate that paleo SST reconstructions in Fiji using fossil cores may grant the need for composite datasets and site-specific calibrations in order to accurately quantify absolute interannual temperatures.

The reconstructed SST (Sr/Ca) fits instrumental SST, but cold deviations (positive Sr/Ca anomalies) from instrumental data are observed during periods of thermal stress (Figure 4.6.C). SST residuals, calculated as the difference between reconstructed SST and instrumental SST, show lower SST reconstructed than instrumental SST (cold bias) during 2000 to 2002, 2005 to 2007 and 2015 to 2016 by around 2.5°C less on average over the entire period (Figure 4.6.D). In a similar way, reconstructed SST (Li/Mg) shows cold deviations of more than 2.5°C during 2000 to 2002, 2006 to 2009, and 2014 to 2015 (Figure 4.7.D). The cold-biased periods in both SST proxies (Sr/Ca and Li/Mg seem to overlap with years of elevated thermal stress.

The breakage in the El/Ca-SST relationship with thermal stress has been observed before in Sr/Ca (D'Olivo and McCulloch 2017; D'Olivo et al. 2018) and was attributed to the coral physiology response to thermal stress. Under thermal stress it has been observed how corals can limit calcification even when there are no signs of bleaching or high-density bands (Chapter 3). Based on the Marchitto et al. (2018) biomineralization model discussed above, under decreased calcification Rayleigh fractionation would be stronger (resulting in low Sr/Ca and higher Li/Ca and Mg/Ca). Our observations here show elevated Sr/Ca under thermal stress (and low calcification). This disconnect could be due to thermal stress impacting at cellular processes and these episodic events being different from chronic low calcification (as seen in Nananu-i-Ra corals).

X-rays and CT scans of the analysed colonies can help identify those periods of time where the studied colonies underwent stress (e.g., the presence of high-density bands or reduced calcification; DeCarlo and Cohen 2017) and therefore periods where the Sr/Ca-SST relationship might be broken or altered. However, this method presents caveats, especially when working with robust corals such as massive *Porites* spp., as that high density bands might not occur even when the coral is experiencing thermal stress (as we have seen in Chapter 3). Coral samples of this study do not show high density bands during known periods of widespread bleaching in Fiji and/or elevated DHW (e.g., 2000, 2006, 2014-2016; Vuki et al. 2000; Ellison and Fiu 2010; McClanahan et al. 2020). Despite the lack of high-density bands, several cores show partial growth scars and presence of endolithic algae in 2015 and 2016 (See core X-rays in Appendix A) which hint at an interplay of factors during the most recent period of thermal stress and the importance of considering other features related to environmental changes, beyond high density bands. These observations grant the need for further research on biomineralization processes at ECF and cellular level, and how coral physiology responds to different environmental factors in Fiji.

Data shows how coral colony replication and Sr/Ca averaging can reduce thermal stress bias if enough colonies are replicated (Sayani et al. 2019). Statistical modelling of the averaged Sr/Ca signal shows how annually averaged SST residuals (the mean difference of reconstructed SST-Sr/Ca and satellite SST per year) is a function of thermal stress (negative correlation), but the SST residual is limited to < 0.5°C when 5 or more cores are averaged.

$$\text{SST residuals Sr/Ca} = \text{DHW} + \text{number of cores}; R^2 = 0.55, p < 0.05$$

This correlation between SST residuals, DHW and number of cores is not observed for Li/Mg, and SST residuals remain constant at around 2°C regardless of the number of cores averaged.

$$\text{SST residuals Li/Mg} = \text{DHW} + \text{number of cores}; R^2 = 0.08, p > 0.1$$

This difference between Sr/Ca and Li/Mg averaging and "vital effects" of thermal stress is interesting and implies that the potential of El/Ca composites to constrain the climatic signal can be limited by certain events if they affect all the replicated colonies. It also hints that in Fijian *Porites* spp. Li/Mg is not minimising the physiological imprints of biomineralization, "vital effects" and Rayleigh fractionation as detailed by Marchitto et al. (2018).

The results of this study support the need for measuring several SST proxies simultaneously before applying paleo-reconstructions. In doing so we can explore which proxy shows the best correlation with SST in the studied samples (thus limiting the error in the paleo-reconstruction), as well as improve understanding of the interplay between coral biomineralization and environmental factors.

As discussed in Section 4.4.3., SST is not the only variable influencing coral geochemistry, and in Fiji, seawater turbidity is of special importance as its gradient is reflected in reef-specific skeletal growth and El/Ca. Sr/Ca reconstructed SST shows a warm bias (low Sr/Ca between the years 2010 to 2012). This event is especially interesting during May – August 2011, where the Sr/Ca anomaly is clearly different between samples from the Votua and Suva Reefs (Sr/Ca ~ 8.55 mmol/mol) and Nananu-i-Ra (Sr/Ca ~8.76 mmol/mol). The warm bias is not present in the Li/Mg reconstructed SST, however the decoupling in the signal between the southern (Votua and Suva Reefs; Li/Mg ~ 1.67 mmol/mol) and northern reefs (Nananu-i-Ra; Li/Mg ~ 2.30 mmol/mol) is evident.

This period (2010-2012) with a warming bias in Sr/Ca and decoupling between southern and northern reefs is coeval with a strong La Niña phase. Although it is not the only strong La Niña event that occurred during the duration of our record (another strong La Niña developed in 2007 – 2008), it is the only event developing directly after a strong El Niño (2009 – 2010). ENSO phases change reef-specific environmental conditions in Fiji through changes in both wind and precipitation regimes. During El Niño events in Fiji, the seasons tend to be drier and cooler than normal (due to movement of the SPCZ to the north-east), and the opposite tends to happen during La Niña (Agrawala et al. 2003; Kumar et al. 2014). In agreement, SSS data shows a large negative anomaly in 2011 across all sites and increased daily precipitation (See Chapter 5) as well as differences in monthly seawater turbidity (Figure 4.6.E and Figure 4.7.E.). The large influx of freshwater entering inshore reefs where samples were collected potentially also impacted environmental variables such as light availability, nutrients, turbidity, and salinity, as well as SST. This suggests that in addition to thermal stress, localised environmental factors can impact the geochemical signal of SST proxies in Fiji due to the sensitivity of the skeletogenesis process and coral physiology (as explored in Sections 4.4.2. and 4.4.3.). In addition, Sr/Ca seems to be an accurate SST proxy in Fiji. Overall, in order to be able produce SST reconstruction in this region a composite record obtained from averaging several core replicates is needed.

The geographic location of Fijian reefs is of great importance not only to reconstruct past SST, but also to get a better understanding of past rainfall patterns and SPCZ migration. Work has shown how $\delta^{18}O$ from Fijian massive corals can be used to reconstruct SSS (Bagnato et al. 2004; Linsley et al. 2004; Dassié et al. 2014). Coupling the use of this proxy with Sr/Ca can aid in the reconstruction of water masses due to SPCZ movement as well as sub-annual temperature events. While single core reconstruction from El/Ca can be challenging in Fiji (Juillet-Leclerc et al. 2006; Linsley et al. 2006), the approach taken here combining replicated colonies can extend the possibilities for this region. Sr/Ca records obtained from averaging several core replicates might allow for the smoothing of the “vital effects” imprinted by coral physiology and other environmental variables (e.g., seawater turbidity), unmasking the SST signal.

4.5. Conclusion

The coral skeleton paleotemperature proxies based on Sr, U, Li and Mg ratios with Ca in six Fijian *Porites* spp. coral cores from the period 2001 – 2017 only partially reconstruct SST. Physiological processes (i.e., Ca^{2+} pumping, skeletal deposition, Rayleigh fractionation) and environmental conditions, particularly seawater turbidity, add additional variability on seasonal and interannual timescales. The elemental ratios of each core are correlated between each other, generally following the expected pattern caused by Rayleigh fractionation occurring in the ECF from which the ions are precipitated into the aragonite skeleton. Rayleigh fractionation develops due to the large differences in partitioning coefficients between ions and aragonite. Furthermore, colony-specific differences in absolute El/Ca are induced by differences in Ca^{2+} pump activity which at the same time also exerts a control over Rayleigh fractionation degree (as Ca^{2+} pump increases $[Ca^{2+}]$ and $[Sr^{2+}]$). Thus, any variable capable of influencing Ca^{2+}

pumping (e.g., SST, seawater turbidity) and partition coefficients will, ultimately, exert some degree of control over El/Ca.

El/Ca correlates with skeletal density and drives the differences in absolute El/Ca between colonies. Changes in density (and growth rate) in the six coral cores of this study were linked to a seawater turbidity gradient observed between reef locations around Fiji. Although I did not focus on mechanisms through which reef-specific conditions (e.g., seawater turbidity) can affect physiological processes, I theorise that this gradient has an effect over Ca^{2+} pumping, modifying the rate at which ECF is renewed (which will also affect Rayleigh fractionation). These differences in Ca^{2+} pumping affects the El/Ca signal, partially masking the SST response and thus weakening El/Ca-SST correlations.

These results underpin the importance of combining seasonally resolved coral growth parameters with geochemical proxies and local environmental data to assess the robustness of the proxies in the region and species of study and how the SST record might be biased by coral physiology, skeletal deposition, and other environmental factors. Further research is needed to comprehend the exact processes acting in these corals regarding growth parameters and seawater turbidity. Based on this work, it is important that along with elemental ratio data we prioritize extraction of calcification information via 3D imaging to resolve seasonal growth parameter to assess the robustness of coral temperature proxies and application in different regions/environments. Further it is critical to combine seasonal growth parameters with local environmental data (whether in-situ or remote sensed) to ground truth and underpin the El/Ca-SST calibration and the relationships between density, environment, and El/Ca variations beyond the "calibration" period.

The results of this chapter suggest that in addition to thermal stress, localised environmental factors can impact the geochemical signal of SST proxies in Fiji. Sr/Ca is the most accurate proxy for SST in this region, however further research disentangling the effects of SST, coral physiology and local environment might unlock and improve different proxies for paleoclimate reconstructions. Until then, and in order to be able to produce SST reconstructions in this region, building composites by using several core replicates are needed.

This study reiterates the importance of acquiring a multi-elemental record since measuring and evaluating multiple El/Ca SST-proxies allows for a thorough assessment of processes occurring in the ECF during aragonite precipitation and can improve the accuracy of reconstructions by being able to explore the most adequate proxy. Along with elemental ratios, it is crucial to obtain growth (extension, density, and calcification) data from the studied specimens. 3D imaging (CT scans) is a powerful method to digitally explore growth parameters (extension direction, growth troughs and density anomalies) and guide the geochemical measurement path following the most optimal axis. To further understand the processes that are taking place and modifying El/Ca variability, coral growth and geochemical data coupled to high-resolution local environmental data are key. Although in-situ measurements can be hard to acquire, especially if working on remote and uninhabited areas, remote-sensed data via satellite products offers a wealth of environmental data at high spatial and temporal resolution that has advanced the testing of environment and SST proxies in coral skeletons.

Chapter 5 | Coral Ba/Ca, Mn/Ca and REE records from Fiji Porites spp. and their potential as inshore reef water quality archives

By water, wood and hill, by the reed and willow,
By fire, sun and moon, harken now and hear us!
Come, Tom Bombadil, for our need is near us!
Tom Bombadil

Reef series #1 (MVL)

Chapter 5 | Coral Ba/Ca, Mn/Ca and REE records from Fiji *Porites* spp. and their potential as inshore reef water quality archives

Abstract

Poor water quality in coastal reefs as a result of inland anthropogenic activity can severely impact reef-building corals, making them increasingly vulnerable. Implementation of an integrated coastal management to maintain reef biodiversity and resilience is key to preserve these reefs, however, these efforts lack the necessary temporally and spatially resolved environmental data to assess the impact of catchment changes on downstream inshore reefs. Geochemical records derived from massive hard corals can provide historical timeseries of coastal water quality and aid management efforts to disentangle drivers of sediment load and freshwater discharge in inshore reefs. Here, I present a suite of elemental ratios (Ba/Ca, Mn/Ca and REE/Ca (Y/Ca, La/Ca and Ce/Ca)) extracted from aragonite massive *Porites* spp. skeletons collected from inshore reefs in Viti Levu, Fiji, adjacent to three different catchment settings (i.e., forested, agricultural, urban). I explore the environmental drivers of elemental ratio variability in these records and further identify local processes controlling water quality

Overall, results show El/Ca variability is influenced by periods of increased rainfall and sediment load, in line with previous published studies, but site-specific differences are observed. In the forested catchment, Mn/Ca and REE/Ca variability is linked to seasonal and large runoff periods with differences in rainfall intensity and magnitude causing differences in the coupling of these proxies, whereas Ba/Ca is influenced by primary productivity. In the agricultural catchment, Ba/Ca, Mn/Ca and REE/Ca all are influenced by rainfall and ENSO phases, although wind-driven turbidity seems to be a key role in the spatial and temporal presence of sediments within the water column. In the urban reef, Ba/Ca and Mn/Ca are influenced by both rainfall-driven increase in sediment discharge directly from the adjacent rivers during the wet season, and wind-driven sediment movement being transported during the dry season. These findings reveal that *Porites* spp. El/Ca records from across Viti Levu respond to environmental changes associated with inshore water quality and are dependent on catchment-specific

factors (e.g., land cover, catchment area). Yet, a deep understanding of the land-sea system mechanisms is required before applying these proxies to reconstruct historical environmental records.

5.1. Introduction

Inshore reefs are particularly vulnerable to disruption (Hoegh-Guldberg 1999; Graham et al. 2006), because in addition to global stressors (i.e. climate change), these reefs are also being subjected to rising disturbances as a result of localised anthropogenic activity (Hughes et al. 2003; Pandolfi et al. 2003), which lowers reef resilience and makes them increasingly susceptible to damage and degradation. In order to preserve inshore reefs, and the services they provide to coastal communities, it is imperative to understand how local anthropogenic pressures are affecting and shaping reefs nowadays.

Anthropogenic development can strongly influence coastal ecosystems through changes in the land-based runoff. One of the main local threats to inshore reefs worldwide is deteriorating water quality as a result of terrestrially sourced pollutants, nutrients and sediments (Fabricius 2005; Doney 2010; Burke et al. 2011). In addition to increased terrestrial material, catchment development and land use also have an important role altering the hydrological response to rainfall events, increasing discharge rate and peak, increasing freshwater discharge and low salinity in the reef area, constituting an additional stressor (Faxneld et al. 2010; Ban et al. 2014). The extent of riverine runoff is not only dependent on land use (Risk 2014; Mateos-Molina et al. 2015) but also on other catchment specific factors such as soil type, type of vegetation cover, terrain slope (Roberts et al. 2017), and the climatic/rainfall regime (Bridge 2009). Land-based pollution and runoff can increase sedimentation in the coastal environment, leading to coral smothering, increased water turbidity reducing the amount of light available for photosynthetic processes, and increased dissolved nutrients leading to algal blooms, including macroalgae that outcompetes corals and limits coral larvae recruitment (e.g., Fabricius 2005; Restrepo et al. 2016).

In the South West Pacific, coral reefs are highly diverse and of great importance for the coastal communities that depend on them for subsistence, coastal protection and livelihood (Lovell and Whippy-Morris 2009). In Fiji, over 75% (627,954) of the population live within 5 km of the coast (Andrew et al. 2019) and Viti Levu, as the largest island, is the population centre (80% of the population – 715,000) of Fiji.

Communities use specific strategies to limit local stressors for reefs, and to buffer the damaging effect of climate change (O'Leary et al. 2017; Kitolelei and Kakuma 2022). However, inshore reefs of Viti Levu are still impacted by pollution and sedimentation (Whippy-Morris 2009) due to poor land practices (burning, deforestation) and changes in the watershed that increase soil erodibility and sediment runoff (Brown et al. 2017a, 2017b; Andrello et al. 2022). The Fiji National Biodiversity Strategy and Action Plan is aiming to protect 30% of its marine territory by 2025 (Department of Environment, Government of Fiji 2020), and acknowledges the importance of good catchment and forest management to limit the threat to inshore reef ecosystems (Jupiter et al. 2012; Brown et al. 2017a). However, potential benefits of land protection to inshore reefs in Fiji are highly variable depending on where the protected land is (Brown et al. 2017a, 2017b), and therefore, a record of the links between catchment use, vegetation cover, sediment runoff, river turbidity and nearshore water quality is essential for adequately implement resilience-based management strategies.

Catchments across Viti Levu can be very different depending on location due to climatic differences (leeward versus windward), size, terrain slope, land use and degree of forest cover (Figure 5.1.), and the influence of these factors over soil erosion and catchment hydrology. The tropical soils of Viti Levu are characterised by a deep weathering, with a considerable higher permeability and porosity compared to the underlying parent rock (Ram et al. 2019), which favours saturation under wet conditions and leads to extensive sediment runoff (Ram et al. 2019). Furthermore, the type of vegetation covering the land can also have a considerable impact in the hydrological system of a watershed where mature forest limits physical erosive capacity of rainfall and increase transpiration (Bartley et al. 2014; Roberts et al. 2017), therefore increasing soil saturation threshold. As such, magnitude and sources of terrestrial runoff into the coastal system and subsequent decline of coastal water quality highly differs across locations (Álvarez-Romero et al. 2014).

To fully understand the environmental mechanisms controlling the nature of terrestrial runoff and how catchment changes impact inshore reefs (Jupiter et al. 2008; De'ath et al. 2012) in Vit Levu, an immense wealth of environmental information and data is needed. Historical data of inshore water quality in Viti Levu is limited to a few localities near Suva and along the Coral Coast, and to specific set of pollutants. For example, in Suva Harbour, studies have investigated sediment delivery processes (Singh and Aung 2008), heavy metal pollution (Naidu and Morrison 1994; Maata and Singh 2008; Chand et al. 2011; Arikibe and Prasad 2020) and Tri(n-bultyl)tin (Stewart and De Mora 1992) from industrial sources; trace metal content in sediments from the Namuka Reef (Collen et al. 2011); and nutrient (nitrates and phosphates) concentration in inshore reefs (Mosley and Aalbersberg 2003; Tamata 2007) and sediment load and river turbidity in the Coral Coast (Ram and Terry 2016). These records, however, only provide a snapshot of information and lack sufficient spatial or temporal resolution to fully understand the relationships between terrestrial runoff and reef degradation (Fabricius 2005). This information is critical to understand how Fijian inshore reefs respond to specific disturbances and how they have changed in recent decades. Therefore, in order to preserve the services that inshore reefs provide for the Fijian community, insights on historical inshore water quality encompassing acute and chronic disturbances from terrestrial discharge can help understand drivers of variations in benthic cover and coral growth rates in these reefs (Ostrander et al. 2000).

In this framework, remote sensed data has the potential to identify sources of sediment runoff into inshore reefs (e.g., Brown et al. 2017a). Remotely sensed imagery (and the derived environmental data products) is freely available, relatively cheap and offers global coverage, often at a range of both spatial and temporal scales (Lechner et al. 2020), facilitating their use by workers in many fields, including scientists, reef conservation stakeholders and managers. Remote sensing is a powerful tool to understand the environment; however, data is only available from the 1970s onwards (for example, the Landsat program was launched in 1972). Furthermore, its temporal resolution can be diminished during specific seasons/events of interest due to cloud cover, and coastal and reef-specific processes might not be discernible due to spatial resolution (both in area and within the water column). While advances in remote sensing for water quality monitoring have provided a successful method to estimate optically active water parameters (e.g., suspended sediments, chlorophyll-a), assessment of non-optical parameters (e.g., nutrient concentration, dissolved oxygen levels, pathogens) remains a challenge (Sagan et al. 2020).

A novel approach that complements and builds upon both direct environmental data are records from geochemical tracers in coral skeletons. Coupled records of remote sensed and coral-derived environmental data fill critical gaps in both spatial and temporal coverage of climate and coastal water quality variability in tropical and subtropical regions. They inform us how reef-building corals are responding to both sustained and intermittent environmental changes (Lough 2011) as a result of anthropogenic activity, and aid in identifying specific factors and sources of coastal pollution enabling better management strategies. High-resolution reconstruction of precipitation and salinity (e.g., Gallup et al. 2006; Wu and Grottoli 2010; Grove et al. 2013), and water quality, in particular sediment or nutrient load (e.g., Shen and Boyle 1987; Lewis et al. 2007; Moyer et al. 2012; Inoue et al. 2014), can be obtained from massive reef building *Porites* spp. corals. This coral genus is widely distributed in the Indo Pacific, its specimens are resistant to erosion and breakage, and have a lifespan of hundreds of years (Veron 2000). These characteristics, together with their annually banded skeletons (Knutson et al. 1972), makes them invaluable environmental archives.

The ratios of Ba, Mn, and rare earth elements (REEs) to calcium in coral aragonite have been used as proxies to inform terrigenous discharge and sediment movements in tropical coastal regions (e.g., Fallon et al. 2002; Alibert et al. 2003; McCulloch et al. 2003; Jupiter 2008; Maina et al. 2012; Prouty et al. 2014). These trace elements found dissolved in seawater as free ions, have a similar ionic radii and charge to the Ca^{2+} ion and can easily substitute for Ca^{2+} in the aragonite lattice of *Porites* spp. skeleton (Shannon, 1976). Further, they substitute in similar proportions to the ambient sweater concentration (distribution coefficient ≈ 1) (Alibert et al. 2003; Akagi et al. 2004; Sinclair and McCulloch 2004; Lewis et al. 2007; LaVigne et al. 2016), thus reflecting the environment in which the skeleton was mineralised. These elements are predominantly sourced to the coastal reefs adsorbed onto suspended fluvial sediment particles (i.e., clay particles), where they suffer desorption from the particulate matter in the estuarine mixing zone (as reviewed by Saha et al. 2016). However, movements of the newly desorbed ions across the river plume, their residence time in coastal waters and incorporation into coral aragonite differ depending on the element and site-specific environmental conditions. For this reason, a multi-proxy approach to terrigenous discharge records has the potential to provide a more comprehensive insight of the catchment-coastal ecosystem and what factors favour delivery of freshwater, sediments, and pollutants into the inshore reefs.

Ba/Ca content in coral skeletons from inshore reefs is applied to reconstruct surface biogeochemical processes and terrestrial discharge (Alibert et al. 2003; McCulloch et al. 2003; Lewis et al. 2007; Prouty et al. 2010; Grove et al. 2013). However, the biogeochemical cycle of Ba in coastal regions is not fully understood, which complicates the interpretation of the Ba/Ca signal as a river discharge proxy. For example, some studies did not find a correspondence of elevated Ba/Ca periods with flood events and/or river discharge (Lewis et al. 2007, 2012; Saha et al. 2018; Tanzil et al. 2019). In addition other events such as coastal upwelling (Tudhope et al. 1996), algal blooms (Sinclair 2005a), SST influence (Grove et al. 2012), and Ba released from sediment fluxes and groundwater seeps (Prouty et al. 2010) have also been observed to affect the coral Ba/Ca signal.

Coral Mn/Ca has been used as a proxy to reconstruct primary productivity, terrestrial influx, upwelling, and wind-driven sediment mixing and oxidation processes in the water column (Wyndham et al. 2004; Jupiter et al. 2008; Inoue et al. 2014; Sayani et al. 2021; Chapman et al. 2022). Yet, the biogeochemical cycle of Mn in coastal reefs presents some complexities where the availability of Mn^{2+} dissolved in the water column (and thus available for coral incorporation) depends on the salinity and the net amount of suspended particles being incorporated to the system from river discharge, but it is also influenced by photo-reductive dissolution and a complex oxidation-reduction cycle occurring in the coastal sedimentary environment (Shen et al. 1992b; Lewis et al. 2012), which can potentially complicate the interpretation of the proxy.

REEs/Ca (i.e., Y/Ca, La/Ca, Ce/Ca) are used to reconstruct terrestrial sediment input and riverine influence in inshore reefs (e.g., Fallon et al. 2002; Akagi et al. 2004; Wyndham et al. 2004; Jupiter 2008), due to the more conservative behaviour (than Ba and Mn) within the estuarine mixing zone and not being influenced by biogeochemical processes (i.e., primary productivity) (Lewis et al. 2007).

The inshore reefs around Viti Levu are an ideal location to explore the application of terrestrial input proxies (i.e., Ba/Ca, Mn/Ca, and REE/Ca) as a means to provide long-term water quality information. The differences in catchment size, land-use and rainfall/climatic regime across the locations of this study are likely to be reflected as site-specific differences in coastal water quality across time, and therefore reflected in the coral El/Ca signal. These characteristics inform how reefs are influenced by catchment-specific environmental parameters, supporting decision-making in the "ridge-to-reef" management approach to protect Fijian marine ecosystems.

In this chapter I assess how skeletal Ba/Ca, Mn/Ca and REE in massive *Porites* spp. corals vary between four different catchments (varying catchment area, land-cover, population pressure and climatic conditions) to explore localized processes (e.g., rainfall-driven versus wind-driven increased turbidity) impacting the reef environment and the interpretation of El/Ca records. I compare the El/Ca spatial variability across 2001 – 2016 in Viti Levu to in-situ observational data and remote-sensing data to validate the mechanistic understanding proposed and ground truth drivers of El/Ca variability. Overall, I show that application of this proxy in Fiji is promising for reconstructing changes in runoff and wind induced changes in turbidity but requires a local understanding of different climatic and environmental processes (e.g., rainfall patterns, winds, surface currents) at the reef scale.

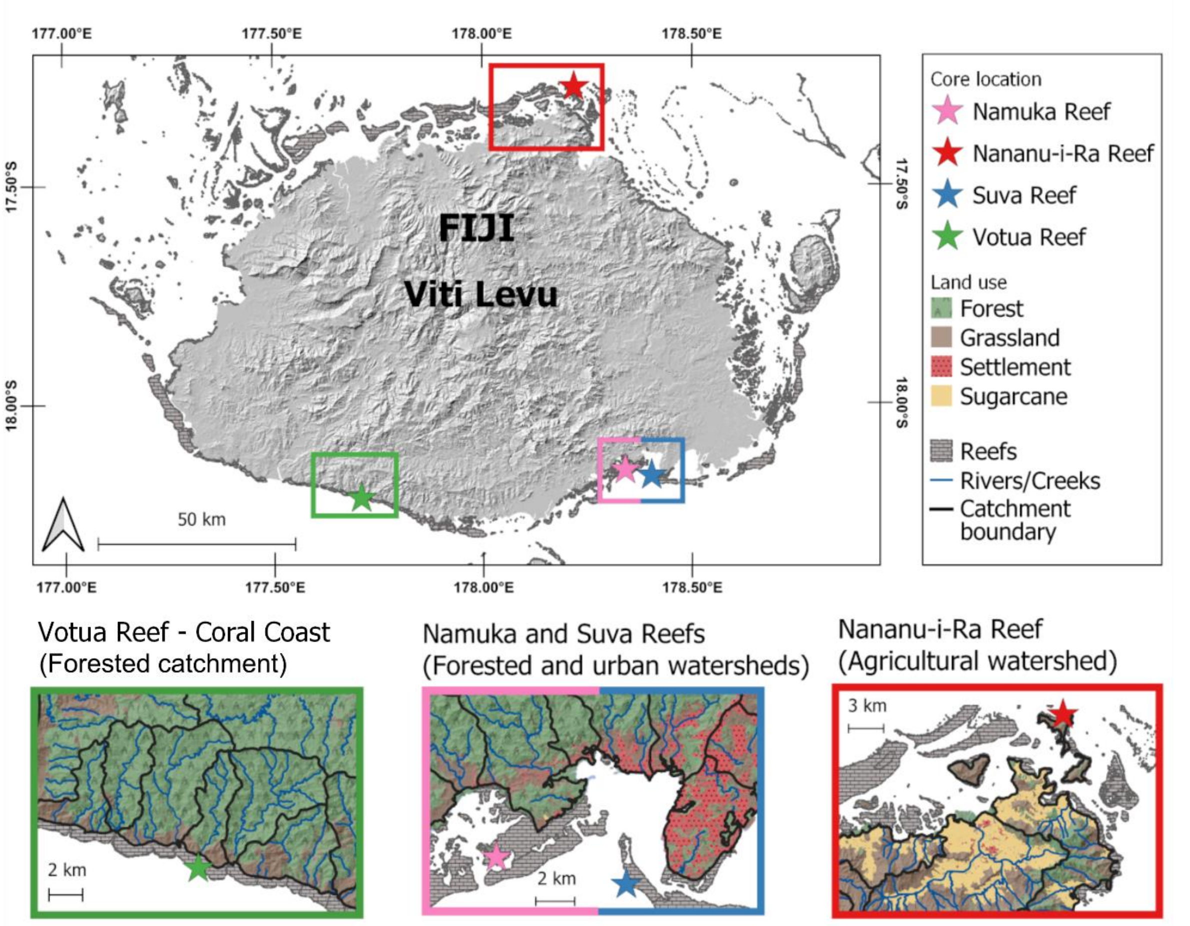

Figure 5.1. Map of Viti Levu (Fiji). Star symbols represent the coring locations of the samples of this study. Cores VOT17_1 and VOT17_2 were extracted from the Votua Reef (western Coral Coast). NAM17_1 was extracted from Namuka Reef. FP17_1 was extracted from the Suva Reef. NAN17_2 and NAN17_5 were extracted from the shores of Nananu-i-Ra

5.2. Methods summary

5.2.1. Reef environmental data

Instrumental environmental data was collected, when available, between 2001 – 2017 (Figure 5.2.). Detailed information on the sources of the environmental data is found in Chapter 2 – Section 2.6.. Daily rainfall data (2001 – 2017) was collected from the closest available weather stations to each location of this study, and was provided by the Fiji Meteorological Services. The Votua, Suva, and Namuka Reefs were paired with Laucala Bay rainfall stations (located at < 15 km distance for Suva and Namuka Reefs, and ~80 km for Votua Reef), whereas Nananu-i-Ra was paired with data from the Penang Mill weather station (< 15 km). Monthly rainfall was used in this Chapter and was calculated as the accumulated rainfall over the duration of each month (mm/month). Near-daily inshore reef water quality for each location was derived from the diffuse attenuation coefficient at a wavelength of 490 nm (K_d490 (m^{-1})) satellite products from MODIS-Aqua (spatial resolution of 4 km) from 04/07/2022 (earliest available data) until 30/05/2017. Chlorophyll-a concentration (mg/m^3) was also retrieved but is so strongly correlated with K_d490 m^{-1} data ($R^2 > 0.90$; See Chapter 2 – Section 2.6.4.) that only the K_d490 data is shown. Monthly seawater turbidity (and chlorophyll- a) was obtained as the arithmetic mean of daily datapoints. Daily wind speed for each location of this Chapter was obtained from CCMP satellite product from 2002 until 2017. Monthly wind speeds were calculated as the arithmetic mean of daily data over each month. SSS was obtained from level-3 CATSD Ocean Salinity product at daily resolution, for each location, between 2010 – 2017. Monthly SSS was calculated as arithmetic mean of daily data. Daily SSTs for each location were obtained from the OISST dataset covering the period 2001 – 2017. Monthly SSTs were calculated as the arithmetic mean of daily SSTs.

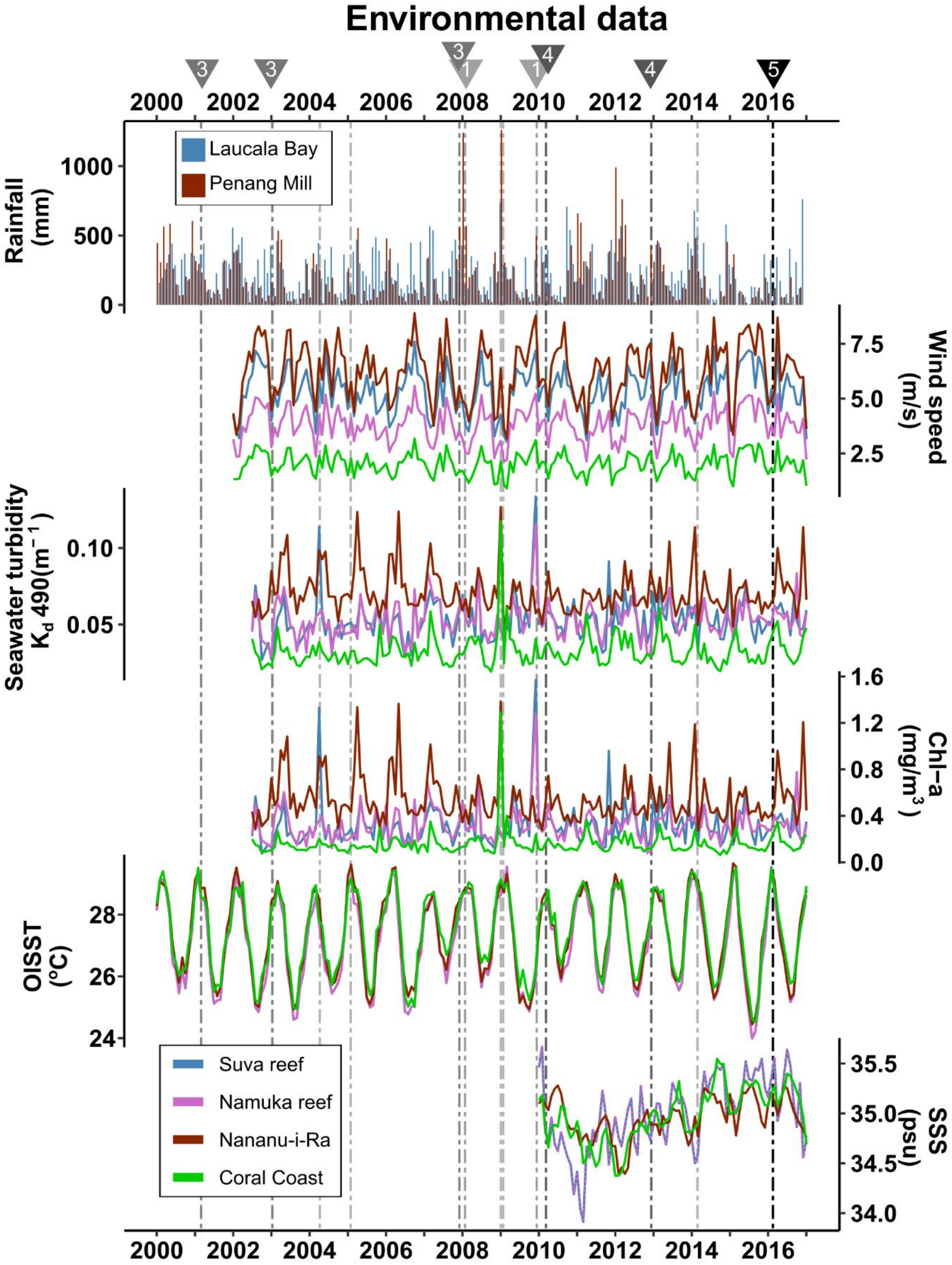

Figure 5.2. Time series of monthly resolved environmental data explored in this Chapter. Rainfall corresponds to Laucala Bay (paired to corals from Coral Coast, Namuka and Suva) and Penang Mill (paired to corals from Nananu-i-Ra). Line colours in the rest of the plots correspond with each location studied. Gray vertical lines depict tropical storms (lighter) and cyclones. Triangles above plot depict cyclone category.

5.2.2. Coral selection and preparation

Cores from six massive *Porites* spp. colonies across four different locations were selected to investigate catchment influence and water quality proxies in inshore reefs (Figure 5.1. and Figure 5.3.). The four study locations included two inshore reefs adjacent to small and forested catchments (Votua and Namuka Reefs), one reef in the vicinity of a catchment with high presence of sugarcane crops and grasslands (Nananu-i-Ra) and one urban reef (Suva Reef). More information on these locations is presented in Chapter 2 – Section 2.2. Two replicate cores were collected at each location where available, with one longer core to explore temporal variability and a shorter sample to investigate local reproducibility of geochemical records. For the Coral Coast site at Votua, two cores, VOT17_1 and VOT17_2, were collected within ~10 m of each other. In Nananu-i-Ra, I chose NAN17_2 as the longer record because it showed the highest linear extension of these cores, therefore opening the potential for higher temporal resolution of geochemical signature, and due to its clear growth along a main axis. We chose NAN17_5 as replicate core because it did not show signs of bioerosion or areas with clear differences in skeletal density (unlike NAN17_1 and NAN17_3) and showed a clear and linear growth across a single main transect. These two colonies were located ~ 1 km from each other. One core (long core: FP17_1) was collected at the Suva reef, at the entrance of Suva Harbour (Figure 5.1.). This core showed a clear seasonal growth of density bands and uninterrupted growth. As a replicate core for FP17_1 in Suva Harbour, then, we chose a specimen from the nearest available location, Namuka reef (NAM17_1), at a distance of ~ 4 km (Figure 5.3.).

5.2.3. Growth parameters

Growth parameters from these coral cores were obtained from X-ray CT scans. A detail description of the protocol is in Chapter 2 – Section 2.4.2. In summary, skeletal density (g/cm^3) was measured continuously along the major growth axis based on the CT imaging (following methods in Cantin et al. (2010)). Annual linear extension rates (cm/yr) were obtained from both X-ray images visualising seasonal density bands, by measuring distance across the major growth axis from high density band to the following, and from density profiles of each coral core measuring distance between density maxima and minima (Lough and Cooper 2011). The calcification rate ($g\ CaCO_3/cm^2 \cdot yr$) was also obtained as a product of the previous two growth parameters. For the purposes of this chapter, we used density as a measurement of skeletal growth due to its availability at the same time resolution as El/Ca (monthly), in contrast to linear extension and calcification, which are obtained at annual resolution.

5.2.4. Analytical techniques – LA-ICPMS

The coral slabs were analysed by LA-ICPMS for Ba, Mn, Y, La, Ce and Ca (among others; See details in Chapter 2 – Section 2.4.1.) following the major growth axis. The laser slit dimensions were 50x200 µm, laser pulse rate was set to 10 Hz and on-sample fluence was of 2.5 J/cm^3 (See method development; Chapter 2 – Section 2.4.1.2.). Each coral sample was ablated (and El/Ca measured) three times (three transects) on the exact same path. The first transect served as a cleaning ablation, removing the outer ~0.50 µm of the ablation path surface, and exposing a fresh surface for subsequent analysis. Elemental ratios of proxies explored in this Chapter were obtained from the third transect (following methods by Fallon et al. 2002). The standards NIST610, NIST612, NIST614 and JCp–1 were measured at the beginning and end of each coral transect. Furthermore, alternating NIST612 + NIST610, NIST612 + NIST614 and NIST612 + JCp–1 were measured every five sub-transects.

5.2.5. Coral chronology

Annual age models obtained from CT scans (band counting and density minima and maxima) were refined following standard approaches (Felis et al. 2009). Monthly resolved chronologies were extrapolated using the annual chronology obtained from CT scans, the location of the sample at the time of its collection (May 2017) and subsequent alignment in peaks and troughs of Sr/Ca with SST assuming an inverse correlation between Sr/Ca–SST seen elsewhere (e.g., DeLong et al. 2014). Despite all El/Ca being explored for chronology refinement, Sr/Ca was chosen for showing consistent significant correlations with SST (See Chapter 4 – Section 4.3.2.1.) and clear seasonality in each of the cores of this study. El/Ca timeseries in this Chapter were explored between 2001 to 2016 (unlike Chapter 4, where the studied period is 2001 to 2017) due to elevated Ba/Ca observed on the tissue layer of several samples. As such, the El/Ca data corresponding to this skeletal portion was removed.

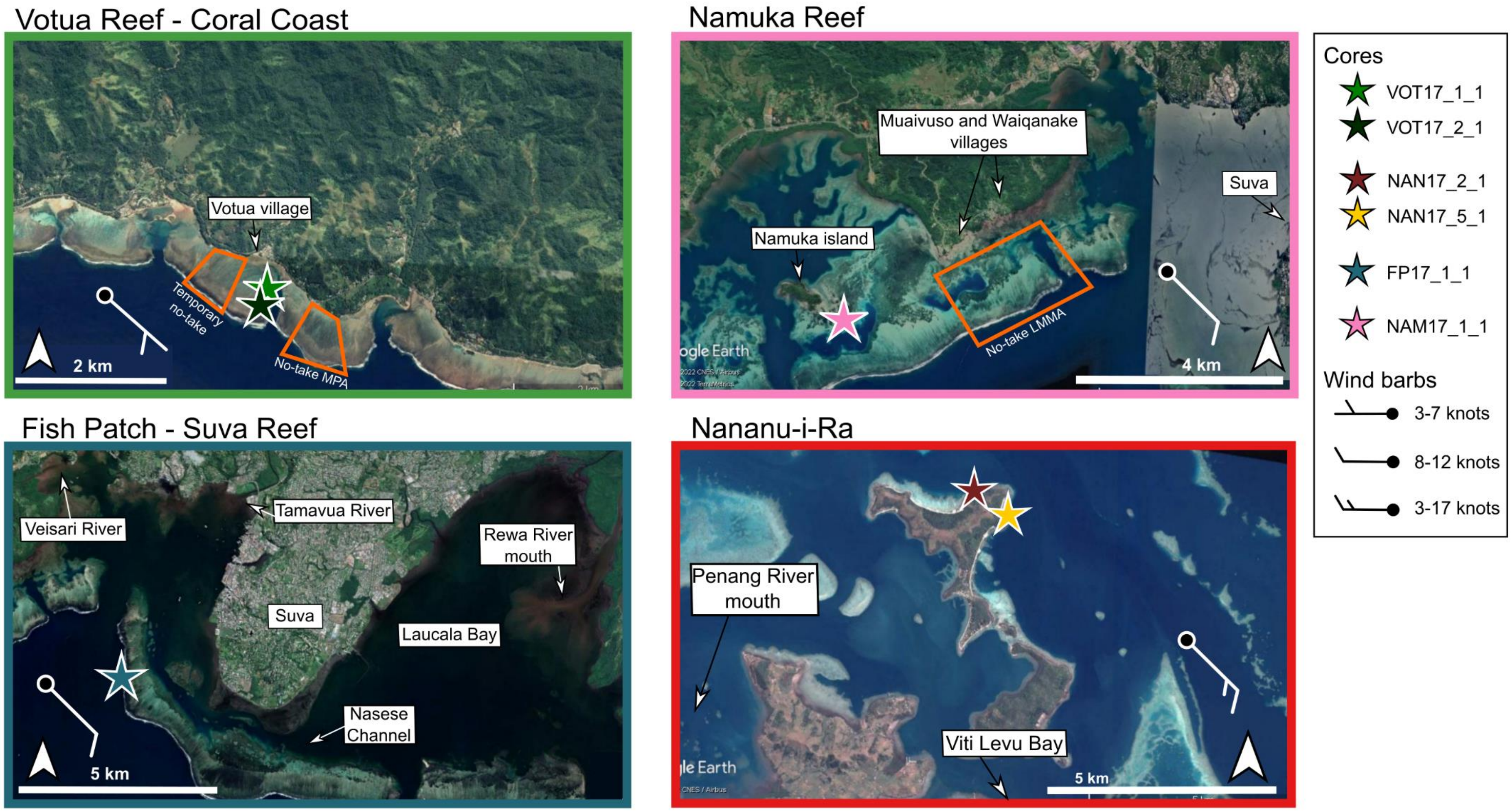

Figure 5.3. Satellite images from the four locations of this study. Star symbols are the locations of each coral sample. Note different scale bars across each satellite image. Source: Google Earth.

5.2.6. Data processing

Each individual laser ablation transect was processed using the Python package LAtools (Branson et al. 2019) following an established protocol. Each transect was background corrected, despiked, normalised to ^{43}Ca and calibrated against NIST614. Analytical reproducibility of the standard material was monitored throughout every day of analysis. It is reported as internal reproducibility (mean El/Ca and %RSD), and external accuracy (measured value/reported value) and precision (2x SD of accuracy) (See detail in Chapter 2 – Section 2.4.1.4). Accuracy and precision of Ba/Ca (1.06% and 2.24% respectively), Mn/Ca (3.77% and 4.95%), Y/Ca (1.96% and 3.48%), La/Ca (1.95% and 2.86%) and Ce/Ca (5.45% and 2.85%) were all below 5%RSD, except Ce/Ca being only marginally higher (5.45%), thus considered adequate.

After refining the chronology of each coral transect, the resolution of the raw data was calculated to be nearly-weekly (based on the number of datapoints and skeletal extension of each sample). Weekly data was then averaged at monthly time-scales (1 datapoint per month).

All statistical analyses were performed in R. Pearson's correlation (with a significance of 95%) were used to calculate correlations between El/Ca, and between El/Ca and environmental variables.

5.3. Results

5.3.1. Mean El/Ca values

5.3.1.1. Ba/Ca

Mean coral Ba/Ca values for the common period (2012 – 2016) in each core range from 3.15 µmol/mol (in VOT17_2) to 6.44 µmol/mol (in VOT17_1), both extremes being from the two cores from the Votua Reef on the Coral Coast (Figure 5.4.; Table 5.1.). The difference between mean Ba/Ca values between replicates at each site range from 0.86 µmol/mol (in Nananu-i-Ra) to 3.29 µmol/mol (at Votua Reef). Differences in the mean Ba/Ca values between sites (inter-site), which incorporated the values from both replicate cores at each site when available, are up to 1.54 µmol/mol (Table 5.1.).

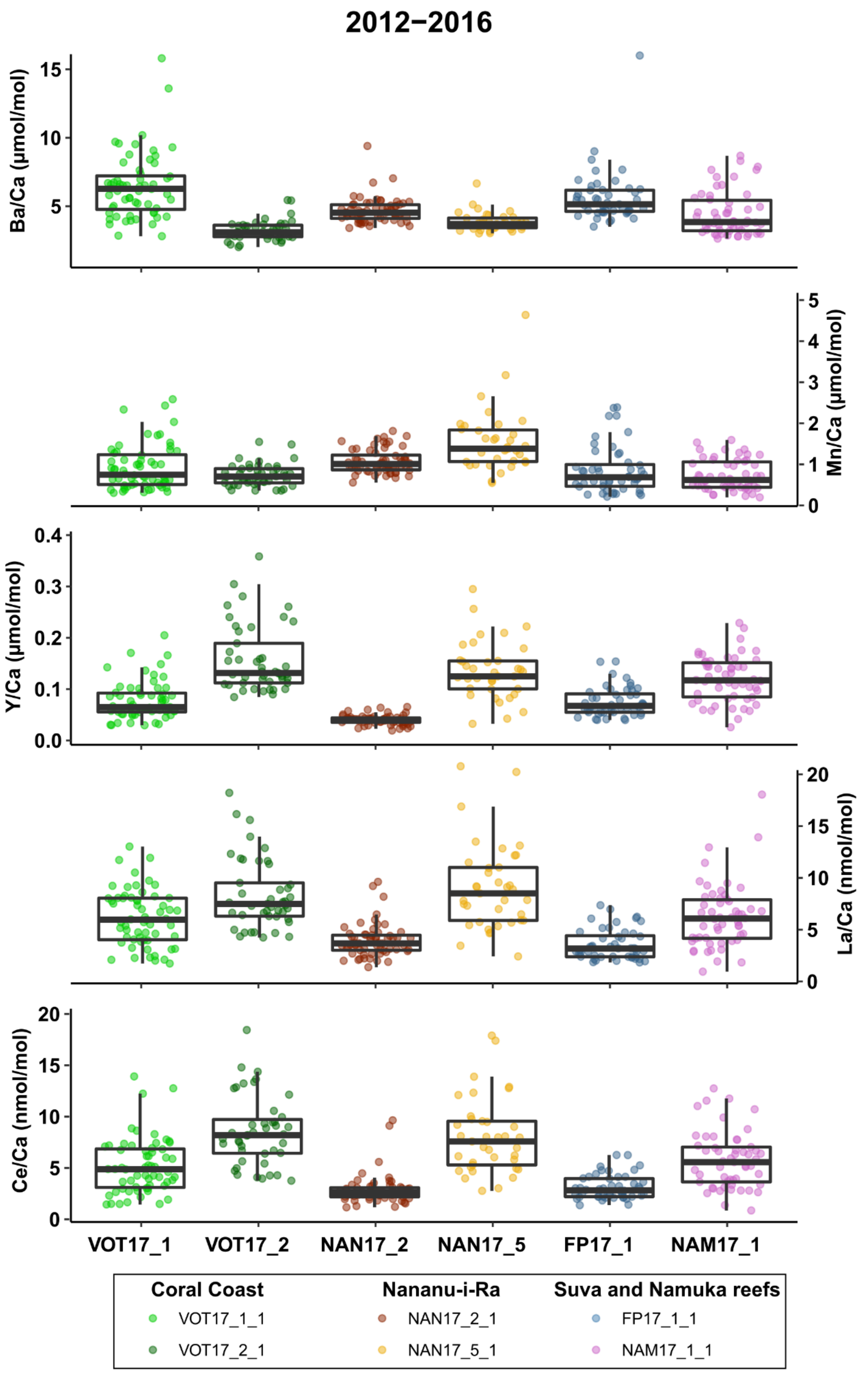

Figure 5.4. Monthly resolved El/Ca data from each coral sample for the common period to all records (2012 - 2017).

5.3.1.2. Mn/Ca

Mean Mn/Ca values for the interval 2012 – 2016 in each coral core range from 0.74 µmol/mol (NAM17_1) to 2.02 µmol/mol (NAN17_5) (Figure 5.4.; Table 5.1.). The difference in mean Mn/Ca values across replicates within each location is 0.18 µmol/mol for the Votua Reef, and 0.94 µmol/mol for Nananu-i-Ra. Differences in mean Mn/Ca across sites are up to 0.71 µmol/mol (Table 5.1.).

Table 5.1. Mean trace element ratios (and relative SD (%)) for each coral for the common period to all the geochemical records (2012 – 2016).

Location	Core	Ba/Ca (umol /mol)	RSD (%)	Mn/Ca (umol/ mol)	RSD (%)	Y/Ca (umol /mol)	RSD (%)	La/Ca (nmol/ mol)	RSD (%)	Ce/Ca (nmol/ mol)	RSD (%)
Votua	VOT17_1	6.44	37%	0.93	59%	0.08	48%	6.14	44%	5.17	52%
	VOT17_2	3.15	25%	0.75	37%	0.16	41%	8.37	40%	9.10	45%
Nananu-i-Ra	NAN17_2	4.70	20%	1.08	27%	0.04	23%	3.95	40%	2.87	50%
	NAN17_5	3.84	18%	2.02	104 %	0.14	41%	9.07	46%	8.06	45%
Suva	FP17_1	6.07	57%	0.86	67%	0.08	37%	3.57	41%	3.12	38%
Namuka	NAM17_1	4.47	37%	0.74	51%	0.12	37%	6.29	50%	6.17	67%

5.3.1.3. REE (Y/Ca, La/Ca, Ce/Ca)

During the common period (2012 – 2016) mean Y/Ca ranges from 0.04 µmol/mol (NAN147_2) to 0.16 (VOT17_2) (Figure 5.4.; Table 5.1.). Differences between the mean Y/Ca values of replicates at both Votua and Nananu-i-Ra are 0.08 µmol/mol and 0.10 µmol/mol respectively. Differences across sites range between 0.03 to 0.09 µmol/mol (Table 5.1.).

For La/Ca, mean values range from 3.57 nmol/mol (FP17_1) to 9.07 nmol/mol (NAN17_5) (Figure 5.4.: Table 5.1.). At Votua, the difference between mean values of replicates is 2.23 nmol/mol. In Nananu-i-Ra, the difference between mean La/Ca values is 5.12 nmol/mol. Differences in mean La/Ca across sites range between 0.22 nmol/mol and 3.68 nmol/mol (Table 5.1.).

Finally, mean coral Ce/Ca values across cores range from 2.87 nmol/mol (NAN17_2) to 9.10 nmol/mol (VOT17_2) (Figure 5.4.; Table 5.1.). At Votua, the difference in mean Ce/Ca values between replicates is 3.93 nmol/mol. At Nananu-i-Ra, the mean Ce/Ca difference between replicates is 5.19 nmol/mol. Differences in mean Ce/Ca across sites range from 0.71 nmol/mol to 4.01 nmol/mol (Table 5.1.).

5.3.2. Reproducibility and correlation between El/Ca records

5.3.2.1. El/Ca reproducibility within sites

Monthly resolved paired records in Nananu-i-Ra (NAN17_2 and NAN17_5) were only correlated for REE/Ca (Pearson's r ~0.22, $p < 0.05$), whereas the Votua cores (VOT17_1 and VOT17_2) correlate in both Ba/Ca (Pearson's r= 0.44, $p < 0.05$), and Mn/Ca (Pearson's r = 0.46, $p < 0.05$) (Table 5.2.).

Table 5.2. Reproducibility of geochemical record. Correlation (Pearson's r) values between replicate colonies within each reef location. Significant values ($p < 0.05$) are indicated in bold.

	Cores	Ba/Ca	Mn/Ca	Y/Ca	La/Ca	Ce/Ca
Votua Reef	VOT17_1:VOT17_2	**0.44**	**0.46**	0	0	0
Nananu-i-Ra	NAN17_2:NAN17_5	0	0.15	**0.21**	**0.22**	**0.22**
Suva/ Namuka Reefs	FP17_1:NAM17_1	0	**0.75**	**0.28**	0.1	0.1

5.3.2.2. El/Ca correlation within samples

Monthly mean Ba/Ca and Mn/Ca ratios correlate internally within all the cores (Table 5.3.). Similarly, correlation between REEs is high in all the samples (Pearson's r ~0.80, $p < 0.05$) (Table 5.3.). Significant relationships between Ba/Ca and all REEs are only present in NAN17_2 (Pearson's r ~ 0.50, $p < 0.05$), whereas Mn/Ca correlates with all REEs at VOT17_1, NAN17_2 and NAN17_5 (Pearson's r = 0.15 – 0.46, $p < 0.05$).

5.3.2.3. El/Ca correlation across samples and sites

Monthly resolved El/Ca are rarely correlated across locations, with the exception of Mn/Ca, which is significantly correlated between most samples (Pearson's r =0.41, $p < 0.05$) except between VOT17_1:NAN17_5, VOT17_2:NAN17_5, FP17_1:VOT17_2, and NAN17_5:NAM17_1 (Table 5.4.). Ba/Ca is significantly correlated between Votua samples and Namuka (VOT17_1:VOT17_2:NAM17_1; Pearson's r > 0.44, $p < 0.05$). REE (Y/Ca, La/Ca, Ce/Ca) are only significantly correlated between VOT17_1 and NAM17_1 (Pearson's r > 0.44, $p < 0.05$) (Table 5.4.).

Table 5.3. Correlation between trace element ratios within each core sample. Significant values ($p < 0.05$) are indicated in bold.

	Votua Reef		**Nananu-i-Ra**		**Suva**	**Namuka**
	VOT17_1	VOT17_2	NAN17_2	NAN17_5	FP17_1	NAM17_1
Ba/Ca:Mn/Ca	**0.36**	**0.66**	**0.58**	**0.35**	**0.51**	**0.46**
Ba/Ca:Y/Ca	0.02	-0.05	**0.4**	-0.18	0.03	0.17
Ba/Ca:La/Ca	**0.16**	0.06	**0.51**	-0.2	0.13	0.1
Ba/Ca:Ce/Ca	0.04	0.09	**0.49**	-0.11	0.07	-0.02
Mn/Ca:Y/Ca	**0.46**	0.23	**0.14**	**0.34**	0.11	-0.05
Mn/Ca:La/Ca	**0.4**	**0.33**	**0.21**	**0.29**	0.1	-0.11
Mn/Ca:Ce/Ca	**0.31**	**0.33**	**0.16**	**0.32**	0.09	**-0.24**
Y/Ca:La/Ca	**0.88**	**0.96**	**0.85**	**0.94**	**0.9**	**0.76**
Y/Ca:Ce/Ca	**0.72**	**0.95**	**0.68**	**0.93**	**0.92**	**0.54**
La/Ca:Ce/Ca	**0.87**	**0.98**	**0.93**	**0.97**	**0.91**	**0.92**

Table 5.4. Correlation of El/Ca across locations. Significant values ($p < 0.05$) are indicated in bold.

	Ba/Ca	**Mn/Ca**	**Y/Ca**	**La/Ca**	**Ce/Ca**
VOT17_1:NAN17_2	0	**0.62**	0	0	0
VOT17_1:FP17_1	0	**0.61**	0	0	0
NAN17_1:FP17_1	0	**0.65**	0	0	0
VOT17_1:NAN17_5	0	0	0	0	0
VOT17_1:NAM17_1	**0.44**	**0.61**	**0.52**	**0.44**	**0.37**
NAN17_2:VOT17_2	0	**0.45**	0	0	0
NAN17_2:NAM17_1	0	**0.62**	0	0	0
FP17_1:VOT17_2	0	0	0	0	0
FP17_1:NAN17_5	0	**0.53**	0	0	0
VOT17_2:NAM17_1	**0.61**	**0.41**	0	0	0
VOT17_2:NAN17_5	0	0	0	0	0
NAN17_5:NAM17_1	0	0	0	0	0

5.3.3. Temporal variability

5.3.3.1. Ba/Ca

When discussing temporal variability of Ba/Ca in the VOT17_1 core (Figure 5.5.), we are distinguishing between the 2 sections (pre and post 2009) that show a step in geochemical profile and baseline. Sample VOT17_1 (Pre 2009) shows a maxima event during October 2000 (7.52 µmol/mol), with a fairly constant baseline and no pronounced troughs. VOT17_1 (Post 2009) shows maxima events in October 2008 through 2011 (~9.00 µmol/mol), December 2012 (10.12 µmol/mol), May 2014 (10.18 µmol/mol), November 2015 (13.15 µmol/mol). Seasonality is not evident in any of the sections of this sample, but it seems that Ba/Ca peaks are recorded through the wet season. VOT17_2 (Figure 5.5.) shows elevated Ba/Ca events in January 2014 and March 2016 (5.21 µmol/mol), and though seasonality is not present either, it seems that elevated Ba/Ca values are also recorded during the wet season. VOT17_1 shows a correlation with seawater salinity (Pearson's r = 0.39, p <0.05). This relationship with SSS is similar to that observed in the replicate core VOT17_2_1 (Table 5.5.).

In the long core NAN17_2 (Figure 5.6.), maximum Ba/Ca is recorded in October 2008 (7.82 µmol/mol), while minimum Ba/Ca values are recorded in January 2007 and March 2009 (3.07 µmol/mol). There is a sharp drop in Ba/Ca following the maximum Ba/Ca event in October 2008 that aligns with the severe flooding event of January 2009 (Brown et al. 2017c). Limited seasonality can be observed, with elevated values found generally later in the year (September to November) and lower values between December to February. In the replicate colony NAN17_5 (Figure 5.6.) maximum values are recorded in August 2012 (6.82 µmol/mol), and lowest values are found consistently before January 2012 and between December 2012 to February 2014 (~ 3.00 µmoll/mol). Seasonality is less obvious in NAN17_5 than in NAN17_2 but values seem to be elevated during a month or two around June-September, yet this is not present every year. Only Ba/Ca in NAN17_5 was found to have a significant correlation with rainfall (Pearson's r = -0.28, p < 0.05), and no other correlation with environmental variables was observed (Table 5.5.).

In FP17_1 (Figure 5.7.) Ba/Ca maxima are recorded in January 2003, February 2004 and November 2015 (~8.00 µmol/mol). Minimum values are found in February 2009 and April 2010 (~3.00 µmol/mol). Both these minima events are characterised by occurring immediately after a high Ba/Ca event. Despite showing periods of elevated Ba/Ca that are sustained over several months (2003, 2004 – 2005, 2009, 2013, 2015) a clear seasonal signal cannot be identified in this record. Yet, when present, Ba/Ca seems to peak around November – March. For NAM17_1 (Figure 5.7.), maxima Ba/Ca events are recorded in late 2011 and early 2012 (8.54 µmol/mol), while lowest recorded signal happens in mid-2013 (2.50 µmol/mol). Sub-annual seasonality is not present in this sample, but there are elevated values during the 2011 – 2012 and 2013 – 2014 summers, while remaining low during 2012 – 2013. Ba/Ca in FP17_1 is correlated with SSS

(Pearson's r = 0.26, $p < 0.05$) and wind speed (Pearson's r = 0.13, $p < 0.05$). On the other hand, Ba/Ca in NAM17_1 is not correlated with any environmental variable (Table 5.5.).

Table 5.5. Correlations between coral El/Ca and environmental variables of each sample. Only significant correlations ($p < 0.05$) are reported.

VOT17_1	**Rainfall**	**Wind speed**	**K_d490**	**Chl-a**	**SST**	**SSS**
Ba/Ca	-0.11	0.01	0.07	0.08	-0.02	**0.39**
Mn/Ca	**0.21**	-0.07	0.15	0.11	0.12	0.13
Y/Ca	**0.36**	**-0.22**	0.08	0.04	**0.2**	-0.17
La/Ca	**0.2**	-0.1	0.07	-0.01	0.08	-0.03
Ce/Ca	**0.23**	**-0.17**	0.01	-0.01	**0.15**	-0.15

VOT17_2	**Rainfall**	**Wind speed**	**K_d490**	**Chl-a**	**SST**	**SSS**
Ba/Ca	-0.11	0.17	0.01	0.06	-0.02	**0.31**
Mn/Ca	0.19	-0.12	**0.36**	**0.39**	0.01	0.18
Y/Ca	**0.35**	-0.19	0.08	0.17	0.09	-0.02
La/Ca	**0.41**	**-0.31**	0.02	0.13	0.22	0.13
Ce/Ca	**0.4**	-0.29	0.07	0.17	0.17	0.08

NAN17_2	**Rainfall**	**Wind speed**	**K_d490**	**Chl-a**	**SST**	**SSS**
Ba/Ca	-0.02	0.01	-0.02	-0.03	-0.06	0.09
Mn/Ca	-0.12	0.03	-0.01	-0.02	-0.11	0.21
Y/Ca	-0.07	0.05	-0.07	-0.07	-0.14	0.21
La/Ca	-0.06	-0.03	-0.07	-0.07	-0.12	0.04
Ce/Ca	-0.07	0.01	-0.07	-0.07	-0.12	-0.1

NAN17_5	**Rainfall**	**Wind speed**	**K_d490**	**Chl-a**	**SST**	**SSS**
Ba/Ca	**-0.28**	-0.11	-0.04	-0.02	-0.01	0.2
Mn/Ca	-0.11	0.06	-0.18	-0.19	0.01	-0.08
Y/Ca	-0.08	-0.09	0.13	0.12	-0.08	0.15
La/Ca	0.04	-0.2	0.06	0.05	-0.01	-0.01
Ce/Ca	0.06	-0.25	0.11	0.09	0.06	-0.09

FP17_1	**Rainfall**	**Wind speed**	**K_d490**	**Chl-a**	**SST**	**SSS**
Ba/Ca	0.02	**0.13**	0.04	0.01	0.05	**0.26**
Mn/Ca	0.04	**0.16**	0.09	0.06	0.09	**0.24**
Y/Ca	-0.08	**0.17**	-0.13	-0.1	**-0.26**	0.01
La/Ca	-0.04	0.08	**-0.17**	**-0.15**	**-0.21**	-0.08
Ce/Ca	0.02	0.03	**-0.17**	**-0.14**	**-0.2**	-0.07

NAM17_1	**Rainfall**	**Wind speed**	**K_d490**	**Chl-a**	**SST**	**SSS**
Ba/Ca	-0.09	0.06	0.09	0.1	-0.07	0.09
Mn/Ca	**-0.31**	0.24	0.09	0.05	-0.01	**0.36**
Y/Ca	-0.07	0.19	0.04	0.06	**-0.26**	-0.02
La/Ca	-0.09	0.18	0.02	0.04	-0.24	-0.06
Ce/Ca	0.02	0.11	0.08	0.11	-0.23	-0.16

5.3.3.2. Mn/Ca

Unlike with Ba/Ca, the Mn/Ca signal in the VOT17_1 core (Figure 5.5.) does not present differences in mean values or variability pre and post the flooding event in 2009. In this sample, monthly Mn/Ca is correlated with rainfall (Pearson's r = 0.21, $p < 0.05$). Maximum Mn/Ca values are recorded during August 2008 to January 2009 (2.52 µmol/mol) and for a series of short-lived events between June 2015 and November 2016 (~3.10 µmol/mol). Seasonal variability becomes more apparent from 2012 onwards, and monthly peaks seem to occur between January and April every year. There is a sharp drop during 2009 in Mn/Ca following the maxima period of 2008 – 2009, and it is not until mid-2010 that baseline values return to pre-2009 ranges. VOT17_2_1 shows a positive corelation with K_d490 and Chl-a (Pearson's r ~ 0.37, $p < 0.05$). Mn/Ca maxima is found during a sharp event in February 2013 (2.12 µmol/mol) and in early 2016 following TC Winston (2.08 µmol/mol). Mn/Ca in this sample shows sub-annual seasonality, with elevated concentrations during January to March, and low Mn/Ca signal between July to November (Table 5.5.).

In sample NAN17_2, the maximum Mn/Ca signal (Figure 5.6.) occurs in early 2016 (1.50 µmol/mol), and there are also elevated Mn/Ca events in November 2005 and January 2006 as well as late 2008 (~1.20 µmol/mol). Lowest Mn/Ca are registered through 2009 and 2010, staying at around 0.80 µmol/mol. Seasonality cannot be detected in this samples, but there is a long-term increase in the Mn/Ca trend from 2011 onwards with a dip in early 2014. In the replicate colony NAN17_5 (Figure 5.6.) an abrupt event is registered in December 2013 reaching a Mn/Ca concentration of 5.50 µmol/mol. Another elevated event is detected in late 2015 where Mn/Ca reached 4.50 µmol/mol. Minimum values were registered during January 2014 with 0.93 µmol/mol. Although seasonality is not present in the signal of this colony either, the general increasing trend observed in NAN17_2 is also present here. Mn/Ca signal from samples NAN17_2 and NAN17_5 was not correlated with any environmental variable (Table 5.5.).

Maximum Mn/Ca levels in FP17_1 (Figure 5.7.) are recorded over a period between October 2002 and March 2003 (~2.00 µmol/mol) and October 2015 (1.75 µmol/mol), and minima Mn/Ca are found during January 2009 (0.33 µmol/mol). From 2013 onwards Mn/Ca in this samples shows an increasing trend, but no seasonality is found on the duration of the record. For NAM17_1 (Figure 5.7.), maximum Mn/Ca values are recorded in late 2015 (2.75 µmol/mol), minimum levels are recorded during early 2013 (0.45 µmol/mol). Similarly, to FP17_1, an increased trend is observed from 2013, but no sub annual seasonality is detected. Mn/Ca signal in FP17_1 (Table 5.5.) is correlated with SSS (Pearson's r = 0.24, $p < 0.05$) and wind speed (Pearson's r = 0.16, $p < 0.05$). For NAM17_1, Mn/Ca signal shows a correlation with rainfall (Pearson's r = -0.31, $p < 0.05$), and salinity (Pearson's r = 0.36, $p < 0.05$) (Table 5.5.).

5.3.3.3. REE (Y/Ca, La/Ca, Ce/Ca)

At Votua, a clear seasonality in REE/Ca ratios is present, where annual maxima occur between January and April, and annual minima occur around June – July of each year (Figure 5.5.). For sample VOT17_1, maximum events are identified in 2001, 2007, 2008, 2012 and 2014. For VOT17_2, maximum events are recorded in 2013, 2014 and 2016. REE/Ca values in sample VOT17_1 are significantly correlated with SST (Pearson's r ~0.17, $p < 0.05$), rainfall (Pearson's r = 0.20 – 0.36, $p < 0.05$) and wind speed (Pearson's r ~ -0.20, $p < 0.05$). Values in sample VOT17_2 is significantly correlated with rainfall (Pearson's r = 0.35 – 0.41, $p < 0.05$) and wind speed (Pearson's r =-0.31, $p < 0.05$) (Table 5.5.).

REE/Ca profiles in Nananu-i-Ra (Figure 5.6.) are very similar for each sample, and Y/Ca, La/Ca and Ce/Ca ratios are strongly correlated. In NAN17_2 maximum REE/Ca values are reached in early 2008 and late 2011, and REE/Ca minima occur between March and June 2010. There is seasonality observed in all REE elements, with peaks occurring around June–September and troughs present during November – March. For NAN17_5, highest REE concentrations are found in June 2012 and February 2014, and lowest REE concentrations are recorded in December 2011. However, temporal variability in these samples is highly abrupt, and clearly different from NAN17_2. There seems to be some seasonality in these samples, as well as a double annual peak in REE concentrations, the first one happening around Apr–May and a later one Around Nov–Dec, however, this double peak is not present on every year of the record. REE/Ca values in these samples were not found to have any correlation with environmental variables ($p > 0.1$) (Table 5.5.).

In FP17_1 (Figure 5.7.), maximum REE/Ca events are recorded in November 2001, October 2003, August 2006, September 2007 and May 2012, while lowest values are recorded in March 2005, May 2010 and May 2011. There is a clear sub annual seasonality in the REE signal of these samples, with elevated REE/Ca peaks usually happening between September and December every year, while minimum values are recorded immediately after, during January–March. For NAM17_1 (Figure 5.7.), maximum values are recorded in November 2011 to January 2012, December 2012, February–March 2015 while the interval with the lowest REE/Ca values is during December 2013/January 2014, and January 2015. Seasonality is not clear in this record. REE/Ca values in FP17_1 are correlated with SST (Pearson's r ~-0.20, $p < 0.05$), and K_d490 and Chl-a (Pearson's r ~-0.15, $p < 0.05$). In NAM17_1, the REE/Ca (Y/Ca) signal is somewhat correlated with SST (Pearson's r = -0.26, $p < 0.05$) (Table 5.5.).

5.4. Discussion

The following discussion presents coral Ba/Ca, Mn/Ca and REE/Ca (Y/Ca, La/Ca and Ce/Ca) records at each location and focuses on: i) intra-site and inter-site El/Ca variability in context with other studies (Section 5.4.1.) and ii) exploring environmental drivers of temporal variability in El/Ca records (Section 5.4.2). I propose that the successful application of these proxies to assess terrestrial runoff patterns on the sub-annual timescale in Fiji requires a site-specific understanding of the dominant controlling factors on sediment and freshwater delivery including rainfall and its links to runoff, the role of wind on local turbidity, and land-use and coastal development.

5.4.1. Intra- and inter-site variations in elemental records

5.4.1.1. Ba/Ca

Coral Ba/Ca was found to be highly variable at both the intra- and inter-site level. There is poor replication in mean Ba/Ca within site (ΔBa/Ca of replicates > 0.86 µmol/mol) and, in addition, intra-site offsets are larger than between sites (ΔBa/Ca between sites > 0.18 µmol/mol; Calculated by comparing average Ba/Ca of each site) (Table 5.1.). In addition, the only Ba/Ca time series that were consistent between cores were at Votua Reef (Pearson's r = 0.44; Table 5.2.).

Highly variable replicability of Ba/Ca from *Porites* spp. records has been reported in previous studies from Fiji and other locations. Jupiter et al. (2010) analysed *Porites* spp. Ba/Ca from two coastal locations in Kubulau (Vanua Levu, Fiji; 60 km north of Viti Levu, Figure 5.1.) and found large variability in mean Ba/Ca across reefs (3.69 to 13.50

µmol/mol; n=2). Similarly, two *Porites* spp. cores collected from Dennis Patch in the Suva Reef (~2 km away from Fish Patches) recorded mean Ba/Ca values of 6.15 and 15.9 µmol/mol (S. Albert, *Pers. Comm*.). Lewis et al. (2018) analysed Ba/Ca from *Porites* spp. from five locations in the GBR (two replicate cores per location) and found contrasting differences in mean Ba/Ca between replicates, ranging between 1.13 and 8.49 µmol/mol. In Singaporean reefs the difference in mean Ba/Ca between site replicates was found to be ~ 1.50 µmol/mol (Tanzil et al. 2019), and in the Caribbean mean Ba/Ca differences in *Porites* spp. was of 0.17 µmol/mol (LaVigne et al. 2016). Regarding reproducibility of Ba/Ca timeseries between replicates, Tanzil et al. (2019) found contrasting results in Singapore's reefs where significantly correlated replicates only show a weak relationship, similar to this study (Pearson's r = 0.22 – 0.53). Furthermore, Lewis et al. (2018) found poor replication between coral colonies in the GBR, but Lavigne et al. (2016) reported excellent agreement between their Gulf of Panama *Porites* spp. replicates (Pearson's r = 0.86 – 0.99).

The inconsistency in Ba/Ca reproducibility in terms of absolute values between colonies within the same location and the low time-series correlations indicate that there can be other factors, in addition to freshwater discharge, that drive Ba concentration in coral aragonite. Instead, colony-specific biological factors could explain the observed differences between colonies ("vital effects"). For example, the incorporation of Ba due to genotypic differences (Allison et al. 2018) or trophic differences favouring ingestion of Ba-rich particles (Tanzil et al. 2019) in some colonies could lead to offsets in Ba/Ca within the same reef. Yet, Fiji coral Ba/Ca values are within the range of other Ba/Ca measurements across the Indo Pacific, including the GBR (3.5 – 7.1 µmol/mol; Alibert et al. 2003; Sinclair and McCulloch 2004; Jupiter et al. 2008; Saha et al. 2018), Singapore (4.35 – 6.21 µmol/mol; Tanzil et al. 2019), Western Pacific Warm Pool (4 µmol/mol; Alibert and Kinsley 2008) and New Caledonia (4 µmol/mol; Quinn and Sampson 2002), and are up to 3 µmol/mol lower than Ba/Ca in *Porites* spp. from Madagascar (6.05 – 6.75 µmol/mol; Grove et al. 2012) and more than 10 µmol/mol lower than values from Guam (14.11 – 18.86 µmol/mol; Prouty et al. 2014).

The highest mean Ba/Ca value is measured in VOT17_1 (post-2009), followed by FP17_1 and NAN17_2. Variability of mean Ba/Ca across locations does not depend on seawater turbidity or terrestrial influence as baseline values from Votua Reef (small wet watershed, low population, lowest turbidity) are around 1 µmol/mol lower than values in Nananu-i-Ra (big watersheds, different rainfall regime, high population and highest turbidity). Similar to the other elements explored below, these results hint at different mechanisms affecting Ba cycling across locations, but also colony specific responses in regard to Ba uptake that increases the intra-site variability. Mechanisms controlling Ba concentration in seawater and coral uptake in each location are discussed in Section 5.4.2.

5.4.1.2. Mn/Ca

Mn/Ca shows a different behaviour within and across sites than that of Ba/Ca records. Mean Mn/Ca has a better replicability than Ba/Ca regarding both mean values and timeseries correlations (Tables 5.1. and 5.2.), something also observed by Lewis et al. (2018), with only Nananu-i-Ra Mn/Ca showing a relatively large difference in mean Mn/Ca (1.10 µmol/mol) and a not significant correlation (Tables 5.1. and 5.2.). Site specific Mn/Ca is different across sites with Nananu-i-Ra (NAN17_5) showing the highest mean Mn/Ca (2.02 µmol/mol), and Namuka (NAM17_1) showing the lowest (0.74 µmol/mol). Although Mn/Ca values in this study are much lower than other samples previously analysed from Fiji, recorded Mn/Ca values fall within range of other *Porites* spp. records. Coral Mn/Ca from Fiji *Porites* spp. showed values of 1.35 µmol/mol in the Suva Reef (S. Albert, *Pers. Comm.*), higher values than those reported in our sample from the Suva Reef (Fish Patch – FP17_1), and between 2.01 µmol/mol to 9.19 µmol/mol in those samples from Kubulau (Jupiter et al. 2010). Recorded Mn/Ca from *Porites* spp. ranges greatly in the literature across several regions (i.e., GBR, Caribbean, Indo-Pacific) where studies found Mn/Ca varying from 41.6 nmol/mol up to 6.74 µmol/mol (e.g. Fallon et al. 2002; Alibert et al. 2003; Carriquiry and Villaescusa 2010; Moyer et al. 2012; Jiang et al. 2017; Saha et al. 2021; Sayani et al. 2021).

The highest Mn/Ca values are measured in both cores from Nananu-i-Ra, which is also the location with highest terrestrial influence and seawater turbidity through the year (See Chapter 3). Yet, Mn/Ca values from the Votua Reef (lowest turbidity, small watershed, low population), Namuka Reef (mid turbidity, small watershed, low population) and Suva Reef (high turbidity, industrial activity, high population) have similar values despite a range of turbidity levels. These Mn/Ca variations across sites, in contrast to environmental gradient, suggests that more localised, site-specific factors might be controlling absolute incorporation of Mn in the aragonite lattice, as explored further in Section 5.4.2.

5.4.1.3. REE (Y/Ca, La/Ca, Ce/Ca)

Intra-reef variability (between replicated samples) and inter-reef variability are similar in terms of the mean REE/Ca value (Table 5.1.). Furthermore, no gradient or site-specific signal in mean REE/Ca is observed. Regarding timeseries correlation between replicates, although Y/Ca was significantly replicated in Nananu-i-Ra and Suva, La/Ca and Ce/Ca were only significantly correlated in Nananu-i-Ra (Table 5.2.). Previous data from Fijian *Porites* spp. show Y/Ca values ranging from 0.28 µmol/mol to 0.45 µmol/mol (Jupiter et al. 2010; S. Albert, *Pers. Comm.*). These Y/Ca values are much higher than those recorded in this study (0.04 – 0.16 µmol/mol), which are closer to values recorded in corals from Puerto Rico (0.04 µmol/mol ; Moyer et al. 2012), and GBR (0.01 µmol/mol to 0.22; Alibert et al. 2003; Sinclair 2005; Jupiter 2008; Saha et al. 2018, 2018, 2021; Leonard et al. 2019), with even lower values being reported from Papua New Guinea (0.007 µmol/mol to 0.010 µmoll/mol, Fallon et al. 2002). Other studies from the GBR, however, recorded higher Y/Ca values than those above (e.g., Lewis et al. 2018). Jupiter et al. (2010) also report ranges of 30 – 130 nmol/mol for La/Ca, and 24.1 – 79.9 nmol/mol for Ce/Ca in Fijian *Porites* spp. As with Y/Ca, these values are considerably higher than those recorded in our samples and also than in other available data from the GBR (Webb and Kamber 2000; Wyndham et al. 2004; Jupiter 2008; Leonard et al. 2019; Saha et al. 2021) whose recorded values (1.07 – 24.10 nmol/mol for La/Ca, and 1.40 – 32.93 nmol/mol for Ce/Ca) are closer to our data, Kiribati (Sholkovitz and Shen 1995) and Papua New Guinea (Fallon et al. 2002).

The wide variability in REE concentrations recorded in different regions and locations is often reported as reflecting differences in terrestrial influence across different reefs, being more or less exposed to sediment plumes (e.g., Leonard et al. 2019; Fallon et al. 2002; Saha et al. 2021; Alibert et al. 2003). As seen before (Chapter 3), seawater turbidity properties are significantly different between coastal sites in Fiji, including those reefs from Vanua Levu (Jupiter et al. 2010) and Dennis Patch (S. Albert, *Pers. Comm.*), yet no gradient or systematic difference is evident in REE/Ca from Fijian coral samples in this study. These REE/Ca variations across sites suggests that other site-specific factors might be controlling incorporation of REE in the aragonite lattice explored further in Section 5.4.2. in a similar manner to Mn/Ca and Ba/Ca.

5.4.2. Controlling factors on site-specific temporal variability in elemental proxies

5.4.2.1. Votua Reef

The Votua Reef, in the Coral Coast, is located in the vicinity of a small catchment which is mainly forested (>90%; Atherton et al. 2005), but inhabited (Figure 5.1. and Figure 5.3.). In this location seasonal climatology has a substantial control over catchment and coastal hydrology, with turbidity being strongly linked to the wet season (See Environmental Data; Chapter 2 – Section 2.6.).

Coral Mn/Ca and REE (Y/Ca, La/Ca, and Ce/Ca) are correlated in both specimens within this site (Table 5.3.) and this reproducibility indicates a strong environmental influence on the record. Periods of both elevated Mn/Ca and REE/Ca occur during wet phases with rainfall events above a threshold delimited by the climatological maximum monthly mean (> 400 mm/month) (Figure 5.5.). These events are usually associated with anomalously high seasonal events (e.g., monsoon) or intervals of abrupt and intense rainfall (e.g., tropical cyclones).

This is evidenced by the peaks in Mn/Ca, although of variable magnitude, that can be observed from November 2000 to June 2002 (1.54 μmol/mol), 2007 (1.03 μmol/mol), 2008 to 2009 (2.34 μmol/mol), 2009 to 2010 (1.34 μmol/mol), with small seasonal peaks (1.08 to 1.48 μmol/mol) in 2012, 2013 and 2014, and from September 2015 to the end of the records (> 1.5 μmol/mol) (Figure 5.5.). Increases in REE/Ca are correlated with these Mn/Ca peaks (Y, La, Ce; Pearson's r > 0.20; Table 5.3.) which occur in November 2000, January 2002, early 2007, early 2008, January 2012, January – February 2013 (despite different magnitude across core replicates), January 2014, January – March 2015 and January – February 2016. However, some differences in peaks and patterns are observed. For example, during the La Niña events of 2005 – 2006 and 2010 – 2011 small, broad peaks are observed in all three REE/Ca records that are not present in the Mn/Ca record. Note also that Mn/Ca shows a broad increase from 2009 until 2010 that is not reproduced in the REE/Ca records. Instead, La/Ca and Ce/Ca (but not Y/Ca) show a sharp increase in January 2009, followed by a trough and a subsequent increase again in April 2009 until 2010. Furthermore, the seasonality is more pronounced (e.g., from 2006 until 2010) in the REE/Ca records.

Overall, the coupling of Mn/Ca and REE (Y/Ca, La/Ca, Ce/Ca) in corals from the Votua Reef with heavy rainfall during the wet season (where accumulated rainfall increases above 400 mm/month) and the positive significant correlation between these El/Ca ratios and rainfall (Pearson's $r > 0.20$) suggests that terrestrial runoff is driving seasonal variations in these records. Interestingly, these intense rainy events occur during La Niña phases, which are characterised by higher frequency of rainfall events than Neutral and El Niño phases, due to the SPCZ moving closer to Fiji (Kumar et al. 2014). Presumably, during the wet season soil moisture in Fiji is elevated and thus during intense rainfall events the soil saturation threshold in this region might be easily reached, increasing sediment runoff into creeks and rivers (Stephens et al. 2018).

Coral Mn/Ca records from Votua Reef record seasonal rainfall conditions as well as short-lived events (such as tropical cyclones and flooding events). While in some regions like in the GBR Mn/Ca has been found to follow SST variability closely, which is attributed to primary productivity (e.g., Alibert et al. 2003; Wyndham et al. 2004), this clear seasonal pattern was absent in the coral Mn/Ca here (correlation SST – Mn/Ca was not significant), and suggests that either the role that primary productivity plays as a sub-annual driver of coral Mn/Ca in the Votua Reef is limited or the limiting factor for primary productivity is not temperature-based.

For coral REE/Ca, early studies showed a significant correlation between REE/Ca values and terrestrial influence, linked to the presence of flood waters (Wyndham et al. 2004) and sedimentation processes (Fallon et al. 2002), thus showcasing its potential for identifying inland processes and their effects on coastal ecosystems. Recently, peaks in REE/Ca (including Y/Ca) were correlated with river discharge, rainfall and turbidity at annual timescales in the GBR by Saha et al. (2019). Although available REE/Ca records showing highly resolved monthly or seasonal changes are limited to two studies in the GBR, they have been successfully linked to rainfall events (Leonard et al. 2019) and terrestrial runoff (Saha et al. 2021) at annual and sub-annual timescales.

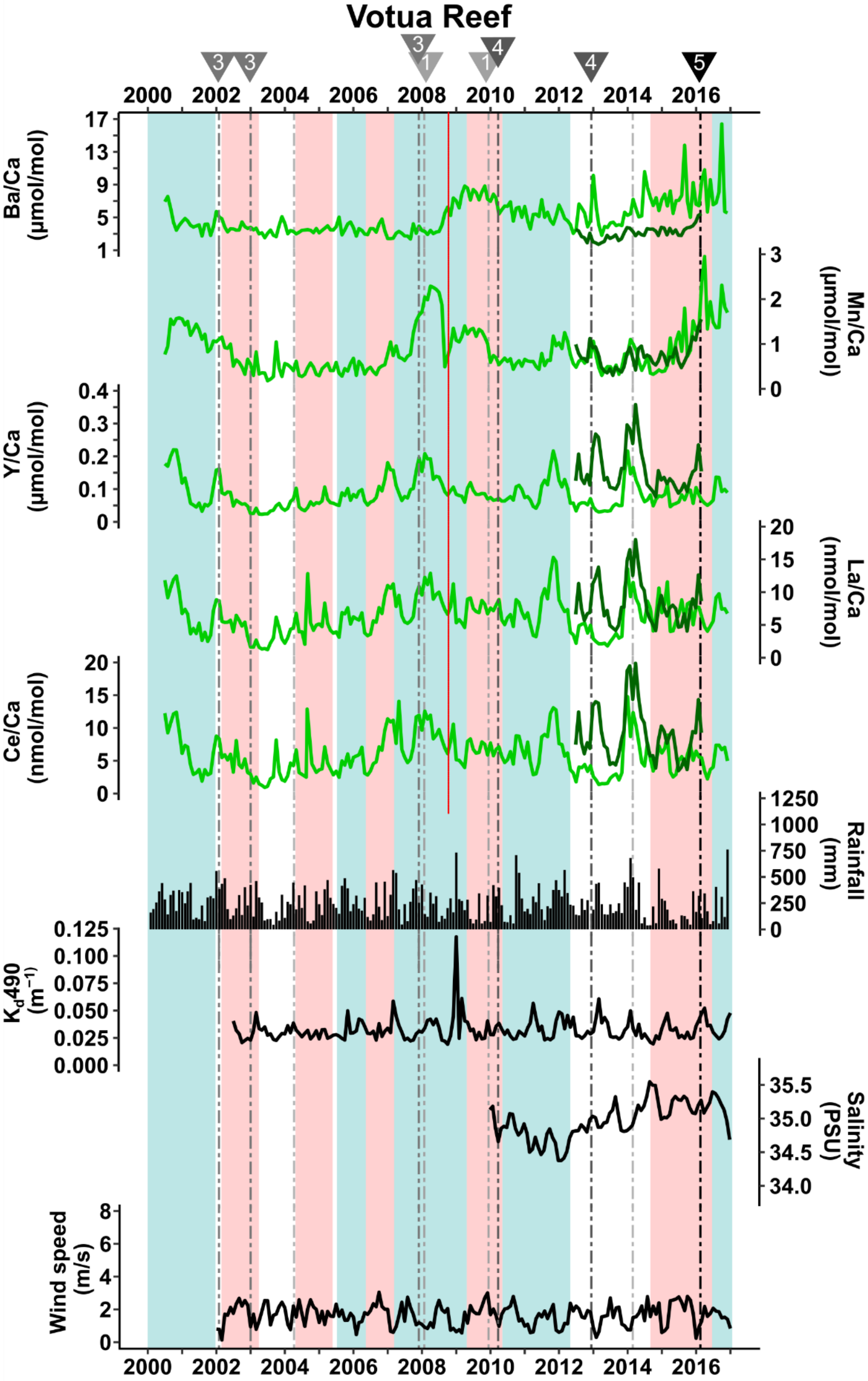

Figure 5.5. Time series monthly mean El/Ca records from samples from the Votua Reef, VOT17_1 (light green) and VOT17_2 (dark green) and environmental variables. Blue years are La Niña phase, and red years are El Niño phase. Gray vertical lines depict tropical storms (lighter) and cyclones. Triangles above plot depict cyclone category. Red vertical line signs the core break.

Building on our coral El/Ca records and covariation between rainfall and El/Ca, a previous study of the Votua watershed hydrology (2009 – 2010) shows that in this area >50% of the cumulated rainfall is produced by low intensity rainfall events (<5 mm/h) (Ram and Terry 2016). Further, this study shows that increases in Votua Creek turbidity are linked to rainfall events with at least 14.5 mm of accumulated rainfall per day, which represents a small percentage (~10%) of the total rainfall events. Importantly, some rainfall events that overcome this threshold (14.5 mm/day) did not produce an increase in creek turbidity (Ram and Terry 2016) and this hints that creek turbidity is not only dependent on total rainfall. This work shows that a combination of maximum rainfall intensity and antecedent moisture conditions (relative wetness or dryness of the soil) play an important role in modifying creek turbidity at Votua.

Influence of creek runoff and sediment load on inshore turbidity and reef chemistry (e.g., Mn^{2+}, REE) has not been investigated in the Votua catchment or in Fiji on a wider scale. However, based on the observations of Ram et al. (2016) and environmental records of rainfall and coastal turbidity (satellite K_d490) response, I postulate that certain rainfall events (those with high intensity or high accumulated rainfall, especially during summer/wet season, November – April) will significantly influence reef turbidity and therefore will be recorded in Mn/Ca and REE/Ca records; this explains the correspondence of Mn/Ca and REE/Ca peaks with wet periods and high accumulated rainfall events in this study. This suggests that application of Mn/Ca and REE/Ca proxies along the Coral Coast (small catchments, with little anthropogenic modification and a typical tropical climate and rainfall regime) are good candidates to reconstruct runoff events associated with seasonal climatic events (i.e., wet periods, intense monsoons, and tropical cyclones).

Although there is a clear correspondence of the seasonal Mn/Ca and REE/Ca peaks, there are two large Mn/Ca (Mn/Ca maxima) events (2009 and 2016) that are not shown in the Y/Ca record (although La/Ca and Ce/Ca show a small increase of ~4 µmol/mol during these periods). The 2009 event corresponds to a high rainfall period (> 750 mm/month) and high turbidity (low light penetration (K_d490) > 0.1 m^{-1}). In January 2009 a persistent monsoon coupled to two consecutive tropical storms caused severe flooding along the Coral Coast (Brown et al. 2017c). In February 2016, Tropical Cyclone Winston (Cat. 5) caused high rainfall and sediment mobilization across the southern coast of Viti Levu despite the storm centre passing further north (Kim et al. 2020). Both these events can cause a large perturbation in the coastal ecosystem by increasing freshwater, sediment input and organic matter in the water column (Yoon and Raymond 2012; Anglès et al. 2015). The latter can induce sub-anoxic conditions, and thereby the reduction of Mn (IV) to Mn (II), which is easily assimilated by corals (Lewis et al. 2012). Further, strong mixing in the water column and resuspension of sediments can favour the release of Mn (II) from the sediment pore waters (Chapman et al. 2022). Reduction of Mn oxides in both sub-oxic pore waters and from particulate matter can cause REE desorption (de Baar et al. 1988; Sholkovitz et al. 1989) favouring the enrichment of light REEs (LREEs; La, Ce). Although Wyndham et al. (2004) argues that the contribution of REE desorption as a result of Mn reduction in increasing coral REE/Ca is minor, this mechanism would show a notable increase of Mn concentration weakly followed by LREE (as seen here).

I, therefore, postulate, that during these two high-energy events the nature of the sediments imported into the coastal system were different than those during regular seasonal rainfall events, altering the source of elements (and the recorded signal). Overall, Mn/Ca, and REE/Ca values to some extent, also show sensitivity to addition of organics associated with large flood events. This sensitivity, and the role of organic matter in increasing absolute coral El/Ca, needs to be considered when applying this proxy to reconstruct changes in environmental conditions. For example, one way to delineate these events would be to assess both proxies and depending on coupling between Mn/Ca and REE/Ca changes, or lack of thereof, events associated with organic matter delivery could be disentangled from other events.

Overall, the robustness of coral Mn/Ca and REE/Ca as river discharge proxies and their ability to record short-lived events or seasonal changes in Fiji are dependent on multiple factors such as (1) the sensitivity of the coral proxy to changes in the environment (e.g., changes in the sediment load and river runoff), (2) hydrodynamics of the land-coastal system, as it regulates river discharge, sediment input and the nature of runoff (e.g., dissolved nutrients, organic-rich particles, fine v. coarse), and (3) reef specific factors (i.e., productivity/sediment mixing).

The Ba/Ca record in corals from the Votua Reef lack seasonal variability, in contrast to the other explored proxies (Mn/Ca, Y/Ca, La/Ca and Ce/Ca). Only two periods show elevated Ba/Ca: between 2009 and 2010 (closely aligned with a broad peak in Mn/Ca values), and the progressive increase in Ba/Ca values with sharp (increasing up to 15 µmol/mol) peaks from November 2015 until the end of the record (again, similar to the Mn/Ca increase over the same interval). It is important to note how coral Ba/Ca values show a baseline increase in Ba/Ca (3 µmol/mol higher; long core VOT17_1) from 2009 onwards. The lack of correlation between Ba/Ca and river discharge is not unique to this study (e.g., Lewis et al. 2007) and other drivers related to changes in the reef environment must be considered. In the above section we link periods of elevated Mn/Ca, La/Ca and Ce/Ca with changes in oxidative processes taking place in the water column making these elements more bioavailable. Here I propose that this baseline shift in Ba/Ca is linked to the specific change in local primary productivity during the 2009 flooding event. Environmental data shows how reef turbidity sharply increased following this event, and de-coupling of Mn/Ca and REE/Ca suggest a sudden change in the nature and source of sediment runoff.

Primary productivity has been seen to drive seasonal Ba/Ca (Sinclair 2005a; Lewis et al. 2012; Saha et al. 2016, 2018) due to barite formation favoured by algal blooms (Gillikin et al. 2006). A previous study on nutrient variability along the Coral Coast found that both nitrates and phosphates are highly variable (NO_3^-: 0.13 – 7.64 µM; PO_4^{3-}: 0.04-0.98 µM; Tamata 2007) and also sourced to the inshore reefs by creeks and rivers. This study observes how increase of nutrients, and specifically nitrate levels, are strongly linked to rainfall events. Yet, the level of phosphates in the coastal region during rainfall events is variable and changes with the type of event due to the varying source of phosphates. Some rainfall events favour sediment mobilisation from crops (increase of phosphates in reefs), while other events favour dilution of wastewaters (decrease of phosphates in reefs) (Tamata 2007). Building on this, I suggest that both the flood event of 2009 and the tropical cyclone in 2016 had the potential to increase the terrigenous delivery into the coastal ecosystem, which is supported by the sharp increase (by 0.050 m^{-1}) in seawater turbidity (K_d490) and chlorophyll-a during the flooding event, increasing the concentration of nutrients in the reef and promoting primary productivity (algal bloom and organic matter increase), altering the biogeochemical cycle of Ba/Ca (and Mn/Ca, see previous paragraphs) in this location.

Furthermore, this increase in Ba/Ca occurs in tandem with a break in the coral core between the two sections (pre-2009 and post-2009). Although linear extension is not affected during this period, annual density for 2009 remains low until 2010, when the seasonal density cycle recovers (See Chapter 4 – Figure 4.7.). Growth anomalies as a response to freshwater pulses and flood have previously been observed in *Porites* spp. (e.g., Hendy et al. 2007; Lough and Cantin 2014). This growth anomaly is not observed during the 2016 event, which suggests the context and impact on coral cores in these two events are different. While the 2009 occurred during a moderate La Niña (wetter than usual conditions), the 2016 tropical cyclone happened during a strong El Niño (drier than usual conditions) and following two years of high thermal stress that had already affected coral growth (Chapter 3). Potentially, these two very different environmental periods might also alter the source and the N:P ratios of nutrients in the reef. Tamata (2007) showed that while rainfall/river discharge always increased coastal N concentration, the concentration of P was variable depending on whether river runoff was dominated by surface sediment from agricultural lands or by settlement wastewater. The varying concentration of nutrients might have played a role on the diverse coral growth response as periods of elevated nutrients have been shown to have a variable impact on coral growth (Marubini and Davies 1996; Donovan et al. 2020).

As discussed above, although the threefold baseline increases in Ba/Ca of VOT17_1 complicates its interpretation as a runoff proxy, the record suggests primary productivity plays an important role in modifying coral Ba/Ca at this site as shown in other studies. Replicate Ba/Ca records from VOT17_2, however, show a similar average Ba/Ca value to the baseline values from VOT17_1 prior to 2009. This suggests that either VOT17_2 did not suffer a baseline increase following the 2009 flooding, or that that mean Ba/Ca is different across colonies, even from the same reef (Tanzil et al. 2018). As described in previous section, a range of factors could alter the mean and temporal variability of coral Ba/Ca, and more work confirming the presence or absence of diagenetic barite in the coral skeleton using imaging techniques to disentangle the sources of Ba is necessary. Nevertheless, bringing together all the proxies and findings (elevated Ba/Ca and Mn/Ca, low La/Ca and Ce/Ca and no Y/Ca increase during 2009 and 2016) hints that it is changes in primary productivity, organic matter and bacterial processes occurring following abrupt flooding events and they are important to consider when thinking about nutrient inputs into inshore reefs.

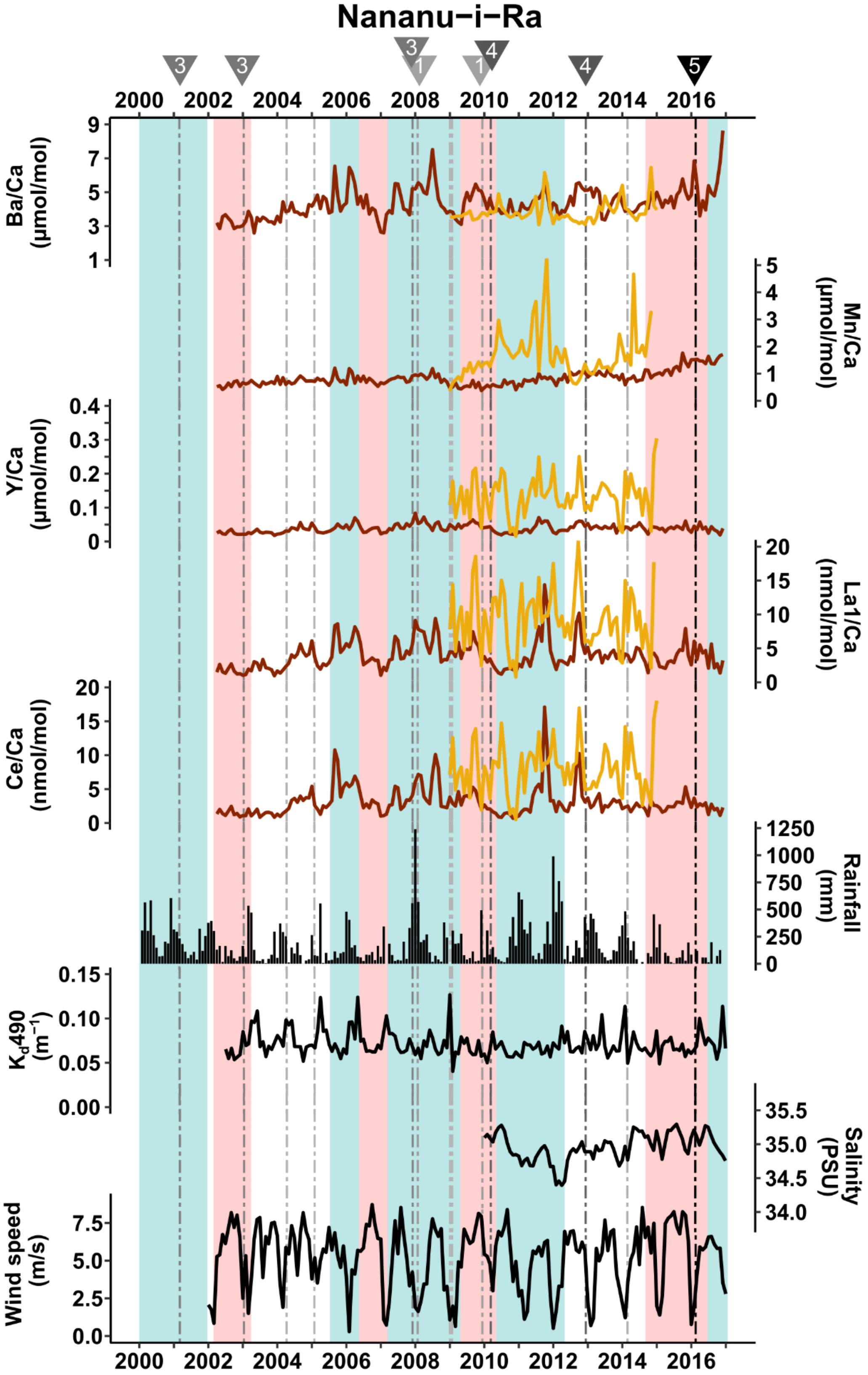

Figure 5.6. Time series monthly mean El/Ca records from samples from the Nananu-i-Ra, NAN17_2 (brown) and NAN17_5 (ochre) and environmental variables. Blue years are La Niña phase, and red years are El Niño phase. Gray vertical lines depict tropical storms (lighter) and cyclones. Triangles above plot depict cyclone category.

5.4.2.2. Nananu-i-Ra

Nananu-i-Ra is a small offshore island of 3.5 km^2, situated in the north-eastern coast of Viti Levu, at ~3 km distance from the Ra province. The island has low anthropogenic development, and its low-lying hills are mostly covered by grassland (Figure 5.1.). Besides island surface runoff, the most proximal sources of terrigenous sediments are the Penang River (mouth ~10 km) and Viti Levu Bay (~17 km), whose catchments cover an extensive area, are heavily populated and dedicated mostly to grassland, farming and sugarcane crops. Furthermore, the coral colonies (NAN17_2 and NAN17_5) are found in areas of reef with hydrographic differences (Figure 5.3.). We expand on these micro-scale differences below.

In the long core (NAN17_2; 2002 to 2016) the explored proxies (Ba/Ca, Mn/Ca, REE (Y/Ca, La/Ca and Ce/Ca) are significantly correlated with each other (Pearson's r = > 0.14; Table 5.3.), in contrast to all other locations. Seasonal Ba/Ca, Mn/Ca and REE/Ca peaks are coordinated during 2005 to 2006, 2007 to 2008, 2009, 2011, 2012, and end of 2015 to 2016. Although the nature of the peaks varies for each proxy across the time interval, showing broader El/Ca peaks before 2009 and sharper El/Ca peaks during events post-2009. For example, during 2008 there is a pronounced difference in El/Ca peaks in comparison to 2015 (ΔBa/Ca= 0.20 µmol/mol, ΔMn/Ca= 0.30 µmol/mol, ΔY/Ca= 0.45 µmol/mol, ΔLa/Ca = 3 nmol/mol, ΔCe/Ca= 5 nmol/mol; Figure 5.6.). The seasonal profile in El/Ca values contrast with the Votua Reef, with "double peaks" or high frequency variability occurring within the seasonal maxima, particularly evident during 2005-06 and 2007-08 (La Niña phases), and also in the 2016 event. Overall, higher El/Ca peaks correspond to several La Niña phases (2005-2006, 2007-2008, 2010-2012) whereas smaller El/Ca peaks observed in 2006 and 2016, for instance, correspond to an El Niño phase. However, high peaks in El/Ca occurred alongside strong tropical cyclones (Cat. 4 and 5 respectively) in 2012 and 2016.

In the short core of this location (NAN17_5; 2009 to 2015), correlations between El/Ca are limited to Ba/Ca and Mn/Ca (Pearson's r = 0.35, Table 5.3.), Mn/Ca and REE/Ca (Pearson's r > 0.29, Table 5.3.) and REE/Ca (Pearson's r >0.93, Table 5.3.). Mn/Ca and REE/Ca values vary on monthly timescales in contrast to the other core, with sharp high peaks and deep troughs. The differences in expression of sub-annual variations between the long and short core are not surprising as these two colonies occupy opposing sides of Nananu-i-Ra island (Figure 5.3.; Chapter 2 – Section 2.2.2.). NAN17_5 is on an east-facing reef slope and exposed to strong surface current and winds (from southeast to northwest). NAN17_2 is on a bay facing the north-west of the small island and it is sheltered from these strong surface currents and wind. The mechanisms in which these differing hydrographic conditions can potentially drive the site-specific El/Ca monthly variability, assuming a constant and similar runoff source, of the geochemical signal are: i) reef specific conditions, and ii) differences in colony boundary diffusion layer (BDL) thickness (Shashar et al. 1996; Gardella and Edmunds 2001; Chang et al. 2009) and concentration and dilution of trace elements in the BDL.

The resolution of remote sensed data (4 km) does not allow us to examine scenario (i) but I propose that reef specific conditions, such as changes in wind, sediment residence time, and degree of flushing to the open ocean, are manifest as higher frequency El/Ca variability in the exposed coral colony record (NAN17_5). Seasonal turbidity profiles have higher variability than other sites with monthly turbidity having high frequency variability between January and April in this location, while in the Votua Reef turbidity maxima is reached only in January. However, higher resolution in situ and remote sensed environmental data (e.g., seawater turbidity) are needed to corroborate this hypothesis. In scenario (ii) I propose that trace elements being incorporated into the coral aragonite are initially dissolved in the immediate seawater to the coral colony (BDL), and that the rate at which these elements are incorporated do not only depend on elemental geochemistry but also on the hydrodynamics of the BDL (Chang et al. 2009). Increasing flow speed has been observed to decrease BDL thickness (Jimenez et al. 2011) and increase turbulence of the flow (Gardella et al. 2001). Assuming that seawater current (flow speed) are very different across sites, the exposed NAN17_5 coral will experience high flow speed, which is likely to explain the sharp peaks and extreme month-to-month variability of El/Ca, as concentration of trace elements in the BDL changes with seawater influx and flow turbulences. Further supporting this hypothesis, SST proxies in NAN17_5 (investigated in Chapter 4) do not show the high frequency variability shown by Mn/Ca and REE/Ca, supporting that this is micro-scale environmental signal, rather than "vital effects" on NAN17_5. For the remainder of the discussion, we focus on the long core (sheltered NAN17_2) as the record is longer enabling comparison with other records over a 15-year period. Further, the sheltered nature of the core site might limit its exposure to non-runoff factors.

Overall, the coupling of proxies (Ba/Ca, Mn/Ca, REE/Ca) in NAN17_2 indicates that they are all influenced by similar environmental factors. The largest peaks in El/Ca occur during wet periods (i.e., La Niña phase) characterised by both a higher number of rainfall events and a higher precipitation in each event (Kumar et al. 2014). Average accumulated rainfall per month in Nananu-i-Ra is 192 mm with above average accumulated rainfall recorded in 60% of the months during La Niña phases in contrast to El Niño phases (10%). This correspondence between El/Ca peaks and rainy periods suggests that freshwater and sediment discharge into the coastal system are being recorded by these proxies. However, correlation analysis shows no significant relationship between environmental variables and elemental ratios. A closer inspection detects that peak-to-peak correspondence is limited with an offset (2-4 months) between peak rainfall and peak El/Ca, and also a small proportion of lower peaks are observed within the high rainfall period window. For example, between November 2007 and February 2008 the accumulated rainfall is several mm above average (including a major rainfall recorded in January 2008), but the highest El/Ca peak is not recorded simultaneously during this period. This offset in timing of peaks has been shown before in other regions ranging from 1-2 months to 1 year (e.g. Moyer et al. 2012; Chen et al. 2020; Sayani et al. 2021). I propose that the offset in timing is attributed to the seasonal interaction between wind and rainfall and its impact on site specific turbidity.

Seawater turbidity in Nananu-i-Ra follows a variable seasonal pattern with 2 maxima per year: in December-January (when maximum rainfall occurs), and in April-May (when wind strength starts increasing). The environmental data shows how average seasonal peak turbidity is weakly coherent with peak rainfall, showing an increase after the wet season (rainfall seasonal peak is December – April), and when winds start strengthening in Fiji (wind seasonal peak is June – October). There are two potential sources of river runoff from Viti Levu into Nananu-i-Ra (Penang River and Viti Levu Bay, with several small rivers and creeks discharging there). I hypothesise that during the wet season (November – April), sediment from these two sources enters nearshore environments and resides there, not reaching Nananu-i-Ra immediately after. This area has a shallow bathymetry and several islets, cays and barrier-like reefs around coastal Viti Levu. Due to these geomorphological and hydrological features, strong wind-driven surface currents (from southeast towards northwest) at the beginning of the dry season (winds start strengthening in April) are then able to mobilise the sediment sourced to nearshore environments during the previous months. During this process, the mobilised water masses reach Nananu-i-Ra and as such are recorded by the coral, evident by the timing of peak El/Ca aligning with the period when winds start strengthening in this region. Thus, the observed double peak in turbidity (weak increase in December – January and strong increase in April – May) and the high frequency variability of El/Ca between December – May are attributable to both surface runoff from Nanau-i-Ra and wind-mixed sediments available in the coastal ecosystems.

Another process contributing to this offset between rainfall and El/Ca could be related to the residence time of dissolved trace metals in the coastal seawater, resulting in the offset in the peak timing. For example, it was found that Ba, Mn, and Y show different desorption levels in the Burdekin River estuarine mixing zone (Lewis et al. 2018) and that Mn and Y have a longer residence time than Ba in the GBR lagoon (Brodie et al. 2012). Furthermore, it has been observed that coral Mn/Ca and Y/Ca ratios record major terrestrial runoff and prolonged perturbations rather than peaks corresponding to riverine plumes (Lewis et al. 2007, 2018; Moyer et al. 2012), as incorporation of Mn and Y in corals is less easily substituted for Ca than Ba (Saha et al. 2016).

This review of coral El/Ca records in Nananu-i-Ra hints that changes are not solely influenced by river and surface runoff, but that transport of sediment and mixing due to winds are also key. However, statistical methods explored here fail to find a correlation of the coral record with environmental variables. The hypothesis proposed here combines the effects of surface runoff with wind-driven sediments as an explanation for offset in peak timing due to residence time of elemental concentrations.

The observed coherence among Ba/Ca, Mn/Ca and REE/Ca in Nananu-i-Ra is a strong indication that they are indeed recording environmental changes in this reef and have potential to reconstruct past rainfall and climatic events (like ENSO phases). However, this potential is obscured by limited correlation between environment and El/Ca. Although I propose several mechanisms to account for this offset, more site-specific environmental information is needed to support this idea. While remote sensed data has been key in understanding the role of both rainfall and wind as drivers of turbidity in the coast of Nananu-i-Ra, this data lacks enough spatial resolution to decipher the exact mechanisms and source of sediments (island surface runoff versus wind-transported sediments) by which coral Ba/Ca, Mn/Ca and REE/Ca are increased in the coral record during specific periods. In-situ measurements of water quality can aid in elucidating the precise control of coral El/Ca in Nananu-i-Ra. Furthermore, oxygen stable isotopes ($\delta^{18}O$) and Sr/Ca records can aid in deconvolving coastal salinity, thus determining the role of surface runoff in this location.

5.4.2.3. Suva Reef and Namuka Reef

a. *Suva Reef*

Fish Patch is located in the Suva Reef and within the Suva Harbour, a highly populated and industrialised area (Naidu and Morrison 1994). This location receives direct fresh-water influx from the small Lami, Veisari and Tamavua rivers, which discharge into the harbour area, and indirectly from the Rewa river discharging into Laucala Bay, east of Suva, where suspended sediments in the water column are transported towards Fish Patch by the southeast trade winds (Singh and Aung 2008). Long core FP17_1 shows a consistent seasonal pattern across all REE/Ca (Y/Ca, La/Ca and Ce/Ca) with a peak between September and October and similar seasonal amplitude across the length of the record. REE/Ca variations show a significant and direct correlation with wind (Pearson's r ~ 0.17; Table 5.5.), and an inverse correlation with SST (Pearson's r ~ -0.20; Table 5.5.). No correlation is found between REEs and Ba/Ca or Mn/Ca, hinting at different environmental controls for this set of proxies in Suva Harbour. For REE/Ca, the pronounced seasonal peaks occur during the dry season (May – October) and this supports the hypothesis that sediment reaching Fish Patch is not associated with discharge from river runoff. Several studies have reported that sediment discharged in the Laucala Bay by the Rewa River remains in the Suva lagoon, rather than being flushed into the open ocean (N'Yeurt 2001; Quinn and Kojis 2008; Singh and Aung 2008), increasing the turbidity of these waters during the wet season (November – April). While coarser sediments are deposited in Laucala Bay, the finer portion remain suspended in the seawater and are transported into the Suva Habour via Nasese channel (Figure 5.3.) by the action of the strong South-East trade winds (which are stronger during dry season; between May – October) (N'Yeurt 2001; Singh and Aung 2008). The delivery of these fine-grained sediments can be associated with enrichment of REE (Zhang et al. 2002; Tranchida et al. 2011), where organic particle-rich waters influence a conservative mixing behaviour of REE in the estuarine region (Merschel et al. 2017), elongating the residence time of these elements in the wind-mixed water mass, in contrast to Ba and/or Mn. Furthermore, I propose that the positive correlation with salinity is a product of the wind seasonality, rather than a direct influence of salinity.

In contrast to the REE/Ca records, the Ba/Ca and Mn/Ca records lack a pronounced seasonal pattern, and instead show variability on annual timescales. There is coherence and synchronicity between Ba/Ca and Mn/Ca records (Pearson's r = 0.51; Table 5.3.) hinting that similar processes are driving some of the changes seen in the records. Both Ba/Ca and Mn/Ca in FP17_1 show a correlation with salinity (Pearson's r > 0.24; Table 5.5.) and to a lesser extent, wind speed (Pearson's r > 0.13; Table 5.5.).

Outside of the 2004 event, Ba/Ca and Mn/Ca show increases associated with several El Niño (2002, 2009, 2015) and La Niña phases (2007, 2008). During La Niña phases in 2007 and 2008 there is an increase of Ba/Ca (~5 µmol/mol) and Mn/Ca (1 µmol/mol). During El Niño phases in 2002 and 2009, there is an extended increase in Mn/Ca (max. 1.92 µmol/mol) and Ba/Ca (max. 7.90 µmol/mol) and a sharp Ba/Ca is recorded with small increase in Mn/Ca. The Ba/Ca and Mn/Ca increases that occur during La Niña phases are associated with tropical cyclones or storms (e.g., two tropical cyclones in early 2008 and two tropical storms in 2009 + monsoon flood; (Brown et al. 2017c)). This suggests that during La Niña phases, river discharge (Tamavua and Veisari rivers) and sediment runoff are reaching this location and that these elevated sediment load events are recorded by the coral. Interestingly, during El Niño phases, increases in Ba/Ca are not as strongly mirrored by Mn/Ca, hinting that during these periods a different mechanism is controlling the changes evident in these records. REE/Ca records show that wind-driven sediment transport is an important influence of suspended sediment concentration in Fish Patch. A potential hypothesis that could explain the decoupling between Ba/Ca and Mn/Ca during El Niño phases is interplay of delivery of sediment transport via wind-driven versus runoff. I propose that during the wet season, increased sediment volumes are discharged into the Laucala Bay, but also organic particulate matter (Singh and Aung 2008). These conditions, and specifically delivery of organics, favour reduction of Mn (IV) and Mn (III) into Mn (II), eventually leading to effective scavenging of dissolved Mn (Chen et al. 2022) by marine organisms and/or adsorption onto carbonate particles (Ouddane et al. 1997) in Laucala Bay. The discharge that would reach the coral head in Fish Patch (transported by winds) would have a lower Mn/Ca than expected resulting in smaller Mn/Ca peak in comparison to Ba/Ca, as for example the peaks observed during El Niño in 2006 (Ba/Ca = 5.1 μmol/mol, Mn/Ca = 0.7 μmol/mol) and 2009 (Ba/Ca = 6.2 μmol/mol, Mn/Ca = 0.6 μmol/mol).

Across 2004, there is a pronounced increase in Ba/Ca (max. Ba/Ca = 8.3 μmol/mol) and to a smaller extent, an increase in Mn/Ca (max. Mn/Ca = 1.0 μmol/mol), which corresponds to a period of local development. From February 2004 until November 2005, development works took place at Suva Port, in Suva Harbour, less than 4 km away from where the colony cored was found (ADB 2008). This work included coastal dredging and land reclamation of mudflats and mangroves to extend the size of King's Warf in Suva Port and was expected to increase turbidity and silt in the coastal area as a result (ADB 2008). As such, Ba/Ca shows an increase during the duration of the works. Similar prolonged enrichments of Ba/Ca rather than sharp peaks related to specific events, have been previously observed in Fiji in inshore cores near mines (Jupiter et al. 2010), but also in other regions as a result of tidal resuspension and release of Ba accumulated in bottom sediments and mangroves (Jupiter et al. 2008; Prouty et al. 2010). The smaller increase in Mn/Ca could be associated with this increase in sediments associated with port development although the difference in amplitude between Ba and Mn is not straightforward to explain.

Overall, records from this region are showcasing two unique signatures related to wind vs run off delivery of sediment to the coral site across interannual timescales. Further, port development and related works associated with development of Suva are showcased in Ba/Ca and to lesser extent Mn/Ca records which shows the potential in this region to explore long-term changes in development.

b. Namuka Reef

The Namuka reef is located west of Suva Harbour, in the vicinity of small catchments with a high forest cover (~80%), some grassland and mangroves in the coastal limit. Two settlements are found nearby Muaivuso and Waiqanaki (Figure 5.1. and Figure 5.3.). Terrigenous influence into the reef might be sourced by surface runoff from the coastal area and villages, as no evident creeks discharge directly onto the reef.

In NAM17_1, REE/Ca records shows higher frequency variability and lack a clear seasonal signal with higher values recorded between August to November. Similar to Fish Patch, REE/Ca values are highly correlated (Pearson's r > 0.55; Table 5.3.), and so are Ba/Ca and Mn/Ca (Pearson's r = 0.46; Table 5.3.). Furthermore, only Mn/Ca shows a correlation with Ce/Ca (Pearson's r = -0.24; Table 5.3.). Ba/Ca does not show correlations with any environmental parameter, while Mn/Ca appears correlated with rainfall (Pearson's r= -0.31; Table 5.5.) and SSS (Pearson's r= 0.36; Table 5.5.) and Y/Ca is correlated with SST (Pearson's r= -0.26; Table 5.5.). The high-frequency variability at monthly timescales observed in this sample hints that the environment at Namuka Reef is considerably more dynamic than that of nearby Fish Patch, which is not surprising given the differences in depth between the two coring locations (Fish Patch = 8 – 10 m, Namuka = 3 – 4 m). Nevertheless, when long-term trends are explored, REE/Ca patterns at Namuka are similar to those in Fish Patch, with a broad scale increase in 2013, potentially associated with a tropical cyclone event. Similarities between Namuka and Fish Patch are also observed in the long-term trend of the Mn/Ca records. This suggest similar environmental drivers in these two proximal locations, but due to the short span of NAM17_1 (6 years) it is complicated to fully ascertain the mechanisms at play.

The Ba/Ca records shows two peaks in 2012 (8.2 μmol/mol) and 2014 (8.2 μmol/mol), with the latter being associated with an increase of Mn/Ca (1.3 μmol/mol). The presence of a Ba/Ca peak during both La Niña and El Niño phases with an Mn/Ca increase only during El Niño suggests that two different mechanisms are behind these increments. The large peak of Ba/Ca during 2012 can potentially be linked to a severe flooding experienced in Fiji in March 2012 (Brown et al. 2017c), caused by a tropical depression. This flooding was more severe in the north-east side of Viti Levu, but sediment runoff might have been increased as a result of this weather system, leading to alteration in the Ba cycle similar to those in the Coral Coast.

Overall, there are hints of similar mechanisms in the coastal systems driving El/Ca changes at Namuka and Fish Patch, but further investigation of the differences and similarities between these reefs would require comparison of longer records than those available for Namuka Reef. I conclude that although there seems to be an influence of water quality properties on Ba/Ca, Mn/Ca and REE in Namuka, decadal length records are key to decipher the precise controls of each proxy.

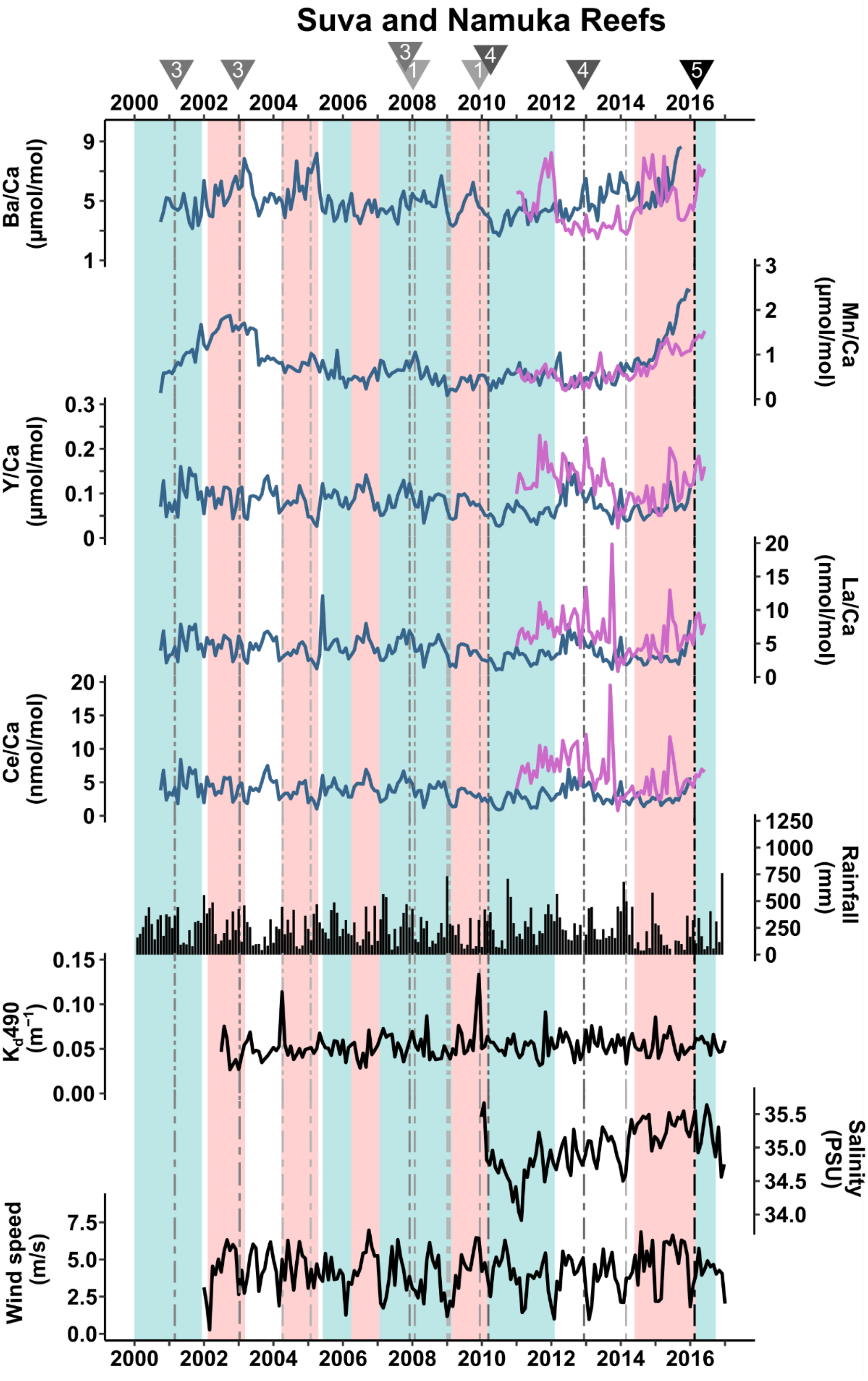

Figure 5.7. Time series monthly mean El/Ca records from samples from the Suva and Namuka reefs, FP17_1 (dark blue) and NAM17_1 (pink) and environmental variables. Blue years are La Niña phase, and red years are El Niño phase. Gray vertical lines depict tropical storms (lighter) and cyclones. Triangles above plot depict cyclone category.

5.5. Conclusion

I examined Ba/Ca, Mn/Ca and REE (Y/Ca, La/Ca and Ce/Ca) records from six *Porites* spp. colonies from four different inshore reefs in Viti Levu (Fiji). These coral proxies reveal different mechanisms across Viti Levu driving changes in inshore water quality.

I show that Mn/Ca and REE/Ca values at Votua Reef, an inshore reef with small and forested catchments, is a promising proxy of seasonal and large runoff events. Moreover, a multiproxy approach (including Ba/Ca) can also identify events that are linked to potential changes in nutrient delivery with a high degree of coastal perturbation. Further work examining river catchment hydrology coupled to in-situ water quality measurements would aid in the determination of controls on Mn and REE sources, as well as rainfall thresholds recorded. On the other hand, the application of Ba/Ca proxy in this location seems to be complicated by non-sediment discharge controls and further work on ascertaining the impact of algal blooms and primary productivity in the water columns is necessary to aid in the interpretation of Votua Ba/Ca.

Coral Ba/Ca, Mn/Ca and REE/Ca records from Nananu-i-Ra (an offshore island with low degree of coastal development, located off the north coast off the Ra province, which is characterised by extensive sugarcane crops) show a potential to reconstruct changes in rainfall and ENSO phases, however the record is more complex than that of Votua. We hypothesise that El/Ca records from this region are linked to variations in rainfall and uniquely in this region both wind-driven sediment mixing and sediment resident time within the water column. Corals from Nananu-i-Ra show influence from both local surface runoff (Nananu-i-Ra island) and distant river discharge (from Viti Levu). Importantly, reef-scale hydrography exerts an important control over coral El/Ca variability.

Finally, coral Ba/Ca, Mn/Ca and REE/Ca from the Suva Reef (an urban reef surrounding Suva, and by Suva Harbour) are influenced by two different mechanisms delivering sediment to the coral colony location. In these mechanisms, either rainfall events during wet periods or wind-driven mixing mobilise sediment to the reef, although from different sources. Rainfall events deliver sediments from small catchments around Suva Harbour, which are typically recorded in the *Porites* spp. skeleton as elevated Ba/Ca and Mn/Ca values. Wind-driven mixing delivers sediments from Laucala Bay (sourced by the Rewa River) showcasing seasonal peaks in REE/Ca, Ba/Ca but limited

Mn/Ca. In the Namuka Reef, El/Ca changes suggest similar mechanisms to the Suva Reef are driving the coral record; however longer records are required to confirm this.

This chapter reveals that *Porites* spp. El/Ca records from across Viti Levu, Fiji, record changes in key processes associated with river runoff, wind-driven sediment mixing, and reef-specific controls. Further, the decadal El/Ca records from across Viti Levu showcase that inshore water quality in Fiji is highly localised and dependent on catchment-specific factors, which has implications for management initiatives as local assessments are critical. A thorough examination of the inventories of Ba, Mn and REEs from catchment to coast would be useful to disentangle proxy systematics and link catchment specific processes to El/Ca records and unlock the potential of obtaining long-term records of past inshore water quality from Fijian inshore reef.

Chapter 6 | Synthesis and direction for future work

Don't adventures ever have an end? I suppose not.
Someone else always has to carry on the story.

Bilbo Baggins

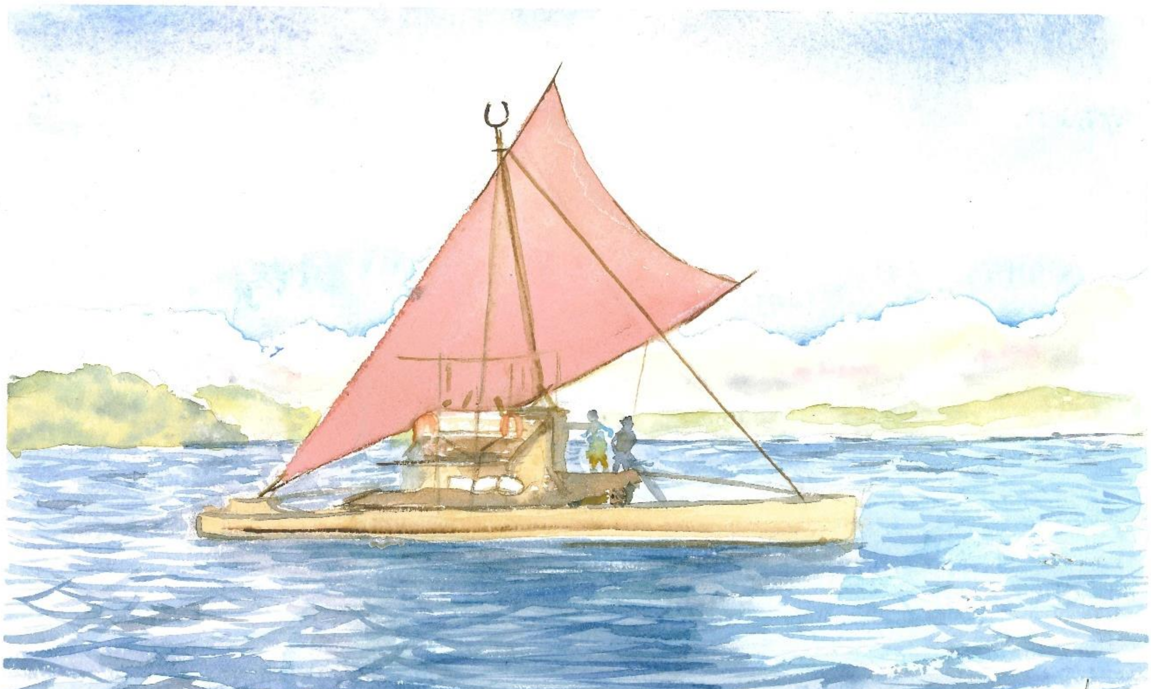

Reef series #2 (MVL)

Chapter 6 | Synthesis and direction for future work

6.1. Thesis summary

Inshore reefs are threatened by climate change and the effects it is exerting upon the ocean (i.e., seawater warming, ocean acidification), and by local impacts derived from anthropogenic activity in coastal areas (e.g., overfishing) or within adjacent catchments leading to degraded water quality (e.g., development, land use changes). These pressures can affect coral growth, reduce reef resilience, and cause ecosystem shifts from coral- to algal-dominated reefs, resulting in the loss of key ecosystem services upon which coastal communities rely to sustain their livelihood.

Fiji sustains nearly 3.5% of the world's coral reefs, with one of the most diverse reef systems in the South West Pacific. The country's economy and the livelihood of coastal dwellers is heavily dependent on coral reefs, yet some reefs are experiencing considerable threats and impacts from the global and local scale stressors described above. Hence, maintenance (or even increase) of the resilience of these reefs is key in sustaining the > 70% of Fijian people inhabiting coastal areas.

Resilience based management (RBM) is a tool that focuses on maintaining the resilience of coral reefs and the people supported by them as a fully coupled socio-ecological system. In Fiji, increasing efforts towards a full RBM are being implemented by the government, non-governmental organisations and the coastal communities working to limit local threats to coastal reefs, including those derived from inland activity (i.e., sediment, nutrient and pollution input). However, for this management to be effective, a deep understanding of the interplay of environmental and climatic mechanisms, alongside an understanding of the impacts of such processes on reef building calcifiers, is needed. This requires a large amount of environmental and coral growth data at sufficient spatial (reef-specific) and temporal (daily to interannual) resolution, which often is lacking.

In this context, the aragonitic skeletons of massive *Porites* spp. corals are valuable archives of both coral growth and environmental change. These records have a great potential to help us understand how reef conditions have changed across time, the factors that drove this change, and how the growth of these organisms varied alongside. By coupling sclerochronological records with environmental data derived from coral geochemical proxies (i.e., SST and water quality) a powerful wealth of information of past climatic events, environmental changes and coral growth variability can aid in decision making for effective coastal and land management.

In this thesis, I explore massive *Porites* spp. cores collected from inshore reefs in Viti Levu, Fiji. I use sclerochronological and geochemical proxies to obtain coral growth and environmental records from the cores and i) examine drivers of coral growth across the interval 1998–2016, ii) explore the use of SST proxies to investigate the impacts of climate change on inshore reef temperature and iii) determine site-specific controls on terrigenous input proxies.

Results show that i) mean coral growth is influenced by seawater turbidity, but trends are also tied to thermal stress. Thus, local seawater quality is an important driver of coral growth alongside climate; ii) Geochemical SST proxies show seasonal changes correlated with SST variability, however disruptions to the El/Ca-SST relationship are also recorded. These disruptions are caused by the influence of seawater turbidity conditions over biomineralization and physiological processes ("vital effects"), thus masking the SST signal; and iii) Runoff proxies reflect seasonal precipitation patterns and runoff, clearly linking catchment land-use and reef conditions. These observations suggest that local conditions, and the specific mechanisms linking land and coast, need to be considered to evaluate the impacts of environmental changes on massive reef-building corals, and to interpret both sclerochronological and geochemical records in this region. Importantly, these results suggest that action over any of these factors (for example, RBM that focuses on diminishing sediment runoff into reefs) might improve the resilience of reef-building corals in the face of climate change.

Below, I detail the three aims for this thesis outlined in Chapter 1, highlight the importance of the key findings and provide context for the development of these aims, and propose future work that will advance knowledge on these topics.

Aim 1: Examine the variability of coral growth across different inshore reefs and across time in Fiji

In Chapter 3 I show coral growth records across several locations in Fiji between 1998 and 2016 and link the role of both regional and local environmental factors and stressors in driving mean growth and interannual variability. Elevated values of seawater turbidity are correlated with lower mean skeletal extension and calcification rates in *Porites* spp. colonies. This is especially evident in cores from Nananu-i-Ra (agricultural catchment; most turbid $K_d490 = 0.07$), which show the lowest coral extension rates (~7.50 mm/yr), and Votua Reef (forested catchment; least turbid $K_d490 = 0.03$), which show the highest coral extension rates (~15.00 mm/yr). Therefore, we conclude that differences in seawater turbidity between locations determine the linear extension gradient observed in different cores from this study. However, this is not the only factor driving skeletal growth in massive *Porites* spp. in Fiji. All four locations explored in this thesis show a significant decrease in growth rate between 2013 and 2016, unprecedented in the coral record of this study. The relative decrease ranged between 12.50 and 19.40% depending on location and appears to have been caused by a period of elevated thermal stress experienced across the Indo Pacific (including Fiji) throughout 2014 to 2016.

Some studies have shown how coastal turbidity and biodiversity loss in Fiji is linked to catchment activity (Brown et al. 2017a, 2017b), and reef managers in Fiji are focusing on RBM that increases the resilience of reefs to mitigate global stressors (i.e., ocean warming). However, the results of this chapter show how thermal stress affected coral growth across all locations regardless of water quality, suggesting that under a scenario of amplified global warming and persistent thermal stress local management might not be enough to palliate the effects of climate change. Yet, it is important to note that although relative decline in growth is similar across all locations, absolute rates of growth differ greatly, with massive corals in turbid reefs at a higher risk of collapse and conversion into algal-dominated systems.

Reconstructions of coral growth, environmental change and climatic change have the potential to provide a deeper understanding of how specific events and/or gradual changes have modified reef environments and impacted reef-building corals in the past. Coupled coral sclerochronological and geochemical records can aid in this quest, disentangling the nature of historical impacts of anthropogenic and climatic change. However, a thorough investigation of the potential of these corals as geochemical archives must be carried out.

Aim 2: Investigate the potential of *Porites* spp. corals from inshore reefs in Fiji as SST archives.

In Chapter 4 I examined a suite of El/Ca ratios that have been proposed as SST proxies (i.e., Sr/Ca, Li/Ca, Mg/Ca, Li/Mg and Sr-U) from six *Porites* spp. cores across four inshore reefs. This study represents the first exploration of a suite of SST-proxies in Fiji in conjunction with contemporaneous coral growth information. Results showed that single core proxies only partially co-varied with seasonal seawater temperature changes ($R^2 < 0.20$) limiting their potential to reconstruct SST, with Sr/Ca being consistently the most accurate SST proxy.

Further analysis of core geochemical data showed how co-variability of El/Ca followed Rayleigh fractionation mechanisms (for example, a simultaneous increase in Sr/Ca and decrease in Mg/Ca), and that the degree of Rayleigh fractionation was different across reefs (for example, cores in Nananu-i-Ra showed stronger Rayleigh fractionation). In addition, core El/Ca data showed a varying degree of correlation with density, depending on the proxy ($R^2 = 0.13 – 0.46$). Here, I argue that this correlation of El/Ca data with core density is caused by the influence of coral physiological processes leading to skeletal deposition (i.e., Ca^{2+} pumping, biomineralization), which adds additional variability on the El/Ca signal beyond SST, on seasonal and interannual timescales. Therefore, colony-specific differences in mean El/Ca are induced by differences in Ca^{2+} pump activity, which at the same time also exerts a control over Rayleigh fractionation. I found that although core El/Ca data weakly correlated with seawater turbidity (at annual timescales), changes in density (and growth rate) in the six coral cores of this study were linked to a seawater turbidity gradient observed between reef locations around Fiji. Thus, I argue that this gradient has an effect on Ca^{2+} pumping, modifying the rate at which ECF is renewed. Ultimately, any variable capable of influencing Ca^{2+} pumping (e.g., SST, seawater turbidity) and element partition coefficients will, then, exert some degree of control over El/Ca.

To overcome these “vital effects” and the limitations for Fijian paleotemperature reconstructions, I combine the six single-core Sr/Ca timeseries from all locations into one “composite signal”. This methodology improves the Sr/Ca-SST calibration (R^2 = 0.40) by smoothing out the reef-specific “vital effects” influenced by local hydrographic conditions so that only the regional SST signal remains. However, this method still presents caveats and limitations, for example due to climatic regional events (e.g., ENSO) that can alter reef environmental conditions across the entire region and thus being reflected across all sampled cores. Nevertheless, this study restates the importance of multi-proxy measurements, as this approach enables the investigation of calcification processes impacting SST proxies and the acquisition of more robust records as a result.

Aim 3: Investigate the terrigenous influence in inshore reefs in Fiji as recorded in *Porites* spp. skeletal geochemistry.

Understanding the mechanisms behind poor water quality in coastal ecosystems is key for implementing successful management strategies, but this requires robust historical datasets. The use of geochemical proxies from massive *Porites* spp. can provide information on coastal water quality. In Chapter 5, I present a suite of elemental ratios (Ba/Ca, Mn/Ca, and REE/Ca (Y/Ca, La/Ca, and Ce/Ca)), that are widely used as terrigenous input proxies in coastal areas, from six *Porites* spp. cores across four inshore reefs.

Results showed that El/Ca variability in corals successfully recorded freshwater discharge and/or sediment input. In addition, results highlight that different environmental and climatic mechanisms drive water quality changes in inshore reefs in Viti Levu, and that fully unveiling these processes is key before applying these proxies for water quality and climatic reconstructions.

In general, high rainfall events during the wet season and La Niña phases are commonly recorded across sites, but small differences affect water quality at each location on monthly timescales. For example, data suggest that at the Votua Reef seawater turbidity is a rainfall-driven process, while in Nananu-i-Ra it is both rainfall- and wind-driven. In the Votua Reef (forested catchment) Mn/Ca and REE/Ca signals show a high degree of co-variability and correlate with seasonal large rainfall events (potentially large runoff). Interestingly, there seems to be a decoupling of Mn/Ca and REE/Ca signal during extraordinarily large rainfall and flooding events, which I argue is due to a change in the sediment and/or nutrient source to waterways and finally reef waters. Ba/Ca, however, does not seem to be principally influenced by sediment input; instead, I suggest that primary productivity and algal blooms might be the main controlling factor in Ba cycling and Ba incorporation in the coral skeleton. In Nananu-i-Ra (agricultural catchment) all analysed proxies (Ba/Ca, Mn/Ca and REE/Ca) were correlated, and furthermore their variability corresponded with wet periods with high rainfall events and La Niña phases. However, observations of environmental data in this location suggest that seasonal seawater turbidity is not only influenced by rainfall, but that wind-mixing is also responsible for increased seawater turbidity. As such, deriving specific meteorological and climatic events from coral records in this location is complicated by these overlapping mechanisms, and a deep understanding of the estuarine mixing zone and reef area are required. In the Suva Reef, on the other hand, co-variability of Ba/Ca and Mn/Ca seems to reflect direct sediment input into the Suva Harbour area during rainfall events in the wet season. Importantly, Ba/Ca and REE/Ca (but not Mn/Ca) also show co-variability, and this seems to be driven by wind-transported sediments from Laucala Bay during the dry season and El Niño phase. Therefore, the source of sediments to the Suva reef influenced by different climatic events, and thus presents a contrasting El/Ca signal.

Overall results show that water quality in inshore reefs in Viti Levu is highly localised and influenced not only by the climatic regime and meteorological events, but by the nature of the catchments adjacent to these areas. Furthermore, *Porites* spp. corals can be used as long-term archives of coastal water quality histories, but a deeper understanding of the linkages between catchment land use, hydrology, climate, and coastal water quality are needed before carrying out robust interpretations.

6.2. Future work

This study constitutes the first investigation applying both sclerochronological records and a suite of elemental proxies to examine *Porites* spp. from inshore reefs in Fiji and shows how coral records from this region are promising archives for investigating past changes. However, further work is necessary to understand the coral physiological processes at play during skeletal deposition and increase the robustness and strength of these records by underpinning knowledge of how a coral calcifies. The future work, detailed below, will be focused towards acquiring a better understanding of coral growth processes and environmental changes, as well as the relationship between them. This will be achieved by expanding the coral core archive to include a wider range of species, longer temporal coverage, and additional replicates, including other geochemical proxies that help constrain coral physiological and environmental processes, and a deeper characterisation of in-situ environmental conditions.

6.2.1. Chapter 3: Coral growth records

While this study shows how coral growth and biomineralization processes are influenced by both seawater turbidity and thermal stress, these observations are based solely on records from *Porites* spp., a dominant reef builder. By including different massive coral genera and replicate growth analysis in future work, it will be possible to discern genus-specific environmental stressor thresholds and deduce whether certain impacts are widespread or constrained to certain species. Studies show how different coral genera present varying degrees of calcification sensitivity to thermal stress (Carricart-Ganivet et al. 2012) and varying growth response to changes in seawater turbidity and sedimentation (Browne et al. 2015; Jones et al. 2020). Furthermore, *Porites* spp. is considered to show greater resilience to bleaching, and bleach-induced mortality (Mumby et al. 2001) than other Scleractinia genera. In addition, the potential of turbid reefs to protect against thermal stress also depends on coral genera, with *Porites* spp. being the genus that benefits the least from the turbidity shielding (Cacciapaglia and van Woesik 2016). As such, the conclusions obtained here and their importance to evaluate the implications of future environmental and climate change on reef accretion are limited to *Porites* spp. and cannot be extrapolated to other reef-builders.

The expansion of growth records from inshore reefs in Fiji could potentially include other reef-building species present in Fijian reefs (e.g., *Diploastrea heliopora*, *Pavona* spp., *Pocillopora* spp., *Tridacna* spp.) (Lovell and McLardy 2008). Of these, *Diploastrea heliopora* is increasingly being used as archive of both sclerochronological and geochemical proxies (Watanabe et al. 2003; Bagnato et al. 2004, 2005; Cantin et al. 2010; Dassié and Linsley 2015; Ramos et al. 2017) due to its wide distribution in the Indo Pacific (Veron 2000) and their low extension rates (i.e., 2–6 mm/yr), which favours the acquisition of longer temporal records than in *Porites* spp. Furthermore, *Diploastrea heliopora* has a dense skeleton showing higher resistance to bioerosion and wave energy, and support a longer life span (of more than 800 years) (Bagnato et al. 2004). Future work obtaining growth records from *Diploastrea heliopora* to replicate and extend *Porites*-based sclerochronological (and geochemical) records, could improve long-term reconstructions of regional climate and coral growth variability (Ramos et al. 2017).

Although it has not been addressed in this thesis, local and global stressors can also impact the abundance and presence of coral bioeroders such as sponges, urchins, and microendolithic organisms (e.g., algae, fungi) (Glynn and Manzello 2015) and the role they play in the net balance of carbonate production in reefs (Perry et al. 2014). Coral skeletal microbiota is complex, and has only recently become the subject of studies focusing on its role in the coral energy balance and decalcification of the skeletal matrix (as reviewed by Ricci et al. 2019). Observed grey bands parallel to coral growth (as those observed in some cores of this study) have been attributed to seasonal increased activity of boring algae (Risk et al. 1987) and further attack and consumption of these algae by endolithic fungi, causing the dark pigmentation in the coral skeleton (Priess et al. 2000). Yet, the environmental variables that originates the endolithic algae in the first place seem to be reef- or regional-specific. The *Porites* spp. cores used for this study present different degrees and types of bioerosion (See Appendix A). For example, burrow-like macro-bioerosion (likely caused by sponges) is observed in one core from Nananu-i-Ra (NAN17_3). Seasonal grey bands (likely related to the presence of fungi; Priess et al. 2000) are present in both cores from the Votua Reef, across the entire span of the core. Endolithic algae are present in cores from Namuka Reef while the core from nearby Suva Reef does not show any sign of macro- or micro-bioerosion. Future work characterising bioerosion processes in these Fijian cores coupled to coral growth and environmental records can inform us about specific processes that favour their presence (e.g., overfishing, increased nutrients) and their effect on coral structural integrity. In addition, expanding records to other species, as described above, will also benefit the characterisation of bioerosion. Differences in skeletal density (e.g., between *Porites* spp. and *Diploastrea heliopora*) are likely to drive different rates and types of bioerosion. Previous work on *Diploastrea heliopora* cores from Fiji suggested that periodic bands of endolithic algae were related to ENSO phases, although the direct causes increasing bioerosion were not explored (Bagnato 2003). Future work focused on skeletal thin sections microscopy and/or micro-CT imaging can shed light on how microbioerosion affects skeletal structure (e.g., lowered skeletal density, increased mineral dissolution) and diagenesis, necessary to improve the robustness of both sclerochronological and geochemical records, and gain a deeper understanding of how reef-specific processes are influencing coral bioerosion in Fiji.

Both the increase in coral records (in time, number of replicates and coral genera) and the investigation of skeletal bioerosion will benefit of the application of numerical models of coral skeletal growth (extension and/or density). Discerning among different environmental variables and measuring their degree of influence over coral growth is key for assessing future changes accurately. It has been observed how different environmental and climatic variables exert a simultaneous influence over coral growth parameters (e.g., this study, Lough and Barnes 2000; Cooper et al. 2008; D'Olivo et al. 2013; Mollica et al. 2018), but delimiting the extent of each one individually, and potential synergies between them can be challenging. Growth modelling can isolate the effects of different factors and quantify their respective contributions to either extension rates or skeletal density (e.g., Guo et al. 2020). Modelling of coral growth in inshore reefs in Fiji would aid in acquiring a better understanding of reef-builders skeletal integrity over the 21st century under the expected climatic changes for Fiji.

6.2.2. Chapter 4: Coral SST proxies

The work in this thesis shows that although Sr/Ca, Li/Ca, Mg/Ca, and U/Ca in Fijian inshore *Porites* spp. records seawater temperature, coral biomineralization and physiological processes are altering the skeletal geochemical signal. However, future work focusing towards understanding these physiological processes and how they link to coral growth data, will help in gaining a better understanding of changes in ECF chemistry across space and time and potentially increase the robustness of paleotemperature reconstructions.

For example, by exploring boron-based proxies (boron isotopic composition ($\delta^{11}B$) and B/Ca) in the cores of this study, coupled to the existing El/Ca measurements and growth records, we could constrain colony specific differences in Ca^{2+} pumping, $[CO_3^{2-}]$ and DIC changes and obtain a better understanding on how environmental conditions (i.e., seawater turbidity, SST) influence skeletal deposition and how this, in exchange, affects the geochemical signal ("vital effects"). The $\delta^{11}B$ of coral aragonite reflects the pH of the ECF at the time of calcification (Holcomb et al. 2014). These isotopic measurements can be combined with estimations of $[CO_3^{2-}]$ in the ECF derived from B/Ca measurements to constrain the full carbonate system (as reviewed DeCarlo et al.

2018). Scleractinian corals have been shown to up-regulate the pH of their ECF from that of seawater in order to facilitate calcification, and this pH-buffering capacity of corals is species-specific (McCulloch et al. 2012). Furthermore, coral up-regulation not only changes across species, but also within a single colony across time. For example, Knebel et al. (2021) measured $\delta^{11}B$ within one colony of *Porites* spp. and found that ECF pH up-regulation changed seasonally following variability of SST, which is likely related to the effect of SST over calcification rate. Thus, the information provided by $\delta^{11}B$ can help to inform how coral physiology changes across reefs and across time in Fiji.

Following the newly acquired better appreciation of the calcification system and how reef-specific differences affect *Porites* spp. (and other massive coral species ; e.g., *Diploastrea heliopora*), numerical modelling of geochemical and calcification records can inform us on the precise drivers (i.e., SST v. ocean acidification v. salinity) of skeletal deposition rates and how future changes will affect different regions. This modelling approach has the potential to improve seasonally resolved coral records of climate, and to understand the relationship between coral calcification and climate change (e.g., Guo 2019; McCraw 2020).

Another method that can complement the information gained on the functioning of the calcification system in corals is elemental and isotopic mapping across several skeletal structures (e.g., corallite walls, columella, pali, septa) to show how skeletal deposition and ECF chemical signature influence micro-scale geochemical variability within the coral skeleton. For example, Chalk et al. (2021) used LA-ICPMS to map El/Ca and $\delta^{11}B$ distribution in *Siderastrea siderea*, and found that geochemical composition changed not only in time, but also spatially, with clear differences between corallite walls and columella. Further, Shirai et al. (2012) used Electron Probe Micro-Analysis (EPMA) and observed sub-daily growth increments in cultured *Porites australensis* measuring enrichments in Sr/Ca. These analytical techniques allow for fine in-situ spatial measurements of isotopic and elemental ratios at high resolution and facilitate the exploration of the full carbonate system at the site of calcification. In addition to elemental and isotopic mapping, Raman spectroscopy of skeletal material can be useful to include as part of the multi-proxy multi-method approach to better characterise coral calcification processes, as it has been used to derive the aragonite saturation state ($\Omega_{aragonite}$) of the ECF (DeCarlo et al. 2017b; DeCarlo 2018).

The results of this chapter suggest that seawater turbidity plays an important role influencing coral physiology, and this is recorded in the skeletal elemental composition. A different line of work that can be highly valuable in informing about the environmental influences over the coral carbonate system would be ex-situ coral culturing, where seawater conditions (i.e., turbidity, SST) can be precisely manipulated and accounted for. Further measurements of El/Ca SST-proxies (i.e., Li/Ca, B/Ca, Mg/Ca, Sr/Ca, U/Ca) and δ^{11}B in these cultured corals can then be used to constrain the mechanisms behind seawater turbidity and coral physiology, and how it impacts SST proxy elemental ratios (e.g., Anthony and Connolly 2004).

Alternatively (or simultaneously), these elemental and isotopic measurements can be done on an increased number of coral cores and other species (e.g., *Diploastrea heliopora*), especially from reefs where bleaching events were observed in the past, to gather information on how thermal stress impacts SST proxy signal to avoid potential bias in paleo-reconstructions (e.g., Clarke et al. 2017; D'Olivo and McCulloch 2017).

In addition to the further coral work explored above, in-situ monitoring of seawater conditions at high resolution (spatially and temporally) in Fijian inshore reefs would benefit the examination of coral growth and environmental proxies. Deploying a dense network of seawater temperature loggers, and coupling this information to coral records, would help investigate how climatic events might affect coral growth. This will lead to an improvement of El/Ca-SST calibrations by discerning whether certain events leading to abnormal growth might be affecting El/Ca incorporation into coral aragonite beyond SST.

6.2.3. Chapter 5: Coral terrigenous input proxies

Ba/Ca, Mn/Ca, and REE/Ca (Y/Ca, La/Ca, and Ce/Ca) measurements in inshore *Porites* spp. show how both catchment land-use, and meteorological and climatic events alter reef water quality. However, these factors can vary across site and have different seasonal patterns. In addition, reef geomorphology and wind-driven surface current play a key role in some locations. Coral El/Ca records show variability linked with rainfall events and runoff. However, the precise mechanisms leading to increased terrigenous influence in reef areas (spatially and temporally) are site-specific and still unknown. More work needs to be carried out to inform us about land-based activities and climatic patterns (rainfall v. wind) influencing runoff and nutrient input. For example, further information on sediment runoff and nutrient concentration will help investigate the coupled observations on K_d490 and chlorophyll-a across all sites and how these processes are connected. In addition, in the Votua Reef Ba/Ca seems to be linked to primary productivity and a better interpretation of this signal will be benefitted by improving our understanding of nutrient cycling in coastal areas. This deep understanding of environment mechanisms is key to produce robust environmental datasets that pre-date observations and then to link to coral growth patterns across site and time.

Skeletal nitrogen isotopes ($\delta^{15}N$) measured in corals can be used to characterise the source of nutrient load (Yamazaki et al. 2011; Murray et al. 2019). Distinguishing among nitrogen sources helps to shed light on anthropogenic nitrogen fluxes into reef ecosystems, and it is critical to design and evaluate effective mitigation and management measures. In addition, coral P/Ca has also been reported to record coastal P runoff ($PO_4^{3-}{}_{sw}$) and pollution as increased P/Ca (Alibert et al. 2003; LaVigne et al. 2010). Previous studies of nutrients in the Coral Coast (Fiji) have shown how the ratio N:P and source of nutrients changes spatially and across time (Mosley and Aalbersberg 2003; Tamata 2007). Coupling $\delta^{15}N$ and P/Ca measurements in the coral samples of this study could elucidate the temporal variability of nutrient concentration and ratio in the reef environment and how this might be linked to specific events (e.g., tropical cyclones, monsoon, ENSO phases). This, coupled to coral growth records would provide a deeper understanding of the mechanistic processes impacting reef water quality and coral growth response. For example, this information would allow to evaluate whether addition of nutrients leads to change in coral growth, and if so, the coral tolerance thresholds. In addition, this will inform us whether the concentration of N and P in reef areas exert a control over coral growth independently of each other, or the balance of N to P is important. Furthermore, these new records could also aid in the understanding on susceptibility of corals to bioerosion under increased nutrients and acidification environments (DeCarlo et al. 2015a).

More work to expand on the potential sources of runoff can be achieved by the application of Ba isotopes ($\delta^{138}/^{134}Ba$) from coral skeletal material. The observed complications disentangling coral Ba/Ca signal and its potential environmental drivers (i.e., Ba concentration in seawater, primary productivity, SST) complicates its application as runoff proxy. Results of this study show how Ba/Ca in the Votua Reef seems to be impacted by other factors (primary productivity). Recent work has shown how $\delta^{138}/^{134}$Ba in shallow water corals is a robust proxy for tracing water masses, water mixing and Ba cycling in the reef ecosystem, independently of other factors (e.g., primary productivity) (Pretet et al. 2015; Hsieh et al. 2022). Ba isotope measurements in *Porites* spp. of this study can help disentangle the drivers of Ba/Ca and also provide another avenue to examine runoff and help understand the coastal processes that might be controlling seawater quality (e.g., river runoff, wind-driven mixing).

Results here show that the studied REE/Ca ratios (Y/Ca, La/Ca and Ce/Ca) are robust proxies for sediment runoff input into the reef ecosystem. Expanding this work by applying solution ICPMS measurements, although decreasing the temporal resolution of the record, would allow for a complete characterisation of the suite of REE (due to the higher analytical sensitivity achieved). REE in marine environments are affected by various biogeochemical processes associated with different complexation behaviour (e.g., adsorption, scavenging, re-mineralization). These processes result in specific fractionations within the group, which are recorded in the coral REE signature (as reviewed by Saha et al. 2016). By examining the full REE suite and their shale-normalised patterns, inter-REE fractionations (e.g., Y/Ho) and anomalies (e.g., Ce/Ce*), which are caused by the different reef-specific biogeochemical processes, they can be used to identify specific sources of sediment flux and biochemical processes affecting the water column (Nguyen et al. 2013; Saha et al. 2019). As such, a better characterisation of catchment-specific processes and geological features, as well as reef-specific conditions, could be linked to coral records.

Characterisation of water chemical properties (e.g., pollutants, nutrients) across the catchment waterways during both the dry and wet season would be valuable to understand how climatic regime and catchment processes affect coastal water quality, and how they relate with reef condition. Furthermore, seawater sampling collection (for analysis of major, minor and trace element analysis) at both surface and at depth in reef-sites over the transect of a year would help investigate freshwater and sediment mixing in the coastal regions. This will allow a better investigation on how environmental changes are linked to both the SST and terrigenous proxies studied here. In addition, through the deployment of a number of marine sensors in Fijian inshore reefs for over a period of one year would provide precise measurements of seawater temperature (as stated above), pH, salinity, turbidity, chlorophyll and nutrient concentration. These highly resolved (spatially and temporally) data would provide invaluable information supporting observations of ecological surveys, by improving characterisation of the carbonate system, water quality and terrestrial inputs and shape what mechanisms are behind certain ecosystem responses.

Finally, and in addition, increasing the number of core replicates from each location would be beneficial for this study as a better characterisation of reef-specific conditions can be constrained. For example, by increasing the number of coral replicates from single colonies we would be able to further investigate intra-colony reproducibility and potential causes of variability. Also, by replicating cores across different areas of a given reef (e.g., distance to shore gradient, reef flat, reef crest) it would be possible to also investigate how variable records are spatially.

6.2.4. Other work

Complementary to all the further work detailed above is the close collaboration with reef managers and engagement with local villages. Reef monitoring is routinely implemented in Fiji to inform managing actions, but it merely provides a snapshot of reef conditions in a moment of time. Paleo reconstructions of coral growth and environmental parameters, however, offer a valuable tool for "retrospective monitoring" informing on anthropogenic influences and expanding the knowledge of past stress to reefs. By close work with reef managers, work can be focused on the acquisition of coral records from reefs that are perceived as important for the community and with potential to successfully implement Locally Managed Marine Areas and improve the resilience of the ecological-social system. This is of great importance to ensure that the information gained with this research is of benefit for the Fijian society. Collaborative work can provide records of the main reef building corals in Fiji (e.g., *Porites* spp.) which will help recognise their susceptibility to seawater quality and thermal stress and establish thresholds. This research can inform how local anthropogenic development have impacted sediment load in coastal areas and how climatic events (e.g., monsoons, flooding) impacted nutrient levels, leading to coral growth alteration. Ultimately, this information is key for the implementation of integrated management strategies.

6.3. Concluding remark

The work of this thesis shows that Fijian inshore massive *Porites* spp. are a robust archive to reconstruct past environmental conditions and coral growth variability. Furthermore, the coupling of sclerochronological and geochemical records carried out in this thesis allows for the exploration of the links between variability in environmental parameters and coral growth, as well as the primary controls on El/Ca incorporation into the coral skeletons and the underpinning physiological mechanisms. Coral paleoreconstructions from Fiji inshore reefs have great potential to provide information on climate and environmental changes across time. This work provides a new understanding of the application of sclerochronological and geochemical proxies in Fijian massive corals. In addition, it provides the starting point for consideration of these records into integrated management strategies and provides coral scientists with an understanding of the resilience and thresholds of a key reef calcifier in this region.

References

Acker JG, Brown CW, Hine AC, Armstrong E, Kuring N (2002) Satellite remote sensing observations and aerial photography of storm-induced neritic carbonate transport from shallow carbonate platforms. Int J Remote Sens 23:2853–2868

ADB (2008) Fiji Islands: Fiji Ports Development Project.

Agrawala S, Ota T, Hagenstad RM, Smith J, Aalst M, Koshy K, Prasad B (2003) Development and climate change in Fiji: focus on coastal mangrove. Environment Directorate Development Co-Operation Directorate. OECD.

Akagi T, Hashimoto Y, F-f F, Tsuno H, Tao H, Nakano Y (2004) Variation of the distribution coefficients of rare earth elements in modern coral-lattices: species and site dependencies. Geochim Cosmochim Acta 68:2265–2273

Al-Horani FA, Al-Moghrabi SM, De Beer D (2003) The mechanism of calcification and its relation to photosynthesis and respiration in the scleractinian coral Galaxea fascicularis. Mar Biol 142:419–426

Alibert C, Kinsley L (2008) A 170-year Sr/Ca and Ba/Ca coral record from the western Pacific warm pool: 1. What can we learn from an unusual coral record? J Geophys Res Oceans 113, C06006.

Alibert C, Kinsley L, Fallon SJ, McCulloch MT, Berkelmans R, McAllister F (2003) Source of trace element variability in Great Barrier Reef corals affected by the Burdekin flood plumes. Geochim Cosmochim Acta 67:231–246

Alibert C, McCulloch MT (1997) Strontium/calcium ratios in modern Porites corals from the Great Barrier Reef as a proxy for sea surface temperature: calibration of the thermometer and monitoring of ENSO. Paleoceanography 12:345–363

Allemand D, Tambutté É, Zoccola D, Tambutté S (2011) Coral Calcification, Cells to Reefs. In: Dubinsky Z., Stambler N. (eds) Coral Reefs: An Ecosystem in Transition. Springer Netherlands, Dordrecht, pp 119–150

Allison N, Cole C, Hintz C, Hintz K, Finch AA (2018) Influences of coral genotype and seawater pCO2 on skeletal Ba/Ca and Mg/Ca in cultured massive Porites spp. corals. Palaeogeogr Palaeoclimatol Palaeoecol 505:351–358

Allison N, Finch AA (2004) High-resolution Sr/Ca records in modern Porites lobata corals: Effects of skeletal extension rate and architecture. Geochem Geophys Geosystems 5:5, Q05001

Allison N, Finch AA (2009) Reproducibility of minor and trace element determinations in Porites coral skeletons by secondary ion mass spectrometry. Geochem Geophys Geosystems 10, Q04003

Allison N, Finch AA, Sutton SR, Newville M (2001) Strontium heterogeneity and speciation in coral aragonite: implications for the strontium paleothermometer. Geochim Cosmochim Acta 65:2669–2676

Allison N, Finch AA, Webster JM, Clague DA (2007) Palaeoenvironmental records from fossil corals: the effects of submarine diagenesis on temperature and climate estimates. Geochim Cosmochim Acta 71:4693–4703

Alpert AE, Cohen AL, Oppo DW, DeCarlo TM, Gaetani GA, Hernandez-Delgado EA, Winter A, Gonneea ME (2017) Twentieth century warming of the tropical Atlantic captured by Sr-U paleothermometry. Paleoceanography 32:146–160

Alpert AE, Cohen AL, Oppo DW, DeCarlo TM, Gove JM, Young CW (2016) Comparison of equatorial Pacific sea surface temperature variability and trends with Sr/Ca records from multiple corals. Paleoceanography 31:252–265

Álvarez-Romero JG, Pressey RL, Ban NC, Brodie J (2015) Advancing land-sea conservation planning: Integrating modelling of catchments, land-use change, and river plumes to prioritise catchment management and protection. PLoS One 10:e0145574

Álvarez-Romero JG, Wilkinson SN, Pressey RL, Ban NC, Kool J, Brodie J (2014) Modeling catchment nutrients and sediment loads to inform regional management of water quality in coastal-marine ecosystems: A comparison of two approaches. J Environ Manage 146:164–178

Amiel AJ, Miller DS, Friedman GM (1973) Incorporation of uranium in modern corals. Sedimentology 20:523–528

Anagnostou E, Sherrell RM, Gagnon A, LaVigne M, Field MP, McDonough WF (2011) Seawater nutrient and carbonate ion concentrations recorded as P/Ca, Ba/Ca, and U/Ca in the deep-sea coral Desmophyllum dianthus. Geochim Cosmochim Acta 75:2529–2543

Andrello M, Darling ES, Wenger A, Suárez-Castro AF, Gelfand S, Ahmadia GN (2022) A global map of human pressures on tropical coral reefs. Conserv Lett 15:e12858

Andrew NL, Bright P, de la Rua L, Teoh SJ, Vickers M (2019) Coastal proximity of populations in 22 Pacific Island Countries and Territories. PLoS One 14:e0223249

Anglès S, Jordi A, Campbell L (2015) Responses of the coastal phytoplankton community to tropical cyclones revealed by high-frequency imaging flow cytometry. Limnol Oceanogr 60:1562–1576

Ankita DP, Kazuo N (2014) Modeling hydrological response to land use change in watersheds of viti levu island, FIJI. J Environ Res Dev 8:492

Anthony KRN, Connolly SR (2004) Environmental limits to growth: physiological niche boundaries of corals along turbidity–light gradients. Oecologia 141:373–384

Anthony KRN, Fabricius KE (2000) Shifting roles of heterotrophy and autotrophy in coral energetics under varying turbidity. J Exp Mar Biol Ecol 252:221–253

Anthony KRN, Kline DI, Diaz-Pulido G, Dove S, Hoegh-Guldberg O (2008) Ocean acidification causes bleaching and productivity loss in coral reef builders. Proc Natl Acad Sci U S A 105:17442–17446

Arikibe JE, Prasad S (2020) Determination and comparison of selected heavy metal concentrations in seawater and sediment samples in the coastal area of Suva, Fiji. Mar Pollut Bull 157:111157

Asia-Pacific Data Research Center Southwest Pacific Enhanced Archive of Tropical Cyclones (SPEArTC). http://apdrc.soest.hawaii.edu/projects/speartc/

Atherton J, Olson D, Farley L, Qauqau I (2005) Fiji watersheds at risk. Watershed Assess Healthy Reefs Fish Final Rep U S Dep State OESI Grant SFJ600 4

Atkinson JE, Collen JD (2000) Environmental setting of Namuka Reef, Suva. Fiji Islands. Suva, Fiji: South Pacific Applied Geoscience Commission.

Australian Bureau of Meteorology and CSIRO (2011) Climate Change in the Pacific: Scientific assessment and new research, volume 2: Country reports, Chapter 5 Fiji Islands.

Avtar R, Rinamalo AV, Umarhadi DA, Gupta A, Khedher KM, Yunus AP, Singh BP, Kumar P, Sahu N, Sakti AD (2022) Land Use Change and Prediction for Valuating Carbon Sequestration in Viti Levu Island, Fiji. Land 11:1274 de Baar HJ, German CR, Elderfield H, Van Gaans P (1988) Rare earth element distributions in anoxic waters of the Cariaco Trench. Geochim Cosmochim Acta 52:1203–1219

Bagnato S (2003) Assessing the paleoclimatic utility of the Indo-Pacific coral genus Diploastrea in a 225-year oxygen isotope record from Fiji. Geology thesis and dissertations, University at Albany, State University of New York

Bagnato S, Linsley BK, Howe SS, Wellington GM, Salinger J (2004) Evaluating the use of the massive coral Diploastrea heliopora for paleoclimate reconstruction. Paleoceanography 19, PA1032

Bagnato S, Linsley BK, Howe SS, Wellington GM, Salinger J (2005) Coral oxygen isotope records of interdecadal climate variations in the South Pacific Convergence Zone region. Geochem Geophys Geosystems 6, Q06001

Bainbridge Z, Lewis S, Bartley R, Fabricius K, Collier C, Waterhouse J, Garzon-Garcia A, Robson B, Burton J, Wenger A, Brodie J (2018) Fine sediment and particulate organic matter: A review and case study on ridge-to-reef transport, transformations, fates, and impacts on marine ecosystems. Mar Pollut Bull 135:1205–1220

Baird AH, Marshall PA (2002) Mortality, growth and reproduction in scleractinian corals following bleaching on the Great Barrier Reef. Mar Ecol Prog Ser 237:133–141

Ban SS, Graham NA, Connolly SR (2014) Evidence for multiple stressor interactions and effects on coral reefs. Glob Change Biol 20:681–697

Banzon V, Smith TM, Chin TM, Liu C, Hankins W (2016) A long-term record of blended satellite and in situ sea-surface temperature for climate monitoring, modeling and environmental studies. Earth Syst Sci Data 8:165–176

Barbour P, Terry J (1998) The hidden economic costs of soil erosion: a case study of the ginger industry in Fiji. J S Pac Agric 5:1–8

Barkley HC, Cohen AL (2016) Skeletal records of community-level bleaching in Porites corals from Palau. Coral Reefs 35:1407–1417

Barkley HC, Cohen AL, Mollica NR, Brainard RE, Rivera HE, DeCarlo TM, Lohmann GP, Drenkard EJ, Alpert AE, Young CW (2018) Repeat bleaching of a central Pacific coral reef over the past six decades (1960–2016). Commun Biol 1:1–10

Barnes DJ, Devereux MJ (1984) Productivity and calcification on a coral reef: a survey using pH and oxygen electrode techniques. J Exp Mar Biol Ecol 79:213–231

Barnes DJ, Lough JM (1992) Systematic variations in the depth of skeleton occupied by coral tissue in massive colonies of Porites from the Great barrier reef. J Exp Mar Biol Ecol 159:113–128

Barnes DJ, Lough JM (1993) On the nature and causes of density banding in massive coral skeletons. J Exp Mar Biol Ecol 167:91–108

Barnes DJ, Taylor RB (2001) On the nature and causes of luminescent lines and bands in coral skeletons. Coral Reefs 19:221–230

Bartley R, Bainbridge ZT, Lewis SE, Kroon FJ, Wilkinson SN, Brodie JE, Silburn DM (2014) Relating sediment impacts on coral reefs to watershed sources, processes and management: A review. Sci Total Environ 468–469:1138–1153

Bates NR, Amat A, Andersson AJ (2010) Feedbacks and responses of coral calcification on the Bermuda reef system to seasonal changes in biological processes and ocean acidification. Biogeosciences 7:2509–2530

Le Bec N, Juillet-Leclerc A, Corrège T, Blamart D, Delcroix T (2000) A coral δ18O record of ENSO driven sea surface salinity variability in Fiji (south-western tropical Pacific). Geophys Res Lett 27:23

Beck JW, Edwards RL, Ito E, Taylor FW, Recy J, Rougerie F, Joannot P, Henin C (1992) Sea-surface temperature from coral skeletal strontium/calcium ratios. Science 257:644–647

Beger M, Grantham HS, Pressey RL, Wilson KA, Peterson EL, Dorfman D, Mumby PJ, Lourival R, Brumbaugh DR, Possingham HP (2010) Conservation planning for connectivity across marine, freshwater, and terrestrial realms. Biol Conserv 143:565–575

Bell JD, Johnson JE, Hobday AJ (2011) Vulnerability of tropical Pacific fisheries and aquaculture to climate change. Summary for Pacific Island Countries and Territories. Secretariat of the Pacific Community, Noumea, New Caledonia

Bellwood DR, Hughes TP, Folke C, Nyström M (2004) Confronting the coral reef crisis. Nature 429, 827–833

Berkelmans R, Jones AM, Schaffelke B (2012) Salinity thresholds of Acropora spp. on the Great Barrier Reef. Coral Reefs 31:1103–1110

Bessat F, Buigues D (2001) Two centuries of variation in coral growth in a massive Porites colony from Moorea (French Polynesia): a response of ocean-atmosphere variability from south central Pacific. Palaeogeogr Palaeoclimatol Palaeoecol 175:381–392

Beyer HL, Kennedy EV, Beger M, Chen CA, Cinner JE, Darling ES, Eakin CM, Gates RD, Heron SF, Knowlton N (2018) Risk-sensitive planning for conserving coral reefs under rapid climate change. Conserv Lett 11:e12587

Birkeland C (1997) Life and Death of Coral Reefs. Springer US, New York

Bolouki Kourandeh M, Nabavi SMB, Shokri MR, Ghanemi K (2018) Variation in skeletal extension, density and calcification of the Scleractinian coral Porites lobate across the northern Persian Gulf. Reg Stud Mar Sci 24:364–369

Bonaldo RM, Pires MM, Junior PRG, Hoey AS, Hay ME (2017) Small Marine Protected Areas in Fiji Provide Refuge for Reef Fish Assemblages, Feeding Groups, and Corals. PLOS ONE 12:e0170638

Branson O, Fehrenbacher JS, Vetter L, Sadekov AY, Eggins SM, Spero HJ (2019) LAtools: A data analysis package for the reproducible reduction of LA-ICPMS data. Chem Geol 504:83–95

Bridge JS (2009) Rivers and Floodplains: Forms, Processes, and Sedimentary Record. John Wiley & Sons,

Brodie JE, Kroon FJ, Schaffelke B, Wolanski EC, Lewis SE, Devlin MJ, Bohnet IC, Bainbridge ZT, Waterhouse J, Davis AM (2012) Terrestrial pollutant runoff to the Great Barrier Reef: An update of issues, priorities and management responses. Mar Pollut Bull 65:81–100

Brown CJ, Jupiter SD, Albert S, Klein CJ, Mangubhai S, Maina JM, Mumby P, Olley J, Stewart-Koster B, Tulloch V, Wenger A (2017a) Tracing the influence of land-use change on water quality and coral reefs using a Bayesian model. Sci Rep 7:4740

Brown CJ, Jupiter SD, Lin H-Y, Albert S, Klein C, Maina JM, Tulloch VJD, Wenger AS, Mumby PJ (2017b) Habitat change mediates the response of coral reef fish populations to terrestrial run-off. Mar Ecol Prog Ser 576:55–68

Brown P, Daigneault A, Gawith D (2017c) Climate change and the economic impacts of flooding on Fiji. Clim Dev 9:493–504

Browne NK, Tay J, Todd PA (2015) Recreating pulsed turbidity events to determine coral–sediment thresholds for active management. J Exp Mar Biol Ecol 466:98–109

Bruland KW, Franks RP (1983) Mn, Ni, Cu, Zn and Cd in the western north atlantic. Trace metals in sea water. Springer, pp 395–414

Bruno JF, Selig ER (2007) Regional decline of coral cover in the Indo-Pacific: timing, extent, and subregional comparisons. PLoS One 2:e711

Bruno JF, Sweatman H, Precht WF, Selig ER, Schutte VGW (2009) Assessing evidence of phase shifts from coral to macroalgal dominance on coral reefs. Ecology 90:1478–1484

Bryant D, Burke L, McManus J, Spalding M (1998) Reefs at risk: a map-based indicator of threats to the world's coral reefs. World Resources Institute. New York, US.

Buddemeier RW, Kleypas JA, Aronson RB (2004) Potential contributions of climate change to stresses on coral reef ecosystems. Coral Reefs Glob Clim Change Pew Cent Glob Clim Change Va USA

Buddemeier RW, Maragos JE, Knutson DW (1974) Radiographic studies of reef coral exoskeletons: Rates and patterns of coral growth. J Exp Mar Biol Ecol 14:179–200

Burke L, Reytar K, Spalding M, Perry A (2011) Reefs at risk revisited. World Resources Institute. New York, US.

Burkepile DE, Hay ME (2006) Herbivore vs. nutrient control of marine primary producers: Context-dependent effects. Ecology 87:3128–3139

Cacciapaglia C, van Woesik R (2016) Climate-change refugia: shading reef corals by turbidity. Glob Change Biol 22:1145–1154

Caesar L, Rahmstorf S, Robinson A, Feulner G, Saba V (2018) Observed fingerprint of a weakening Atlantic Ocean overturning circulation. Nature 556:191–196

Cantin NE, Cohen AL, Karnauskas KB, Tarrant AM, McCorkle DC (2010) Ocean Warming Slows Coral Growth in the Central Red Sea. Science 329:322–325

Cantin NE, Lough JM (2014) Surviving Coral Bleaching Events: Porites Growth Anomalies on the Great Barrier Reef. PLOS ONE 9:e88720

Carballo-Bolaños R, Soto D, Chen CA (2019) Thermal stress and resilience of corals in a climate-changing world. J Mar Sci Eng 8:15

Cardinal D, Hamelin B, Bard E, Pätzold J (2001) Sr/Ca, U/Ca and δ18O records in recent massive corals from Bermuda: relationships with sea surface temperature. Chem Geol 176:213–233

Carilli J, Donner SD, Hartmann AC (2012) Historical temperature variability affects coral response to heat stress. PloS One 7:e34418

Carilli JE, Hartmann AC, Heron SF, Pandolfi JM, Cobb K, Sayani H, Dunbar R, Sandin SA (2017) Porites coral response to an oceanographic and human impact gradient in the Line Islands. Limnol Oceanogr 62:2850–2863

Carilli JE, Norris RD, Black B, Walsh SM, Mcfield M (2010) Century-scale records of coral growth rates indicate that local stressors reduce coral thermal tolerance threshold. Glob Change Biol 16:1247–1257

Carilli JE, Norris RD, Black BA, Walsh SM, McField M (2009) Local Stressors Reduce Coral Resilience to Bleaching. PLOS ONE 4:e6324

Carricart-Ganivet JP, Beltrán-Torres AU, Merino M, Ruiz-Zárate MA (2000) Skeletal extension, density and calcification rate of the reef building coral Montastraea annularis (Ellis and Solander) in the Mexican Caribbean. Bull Mar Sci 66:215–224

Carricart-Ganivet JP, Cabanillas-Terán N, Cruz-Ortega I, Blanchon P (2012) Sensitivity of Calcification to Thermal Stress Varies among Genera of Massive Reef-Building Corals. PLOS ONE 7:e32859

Carricart-Ganivet JP, Merino M (2001) Growth responses of the reef-building coral Montastraea annularis along a gradient of continental influence in the southern Gulf of Mexico. Bull Mar Sci 68:133–146

Carriquiry JD, Horta-Puga G (2010) The Ba/Ca record of corals from the Southern Gulf of Mexico: contributions from land-use changes, fluvial discharge and oil-drilling muds. Mar Pollut Bull 60:1625–1630

Carriquiry JD, Villaescusa JA (2010) Coral Cd/Ca and Mn/Ca records of ENSO variability in the Gulf of California. Clim Past 6:401–410

Case DH, Robinson LF, Auro ME, Gagnon AC (2010) Environmental and biological controls on Mg and Li in deep-sea scleractinian corals. Earth Planet Sci Lett 300:215–225

Casey KS, Brandon TB, Cornillon P, Evans R (2010) The past, present, and future of the AVHRR Pathfinder SST program. Oceanography from space. Springer, pp 273–287

Castillo K, Helmuth B (2005) Influence of thermal history on the response of Montastraea annularis to short-term temperature exposure. Mar Biol 148:261–270

Cesar H, Burke L, Pet-Soede L (2003) The economics of worldwide coral reef degradation. Cesar Environmental Eco-nomics Consulting (CEEC)

Chalk TB, Standish CD, D'Angelo C, Castillo KD, Milton JA, Foster GL (2021) Mapping coral calcification strategies from in situ boron isotope and trace element measurements of the tropical coral Siderastrea siderea. Sci Rep 11:472

Chand V, Prasad S, Prasad R (2011) A study of arsenic contamination by graphite furnace atomic absorption spectrometry in the Lami estuary in Fiji. Microchem J 97:160–164

Chang S, Elkins C, Alley M, Eaton J, Monismitha S (2009) Flow inside a coral colony measured using magnetic resonance velocimetry. Limnol Oceanogr 54:1819–1827

Chapman AU, Thompson DM, Hlohowskyj SR, Carilli JE, Gordon G, Goepfert TJ, Sayani HR, Marchitto TM, Cobb KM (2022) A mechanistic investigation of the coral Mn/Ca-based trade-wind proxy at Kiritimati. Geochim Cosmochim Acta 328:58–75

Chazottes V, Campion-Alsumard L, Peyrot-Clausade M, Cuet P (2002) The effects of eutrophication-related alterations to coral reef communities on agents and rates of bioerosion (Reunion Island, Indian Ocean). Coral Reefs 21:375–390

Chen S, Littley EFM, Rae JWB, Charles CD, Adkins JF (2021) Uranium Distribution and Incorporation Mechanism in Deep-Sea Corals: Implications for Seawater [CO32–] Proxies. Front Earth Sci 9:

Chen T, Li S, Yu K, Zheng Z, Wang L, Chen T (2013) Increasing temperature anomalies reduce coral growth in the Weizhou Island, northern South China Sea. Estuar Coast Shelf Sci 130:121–126

Chen X, Deng W, Wei G, McCulloch M (2020) Terrestrial Signature in Coral Ba/Ca, δ18O, and δ13C Records From a Macrotide-Dominated Nearshore Reef Environment, Kimberley Region of Northwestern Australia. J Geophys Res Biogeosciences 125:e2019JG005394

Chen X, Kwon HK, Joung D, Baek C, Park TG, Son M, Kim G (2022) Role of terrestrial versus marine sources of humic dissolved organic matter on the behaviors of trace elements in seawater. Geochim Cosmochim Acta 333:333–346

Chen X, Wei G, Deng W, Liu Y, Sun Y, Zeng T, Xie L (2015) Decadal variations in trace metal concentrations on a coral reef: Evidence from a 159 year record of Mn, Cu, and v in a Porites coral from the northern South China Sea. J Geophys Res Oceans 120:405–416

Cheung AH, Cole JE, Thompson DM, Vetter L, Jimenez G, Tudhope AW (2021) Fidelity of the Coral Sr/Ca Paleothermometer Following Heat Stress in the Northern Galápagos. Paleoceanogr Paleoclimatology 36:e2021PA004323

Clarke H, D'Olivo JP, Conde M, Evans RD, McCulloch MT (2019) Coral records of variable stress impacts and possible acclimatization to recent marine heat wave events on the northwest shelf of Australia. Paleoceanogr Paleoclimatology 34:1672–1688

Clarke H, D'Olivo JP, Falter J, Zinke J, Lowe R, McCulloch M (2017) Differential response of corals to regional mass-warming events as evident from skeletal Sr/Ca and Mg/Ca ratios. Geochem Geophys Geosystems 18:1794–1809

Clements C, Bonito V, Grober-Dunsmore R, Sobey M (2012) Effects of small, Fijian community-based marine protected areas on exploited reef fishes. Mar Ecol Prog Ser 449:233–243

Cohen AL, Gaetani GA (2010) Ion partitioning and the geochemistry of coral skeletons: solving the mystery of the vital effect. EMU Notes Miner 11:377–397

Cohen AL, Hart SR (2004) Deglacial sea surface temperatures of the western tropical Pacific: A new look at old coral. Paleoceanography 19, PA4031

Cohen AL, McConnaughey TA (2003) Geochemical perspectives on coral mineralization. Rev Mineral Geochem 54:151–187

Cohen AL, McCorkle DC, de Putron S, Gaetani GA, Rose KA (2009) Morphological and compositional changes in the skeletons of new coral recruits reared in acidified seawater: Insights into the biomineralization response to ocean acidification. Geochem Geophys Geosystems 10, Q07005

Cohen AL, Owens KE, Layne GD, Shimizu N (2002) The Effect of Algal Symbionts on the Accuracy of Sr/Ca Paleotemperatures from Coral. Science 296:331–333

Cohen AL, Saenger CP (2006) Tropical Atlantic SSTS at the Last Glacial Maximum derived from Sr/Ca ratios of fossil coral. 2006:PP31A-1735

Cole C, Finch A, Hintz C, Hintz K, Allison N (2016) Understanding cold bias: Variable response of skeletal Sr/Ca to seawater pCO2 in acclimated massive Porites corals. Sci Rep 6:26888

Collen JD, Atkinson JE, Patterson JE (2011) Trace Metal Partitioning in a Nearshore Tropical Environment: Geochemistry of Carbonate Reef Flats Adjacent to Suva Harbor, Fiji Islands. Pac Sci 65:95–107

Collins M, An S-I, Cai W, Ganachaud A, Guilyardi E, Jin F-F, Jochum M, Lengaigne M, Power S, Timmermann A (2010) The impact of global warming on the tropical Pacific Ocean and El Niño. Nat Geosci 3:391–397

Comeau S, Cornwall CE, DeCarlo TM, Krieger E, McCulloch MT (2018) Similar controls on calcification under ocean acidification across unrelated coral reef taxa. Glob Change Biol 24:4857–4868

Comeau S, Edmunds PJ, Spindel NB, Carpenter RC (2014) Diel pCO2 oscillations modulate the response of the coral Acropora hyacinthus to ocean acidification. Mar Ecol Prog Ser 501:99–111

Cooper TF, De'ath G, Fabricius KE, Lough JM (2008) Declining coral calcification in massive Porites in two nearshore regions of the northern Great Barrier Reef. Glob Change Biol 14:529–538

Cooper TF, O'Leary RA, Lough JM (2012) Growth of Western Australian corals in the anthropocene. Science ;335(6068):593-6

Corrège T (2006) Sea surface temperature and salinity reconstruction from coral geochemical tracers. Palaeogeogr Palaeoclimatol Palaeoecol 232:408–428

Crabbe MJC, Smith DJ (2005) Sediment impacts on growth rates of Acropora and Porites corals from fringing reefs of Sulawesi, Indonesia. Coral Reefs 24:437–441

Cuif JP, Dauphin Y, Freiwald A, Gautret P, Zibrowius H (1999) Biochemical markers of zooxanthellae symbiosis in soluble matrices of skeleton of 24 Scleractinia species. Comp Biochem Physiol A Mol Integr Physiol 123:269–278

Cumming R, Aalbersberg WGL, Lovell ER, Sykes HR, Vuki VC (2002) Coral reefs of the Fiji Islands: current issue. https://repository.usp.ac.fj/5177/

Dadhich AP, Nadaoka K (2012) Analysis of Terrestrial Discharge from Agricultural Watersheds and Its Impact on Nearshore and Offshore Reefs in Fiji. J Coast Res 28:1225–1235

D'Angelo C, Wiedenmann J (2014) Impacts of nutrient enrichment on coral reefs: new perspectives and implications for coastal management and reef survival. Curr Opin Environ Sustain 7:82–93

Dassié EP, Linsley BK (2015) Refining the sampling approach for the massive coral Diploastrea heliopora for δ18O-based paleoclimate applications. Palaeogeogr Palaeoclimatol Palaeoecol 440:274–282

Dassié EP, Linsley BK, Corrège T, Wu HC, Lemley GM, Howe S, Cabioch G (2014) A Fiji multi-coral δ18O composite approach to obtaining a more accurate reconstruction of the last two-centuries of the ocean-climate variability in the South Pacific Convergence Zone region. Paleoceanography 29:1196–1213

De'ath G, Fabricius KE, Sweatman H, Puotinen M (2012) The 27–year decline of coral cover on the Great Barrier Reef and its causes. Proc Natl Acad Sci 109:17995–17999

De'ath G, Lough JM, Fabricius KE (2009) Declining Coral Calcification on the Great Barrier Reef. Science 323:116–119

DeCarlo TM (2018) Characterizing coral skeleton mineralogy with Raman spectroscopy. Nat Commun 9:5325

DeCarlo TM, Cohen AL (2017) Dissepiments, density bands and signatures of thermal stress in Porites skeletons. Coral Reefs 36:749–761

DeCarlo TM, Cohen AL, Barkley HC, Cobban Q, Young C, Shamberger KE, Brainard RE, Golbuu Y (2015a) Coral macrobioerosion is accelerated by ocean acidification and nutrients. Geology 43:7–10

DeCarlo TM, Cohen AL, Wong GT, Davis KA, Lohmann P, Soong K (2017a) Mass coral mortality under local amplification of 2 C ocean warming. Sci Rep 7:1–9

DeCarlo TM, D'Olivo JP, Foster T, Holcomb M, Becker T, McCulloch MT (2017b) Coral calcifying fluid aragonite saturation states derived from Raman spectroscopy. Biogeosciences 14:5253–5269

DeCarlo TM, Gaetani GA, Cohen AL, Foster GL, Alpert AE, Stewart JA (2016) Coral Sr-U thermometry. Paleoceanography 31:626–638

DeCarlo TM, Gaetani GA, Holcomb M, Cohen AL (2015b) Experimental determination of factors controlling U/Ca of aragonite precipitated from seawater: Implications for interpreting coral skeleton. Geochim Cosmochim Acta 162:151–165

DeCarlo TM, Harrison HB (2019) An enigmatic decoupling between heat stress and coral bleaching on the Great Barrier Reef. PeerJ 7:e7473

DeCarlo TM, Holcomb M, McCulloch MT (2018) Reviews and syntheses: Revisiting the boron systematics of aragonite and their application to coral calcification. Biogeosciences 15:2819–2834

DeLong KL, Flannery JA, Poore RZ, Quinn TM, Maupin CR, Lin K, Shen C-C (2014) A reconstruction of sea surface temperature variability in the southeastern Gulf of Mexico from 1734 to 2008 CE using cross-dated Sr/Ca records from the coral Siderastrea siderea. Paleoceanography 29:403–422

DeLong KL, Quinn TM, Taylor FW (2007) Reconstructing twentieth-century sea surface temperature variability in the southwest Pacific: A replication study using multiple coral Sr/Ca records from New Caledonia. Paleoceanography 22, PA4212

DeLong KL, Quinn TM, Taylor FW, Shen C-C, Lin K (2013) Improving coral-base paleoclimate reconstructions by replicating 350years of coral Sr/Ca variations. Palaeogeogr Palaeoclimatol Palaeoecol 373:6–24

Department of Environment, Government of Fiji (2020) National Biodiversity Strategy and Action Plan 2020–2025.

Dlugokencky E, Tans P (2022) Trends in atmospheric carbon dioxide, National Oceanic and Atmospheric Administration. https://gml.noaa.gov/ccgg/trends/

Dodge RE, Vaisnys JR (1977) Coral populations and growth patterns: Responses to sedimentation and turbidity associated with dredging. J Mar Res 35: 715-730

D'Olivo JP, Georgiou L, Falter J, DeCarlo TM, Irigoien X, Voolstra CR, Roder C, Trotter J, McCulloch MT (2019) Long-term impacts of the 1997–1998 bleaching event on the growth and resilience of massive Porites corals from the central Red Sea. Geochem Geophys Geosystems 20:2936–2954

D'Olivo JP, McCulloch M (2017) Response of coral calcification and calcifying fluid composition to thermally induced bleaching stress. Sci Rep 7:1–15

D'Olivo JP, McCulloch MT, Judd K (2013) Long-term records of coral calcification across the central Great Barrier Reef: assessing the impacts of river runoff and climate change. Coral Reefs 32:999–1012

D'Olivo JP, Sinclair DJ, Rankenburg K, McCulloch MT (2018) A universal multi-trace element calibration for reconstructing sea surface temperatures from long-lived Porites corals: Removing 'vital-effects.' Geochim Cosmochim Acta 239:109–135

Done TJ, DeVantier LM, Turak E, Fisk DA, Wakeford M, van Woesik R (2010) Coral growth on three reefs: Development of recovery benchmarks using a space for time approach. Coral Reefs 29:815–833

Doney SC (2010) The growing human footprint on coastal and open-ocean biogeochemistry. science 328:1512–1516

Doney SC, Fabry VJ, Feely RA, Kleypas JA (2009) Ocean acidification: the other CO2 problem. Annu Rev Mar Sci 1:169–192

Donovan MK, Adam TC, Shantz AA, Speare KE, Munsterman KS, Rice MM, Schmitt RJ, Holbrook SJ, Burkepile DE (2020) Nitrogen pollution interacts with heat stress to increase coral bleaching across the seascape. Proc Natl Acad Sci 117:5351–5357

Donovan MK, Burkepile DE, Kratochwill C, Shlesinger T, Sully S, Oliver TA, Hodgson G, Freiwald J, Woesik R van (2021) Local conditions magnify coral loss after marine heatwaves. Science 372:977–980

Dougherty G (1988) Heavy metal concentrations in bivalves from Fiji's coastal waters. Mar Pollut Bull 19:81–84

Drake JL, Mass T, Stolarski J, Von Euw S, van de Schootbrugge B, Falkowski PG (2020) How corals made rocks through the ages. Glob Change Biol 26:31–53

Druffel ER (1997) Geochemistry of corals: Proxies of past ocean chemistry, ocean circulation, and climate. Proc Natl Acad Sci 94:8354–8361

Dunbar RB, Wellington GM (1981) Stable isotopes in a branching coral monitor seasonal temperature variation. Nature 293:453–455

Duran A, Collado-Vides L, Burkepile DE (2016) Seasonal regulation of herbivory and nutrient effects on macroalgal recruitment and succession in a Florida coral reef. PeerJ 4:e2643

Dutra LX, Haywood MDE, Singh SS, Piovano S, Ferreira M, Johnson JE, Veitayaki J, Kininmonth S, Morris CW (2018) Impacts of climate change on corals relevant to the Pacific Islands. Pac Mar Clim Change Rep Card Commonw Mar Econ Programme Lond 132–258

Eakin CM (1996) Where have all the carbonates gone? A model comparison of calcium carbonate budgets before and after the 1982–1983 El Nino at Uva Island in the eastern Pacific. Coral Reefs 15:109–119

Edinger EN, Limmon GV, Jompa J, Widjatmoko W, Heikoop JM, Risk MJ (2000) Normal Coral Growth Rates on Dying Reefs: Are Coral Growth Rates Good Indicators of Reef Health? Mar Pollut Bull 40:404–425

Edmunds PJ, Davies PS (1986) An energy budget for Porites porites (Scleractinia). Mar Biol 92:339–347

Elizalde-Rendón E, Horta-Puga G, González-Diaz P, Carricart-Ganivet J (2010) Growth characteristics of the reef-building coral Porites astreoides under different environmental conditions in the Western Atlantic. Coral Reefs 29:607–614

Ellison J, Fiu M (2010) Vulnerability of Fiji's mangroves and associated coral reefs to climate change. World Wildlife Fundation

Elsner JB, Kossin JP, Jagger TH (2008) The increasing intensity of the strongest tropical cyclones. Nature 455:92–95

Endrizzi F, Rao L (2014) Chemical speciation of uranium (VI) in marine environments: complexation of calcium and magnesium ions with [(UO2)(CO3) 3] 4− and the effect on the extraction of uranium from seawater. Chem Eur J 20:14499–14506

England MH, McGregor S, Spence P, Meehl GA, Timmermann A, Cai W, Gupta AS, McPhaden MJ, Purich A, Santoso A (2014) Recent intensification of wind-driven circulation in the Pacific and the ongoing warming hiatus. Nat Clim Change 4:222–227

Enochs IC, Manzello DP, Kolodziej G, Noonan SHC, Valentino L, Fabricius KE, Enochs IC (2016) Enhanced macroboring and depressed calcification drive net dissolution at high-CO 2 coral reefs.

Evans D, Müller W (2018) Automated extraction of a five-year LA-ICP-MS trace element data set of ten common glass and carbonate reference materials: Long-term data quality, optimisation and laser cell homogeneity. Geostand Geoanalytical Res 42:159–188

Eyre BD, Cyronak T, Drupp P, Carlo EHD, Sachs JP, Andersson AJ (2018) Coral reefs will transition to net dissolving before end of century. Science 359:908–911

Fabricius KE (2005) Effects of terrestrial runoff on the ecology of corals and coral reefs: review and synthesis. Mar Pollut Bull 50:125–146

Fabricius KE, De'ath G, Humphrey C, Zagorskis I, Schaffelke B (2013) Intra-annual variation in turbidity in response to terrestrial runoff on near-shore coral reefs of the Great Barrier Reef. Estuar Coast Shelf Sci 116:57–65

Fabricius KE, Langdon C, Uthicke S, Humphrey C, Noonan S, De'ath G, Okazaki R, Muehllehner N, Glas MS, Lough JM (2011) Losers and winners in coral reefs acclimatized to elevated carbon dioxide concentrations. Nat Clim Change 1:165–169

Fabricius KE, Wolanski E (2000) Rapid smothering of coral reef organisms by muddy marine snow. Estuar Coast Shelf Sci 50:115–120

Falkowski PG, Dubinsky Z, Muscatine L, Porter JW (1984) Light and the bioenergetics of a symbiotic coral. Bioscience 34:705–709

Fallon SJ, McCulloch MT, Alibert C (2003) Examining water temperature proxies in Porites corals from the Great Barrier Reef: a cross-shelf comparison. Coral Reefs 22:389–404

Fallon SJ, McCulloch MT, van Woesik R, Sinclair DJ (1999) Corals at their latitudinal limits: laser ablation trace element systematics in Porites from Shirigai Bay, Japan. Earth Planet Sci Lett 172:221–238

Fallon SJ, White JC, McCulloch MT (2002) Porites corals as recorders of mining and environmental impacts: Misima Island, Papua New Guinea. Geochim Cosmochim Acta 66:45–62

Faxneld S, Jörgensen TL, Tedengren M (2010) Effects of elevated water temperature, reduced salinity and nutrient enrichment on the metabolism of the coral Turbinaria mesenterina. Estuar Coast Shelf Sci 88:482–487

FBoS (2017) Census 2017 of Population & Housing.

Felis T, Merkel U, Asami R, Deschamps P, Hathorne EC, Kölling M, Bard E, Cabioch G, Durand N, Prange M (2012) Pronounced interannual variability in tropical South Pacific temperatures during Heinrich Stadial 1. Nat Commun 3:1–7

Felis T, Pätzold J (2003) Climate records from corals. Marine science frontiers for Europe. Springer, pp 11–27

Felis T, Pätzold J, Loya Y (2003) Mean oxygen-isotope signatures in Porites spp. corals: Inter-colony variability and correction for extension-rate effects. Coral Reefs 22, 328–336

Felis T, Suzuki A, Kuhnert H, Dima M, Lohmann G, Kawahata H (2009) Subtropical coral reveals abrupt early-twentieth-century freshening in the western North Pacific Ocean. Geology 37:527–530

Ferrier-Pagès C, Boisson F, Allemand D, Tambutté E (2002) Kinetics of strontium uptake in the scleractinian coral Stylophora pistillata. Mar Ecol Prog Ser 245:93–100

Ferrier-Pagès C, Sauzéat L, Balter V (2018) Coral bleaching is linked to the capacity of the animal host to supply essential metals to the symbionts. Glob Change Biol 24:3145–3157

Fiji Meteorological Service (2006) The Climate of Fiji.

Fiji Meteorological Service (2021) Fiji Climate Summary.

Fiji Sugar Corporation. (2020) Annual report.

Finch AA, Allison N (2008) Mg structural state in coral aragonite and implications for the paleoenvironmental proxy. Geophys Res Lett 35, L08704

Finch AA, Allison N, Sutton SR, Newville M (2003) Strontium in coral aragonite: 1. Characterization of Sr coordination by extended absorption X-ray fine structure. Geochim Cosmochim Acta 67:1197–1202

Folland CK, Renwick JA, Salinger MJ, Mullan AB (2002) Relative influences of the interdecadal Pacific oscillation and ENSO on the South Pacific convergence zone. Geophys Res Lett 29:21-1-21–4

Ford AK, Bejarano S, Nugues MM, Visser PM, Albert S, Ferse SC (2018) Reefs under siege—the rise, putative drivers, and consequences of benthic cyanobacterial mats. Front Mar Sci 5:18

Ford AK, Visser PM, van Herk MJ, Jongepier E, Bonito V (2021) First insights into the impacts of benthic cyanobacterial mats on fish herbivory functions on a nearshore coral reef. Sci Rep 11:1–14

Fowell SE, Sandford K, Stewart JA, Castillo KD, Ries JB, Foster GL (2016) Intrareef variations in Li/Mg and Sr/Ca sea surface temperature proxies in the Caribbean reef-building coral Siderastrea siderea. Paleoceanography 31:1315–1329

Friedlingstein P, O'Sullivan M, Jones MW, Andrew RM, Gregor L, Hauck J, Le Quéré C, Luijkx IT, Olsen A, Peters GP, Peters W, Pongratz J, Schwingshackl C, Sitch S, Canadell JG, Ciais P, Jackson RB, Alin SR, Alkama R, Arneth A, Arora VK, Bates NR, Becker M, Bellouin N, Bittig HC, Bopp L, Chevallier F, Chini LP, Cronin M, Evans W, Falk S, Feely RA, Gasser T, Gehlen M, Gkritzalis T, Gloege L, Grassi G, Gruber N, Gürses Ö, Harris I, Hefner M, Houghton RA, Hurtt GC, Iida Y, Ilyina T, Jain AK, Jersild A, Kadono K, Kato E, Kennedy D, Klein Goldewijk K, Knauer J, Korsbakken JI, Landschützer P, Lefèvre N, Lindsay K, Liu J, Liu Z, Marland G, Mayot N, McGrath MJ, Metzl N, Monacci NM, Munro DR, Nakaoka S-I, Niwa Y, O'Brien K, Ono T, Palmer PI, Pan N, Pierrot D, Pocock K, Poulter B, Resplandy L, Robertson E, Rödenbeck C, Rodriguez C, Rosan TM, Schwinger J, Séférian R, Shutler JD, Skjelvan I, Steinhoff T, Sun Q, Sutton AJ, Sweeney C, Takao S, Tanhua T, Tans PP, Tian X, Tian H, Tilbrook B, Tsujino H, Tubiello F, van der Werf GR, Walker AP, Wanninkhof R, Whitehead C, Willstrand Wranne A, Wright R, Yuan W, Yue C, Yue X, Zaehle S, Zeng J, Zheng B (2022) Global Carbon Budget 2022. Earth Syst Sci Data 14:4811–4900

Gaetani GA, Cohen AL (2006) Element partitioning during precipitation of aragonite from seawater: A framework for understanding paleoproxies. Geochim Cosmochim Acta 70:4617–4634

Gaetani GA, Cohen AL, Wang Z, Crusius J (2011) Rayleigh-based, multi-element coral thermometry: A biomineralization approach to developing climate proxies. Geochim Cosmochim Acta 75:1920–1932

Gagan MK, Ayliffe LK, Beck JW, Cole JE, Druffel ERM, Dunbar RB, Schrag DP (2000) New views of tropical paleoclimates from corals. Quaternary Science Reviews 19: 1 - 5

Gagnon AC, Adkins JF, Erez J (2012) Seawater transport during coral biomineralization. Earth Planet Sci Lett 329:150–161

Gagnon AC, Adkins JF, Fernandez DP, Robinson LF (2007) Sr/Ca and Mg/Ca vital effects correlated with skeletal architecture in a scleractinian deep-sea coral and the role of Rayleigh fractionation. Earth Planet Sci Lett 261:280–295

Gallup CD, Olson DM, Edwards RL, Gruhn LM, Winter A, Taylor FW (2006) Sr/Ca-Sea surface temperature calibration in the branching Caribbean coral Acropora palmata. Geophys Res Lett 33, L03606

Gangaiya P, Tabudravu J, South R, Sotheeswaran S (2018) Heavy metal contamination of the Lami coastal environment, Fiji. S Pac J Nat Appl Sci

Garcia-Soto C, Cheng L, Caesar L, Schmidtko S, Jewett EB, Cheripka A, Rigor I, Caballero A, Chiba S, Báez JC, Zielinski T, Abraham JP (2021) An Overview of Ocean Climate Change Indicators: Sea Surface Temperature, Ocean Heat Content, Ocean pH, Dissolved Oxygen Concentration, Arctic Sea Ice Extent, Thickness and Volume, Sea Level and Strength of the AMOC (Atlantic Meridional Overturning Circulation). Front Mar Sci 8:

Gardella DJ, Edmunds PJ (2001) The effect of flow and morphology on boundary layers in the scleractinians Dichocoenia stokesii (Milne-Edwards and Haime) and Stephanocoenia michilini (Milne-Edwards and Haime). J Exp Mar Biol Ecol 256:279–289

Gardner TA, Côté IM, Gill JA, Grant A, Watkinson AR (2003) Long-term region-wide declines in Caribbean corals. Science 301:958–960

Garland Jr T, Kelly SA (2006) Phenotypic plasticity and experimental evolution. J Exp Biol 209:2344–2361

Gattuso JP, Allemand D, Frankignoulle M (1999) Photosynthesis and calcification at cellular, organismal and community levels in coral reefs: A review on interactions and control by carbonate chemistry. Am Zool 39:160–183

Ghazanfar SA, Keppel G, Khan S (2001) Coastal vegetation of small islands near Viti Levu and Ovalau, Fiji. New Zealand Journal of Botany, 39:4, 587-600

Gillikin DP, Dehairs F, Lorrain A, Steenmans D, Baeyens W, André L (2006) Barium uptake into the shells of the common mussel (Mytilus edulis) and the potential for estuarine paleo-chemistry reconstruction. Geochim Cosmochim Acta 70:395–407

Glynn PW (1996) Coral reef bleaching: facts, hypotheses and implications. Glob Change Biol 2:495–509

Glynn PW, Manzello DP (2015) Bioerosion and coral reef growth: a dynamic balance. Coral reefs in the Anthropocene. Springer, pp 67–97

Goberdhan L, Kininmonth S (2021) Insights into coral growth rate trends in Fiji. Coral Reefs 40:251–266

Goodkin NF, Hughen KA, Cohen AL, Smith SR (2005) Record of Little Ice Age sea surface temperatures at Bermuda using a growth-dependent calibration of coral Sr/Ca. Paleoceanography 20, PA4016

Goreau TJ, Macfarlane AH (1990) Reduced growth rate of Montastrea annularis following the 1987–1988 coral-bleaching event. Coral Reefs 8:211–215

Govan H, Tawake A, Tabunakawai K, Jenkins A, Lasgorceix A, Schwarz AM, Aalbersberg B, Manele B, Vieux C, Notere D, Afzal D (2009) Status and potential of locally-managed marine areas in the South Pacific: meeting nature conservation and sustainable livelihood targets through widespread implementation of LMMAs.

Graham NA, Jennings S, MacNeil MA, Mouillot D, Wilson SK (2015) Predicting climate-driven regime shifts versus rebound potential in coral reefs. Nature 518:94–97

Graham NAJ, Wilson SK, Jennings S, Polunin NVC, Bijoux JP, Robinson J (2006) Dynamic fragility of oceanic coral reef ecosystems. Proc Natl Acad Sci 103:8425–8429

Grottoli AG, Eakin CM (2007) A review of modern coral δ18O and Δ14C proxy records. Earth-Sci Rev 81:67–91

Grottoli AG, Matthews KA, Palardy JE, McDonough WF (2013) High resolution coral Cd measurements using LA-ICP-MS and ID-ICP-MS: Calibration and interpretation. Chem Geol 356:151–159

Grove CA, Kasper S, Zinke J, Pfeiffer M, Garbe-Schönberg D, Brummer G-JA (2013) Confounding effects of coral growth and high SST variability on skeletal Sr/Ca: Implications for coral paleothermometry. Geochem Geophys Geosystems 14:1277–1293

Grove CA, Nagtegaal R, Zinke J, Scheufen T, Koster B, Kasper S, McCulloch MT, van den Bergh G, Brummer GJA (2010) River runoff reconstructions from novel spectral luminescence scanning of massive coral skeletons. Coral Reefs 29:579–591

Grove CA, Zinke J, Scheufen T, Maina J, Epping E, Boer W, Randriamanantsoa B, Brummer G-JA (2012) Spatial linkages between coral proxies of terrestrial runoff across a large embayment in Madagascar. Biogeosciences 9:3063–3081

Guo W (2019) Seawater temperature and buffering capacity modulate coral calcifying pH. Sci Rep 9:1189

Guo W, Bokade R, Cohen AL, Mollica NR, Leung M, Brainard RE (2020) Ocean Acidification Has Impacted Coral Growth on the Great Barrier Reef. Geophys Res Lett 47:e2019GL086761

Hathorne EC, Felis T, James RH, Thomas A (2011) Laser ablation ICP-MS screening of corals for diagenetically affected areas applied to Tahiti corals from the last deglaciation. Geochim Cosmochim Acta 75:1490–1506

Hathorne EC, Felis T, Suzuki A, Kawahata H, Cabioch G (2013) Lithium in the aragonite skeletons of massive Porites corals: A new tool to reconstruct tropical sea surface temperatures. Paleoceanography 28:143–152

Helmle KP, Dodge RE (2011) Sclerochronology. In: Hopley, D. (Ed.), Encyclopedia of Modern Coral Reefs: Structure, Form and Process. Dordrecht, Springer,

Hendy EJ, Gagan MK, Alibert CA, McCulloch MT, Lough JM, Isdale PJ (2002) Abrupt Decrease in Tropical Pacific Sea Surface Salinity at End of Little Ice Age. Science 295:1511–1514

Hendy EJ, Gagan MK, Lough JM, McCulloch M, deMenocal PB (2007) Impact of skeletal dissolution and secondary aragonite on trace element and isotopic climate proxies in Porites corals. Paleoceanography 22, PA4101

Hendy EJ, Lough JM, Gagan MK (2003) Historical mortality in massive Porites from the central Great Barrier Reef, Australia: evidence for past environmental stress? Coral Reefs 22:207–215

Heron SF, Heron ML, Pichel WG (2013) Thermal and Radar Overview. In: Goodman J.A., Purkis S.J., Phinn S.R. (eds) Coral Reef Remote Sensing: A Guide for Mapping, Monitoring and Management. Springer Netherlands, Dordrecht, pp 285–312

Highsmith RC (1979) Coral growth rates and environmental control of density banding. J Exp Mar Biol Ecol 37:105–125

Hoegh-Guldberg O (1999) Climate change, coral bleaching and the future of the world's coral reefs. Mar Freshw Res 50:839–866

Holcomb M, Venn AA, Tambutté E, Tambutté S, Allemand D, Trotter J, Mcculloch M (2014) Coral calcifying fluid pH dictates response to ocean acidification. Sci Rep 4:1–4

van Hooidonk R, Maynard J, Tamelander J, Gove J, Ahmadia G, Raymundo L, Williams G, Heron SF, Planes S (2016) Local-scale projections of coral reef futures and implications of the Paris Agreement. Sci Rep 6:39666

Hsieh Y-T, Paver R, Tanzil JTI, Bridgestock L, Lee JN, Henderson GM (2022) Multi-colony calibration of barium isotopes between shallow-water coral skeletons and in-situ seawater: Implications for paleo proxies. Earth Planet Sci Lett 580:117369

Hughes TP (1994) Catastrophes, phase shifts, and large-scale degradation of a Caribbean coral reef. Science 265:1547–1551

Hughes TP, Anderson KD, Connolly SR, Heron SF, Kerry JT, Lough JM, Baird AH, Baum JK, Berumen ML, Bridge TC, Claar DC, Eakin CM, Gilmour JP, Graham NAJ, Harrison H, Hobbs J-PA, Hoey AS, Hoogenboom M, Lowe RJ, McCulloch MT, Pandolfi JM, Pratchett M, Schoepf V, Torda G, Wilson SK (2018a) Spatial and temporal patterns of mass bleaching of corals in the Anthropocene. Science 359:80–83

Hughes TP, Baird AH, Bellwood DR, Card M, Connolly SR, Folke C, Grosberg R, Hoegh-Guldberg O, Jackson JB, Kleypas J (2003) Climate change, human impacts, and the resilience of coral reefs. science 301:929–933

Hughes TP, Barnes ML, Bellwood DR, Cinner JE, Cumming GS, Jackson JB, Kleypas J, Van De Leemput IA, Lough JM, Morrison TH (2017a) Coral reefs in the Anthropocene. Nature 546:82–90

Hughes TP, Kerry JT, Álvarez-Noriega M, Álvarez-Romero JG, Anderson KD, Baird AH, Babcock RC, Beger M, Bellwood DR, Berkelmans R (2017b) Global warming and recurrent mass bleaching of corals. Nature 543:373–377

Hughes TP, Kerry JT, Baird AH, Connolly SR, Dietzel A, Eakin CM, Heron SF, Hoey AS, Hoogenboom MO, Liu G (2018b) Global warming transforms coral reef assemblages. Nature 556:492–496

Humanes A, Ricardo GF, Willis BL, Fabricius KE, Negri AP (2017) Cumulative effects of suspended sediments, organic nutrients and temperature stress on early life history stages of the coral Acropora tenuis. Sci Rep 7:1–11

Hume B, D'angelo C, Burt J, Baker AC, Riegl B, Wiedenmann J (2013) Corals from the Persian/Arabian Gulf as models for thermotolerant reef-builders: prevalence of clade C3 Symbiodinium, host fluorescence and ex situ temperature tolerance. Mar Pollut Bull 72:313–322

Humphreys J, Clark RWE (2020) Chapter 1 - A critical history of marine protected areas. In: Humphreys J., Clark R.W.E. (eds) Marine Protected Areas. Elsevier, pp 1–12

Iese V, Kiem AS, Mariner A, Malsale P, Tofaeono T, Kirono DGC, Round V, Heady C, Tigona R, Veisa F, Posanau K, Aiono F, Haruhiru A, Daphne A, Vainikolo V, Iona N (2021) Historical and future drought impacts in the Pacific islands and atolls. Clim Change 166:19

Inoue M, Ishikawa D, Miyaji T, Yamazaki A, Suzuki A, Yamano H, Kawahata H, Watanabe T (2014) Evaluation of Mn and Fe in coral skeletons (Porites spp.) as proxies for sediment loading and reconstruction of 50 yrs of land use on Ishigaki Island, Japan. Coral Reefs 33:363–373

Inoue M, Nohara M, Okai T, Suzuki A, Kawahata H (2004) Concentrations of trace elements in carbonate reference materials coral JCp-1 and giant clam JCt-1 by inductively coupled plasma-mass spectrometry. Geostand Geoanalytical Res 28:411–416

IPCC (2021) Climate Change 2021: The Physical Science Basis. Contribution of Working Group I to the Sixth Assessment Report of the Intergovernmental Panel on Climate Change. Cambridge University Press, Cambridge, United Kingdom and New York, NY, USA

IUCN (2009) Navakavu Locally Managed Marine Area.

Jiang W, Yu K-F, Song Y-X, Zhao J-X, Feng Y-X, Wang Y-H, Xu S-D (2017) Coral trace metal of natural and anthropogenic influences in the northern South China Sea. Sci Total Environ 607:195–203

Jimenez G, Cole JE, Thompson DM, Tudhope AW (2018) Northern Galápagos corals reveal twentieth century warming in the eastern tropical Pacific. Geophys Res Lett 45:1981–1988

Jochum KP, Weis U, Stoll B, Kuzmin D, Yang Q, Raczek I, Jacob DE, Stracke A, Birbaum K, Frick DA (2011) Determination of reference values for NIST SRM 610–617 glasses following ISO guidelines. Geostand Geoanalytical Res 35:397–429

Johnson GC, Lyman JM (2020) Warming trends increasingly dominate global ocean. Nat Clim Change 10:757–761

Jones R, Giofre N, Luter HM, Neoh TL, Fisher R, Duckworth A (2020) Responses of corals to chronic turbidity. Sci Rep 10:4762

Juillet-Leclerc A, Thiria S, Naveau P, Delcroix T, Le Bec N, Blamart D, Corrège T (2006) SPCZ migration and ENSO events during the 20th century as revealed by climate proxies from a Fiji coral. Geophys Res Lett 33, L17710

Jupiter S (2008) Coral rare earth element tracers of terrestrial exposure in nearshore corals of the Great Barrier Reef. Proc 11th Int Coral Reef Symp 105–109

Jupiter S, Jenkins ., Koto K, Ah Tong J, Bwebe T, Cakacaka A, Dulunaqio S, Fox M, Kuritani L, Mario S, Naisilisili N, Nand Y, Tukana A, Weeks R, Yakub N (2012) Effects of alteration to catchment and streams on fresh water fish communities of Vanua Levu, Fiji. 17

Jupiter S, Roff G, Marion G, Henderson M, Schrameyer V, McCulloch M, Hoegh-Guldberg O (2008) Linkages between coral assemblages and coral proxies of terrestrial exposure along a cross-shelf gradient on the southern Great Barrier Reef. Coral Reefs 27:887–903

Jupiter S, Tui T, Shah S, Cakacaka A, Moy W, Naisilisili W, Dulunaqio S, Patrick A, Qauqau I, Yakub N (2010) Integrating EBM science to assess marine protected area effectiveness: clues from coral proxies of land disturbance, ecological assessments and socioeconomic surveys.

Jupiter SD, Egli DP (2011) Ecosystem-based management in Fiji: successes and challenges after five years of implementation. J Mar Biol 2011: 940765

Jupiter SD, Wenger A, Klein CJ, Albert S, Mangubhai S, Nelson J, Teneva L, Tulloch VJ, White AT, Watson JE (2017) Opportunities and constraints for implementing integrated land–sea management on islands. Environ Conserv 44:254–266

Kim S, Lee H, Jun K-W (2020) The Impact and Occurrence of Sediment-Mixture Flow due to Cyclone Winston in the Coast of Fiji Island, South Pacific. J Coast Res 95:1460–1466

Kinch J, Anderson P, Richards E, Talouli A, Vieux C, Peteru C, Suaesi T (2010) Outlook report on the state of the marine biodiversity in the Pacific Islands region. Secr Pac Reg Environ Programme Apia

Kirk NL, Weis VM (2016) Animal–Symbiodinium symbioses: foundations of coral reef ecosystems. The mechanistic benefits of microbial symbionts. Springer, pp 269–294

Kitolelei J, Kakuma S (2022) Protecting Fisheries Resources Through Marine Protected Area Networks: Fiji. In: Kakuma S., Yanagi T., Sato T. (eds) Satoumi Science: Co-creating Social-Ecological Harmony Between Human and the Sea. Springer, Singapore, pp 169–190

Klein CJ, Jupiter SD, Selig ER, Watts ME, Halpern BS, Kamal M, Roelfsema C, Possingham HP (2012) Forest conservation delivers highly variable coral reef conservation outcomes. Ecol Appl 22:1246–1256

Klein R, Loya Y (1991) Skeletal growth and density patterns of two Porites corals from the Gulf of Eilat, Red Sea. Mar Ecol Prog Ser 77:253–259

Klein R, Patzold J, Wefer G, Loya Y (1993) Depth-related timing of density band formation in Porites spp. corals from the Red Sea inferred from X-ray chronology and stable isotope composition. Mar Ecol Prog Ser 97:99–104

Klepac CN, Barshis DJ (2020) Reduced thermal tolerance of massive coral species in a highly variable environment. Proc R Soc B 287:20201379

Kleypas J, Hoegh-Guldberg O (2008) Coral reefs and climate change: susceptibility and consequences.

Kleypas JA, Eakin CM (2007) Scientists' perceptions of threats to coral reefs: results of a survey of coral reef researchers. Bull Mar Sci 80:419–436

Knebel O, Carvajal C, Standish CD, Vega E de la, Chalk TB, Ryan EJ, Guo W, Ford M, Foster GL, Kench P (2021) Porites Calcifying Fluid pH on Seasonal to Diurnal Scales. J Geophys Res Oceans 126:e2020JC016889

Knowlton N, Jackson JBC (2008) Shifting baselines, local impacts, and global change on coral reefs. PLoS Biol 6:e54

Knutson DW, Buddemeier RW, Smith SV (1972) Coral chronometers: seasonal growth bands in reef corals. Science 177:270–272

Knutson TR, McBride JL, Chan J, Emanuel K, Holland G, Landsea C, Held I, Kossin JP, Srivastava A, Sugi M (2010) Tropical cyclones and climate change. Nat Geosci 3:157–163

Kuffner IB, Jokiel PL, Rodgers KS, Andersson AJ, Mackenzie FT (2012) An apparent "vital effect" of calcification rate on the Sr/Ca temperature proxy in the reef coral Montipora capitata. Geochem Geophys Geosystems 13, Q08004

Kumar R (2005) Geology, Climate, and Landscape of the PABITRA Wet-Zone Transect, Viti Levu Island, Fiji. Pac Sci 59:141–157

Kumar R, Stephens M, Weir T (2014) Rainfall trends in Fiji. Int J Climatol 34:1501–1510

Langdon C, Broecker WS, Hammond DE, Glenn E, Fitzsimmons K, Nelson SG, Peng T-H, Hajdas I, Bonani G (2003) Effect of elevated CO 2 on the community metabolism of an experimental coral reef. Glob Biogeochem Cycles 17:1011

Lapointe BE (1997) Nutrient thresholds for bottom-up control of macroalgal blooms on coral reefs in Jamaica and southeast Florida. Limnol Oceanogr 42:1119–1131

LaVigne M, Field MP, Anagnostou E, Grottoli AG, Wellington GM, Sherrell RM (2008) Skeletal P/Ca tracks upwelling in Gulf of Panamá coral: Evidence for a new seawater phosphate proxy. Geophys Res Lett 35

LaVigne M, Grottoli AG, Palardy JE, Sherrell RM (2016) Multi-colony calibrations of coral Ba/Ca with a contemporaneous in situ seawater barium record. Geochim Cosmochim Acta 179:203–216

LaVigne M, Matthews KA, Grottoli AG, Cobb KM, Anagnostou E, Cabioch G, Sherrell RM (2010) Coral skeleton P/Ca proxy for seawater phosphate: Multi-colony calibration with a contemporaneous seawater phosphate record. Geochim Cosmochim Acta 74:1282–1293

Lawson KN, Letendre H, Drew JA (2021) Historical Maps provide insight into a century and a half of habitat change in Fijian coasts. Ecol Evol 11:15573–15584

Le Bec N (2001) Reconstitution of sea surface salinity and temperature in the South-Western tropical Pacific Ocean during the last century: multi-proxy study of a scleractinian massive coral (Porites sp) from the Fiji Islands. Universite de Paris-Sud, U.F.R. Scientifique d'Orsay (France)

Le Quéré C, Takahashi T, Buitenhuis ET, Rödenbeck C, Sutherland SC (2010) Impact of climate change and variability on the global oceanic sink of CO2. Glob Biogeochem Cycles 24

Lea DW, Shen GT, Boyle EA (1989) Coralline barium records temporal variability in equatorial Pacific upwelling. Nature 340, 373–376

Lechner AM, Foody GM, Boyd DS (2020) Applications in Remote Sensing to Forest Ecology and Management. One Earth 2:405–412

Leder JJ, Szmant AM, Swart PK (1991) The effect of prolonged "bleaching" on skeletal banding and stable isotopic composition in Montastrea annularis. Coral Reefs 10:19–27

Leonard ND, Welsh KJ, Nguyen AD, Sadler J, Pandolfi JM, Clark TR, Zhao J, Feng Y, Webb GE (2019) High resolution geochemical analysis of massive Porites spp. corals from the Wet Tropics, Great Barrier Reef: rare earth elements, yttrium and barium as indicators of terrigenous input. Mar Pollut Bull 149:110634

Leslie DM (1997) An introduction to the soils of Fiji. Soil and Crop Evaluation Project, Research Division, Ministry of Agriculture, Fisheries. Fiji

Lester SE, Halpern BS, Grorud-Colvert K, Lubchenco J, Ruttenberg BI, Gaines SD, Airamé S, Warner RR (2009) Biological effects within no-take marine reserves: A global synthesis. Mar Ecol Prog Ser 384:33–46

Lewis BM, Nothdurft LD, Nothdurft LN (2016) Expulsion of Symbiodinium by pulsed inflation under hyperthermal stress in Heliofungia actiniformis. Coral Reefs 35:1405–1405

Lewis SE, Brodie JE, McCulloch MT, Mallela J, Jupiter SD, Stuart Williams H, Lough JM, Matson EG (2012) An assessment of an environmental gradient using coral geochemical records, Whitsunday Islands, Great Barrier Reef, Australia. Mar Pollut Bull 65:306–319

Lewis SE, Lough JM, Cantin NE, Matson EG, Kinsley L, Bainbridge ZT, Brodie JE (2018) A critical evaluation of coral Ba/Ca, Mn/Ca and Y/Ca ratios as indicators of terrestrial input: New data from the Great Barrier Reef, Australia. Geochim Cosmochim Acta 237:131–154

Lewis SE, Shields GA, Kamber BS, Lough JM (2007) A multi-trace element coral record of land-use changes in the Burdekin River catchment, NE Australia. Palaeogeogr Palaeoclimatol Palaeoecol 246:471–487

Limalevu L (2008) Land Degradation United Nations Convention to Combat Desertification (UNCCD).

Linsley BK, Dunbar RB, Dassié EP, Tangri N, Wu HC, Brenner LD, Wellington GM (2019) Coral carbon isotope sensitivity to growth rate and water depth with paleo-sea level implications. Nat Commun 10:2056

Linsley BK, Kaplan A, Gouriou Y, Salinger J, deMenocal PB, Wellington GM, Howe SS (2006) Tracking the extent of the South Pacific Convergence Zone since the early 1600s. Geochem Geophys Geosystems 7

Linsley BK, Ren L, Dunbar RB, Howe SS (2000) El Niño Southern Oscillation (ENSO) and decadal-scale climate variability at 10° N in the eastern Pacific from 1893 to 1994: A coral-based reconstruction from Clipperton Atoll. Paleoceanography 15:322–335

Linsley BK, Wellington GM, Schrag DP, Ren L, Salinger MJ, Tudhope AW (2004) Geochemical evidence from corals for changes in the amplitude and spatial pattern of South Pacific interdecadal climate variability over the last 300 years. Clim Dyn 22:1–11

Linsley BK, Zhang P, Kaplan A, Howe SS, Wellington GM (2008) Interdecadal-decadal climate variability from multicoral oxygen isotope records in the South Pacific Convergence Zone region since 1650 AD. Paleoceanography 23

Liu G, Heron SF, Eakin CM, Muller-Karger FE, Vega-Rodriguez M, Guild LS, De La Cour JL, Geiger EF, Skirving WJ, Burgess TFR, Strong AE, Harris A, Maturi E, Ignatov A, Sapper J, Li J, Lynds S (2014) Reef-Scale Thermal Stress Monitoring of Coral Ecosystems: New 5-km Global Products from NOAA Coral Reef Watch. Remote Sens 6:11579–11606

Liu G, Skirving WJ, Geiger EF, De La Cour JL, Marsh BL, Heron SF, Tirak KV, Strong AE, Eakin CM (2017) NOAA Coral Reef Watch's 5km satellite coral bleaching heat stress monitoring product suite version 3 and four-month outlook version 4. Reef Encount 32:39–45

Longerich HP, Jackson SE, Günther D (1996) Inter-laboratory note. Laser ablation inductively coupled plasma mass spectrometric transient signal data acquisition and analyte concentration calculation. J Anal At Spectrom 11:899–904

Lough JM (1991) Rainfall variations in Queensland, Australia: 1891–1986. Int J Climatol

Lough JM (2004) A strategy to improve the contribution of coral data to high-resolution paleoclimatology. Palaeogeogr Palaeoclimatol Palaeoecol 204:115–143

Lough JM (2008) Coral calcification from skeletal records revisited. Mar Ecol Prog Ser 373:257–264

Lough JM (2011) Measured coral luminescence as a freshwater proxy: comparison with visual indices and a potential age artefact. Coral Reefs 30:169–182

Lough JM, Barnes DJ (1990) Intra-annual timing of density band formation of Porites coral from the central Great Barrier Reef. J Exp Mar Biol Ecol 135:35–57

Lough JM, Barnes DJ (1992) Comparisons of skeletal density variations in Porites from the central Great Barrier Reef. J Exp Mar Biol Ecol 155:35–57

Lough JM, Barnes DJ (1997) Several centuries of variation in skeletal extension, density and calcification in massive Porites colonies from the Great Barrier Reef: a proxy for seawater temperature and a background of variability against which to identify unnatural change. J Exp Mar Biol Ecol 211:29–67

Lough JM, Barnes DJ (2000) Environmental controls on growth of the massive coral Porites. J Exp Mar Biol Ecol 245:225–243

Lough JM, Cantin NE (2014) Perspectives on Massive Coral Growth Rates in a Changing Ocean. Biol Bull 226:187–202

Lough JM, Cooper TF (2011) New insights from coral growth band studies in an era of rapid environmental change. Earth-Sci Rev 108:170–184

Lovell E, Whippy-Morris C (2009) Live coral fishery for aquaria in Fiji: sustainability and management. Species Divers 1:0–005

Lovell ER, McLardy C (2008) Annotated checklist of the CITES-listed corals of Fiji with reference to Vanuatu, Tonga, Samoa and American Samoa. Joint Nature Conservation Committee, Peterborough

Lovell ER, Sykes HR (2007) 1 FIJI. Status Coral Reefs Southwest Pac 2004 52:1

Maata M, Koshy K (2001) A study on tributyltin contamination of marine sediments in the major ports of Fiji. S Pac J Nat Appl Sci 19:1–4

Maata M, Singh S (2008) Heavy metal pollution in Suva harbour sediments, Fiji. Environ Chem Lett 6:113–118

Macfarlene DC, Suttie JM, Reynolds SG (2009) FAO Country pasture/forage resource profiles.

Maina J, de Moel H, Vermaat JE, Bruggemann JH, Guillaume MM, Grove CA, Madin JS, Mertz-Kraus R, Zinke J (2012) Linking coral river runoff proxies with climate variability, hydrology and land-use in Madagascar catchments. Mar Pollut Bull 64:2047–2059

Mallela J, Lewis SE, Croke B (2013) Coral Skeletons Provide Historical Evidence of Phosphorus Runoff on the Great Barrier Reef. PLOS ONE 8:e75663

Mangubhai S (2016) Impact of tropical cyclone Winston on coral reefs in the Vatu-i-Ra seascape. Report No. 01/16. Wildlife Conservation Society, Suva, Fiji.

Mangubhai S, Sykes H, Lovell E, Brodie G, Jupiter S, Morris C, Lee S, Loganimoce EM, Rashni B, Lal R, Nand Y, Qauqau I (2019) Chapter 35 - Fiji: Coastal and Marine Ecosystems. In: Sheppard C. (eds) World Seas: an Environmental Evaluation (Second Edition). Academic Press, pp 765–792

Manzello DP (2010) Ocean acidification hotspots: Spatiotemporal dynamics of the seawater CO2 system of eastern Pacific coral reefs. Limnol Oceanogr 55:239–248

Marchitto TM, Bryan SP, Doss W, McCulloch MT, Montagna P (2018) A simple biomineralization model to explain Li, Mg, and Sr incorporation into aragonitic foraminifera and corals. Earth Planet Sci Lett 481:20–29

Marriott CS, Henderson GM, Belshaw NS, Tudhope AW (2004) Temperature dependence of δ7Li, δ44Ca and Li/Ca during growth of calcium carbonate. Earth Planet Sci Lett 222:615–624

Marshall JF, McCulloch MT (2002) An assessment of the Sr/Ca ratio in shallow water hermatypic corals as a proxy for sea surface temperature. Geochim Cosmochim Acta 66:3263–3280

Martínez-Botí MA, Foster GL, Chalk TB, Rohling EJ, Sexton PF, Lunt DJ, Pancost RD, Badger MP, Schmidt DN (2015) Plio-Pleistocene climate sensitivity evaluated using high-resolution CO2 records. Nature 518:49–54

Marubini F, Atkinson MJ (1999) Effects of lowered pH and elevated nitrate on coral calcification. Mar Ecol Prog Ser 188:117–121

Marubini F, Davies PS (1996) Nitrate increases zooxanthellae population density and reduces skeletogenesis in corals. Mar Biol 127:319–328

Mataki M, Koshy KC, Lal M (2006) Baseline Climatology of Viti Levu (Fiji) and Current Climatic Trends1. Pac Sci 60:49–68

Mateos-Molina D, Palma M, Ruiz-Valentín I, Panagos P, García-Charton JA, Ponti M (2015) Assessing consequences of land cover changes on sediment deliveries to coastal waters at regional level over the last two decades in the northwestern Mediterranean Sea. Ocean Coast Manag 116:435–442

McClanahan TR, Donner SD, Maynard JA, MacNeil MA, Graham NA, Maina J, Baker AC, Alemu I JB, Beger M, Campbell SJ (2012) Prioritizing key resilience indicators to support coral reef management in a changing climate. PLoS ONE 7(8): e42884

McClanahan TR, Maina JM, Darling ES, Guillaume MMM, Muthiga NA, D'agata S, Leblond J, Arthur R, Jupiter SD, Wilson SK, Mangubhai S, Ussi AM, Humphries AT, Patankar V, Shedrawi G, Julius P, Ndagala J, Grimsditch G (2020) Large geographic variability in the resistance of corals to thermal stress. Glob Ecol Biogeogr 29:2229–2247

McClanahan TR, Sala E, Stickels PA, Cokos BA, Baker AC, Starger CJ (2003) Interaction between nutrients and herbivory in controlling algal communities and coral condition on Glover^{1}s Reef, Belize . Mar Ecol Prog Ser 261:135–147

McCook LJ (1999) Macroalgae, nutrients and phase shifts on coral reefs: Scientific issues and management consequences for the Great Barrier Reef. Coral Reefs 18:357–367

McCook LJ, Jompa J, Diaz-Pulido G (2001) Competition between corals and algae on coral reefs: A review of evidence and mechanisms. Coral Reefs 19:400–417

McCraw J (2020) Modeling Intra-Annual Variation in Coral Extension Rate Using Multiproxy Geochemical Records from Pacific Corals. M.S., Syracuse University

McCulloch M, Fallon S, Wyndham T, Hendy E, Lough J, Barnes D (2003) Coral record of increased sediment flux to the inner Great Barrier Reef since European settlement. Nature 421:727–730

McCulloch M, Falter J, Trotter J, Montagna P (2012) Coral resilience to ocean acidification and global warming through pH up-regulation. Nat Clim Change 2:623–627

McCulloch MT, D'Olivo JP, Falter J, Holcomb M, Trotter JA (2017) Coral calcification in a changing world and the interactive dynamics of pH and DIC upregulation. Nat Commun 8:1–8

McCulloch MT, Tudhope AW, Esat TM, Mortimer GE, Chappell J, Pillans B, Chivas AR, Omura A (1999) Coral record of equatorial sea-surface temperatures during the penultimate deglaciation at Huon Peninsula. Science 283:202–204

McGregor HV, Gagan MK (2003) Diagenesis and geochemistry of Porites corals from Papua New Guinea: Implications for paleoclimate reconstruction. Geochim Cosmochim Acta 67:2147–2156

McLeod E, Anthony KRN, Mumby PJ, Maynard J, Beeden R, Graham NAJ, Heron SF, Hoegh-Guldberg O, Jupiter S, MacGowan P, Mangubhai S, Marshall N, Marshall PA, McClanahan TR, Mcleod K, Nyström M, Obura D, Parker B, Possingham HP, Salm RV, Tamelander J (2019) The future of resilience-based management in coral reef ecosystems. J Environ Manage 233:291–301

McLeod E, Shaver EC, Beger M, Koss J, Grimsditch G (2021) Using resilience assessments to inform the management and conservation of coral reef ecosystems. J Environ Manage 277:111384

Meissner K, Lippmann T, Gupta AS (2012) Large-scale stress factors affecting coral reefs: open ocean sea surface temperature and surface seawater aragonite saturation over the next 400 years. Coral Reefs 31:309–319

Merschel G, Bau M, Dantas EL (2017) Contrasting impact of organic and inorganic nanoparticles and colloids on the behavior of particle-reactive elements in tropical estuaries: An experimental study. Geochim Cosmochim Acta 197:1–13

Mitsuguchi T, Matsumoto E, Abe O, Uchida T, Isdale PJ (1996) Mg/Ca thermometry in coral skeletons. Science 274:961–963

Mitsuguchi T, Uchida T, Matsumoto E, Isdale PJ, Kawana T (2001) Variations in Mg/Ca, Na/Ca, and Sr/Ca ratios of coral skeletons with chemical treatments: implications for carbonate geochemistry. Geochim Cosmochim Acta 65:2865–2874

Mollica NR, Guo W, Cohen AL, Huang K-F, Foster GL, Donald HK, Solow AR (2018) Ocean acidification affects coral growth by reducing skeletal density. Proc Natl Acad Sci 115:1754–1759

Montagna P, McCulloch M, Douville E, López Correa M, Trotter J, Rodolfo-Metalpa R, Dissard D, Ferrier-Pagès C, Frank N, Freiwald A, Goldstein S, Mazzoli C, Reynaud S, Rüggeberg A, Russo S, Taviani M (2014) Li/Mg systematics in scleractinian corals: Calibration of the thermometer. Geochim Cosmochim Acta 132:288–310

Mora C (2008) A clear human footprint in the coral reefs of the Caribbean. Proc R Soc B Biol Sci 275:767–773

Morrison RJ, Clarke WC, Buresova N, Limalevu L (1990) Erosion and sedimentation in Fiji- an overview. University of the South Pacific, P O Box 1168, Suva (Fiji)

Mosley LM, Aalbersberg WGL (2003) Nutrient levels in sea and river water along the 'Coral Coast' of Viti Levu, Fiji. S Pac J Nat Appl Sci 21:35–40

Moya A, Tambutté S, Tambutté E, Zoccola D, Caminiti N, Allemand D (2006) Study of calcification during a daily cycle of the coral Stylophora pistillata: implications forlight-enhanced calcification'. J Exp Biol 209:3413–3419

Moyer RP, Grottoli AG, Olesik JW (2012) A multiproxy record of terrestrial inputs to the coastal ocean using minor and trace elements (Ba/Ca, Mn/Ca, Y/Ca) and carbon isotopes (δ13C, Δ14C) in a nearshore coral from Puerto Rico. Paleoceanography 27

Mumby P, Chisholm J, Edwards A, Clark C, Roark E, Andrefouet S, Jaubert J (2001) Unprecedented bleaching-induced mortality in Porites spp. at Rangiroa Atoll, French Polynesia. Mar Biol 139:183–189

Mumby PJ (2009) Herbivory versus corallivory: are parrotfish good or bad for Caribbean coral reefs? Coral Reefs 28:683–690

Murray J, Prouty NG, Peek S, Paytan A (2019) Coral Skeleton δ15N as a Tracer of Historic Nutrient Loading to a Coral Reef in Maui, Hawaii. Sci Rep 9:5579

Muscatine L (1990) The role of symbiotic algae in carbon and energy flux in reef corals. Role Symbiotic Algae Carbon Energy Flux Reef Corals 25:75–87

Nagtegaal R, Grove CA, Kasper S, Zinke J, Boer W, Brummer G-JA (2012) Spectral luminescence and geochemistry of coral aragonite: Effects of whole-core treatment. Chem Geol 318–319:6–15

Naidu SD, Morrison RJ (1994) Contamination of Suva harbour, Fiji. Mar Pollut Bull 29:126–130

Nairn MG (2018) Mid-Late Miocene climate constrained by a new Laser Ablation ICP-MS set up. School of Earth and Ocean Sciences, Cardiff University

Nerem RS, Beckley BD, Fasullo JT, Hamlington BD, Masters D, Mitchum GT (2018) Climate-change–driven accelerated sea-level rise detected in the altimeter era. Proc Natl Acad Sci 115:2022–2025

Nezlin NP, DiGiacomo PM (2005) Satellite ocean color observations of stormwater runoff plumes along the San Pedro Shelf (southern California) during 1997–2003. Cont Shelf Res 25:1692–1711

Nguyen AD, Zhao J, Feng Y, Hu W, Yu K, Gasparon M, Pham TB, Clark TR (2013) Impact of recent coastal development and human activities on Nha Trang Bay, Vietnam: evidence from a Porites lutea geochemical record. Coral Reefs 32:181–193

Nie B, Chen T, Liang M, Wang Y, Zhong J, Zhu Y (1997) Relationship between coral growth rate and sea surface temperature in the northern part of South China Sea during the past 100 a. Sci China Ser Earth Sci 40:173–182

Nurhati IS, Cobb KM, Charles CD, Dunbar RB (2009) Late 20th century warming and freshening in the central tropical Pacific. Geophys Res Lett 36

N'Yeurt ADR (2001) Marine algae from the Suva lagoon and reef, Fiji. Aust Syst Bot 14:689

Nyström M, Folke C, Moberg F (2000) Coral reef disturbance and resilience in a human-dominated environment. Trends Ecol Evol 15:413–417

O'Leary JK, Micheli F, Airoldi L, Boch C, De Leo G, Elahi R, Ferretti F, Graham NA, Litvin SY, Low NH (2017) The resilience of marine ecosystems to climatic disturbances. BioScience 67:208–220

Ostrander GK, Armstrong KM, Knobbe ET, Gerace D, Scully EP (2000) Rapid transition in the structure of a coral reef community: the effects of coral bleaching and physical disturbance. Proc Natl Acad Sci 97:5297–5302

Ouddane B, Martin E, Boughriet A, Fischer JC, Wartel M (1997) Speciation of dissolved and particulate manganese in the Seine river estuary. Mar Chem 58:189–201

Pan X, Wong GTF, DeCarlo TM, Tai J-H, Cohen AL (2017) Validation of the remotely sensed nighttime sea surface temperature in the shallow waters at the Dongsha Atoll. Terr Atmospheric Ocean Sci

Pandolfi JM, Bradbury RH, Sala E, Hughes TP, Bjorndal KA, Cooke RG, McArdle D, McClenachan L, Newman MJ, Paredes G (2003) Global trajectories of the long-term decline of coral reef ecosystems. Science 301:955–958

Pandolfi JM, Connolly SR, Marshall DJ, Cohen AL (2011) Projecting Coral Reef Futures Under Global Warming and Ocean Acidification. Science 333:418 LP – 422

Pandolfi JM, Jackson JBC, Baron N, Bradbury RH, Guzman HM, Hughes TP, Kappel C V, Micheli F, Ogden JC, Possingham HP, Sala E (2005) Are U.S. Coral Reefs on the Slippery Slope to Slime? Science 307:1725 LP – 1726

Penn N (1983) The environmental consequences and management of coral sand dredging in the Suva region, Fiji. University of Wales

Perry CT, Murphy GN, Kench PS, Edinger EN, Smithers SG, Steneck RS, Mumby PJ (2014) Changing dynamics of Caribbean reef carbonate budgets: emergence of reef bioeroders as critical controls on present and future reef growth potential. Proc R Soc B Biol Sci 281:20142018

Pfeiffer M, Dullo W-C, Zinke J, Garbe-Schönberg D (2009) Three monthly coral Sr/Ca records from the Chagos Archipelago covering the period of 1950–1995 A.D.: reproducibility and implications for quantitative reconstructions of sea surface temperature variations. Int J Earth Sci 98:53–66

Platt T, Sathyendranath S, Caverhill CM, Lewis MR (1988) Ocean primary production and available light: further algorithms for remote sensing. Deep Sea Res Part Oceanogr Res Pap 35:855–879

Pratchett MS, Munday PL, Wilson SK, Graham NAJ, Cinner JE, Bellwood DR, Jones GP, McClanahan NVCP& TR (2008) Effects of climate -induced coral bleaching on coral -reef fishes — ecological and economic consequences. Oceanography and Marine Biology. CRC Press,

Pretet C, van Zuilen K, Nägler TF, Reynaud S, Böttcher ME, Samankassou E (2015) Constraints on barium isotope fractionation during aragonite precipitation by corals. Depositional Rec 1:118–129

Priess K, Le Campion-Alsumard T, Golubic S, Gadel F, Thomassin BA (2000) Fungi in corals: black bands and density-banding of Porites lutea and P. lobata skeleton. Mar Biol 136:19–27

Printemps J (2008) Mapping Potential Erosion Risks in North Viti Levu (Fiji))using the USLE Model and a GIS.

Prouty NG, Field ME, Stock JD, Jupiter SD, McCulloch M (2010) Coral Ba/Ca records of sediment input to the fringing reef of the southshore of Moloka'i, Hawai'i over the last several decades. Mar Pollut Bull 60:1822–1835

Prouty NG, Jupiter SD, Field ME, McCulloch MT (2009) Coral proxy record of decadal-scale reduction in base flow from Moloka'i, Hawaii. Geochem Geophys Geosystems 10

Prouty NG, Storlazzi CD, McCutcheon AL, Jenson JW (2014) Historic impact of watershed change and sedimentation to reefs along west-central Guam. Coral Reefs 33:733–749

Quinn NJ, Kojis (2008) Variation in coral recruitment on Fijian reefs. Proc 11th Int Coral Reef Symp 105–109

Quinn TM, Sampson DE (2002) A multiproxy approach to reconstructing sea surface conditions using coral skeleton geochemistry. Paleoceanography 17:14-1-14–11

Rahmstorf S, Box JE, Feulner G, Mann ME, Robinson A, Rutherford S, Schaffernicht EJ (2015) Exceptional twentieth-century slowdown in Atlantic Ocean overturning circulation. Nat Clim Change 5:475–480

Ram AR, Brook MS, Cronin SJ (2019) Engineering characteristics of soils prone to rainfall-induced slope failure in Viti Levu, Fiji. Q J Eng Geol Hydrogeol 52:336–345

Ram AR, Terry JP (2014) Land use and erosion risk in small forest catchments on the Coral Coast of Fiji: baseline estimates of sediment inputs to coastal lagoons. 336–344

Ram AR, Terry JP (2016) Stream turbidity responses to storm events in a pristine rainforest watershed on the Coral Coast of southern Fiji. Int J Sediment Res 31:279–290

Ramos RD, Goodkin NF, Siringan FP, Hughen KA (2017) Diploastrea heliopora Sr/Ca and δ18O records from northeast Luzon, Philippines: An assessment of interspecies coral proxy calibrations and climate controls of sea surface temperature and salinity. Paleoceanography 32:424–438

Rasher DB, Hay ME (2010) Chemically rich seaweeds poison corals when not controlled by herbivores. Proc Natl Acad Sci 107 (21) 9683-9688

Raupach MR, Marland G, Ciais P, Le Quéré C, Canadell JG, Klepper G, Field CB (2007) Global and regional drivers of accelerating CO2 emissions. Proc Natl Acad Sci 104:10288–10293

Razak TB, Roff G, Lough JM, Prayudi D, Cantin NE, Mumby PJ (2019) Long-term growth trends of massive Porites corals across a latitudinal gradient in the Indo-Pacific. Mar Ecol Prog Ser 626:69–82

Reed EV, Thompson DM, Cole JE, Lough JM, Cantin NE, Cheung AH, Tudhope A, Vetter L, Jimenez G, Edwards RL (2021) Impacts of Coral Growth on Geochemistry: Lessons From the Galápagos Islands. Paleoceanogr Paleoclimatology 36:e2020PA004051

Restrepo JD, Park E, Aquino S, Latrubesse EM (2016) Coral reefs chronically exposed to river sediment plumes in the southwestern Caribbean: Rosario Islands, Colombia. Sci Total Environ 553:316–329

Reynaud S, Ferrier-Pagès C, Meibom A, Mostefaoui S, Mortlock R, Fairbanks R, Allemand D (2007) Light and temperature effects on Sr/Ca and Mg/Ca ratios in the scleractinian coral Acropora sp. Geochim Cosmochim Acta 71:354–362

Reynaud S, Leclercq N, Romaine-Lioud S, Ferrier-Pagés C, Jaubert J, Gattuso J-P (2003) Interacting effects of CO2 partial pressure and temperature on photosynthesis and calcification in a scleractinian coral. Glob Change Biol 9:1660–1668

Reynolds RW, Smith TM, Liu C, Chelton DB, Casey KS, Schlax MG (2007) Daily High-Resolution-Blended Analyses for Sea Surface Temperature. J Clim 20:5473–5496

Ricci F, Rossetto Marcelino V, Blackall LL, Kühl M, Medina M, Verbruggen H (2019) Beneath the surface: community assembly and functions of the coral skeleton microbiome. Microbiome 7:159

Risk MJ (2014) Assessing the effects of sediments and nutrients on coral reefs. Curr Opin Environ Sustain 7:108–117

Risk MJ, Pagani SE, Elias RJ (1987) Another internal clock: preliminary estimates of growth rates based on cycles of algal boring activity. Palaios 323–331

Roberts M, Hanley N, Williams S, Cresswell W (2017) Terrestrial degradation impacts on coral reef health: Evidence from the Caribbean. Ocean Coast Manag 149:52–68

Robertson T, Greenhalgh S, Korovulavula I, Tikoibua T, Radikedike P, Stahlmann-Brown P (2020) Locally managed marine areas: Implications for socio-economic impacts in Kadavu, Fiji. Mar Policy 117:103950

Robinson JPW, Wilson SK, Robinson J, Gerry C, Lucas J, Assan C, Govinden R, Jennings S, Graham NAJ (2019) Productive instability of coral reef fisheries after climate-driven regime shifts. Nat Ecol Evol 3:183–190

Rodriguez LG, Cohen AL, Ramirez W, Oppo DW, Pourmand A, Edwards RL, Alpert AE, Mollica N (2019) Mid-Holocene, Coral-Based Sea Surface Temperatures in the Western Tropical Atlantic. Paleoceanogr Paleoclimatology 34:1234–1245

Rogers C (1990) Responses of coral reefs and reef organisms to sedimentation. Mar Ecol Prog Ser 62:185–202

Rollion-Bard C, Blamart D (2015) Possible controls on Li, Na, and Mg incorporation into aragonite coral skeletons. Chem Geol 396:98–111

Ross CL, DeCarlo TM, McCulloch MT (2019) Calibration of Sr/Ca, Li/Mg and Sr-U Paleothermometry in Branching and Foliose Corals. Paleoceanogr Paleoclimatology 34:1271–1291

Ryland JS (1981) Reefs of southwest Viti Levu and their tourism potential. Proc Fourth Int Coral Reef Symp 1:293–298

Sagan V, Peterson KT, Maimaitijiang M, Sidike P, Sloan J, Greeling BA, Maalouf S, Adams C (2020) Monitoring inland water quality using remote sensing: potential and limitations of spectral indices, bio-optical simulations, machine learning, and cloud computing. Earth-Sci Rev 205:103187

Saha N, Webb GE, Zhao J-X (2016) Coral skeletal geochemistry as a monitor of inshore water quality. Sci Total Environ 566–567:652–684

Saha N, Webb GE, Zhao J-X, Leonard ND, Nguyen AD (2018) Influence of marine biochemical cycles on seasonal variation of Ba/Ca in the near-shore coral Cyphastrea, Rat Island, southern Great Barrier Reef. Chem Geol 499:71–83

Saha N, Webb GE, Zhao J-X, Lewis SE, Duc Nguyen A, Feng Y (2021) Spatiotemporal variation of rare earth elements from river to reef continuum aids monitoring of terrigenous sources in the Great Barrier Reef. Geochim Cosmochim Acta 299:85–112

Saha N, Webb GE, Zhao J-X, Nguyen AD, Lewis SE, Lough JM (2019) Coral-based high-resolution rare earth element proxy for terrestrial sediment discharge affecting coastal seawater quality, Great Barrier Reef. Geochim Cosmochim Acta 254:173–191

Sayani HR, Cobb KM, Cohen AL, Elliott WC, Nurhati IS, Dunbar RB, Rose KA, Zaunbrecher LK (2011) Effects of diagenesis on paleoclimate reconstructions from modern and young fossil corals. Geochim Cosmochim Acta 75:6361–6373

Sayani HR, Cobb KM, DeLong K, Hitt NT, Druffel ERM (2019) Intercolony δ18O and Sr/Ca variability among Porites spp. corals at Palmyra Atoll: Toward more robust coral-based estimates of climate. Geochem Geophys Geosystems 20:5270–5284

Sayani HR, Thompson DM, Carilli JE, Marchitto TM, Chapman AU, Cobb KM (2021) Reproducibility of Coral Mn/Ca-Based Wind Reconstructions at Kiritimati Island and Butaritari Atoll. Geochem Geophys Geosystems 22:e2020GC009398

Schoepf V, Grottoli AG, Warner ME, Cai W-J, Melman TF, Hoadley KD, Pettay DT, Hu X, Li Q, Xu H (2013) Coral energy reserves and calcification in a high-CO2 world at two temperatures. PloS One 8:e75049

Schönberg CH, Fang JK-H, Carballo JL (2017) Bioeroding sponges and the future of coral reefs. Climate change, ocean acidification and sponges. Springer, pp 179–372

Scoffin TP, Tudhope AW, Brown BE, Chansang H, Cheeney RF (1992) Patterns and possible environmental controls of skeletogenesis of Porites lutea, South Thailand. Coral Reefs 11:1–11

Selig ER, Bruno JF (2010) A global analysis of the effectiveness of marine protected areas in preventing coral loss. PLos One 5:e9278

Shannon RD (1976) Revised effective ionic radii and systematic studies of interatomic distances in halides and chalcogenides. Acta Crystallogr A 32:751–767

Shashar N, Kinane S, Jokiel PL, Patterson MR (1996) Hydromechanical boundary layers over a coral reef. J Exp Mar Biol Ecol 199:17–28

Shaw EC, McNeil BI, Tilbrook B (2012) Impacts of ocean acidification in naturally variable coral reef flat ecosystems. J Geophys Res Oceans 117:1–14

Shen GT, Boyle EA (1987) Lead in corals: reconstruction of historical industrial fluxes to the surface ocean. Earth Planet Sci Lett 82:289–304

Shen GT, Boyle EA (1988) Determination of lead, cadmium and other trace metals in annually-banded corals. Chem Geol 67:47–62

Shen GT, Campbell TM, Dunbar RB, Wellington GM, Colgan MW, Glynn PW (1991) Paleochemistry of manganese in corals from the Galapagos Islands. Coral Reefs 10:91–100

Shen GT, Cole JE, Lea DW, Linn LJ, McConnaughey TA, Fairbanks RG (1992a) Surface ocean variability at Galapagos from 1936–1982: Calibration of geochemical tracers in corals. Paleoceanography 7(5), 563– 588

Shen GT, Dunbar RB (1995) Environmental controls on uranium in reef corals. Geochim Cosmochim Acta 59:2009–2024

Shen GT, Linn LJ, Campbell TM, Cole JE, Fairbanks RG (1992b) A chemical indicator of trade wind reversal in corals from the western tropical Pacific. J Geophys Res Oceans 97:12689–12697

Shepherd A, Ivins ER, Barletta VR, Bentley MJ, Bettadpur S, Briggs KH, Bromwich DH, Forsberg R, Galin N, Horwath M (2012) A reconciled estimate of ice-sheet mass balance. Science 338:1183–1189

Shi Q, Yu K, Chen T, Zhang H, Zhao M, Yan H (2012) Two centuries-long records of skeletal calcification in massive Porites colonies from Meiji Reef in the southern South China Sea and its responses to atmospheric CO2 and seawater temperature. Sci China Earth Sci 55:1–12

Shi W, Wang M (2008) Three-dimensional observations from MODIS and CALIPSO for ocean responses to cyclone Nargis in the Gulf of Martaban. Geophys Res Lett 35

Shi W, Wang M (2010) Characterization of global ocean turbidity from Moderate Resolution Imaging Spectroradiometer ocean color observations. J Geophys Res Oceans 115

Shirai K, Sowa K, Watanabe T, Sano Y, Nakamura T, Clode P (2012) Visualization of sub-daily skeletal growth patterns in massive Porites corals grown in Sr-enriched seawater. J Struct Biol 180:47–56

Sholkovitz E, Shen GT (1995) The incorporation of rare earth elements in modern coral. Geochim Cosmochim Acta 59:2749–2756

Sholkovitz ER, Piepgras DJ, Jacobsen SB (1989) The pore water chemistry of rare earth elements in Buzzards Bay sediments. Geochim Cosmochim Acta 53:2847–2856

Sinclair DJ (2005a) Non-river flood barium signals in the skeletons of corals from coastal Queensland, Australia. Earth Planet Sci Lett 237:354–369

Sinclair DJ (2005b) Correlated trace element "vital effects" in tropical corals: A new geochemical tool for probing biomineralization. Geochim Cosmochim Acta 69:3265–3284

Sinclair DJ, Kinsley LPJ, McCulloch MT (1998) High resolution analysis of trace elements in corals by laser ablation ICP-MS. Geochim Cosmochim Acta 62:1889–1901

Sinclair DJ, McCulloch MT (2004) Corals record low mobile barium concentrations in the Burdekin River during the 1974 flood: evidence for limited Ba supply to rivers? Palaeogeogr Palaeoclimatol Palaeoecol 214:155–174

Sinclair DJ, Williams B, Risk M (2006) A biological origin for climate signals in corals—Trace element "vital effects" are ubiquitous in Scleractinian coral skeletons. Geophys Res Lett 33

Singh A (2020) Benefits of crop diversification in Fiji's sugarcane farming. Asia Pac Policy Stud 7:65–80

Singh AM, Aung TH (2008) Salinity, temperature and turbidity structure in the Suva lagoon, Fiji. Am J Environ Sci 4:266–275

Singh S, Bhat JA, Shah S, Pala NA (2021) Coastal resource management and tourism development in Fiji Islands: a conservation challenge. Environ Dev Sustain 23:3009–3027

Sivaguru M, Todorov LG, Fouke CE, Munro CMO, Fouke KW, Fouke KE, Baughman ME, Fouke BW (2021) Corals regulate the distribution and abundance of Symbiodiniaceae and biomolecules in response to changing water depth and sea surface temperature. Sci Rep 11:2230

Smale DA, Wernberg T, Oliver EC, Thomsen M, Harvey BP, Straub SC, Burrows MT, Alexander LV, Benthuysen JA, Donat MG (2019) Marine heatwaves threaten global biodiversity and the provision of ecosystem services. Nat Clim Change 9:306–312

Smith J, Smith C, Hunter C (2001) An experimental analysis of the effects of herbivory and nutrient enrichment on benthic community dynamics on a Hawaiian reef. Coral Reefs 19:332–342

Smith JM, Quinn TM, Helmle KP, Halley RB (2006) Reproducibility of geochemical and climatic signals in the Atlantic coral Montastraea faveolata. Paleoceanography 21

Smith SV, Buddemeier RW, Redalje RC, Houck JE (1979) Strontium-calcium thermometry in coral skeletons. Science 204:404–407

Souter D, Planes S, Wicquart J, Logan M, Obura D, Staub F (2021) Status of coral reefs of the world: 2020 report.

Spalding M, Phd MDS MA, Ravilious C, Green EP, Programme UNE (2001) World Atlas of Coral Reefs. University of California Press, Stammer D, Engels A, Marotzke J, Gresse E, Hedemann C, Petzold J (2021) Hamburg Climate Futures Outlook 2021: Assessing the plausibility of deep decarbonization by 2050.

Stephens M, Lowry JH, Ram AR (2018) Location-based environmental factors contributing to rainfall-triggered debris flows in the Ba river catchment, northwest Viti Levu island, Fiji. Landslides 15:145–159

Stewart C, De Mora SJ (1992) Elevated tri(n-butyl)tin concentrations in shellfish and sediments from Suva Harbour, Fiji. Appl Organomet Chem 6:507–512

Stewart JA, Robinson LF, Day RD, Strawson I, Burke A, Rae JWB, Spooner PT, Samperiz A, Etnoyer PJ, Williams B, Paytan A, Leng MJ, Häussermann V, Wickes LN, Bratt R, Pryer H (2020) Refining trace metal temperature proxies in cold-water scleractinian and stylasterid corals. Earth Planet Sci Lett 545:116412

Su R, Lough JM, Sun D (2016) Variations in massive Porites growth rates at Hainan Island, northern South China Sea. Mar Ecol Prog Ser 546:47–60

Sully S, Van Woesik R (2020) Turbid reefs moderate coral bleaching under climate-related temperature stress. Glob Change Biol 26:1367–1373

Supriharyono (2004) Growth rates of the massive coral Porites lutea Edward and Haime, on the coast of Botang, East Kalimantan, Indonesia. J Coast Dev 7:143–155

Swart PK, Elderfield H, Greaves MJ (2002) A high-resolution calibration of Sr/Ca thermometry using the Caribbean coral Montastraea annularis. Geochem Geophys Geosystems 3:1–11

Sykes H, Morris C (2007) Status of coral reefs in the Fiji Islands, 2007. South-West Pac Status Coral Reefs Rep

Szmant AM (2002) Nutrient enrichment on coral reefs: is it a major cause of coral reef decline? Estuaries 25:743–766

Takahashi C, Watanabe M (2016) Pacific trade winds accelerated by aerosol forcing over the past two decades. Nat Clim Change 6:768–772

Takahashi T, Sutherland SC, Chipman DW, Goddard JG, Ho C, Newberger T, Sweeney C, Munro DR (2014) Climatological distributions of pH, pCO2, total CO2, alkalinity, and CaCO3 saturation in the global surface ocean, and temporal changes at selected locations. Mar Chem 164:95–125

Tamata UB (2007) Studies of nutrient variability and the consequences for benthic communities on the Coral Coast fringing reefs, Fiji. School of Earth and Environmental Sciences, University of Wollongong

Tambutté S, Holcomb M, Ferrier-Pagès C, Reynaud S, Tambutté É, Zoccola D, Allemand D (2011) Coral biomineralization: From the gene to the environment. J Exp Mar Biol Ecol 408:58–78

Tanaka K, Holcomb M, Takahashi A, Kurihara H, Asami R, Shinjo R, Sowa K, Rankenburg K, Watanabe T, McCulloch M (2015) Response of Acropora digitifera to ocean acidification: constraints from δ11B, Sr, Mg, and Ba compositions of aragonitic skeletons cultured under variable seawater pH. Coral Reefs 34:1139–1149

Tanzil JTI, Brown BE, Dunne RP, Lee JN, Kaandorp JA, Todd PA (2013) Regional decline in growth rates of massive Porites corals in Southeast Asia. Glob Change Biol 19:3011–3023

Tanzil JTI, Brown BE, Tudhope AW, Dunne RP (2009) Decline in skeletal growth of the coral Porites lutea from the Andaman Sea, South Thailand between 1984 and 2005. Coral Reefs 28:519–528

Tanzil JTI, Goodkin NF, Sin TM, Chen ML, Fabbro GN, Boyle EA, Lee AC, Toh KB (2019) Multi-colony coral skeletal Ba/Ca from Singapore's turbid urban reefs: Relationship with contemporaneous in-situ seawater parameters. Geochim Cosmochim Acta 250:191–208

Tanzil JTI, Lee JN, Brown BE, Quax R, Kaandorp JA, Lough JM, Todd PA (2016) Luminescence and density banding patterns in massive Porites corals around the Thai-Malay Peninsula, Southeast Asia. Limnol Oceanogr 61:2003–2026

Terry J p., Lal R, Garimella S (2008) An Examination of Vertical Accretion of Floodplain Sediments in the Labasa River Sugarcane Belt of Northern Fiji: Rates, Influences and Contributing Processes. Geogr Res 46:399–412

Thompson DM (2022) Environmental records from coral skeletons: A decade of novel insights and innovation. WIREs Clim Change 13:e745

Tierney JE, Abram NJ, Anchukaitis KJ, Evans MN, Giry C, Kilbourne KH, Saenger CP, Wu HC, Zinke J (2015) Tropical sea surface temperatures for the past four centuries reconstructed from coral archives. paleoceanography 30:226–252

Tranchida G, Oliveri E, Angelone M, Bellanca A, Censi P, D'Elia M, Neri R, Placenti F, Sprovieri M, Mazzola S (2011) Distribution of rare earth elements in marine sediments from the Strait of Sicily (western Mediterranean Sea): evidence of phosphogypsum waste contamination. Mar Pollut Bull 62:182–191

Trenberth KE, Cheng L, Jacobs P, Zhang Y, Fasullo J (2018) Hurricane Harvey links to ocean heat content and climate change adaptation. Earths Future 6:730–744

Trenberth KE, Jones PD, Ambenje P, Bojariu R, Easterling D, Tank AK, Parker D, Rahimzadeh F, Renwick JA, Rusticucci M (2007) Observations: surface and atmospheric climate change. Climate Change 2007: The Physical Science Basis. Contribution of Working Group 1 to the 4th Assessment Report of the Intergovernmental Panel on Climate Change. Cambridge University Press,

Tudhope AW, Chilcott CP, McCulloch MT, Cook ER, Chappell J, Ellam RM, Lea DW, Lough JM, Shimmield GB (2001) Variability in the El Niño-Southern Oscillation through a glacial-interglacial cycle. Science 291:1511–1517

Tudhope AW, Lea DW, Shimmield GB, Chilcott CP, Head S (1996) Monsoon climate and Arabian Sea coastal upwelling recorded in massive corals from southern Oman. Palaios 347–361

Van Hooidonk R, Maynard JA, Planes S (2013) Temporary refugia for coral reefs in a warming world. Nat Clim Change 3:508–511

Varillon D, Fiat S, Magron F, Allenbach M, Hoibian T, De Ramon N'Yeurt A, Ganachaud A, Aucan J, Pelletier B, Hocdé R (2018) ReefTEMPS: the observation network of the coastal sea waters of the South, West and South-West Pacific. SEANOE

Vega Thurber RL, Burkepile DE, Fuchs C, Shantz AA, McMinds R, Zaneveld JR (2014) Chronic nutrient enrichment increases prevalence and severity of coral disease and bleaching. Glob Change Biol 20:544–554

Veron JEN (2000) Corals of the World. Townsville: Australian Institute of Marine Science. Volumes 1-3.

Veron JEN, Odorico DM, Chen CA, Miller DJ (1996) Reassessing evolutionary relationships of scleractinian corals. Coral Reefs 15:1–9

de Villiers S, Shen GT, Nelson BK (1994) The SrCa-temperature relationship in coralline aragonite: Influence of variability in (SrCa)seawater and skeletal growth parameters. Geochim Cosmochim Acta 58:197–208

Vuki VC, Zann LP, Naqasima MR, Vuki M (2000) The Fiji Islands. In: Seas at the Millenium Chapter 102. Pp. 169-182. Charles Sheppard (Editor) Elsevier ...

Walsh K (2015) Fine resolution simulations of the effect of climate change on tropical cyclones in the South Pacific. Clim Dyn 45:2619–2631

Watanabe T, Gagan MK, Corrége T, Scott-Gagan H, Cowley J, Hantoro WS (2003) Oxygen isotope systematics in Diploastrea heliopora: new coral archive of tropical paleoclimate. Geochim Cosmochim Acta 67:1349–1358

Watanabe T, Minagawa M, Oba T, Winter A (2001) Pretreatment of coral aragonite for Mg and Sr analysis: Implications for coral thermometers. Geochem J 35:265–269

Webb GE, Kamber BS (2000) Rare earth elements in Holocene reefal microbialites: a new shallow seawater proxy. Geochim Cosmochim Acta 64:1557–1565

Weber JN, White EW, Weber PH (1975) Correlation of Density Banding in Reef Coral Skeletons With Environmental Parameters: The Basis for Interpretation of Chronological Records Preserved in the Coralla of Corals. Paleobiology 1:137–149

Wei G, Sun M, Li X, Nie B (2000) Mg/Ca, Sr/Ca and U/Ca ratios of a porites coral from Sanya Bay, Hainan Island, South China Sea and their relationships to sea surface temperature. Palaeogeogr Palaeoclimatol Palaeoecol 162:59–74

Weil E, Smith G, Gil-Agudelo DL (2006) Status and progress in coral reef disease research . Dis Aquat Organ 69:1–7

West JM, Salm RV (2003) Resistance and Resilience to Coral Bleaching: Implications for Coral Reef Conservation and Management. Conserv Biol 17:956–967

Whippy-Morris C (2009) South-west pacific status of coral reefs report.

Williams GJ, Graham NA (2019) Rethinking coral reef functional futures. Funct Ecol. 2019; 33: 942– 947

van Woesik R, Cacciapaglia CW (2021) Thermal stress jeopardizes carbonate production of coral reefs across the western and central Pacific Ocean. PloS One 16:e0249008

van Woesik R, van Woesik K, van Woesik L, van Woesik S (2013) Effects of ocean acidification on the dissolution rates of reef-coral skeletons. PeerJ 1:e208

Wooldridge SA (2017) Instability and breakdown of the coral–algae symbiosis upon exceedence of the interglacial pCO 2 threshold (> 260 ppmv): the “missing” Earth-System feedback mechanism. Coral Reefs 36:1025–1037

Wu HC, Grottoli AG (2010) Stable oxygen isotope records of corals and a sclerosponge in the Western Pacific warm pool. Coral Reefs 29:413–418

Wu HC, Linsley BK, Dassié EP, Schiraldi B, deMenocal PB (2013) Oceanographic variability in the South Pacific Convergence Zone region over the last 210 years from multi-site coral Sr/Ca records. Geochem Geophys Geosystems 14:1435–1453

Wu HC, Moreau M, Linsley BK, Schrag DP, Corrège T (2014) Investigation of sea surface temperature changes from replicated coral Sr/Ca variations in the eastern equatorial Pacific (Clipperton Atoll) since 1874. Palaeogeogr Palaeoclimatol Palaeoecol 412:208–222

Wu Y, Fallon SJ, Cantin NE, Lough JM (2021) Assessing multiproxy approaches (Sr/Ca, U/Ca, Li/Mg, and B/Mg) to reconstruct sea surface temperature from coral skeletons throughout the Great Barrier Reef. Sci Total Environ 786:147393

Wyndham T, McCulloch M, Fallon S, Alibert C (2004) High-resolution coral records of rare earth elements in coastal seawater: biogeochemical cycling and a new environmental proxy. Geochim Cosmochim Acta 68:2067–2080

Yamazaki A, Watanabe T, Tsunogai U (2011) Nitrogen isotopes of organic nitrogen in reef coral skeletons as a proxy of tropical nutrient dynamics. Geophys Res Lett 38

Yoon B, Raymond PA (2012) Dissolved organic matter export from a forested watershed during Hurricane Irene. Geophys Res Lett 39

Zak MR, Cabido M, Hodgson JG (2004) Do subtropical seasonal forests in the Gran Chaco, Argentina, have a future? Biol Conserv 120:589–598

Zann LP (1994) The status of coral reefs in South Western Pacific Islands. Mar Pollut Bull 29:52–61

Zhang C, Wang L, Li G, Dong S, Yang J, Wang X (2002) Grain size effect on multi-element concentrations in sediments from the intertidal flats of Bohai Bay, China. Appl Geochem 17:59–68

Zhao M, Yu K, Zhang Q, Shi Q, Price GJ (2012) Long-term decline of a fringing coral reef in the northern South China Sea. J Coast Res 28:1088–1099

Zoppe SF, Deveaux M, Gischler E (2022) Quantifying skeletal density at high temporal resolution in massive scleractinian corals by using two-dimensional grid-scanning gamma densitometry. Geo-Mar Lett 42:1–14

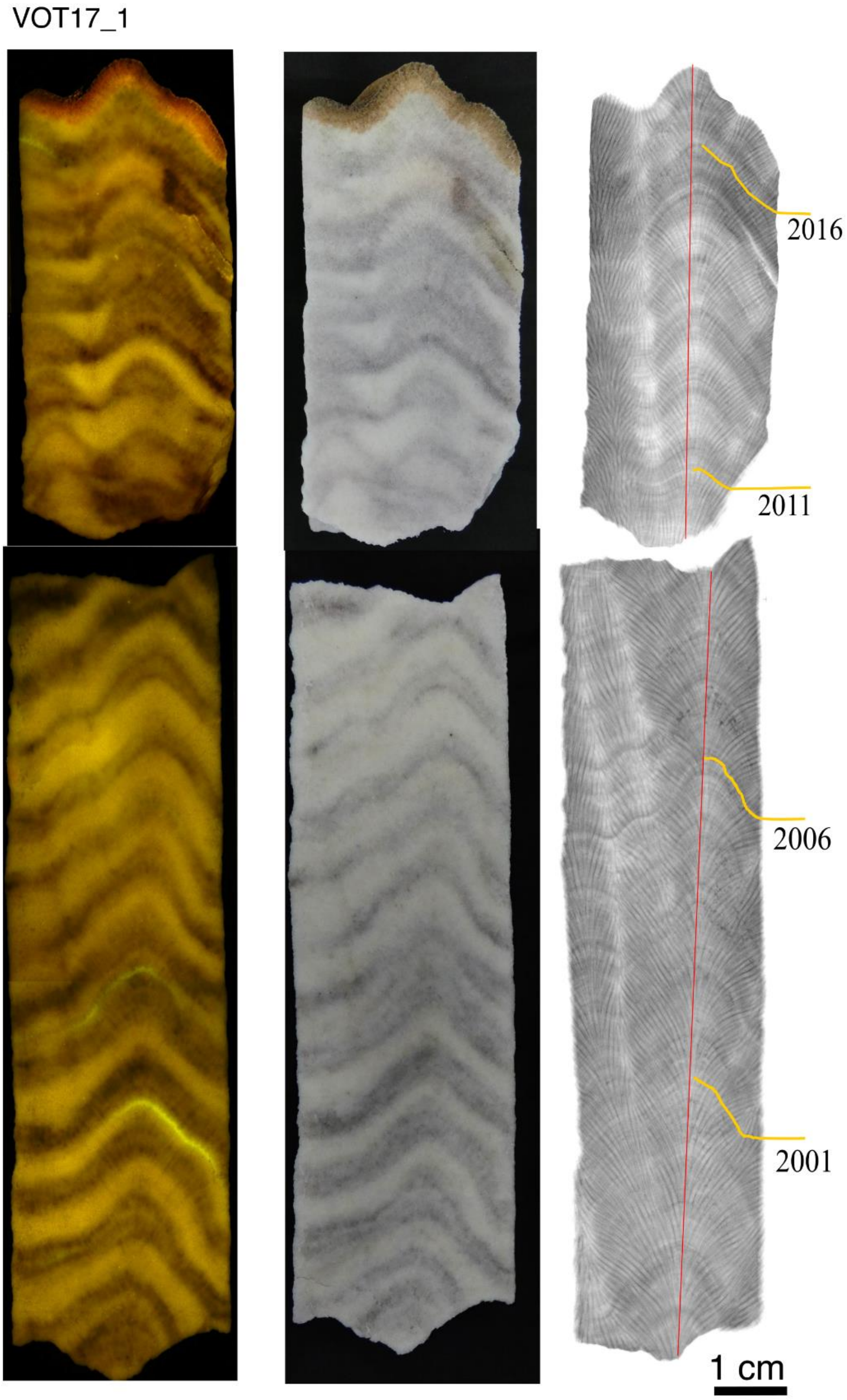

Figure A.1. Photograph of VOT17_1 analysed slab under UV light, white light and positive X-ray imaging.

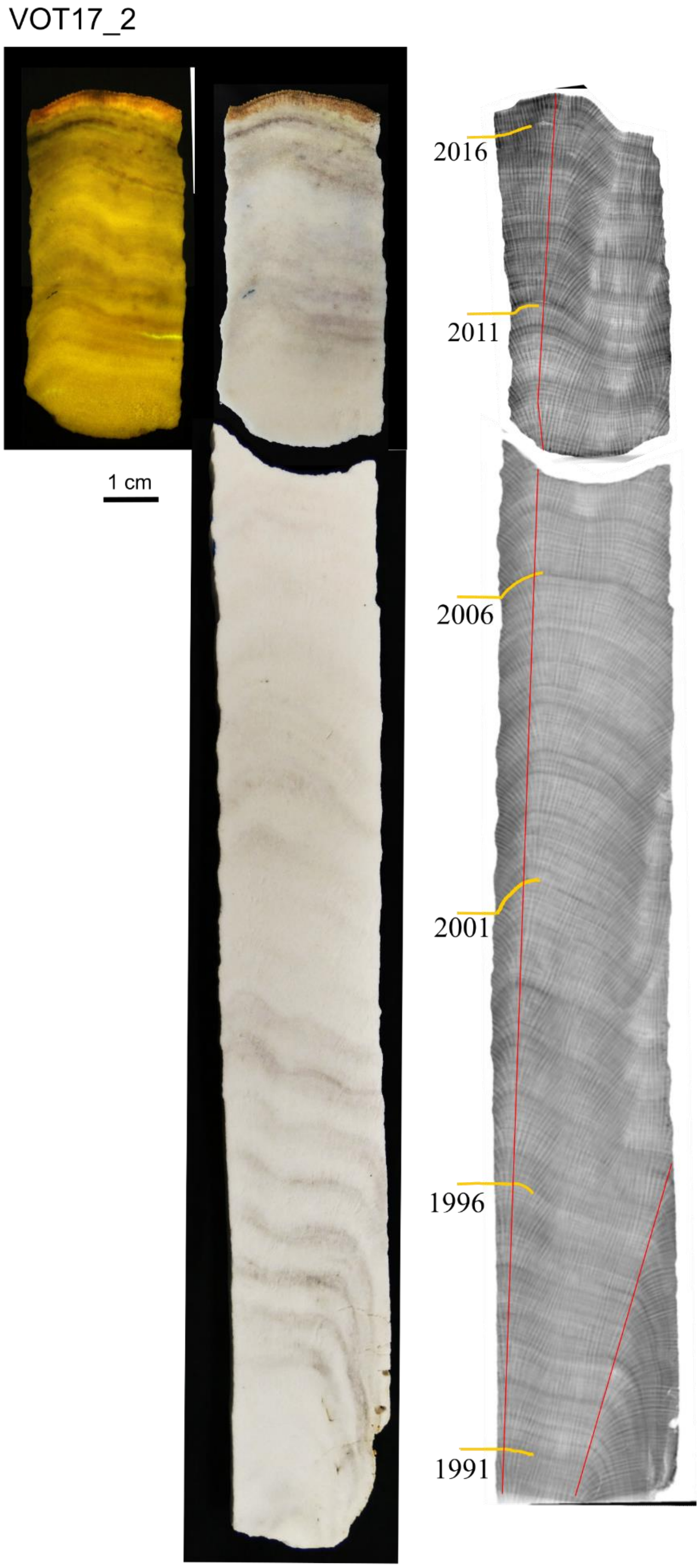

Figure A.2. Photograph of VOT17_2 analysed slab under UV light, white light and positive X-ray imaging.

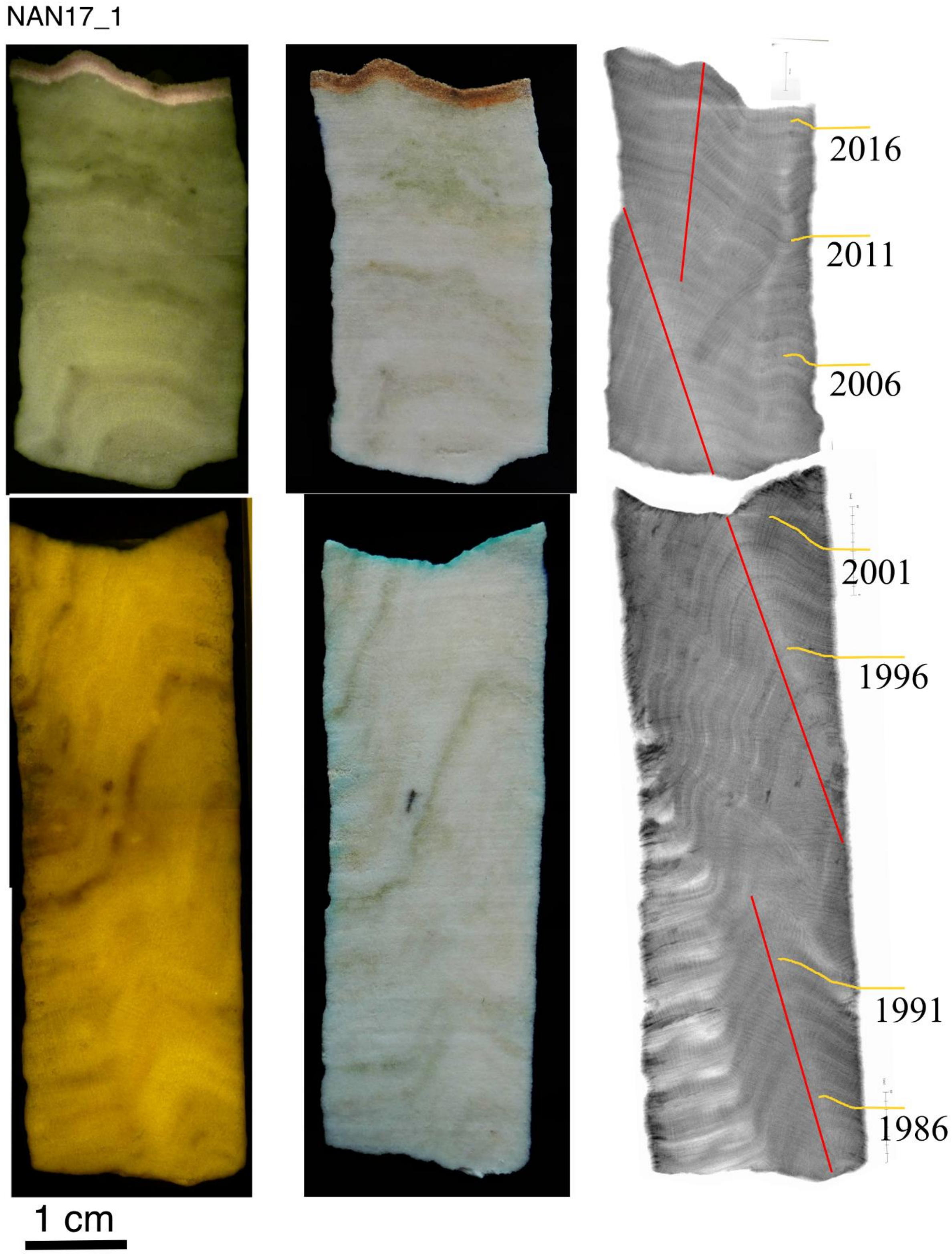

Figure A.3. Photograph of NAN17_1 analysed slab under UV light, white light and positive X-ray

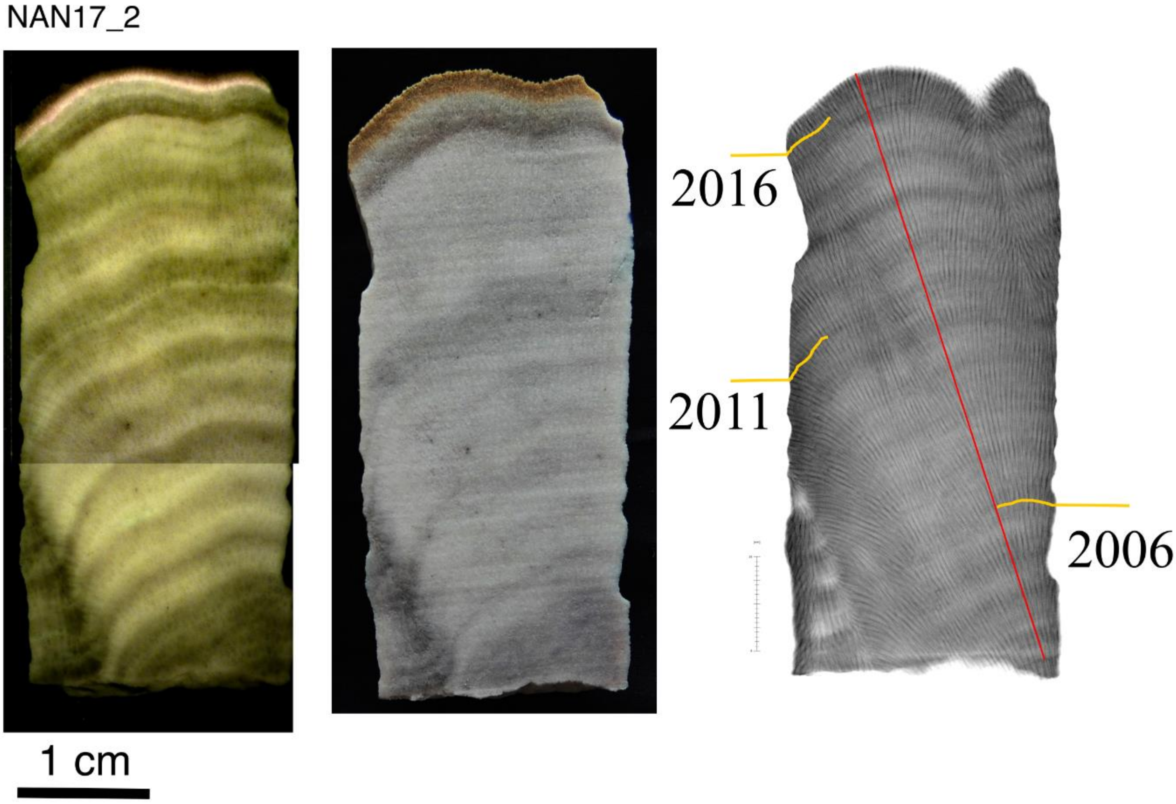

Figure A.4. Photograph of NAN17_2 analysed slab under UV light, white light and positive X-ray

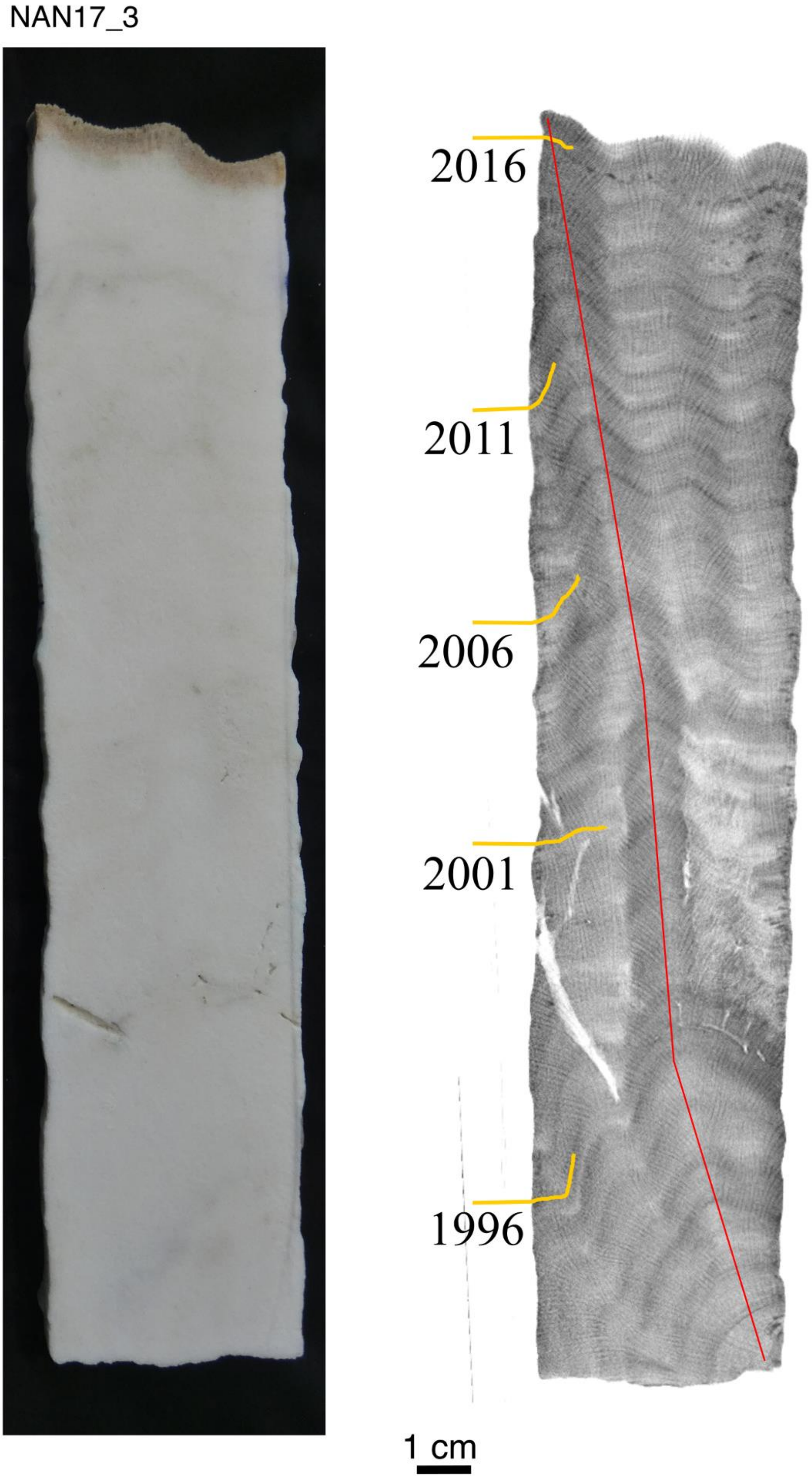

Figure A.5. Photograph of NAN17_3 analysed slab under UV light, white light and positive X-ray

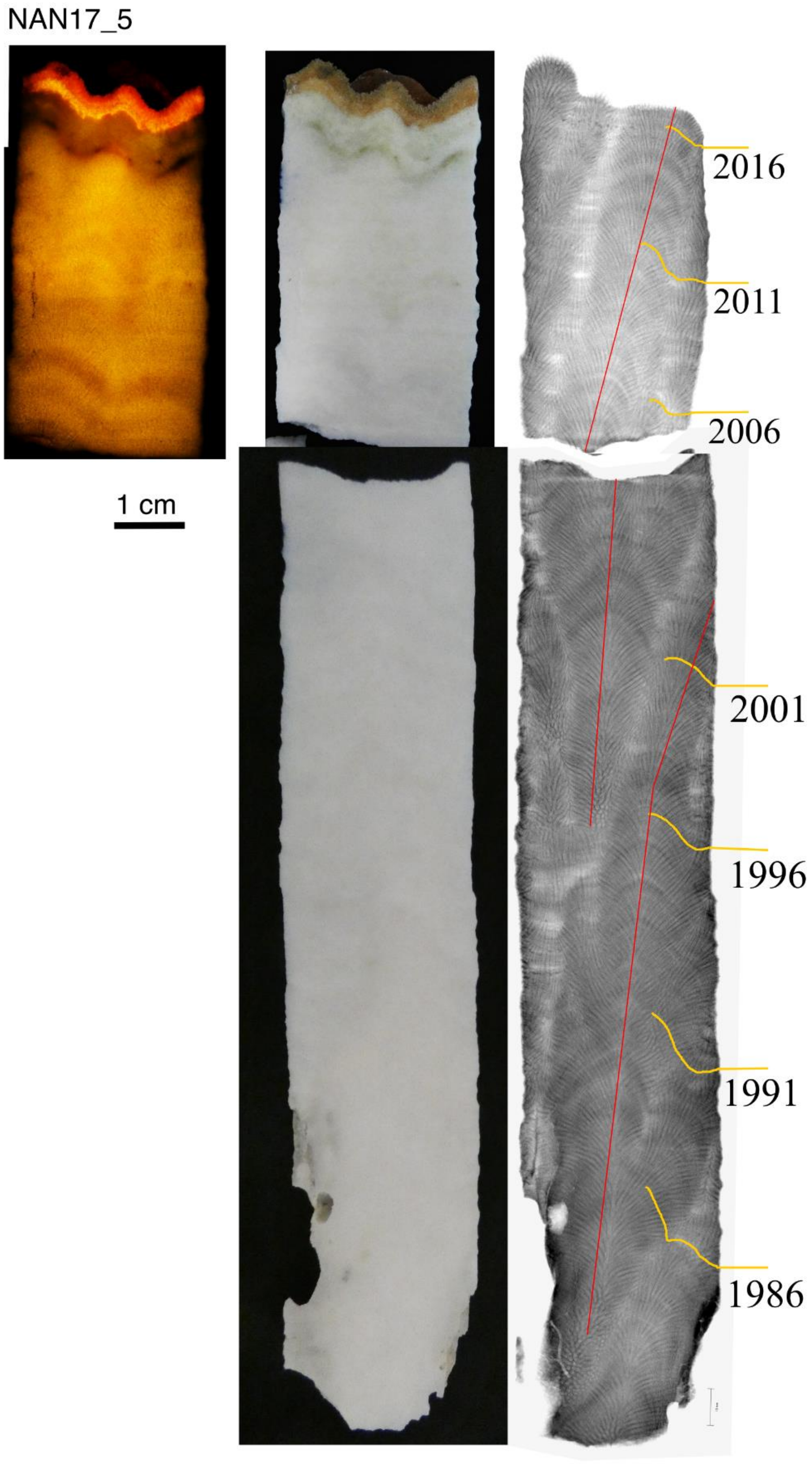

Figure A.6. Photograph of VOT17_1 analysed slab under UV light, white light and positive X-ray

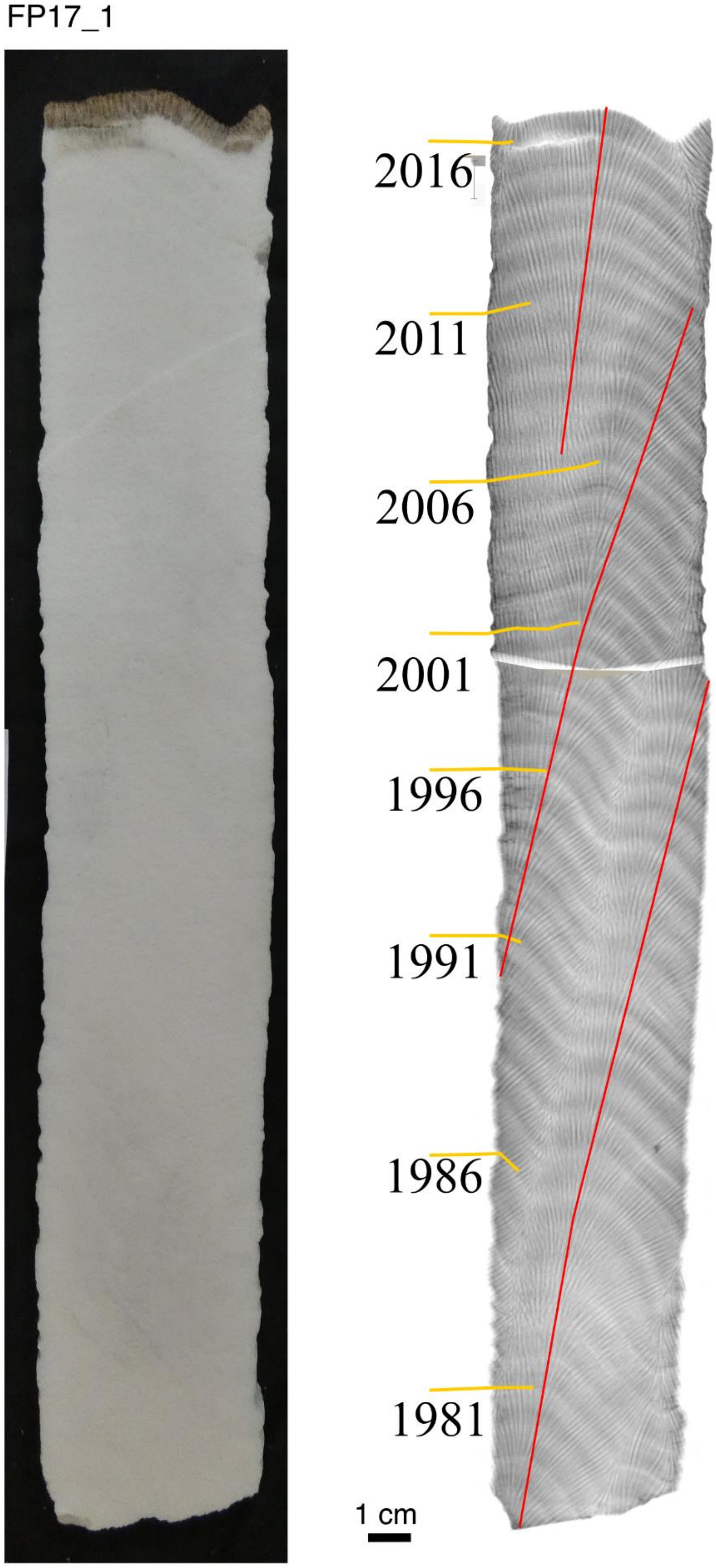

Figure A.7. Photograph of VOT17_1 analysed slab under UV light, white light and positive X-ray

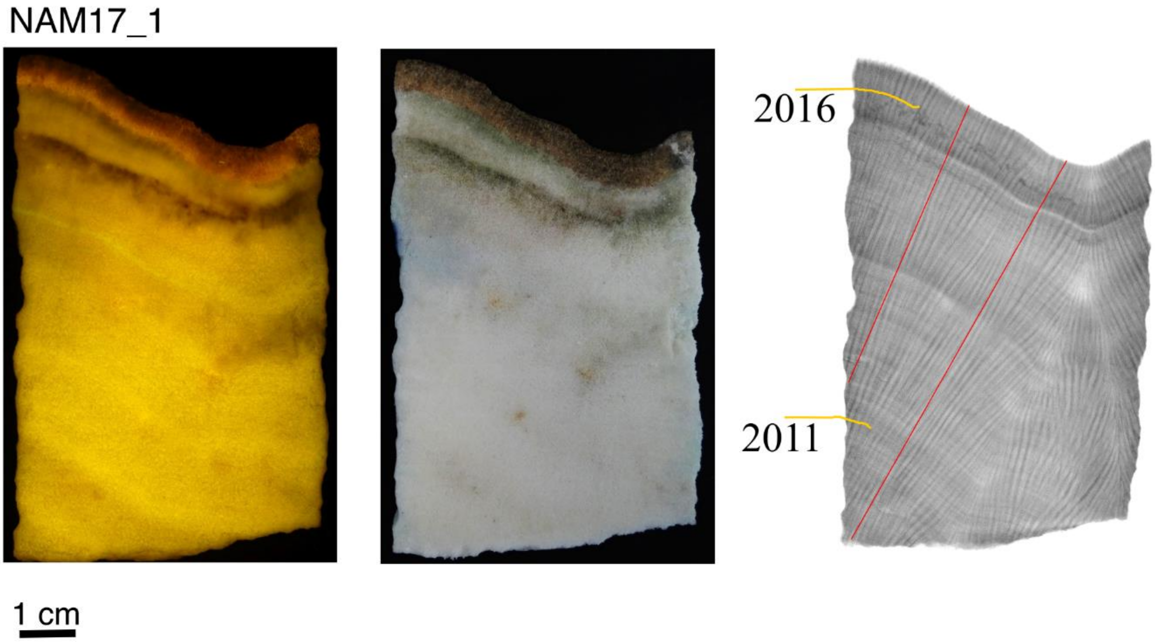

Figure A.8. Photograph of VOT17_1 analysed slab under UV light, white light and positive X-ray

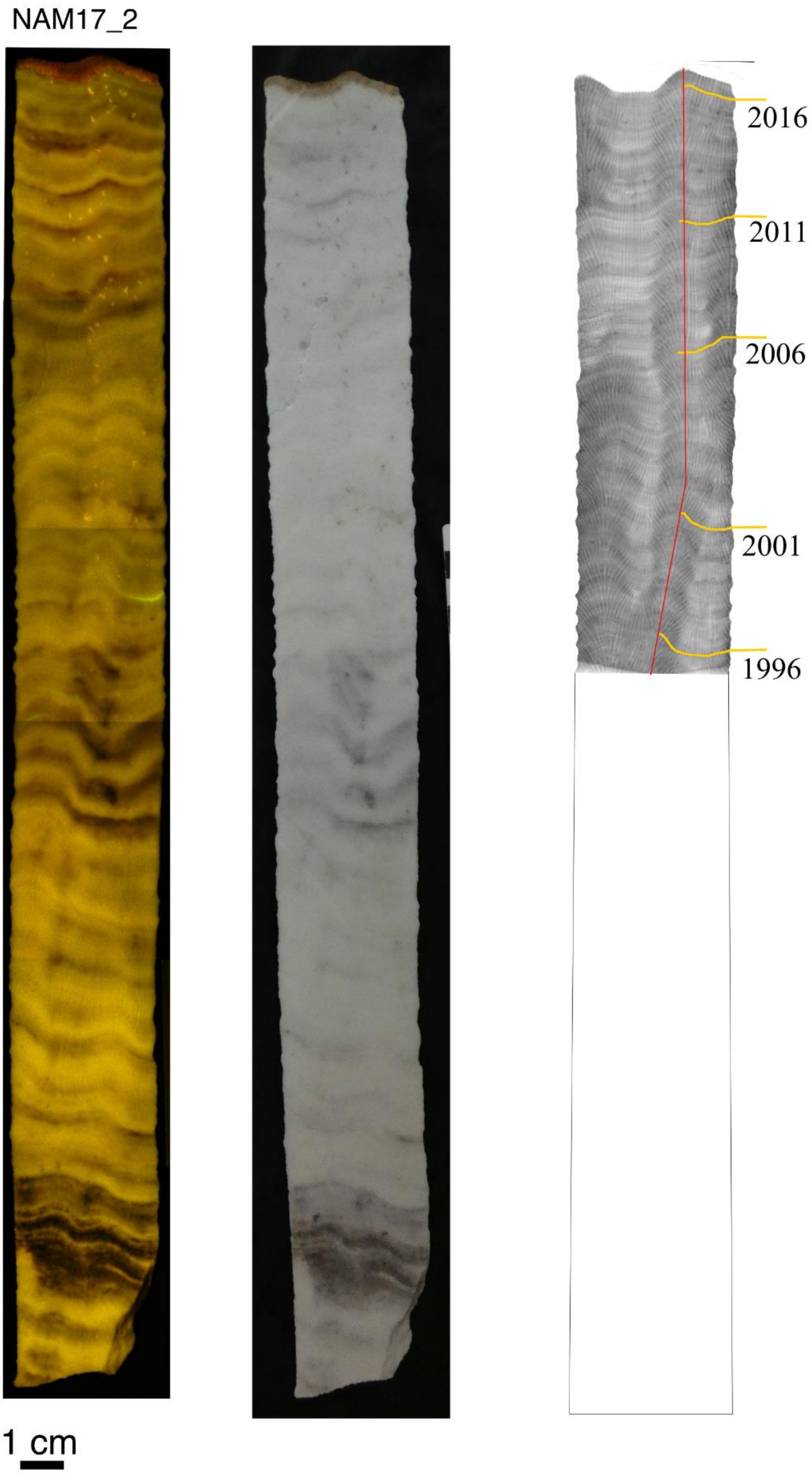

Figure A.9. Photograph of VOT17_1 analysed slab under UV light, white light and positive X-ray

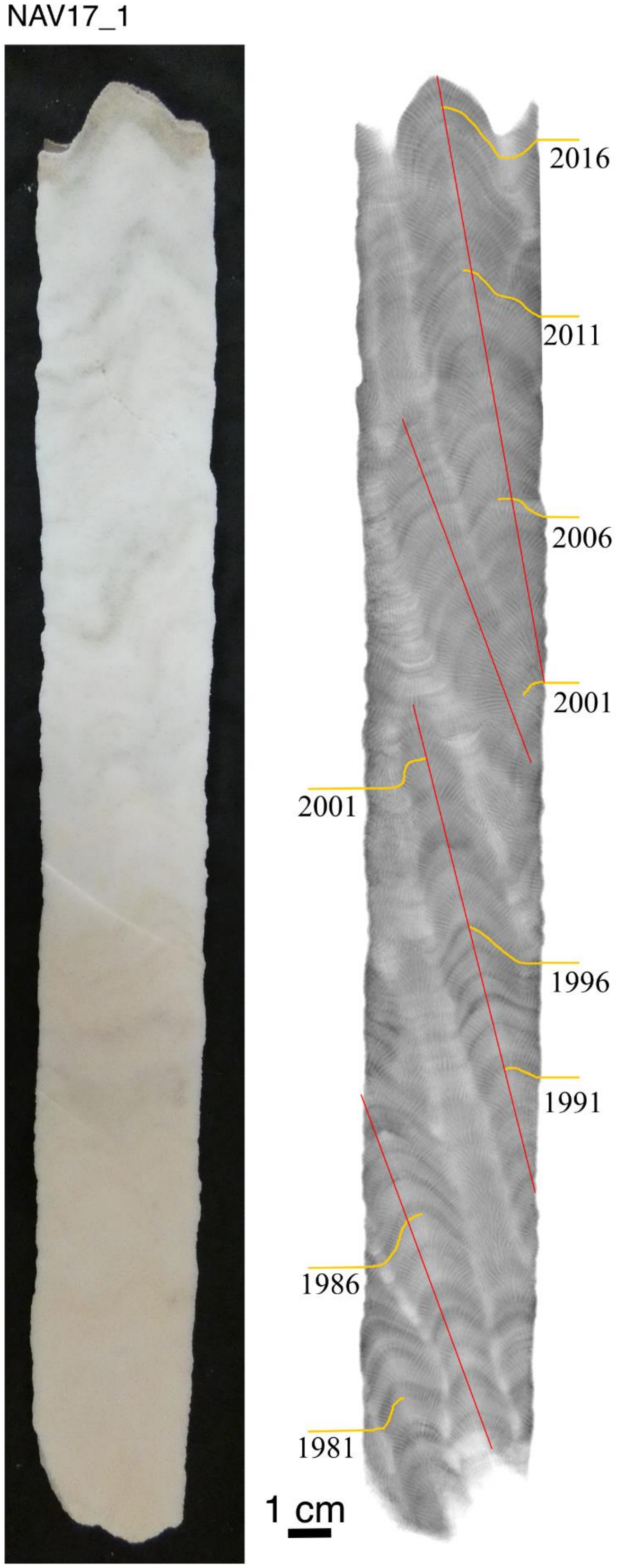

Figure A.10. Photograph of VOT17_1 analysed slab under UV light, white light and positive X-ray

Appendix B: Example of modified chronology of *Porites* spp. sample from Gorberdhan and Kinninmonth (2021)

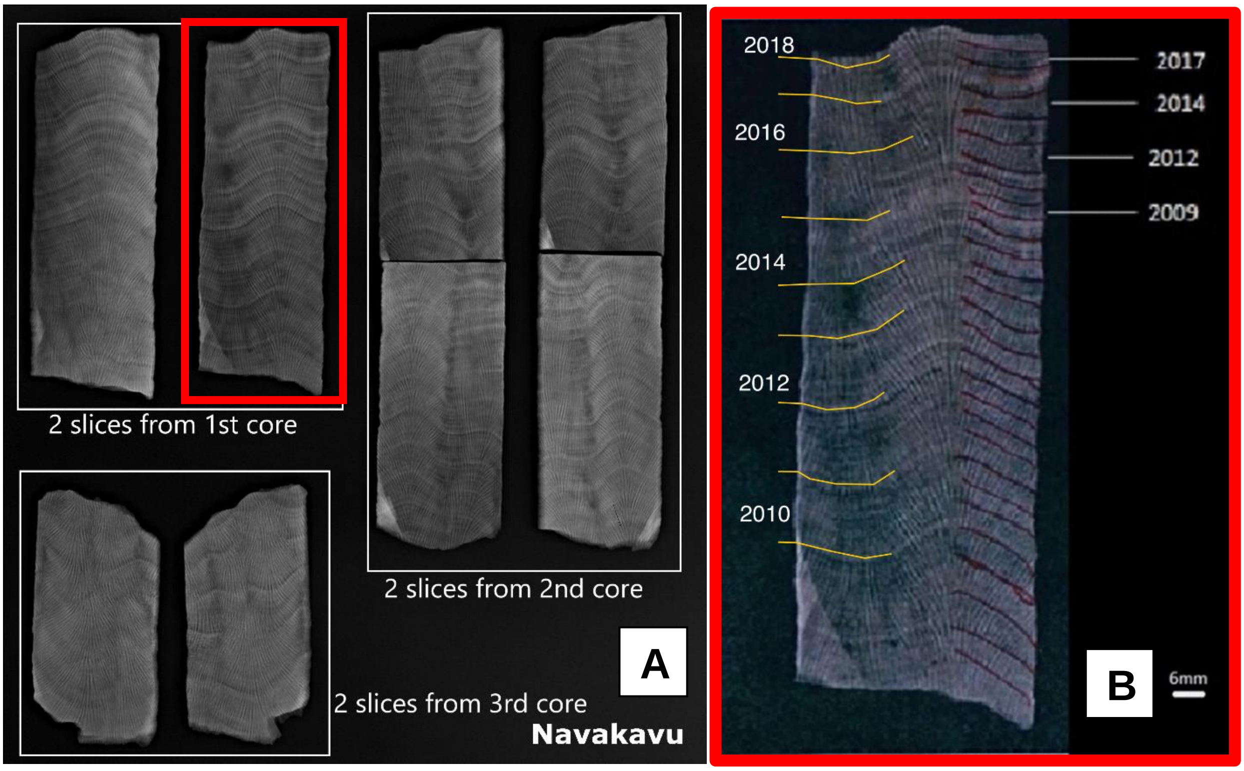

Figure B.1. X-ray slabs from a Porites spp. collected in Navakavu (Namuka Reef) and published in Goberdhan and Kinninmonth (2021). A) Shows all the slabs and sections from the collected core. B) is close-up from slab within red rectangle. Core chronology on the right (white and black lines) is the age model built by Goberdhan and Kinninmonth (2021). Core chronology on the left (yellow lines) is the reinterpreted age model and used in this thesis. The same protocol was followed for all the cores from Goberdhan and Kinninmonth (2021) used in this thesis, although their visual coral age model was not available.

Appendix C: Supplementary figures to Chapter 4 (SST proxies)

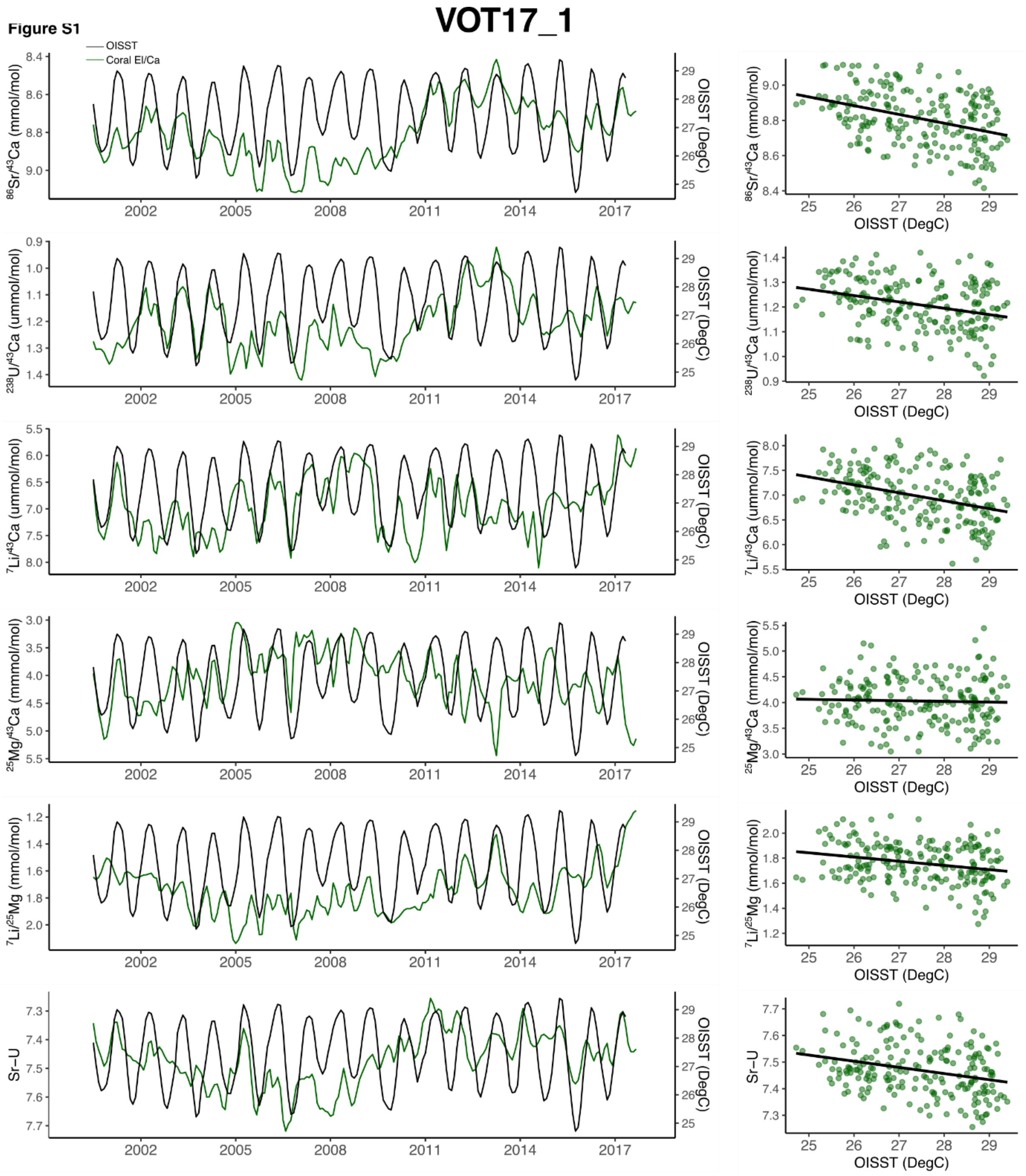

Figure C.1. Left panels: Monthly resolved timeseries of El/Ca records from VOT17_1 and OISST. Right panels: Linear regression (OLS) of El/Ca:SST. Black line represents best linear fit of data.

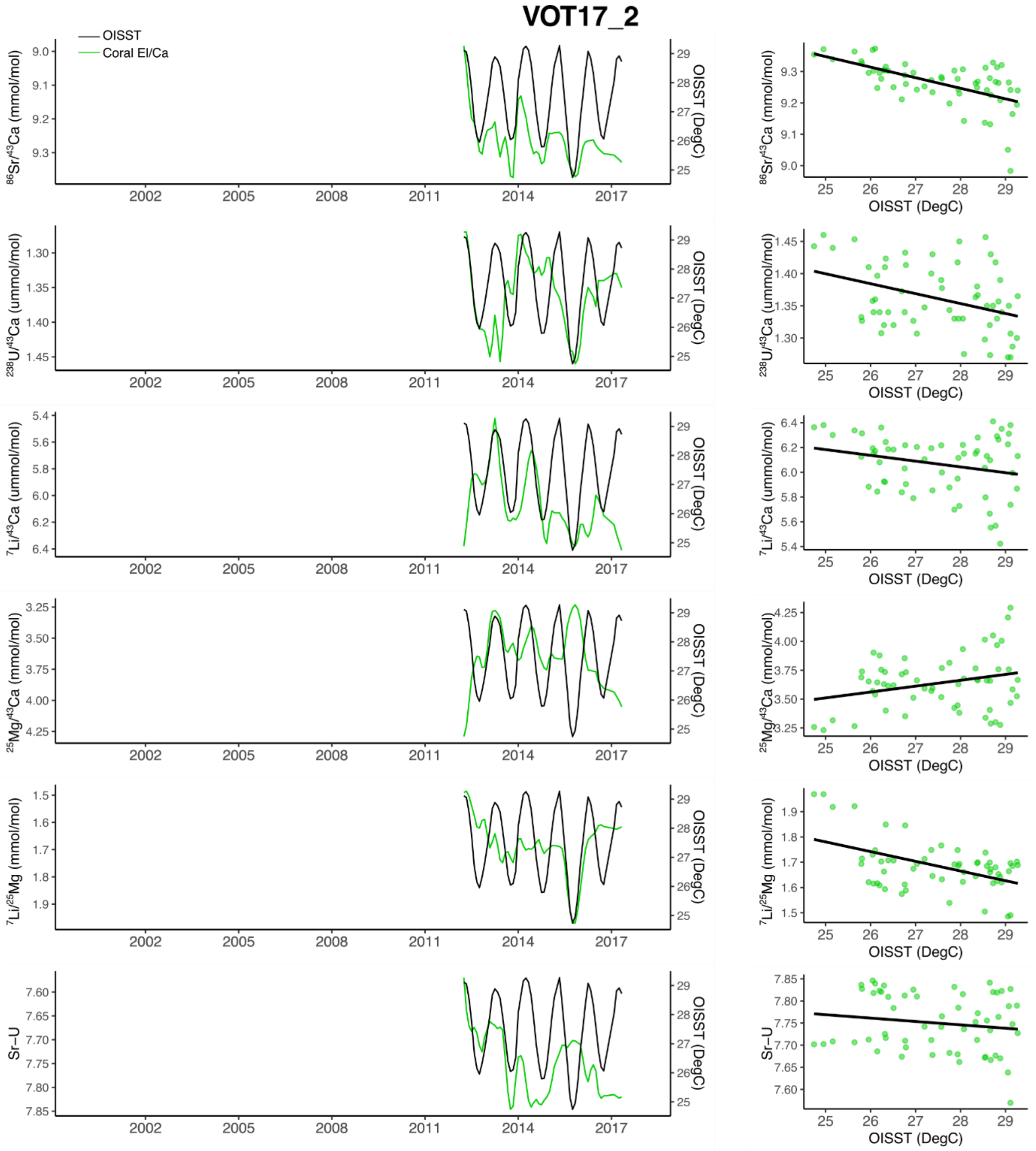

Figure C.2. Left panels: Monthly resolved timeseries of El/Ca records from VOT17_2 and OISST. Right panels: Linear regression (OLS) of El/Ca:SST. Black line represents best linear fit of data.

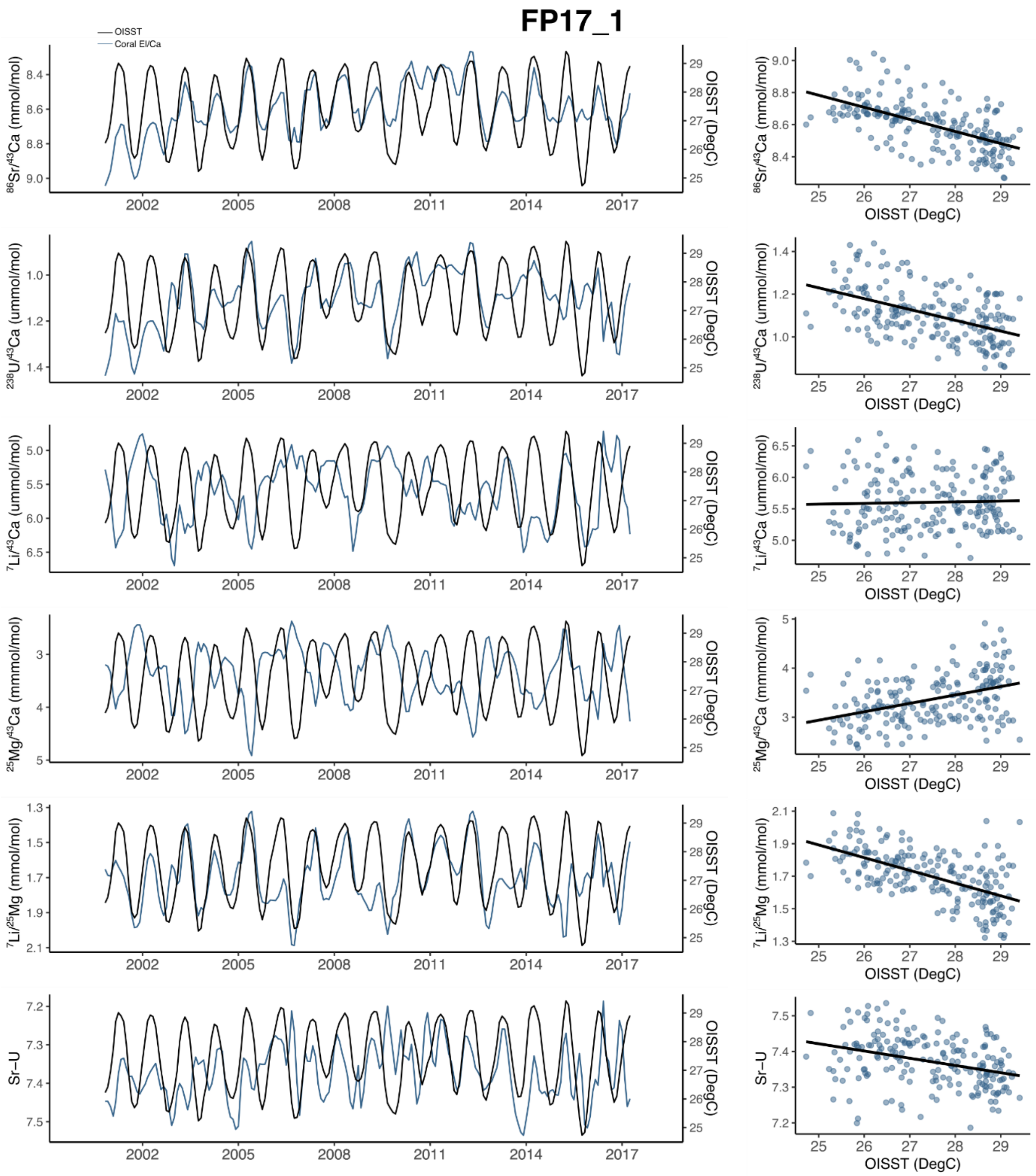

Figure C.3. Left panels: Monthly resolved timeseries of El/Ca records from FP17_1 and OISST. Right panels: Linear regression (OLS) of El/Ca:SST. Black line represents best linear fit of data.

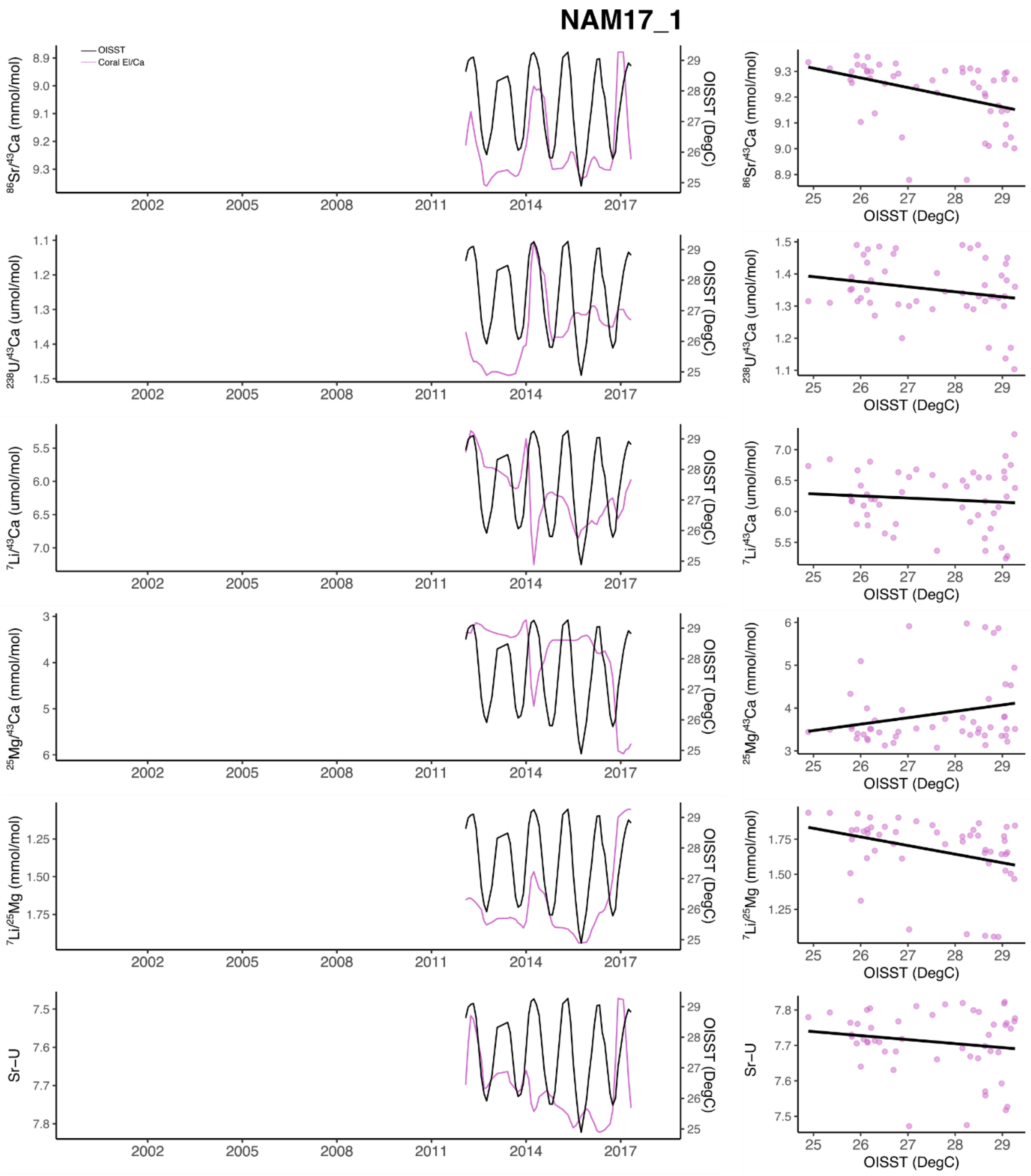

Figure C.4. Left panels: Monthly resolved timeseries of El/Ca records from NAM17_1 and OISST. Right panels: Linear regression (OLS) of El/Ca:SST. Black line represents best linear fit of data.

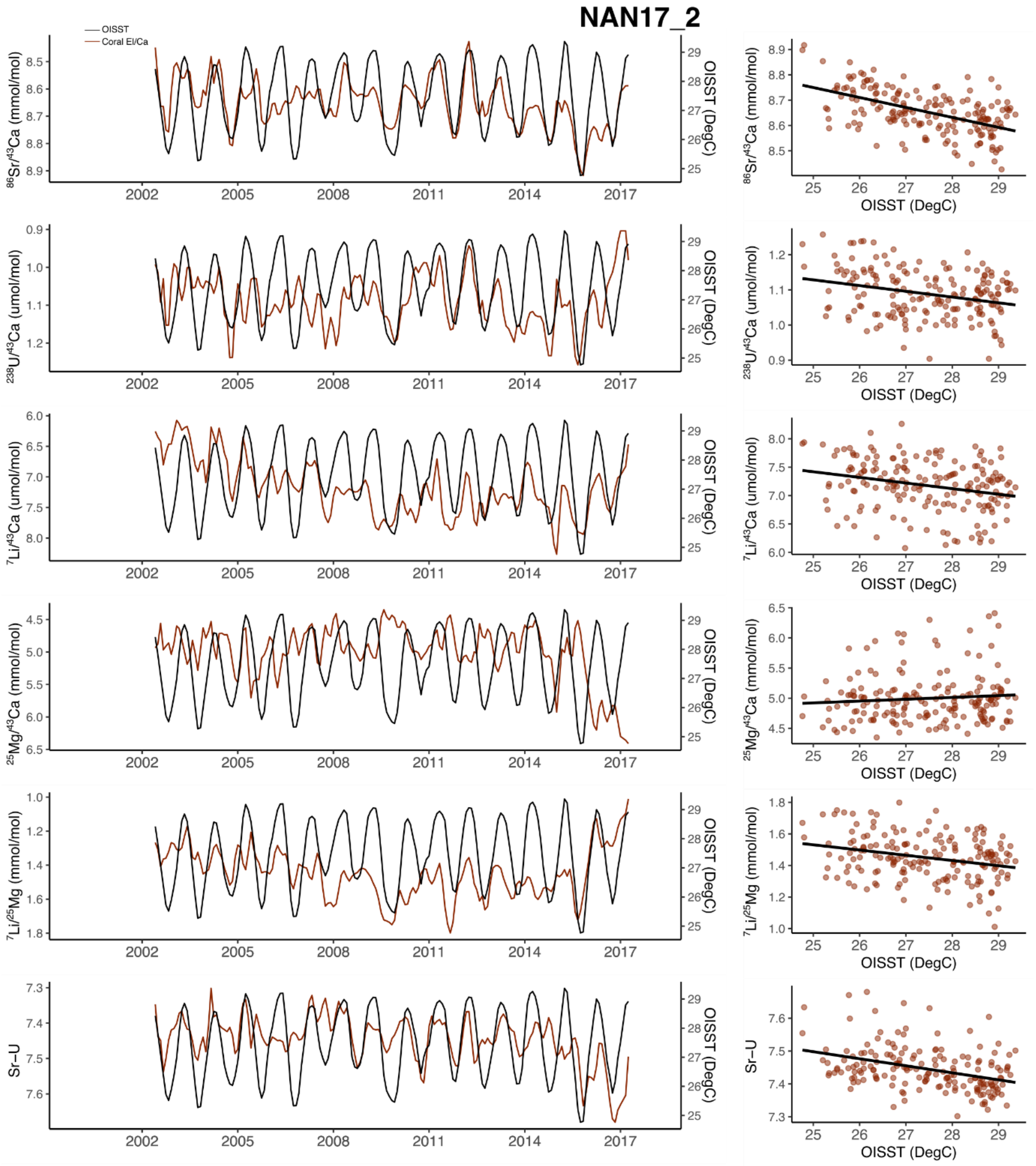

Figure C.5. Left panels: Monthly resolved timeseries of El/Ca records from NAN17_2 and OISST. Right panels: Linear regression (OLS) of El/Ca:SST. Black line represents best linear fit of data.

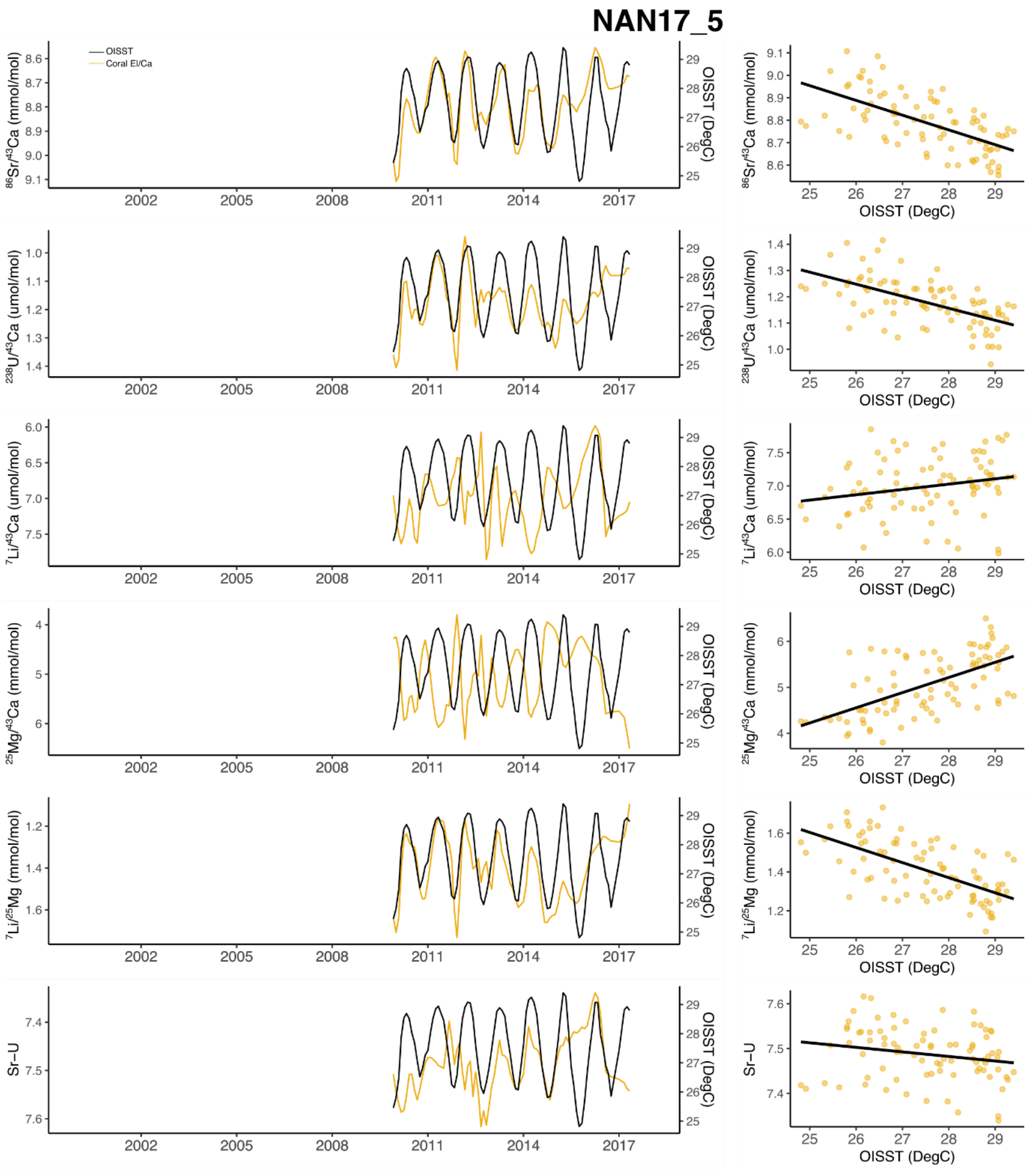

Figure C.6. Left panels: Monthly resolved timeseries of El/Ca records from NAN17_5 and OISST. Right panels: Linear regression (OLS) of El/Ca:SST. Black line represents best linear fit of data.

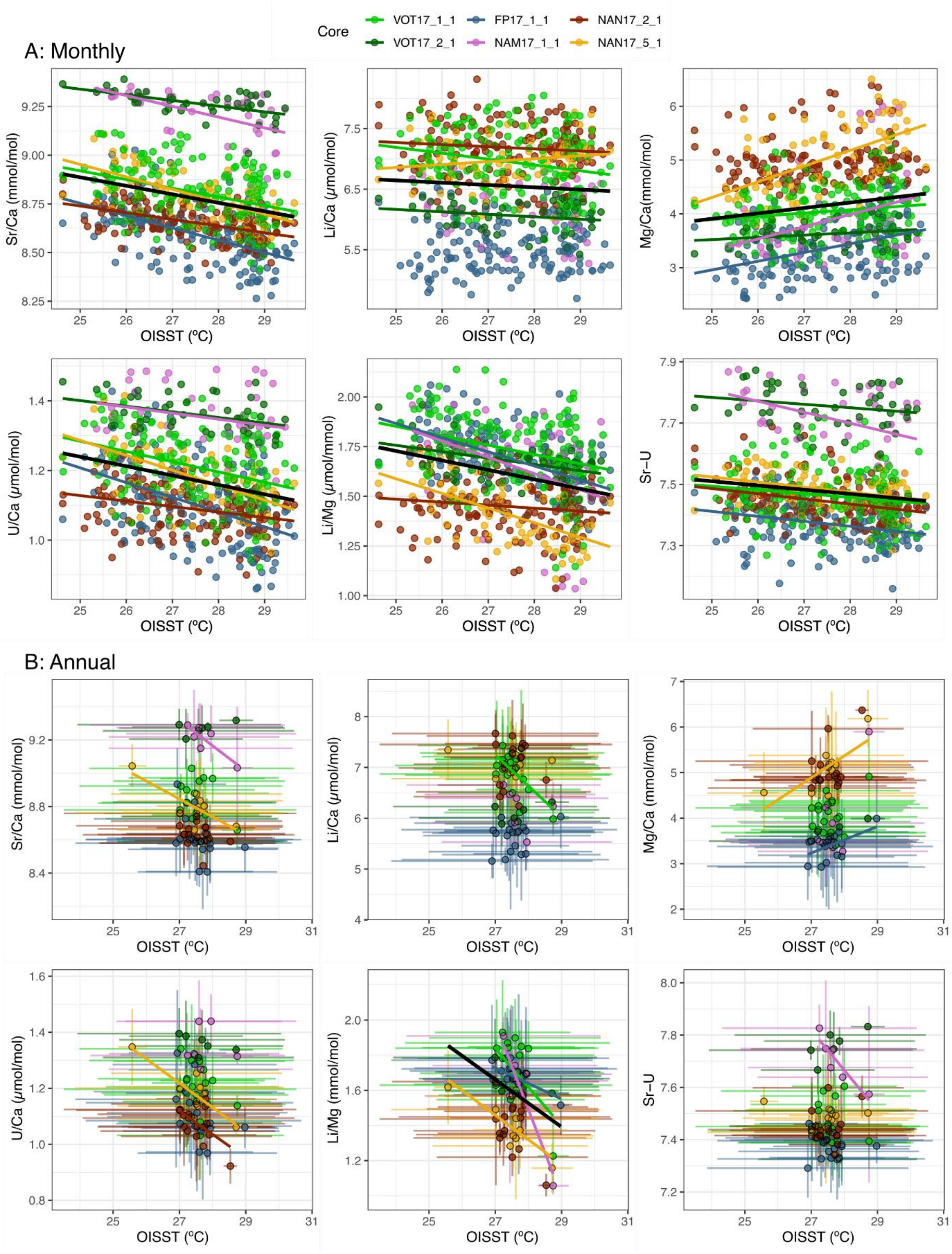

Figure C.7. A) Monthly resolved El/Ca vs SST. B) Annually resolved El/Ca vs SST. Error bars are 2SD. Colour datapoints and linear regressions correspond to single core data. Only significant linear regressions ($p < 0.05$) are included. Black line is the best linear fit considering all data. Equation in each plot correspond to all data.

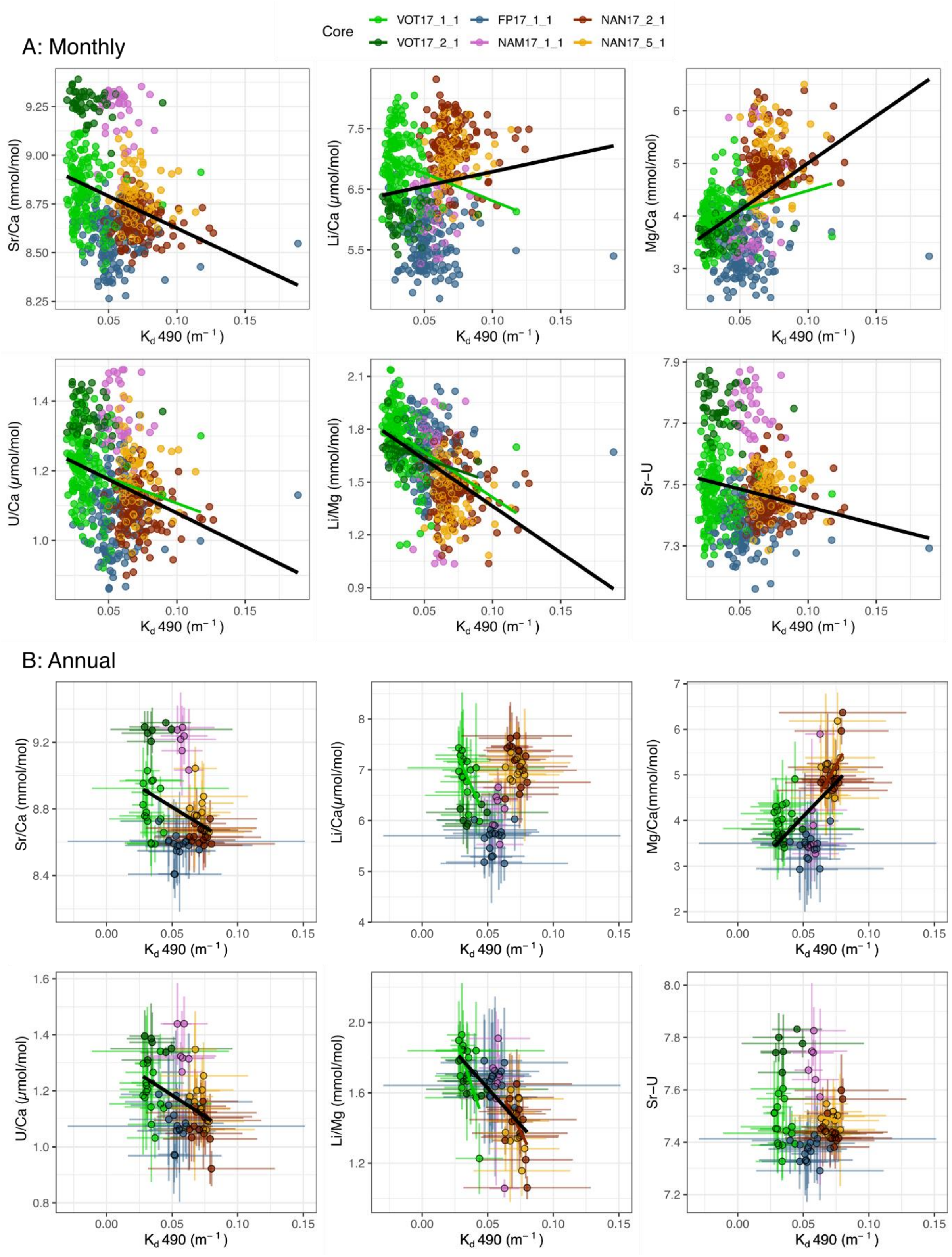

Figure C.8. A) Monthly resolved El/Ca vs seawater turbidity. B) Annually resolved El/Ca vs seawater turbidity. Error bars are 2SD. Colour datapoints and linear regressions correspond to single core data. Only significant linear regressions ($p < 0.05$) are included. Black line is the best linear fit considering all data. Equation in each plot correspond to all data.

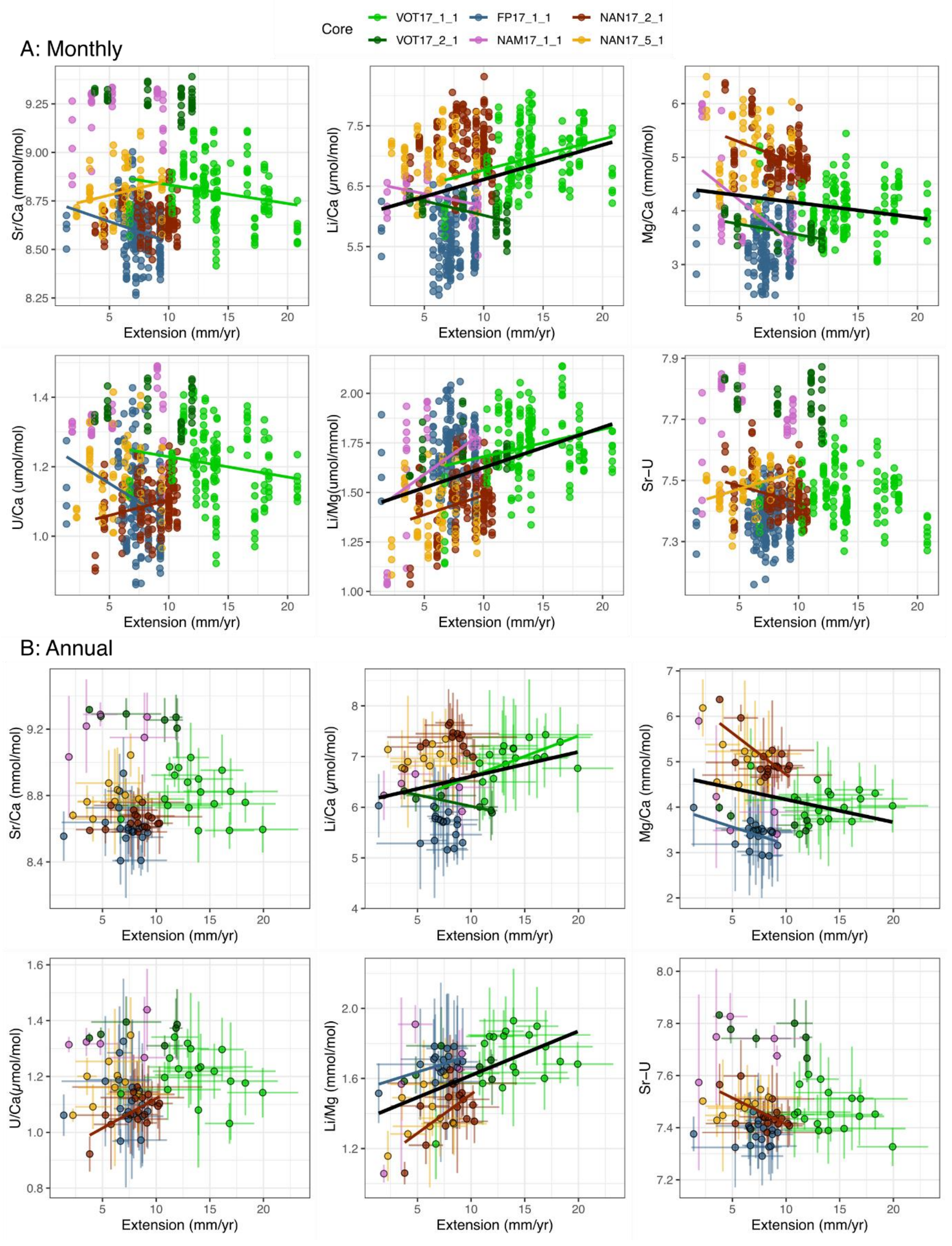

Figure C.9. A) Monthly resolved El/Ca vs core linear extension. B) Annually resolved El/Ca vs core linear extension. Error bars are 2SD. Colour datapoints and linear regressions correspond to single core data. Only significant linear regressions ($p < 0.05$) are included. Black line is the best linear fit considering all data. Equation in each plot correspond to all data.

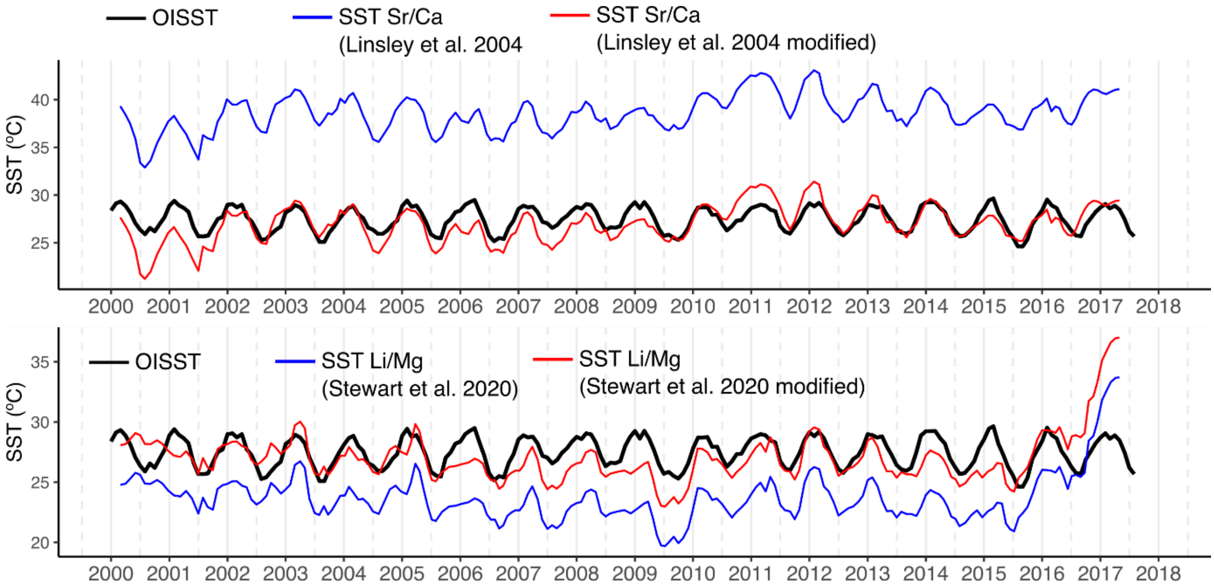

Figure C.10. A) SST reconstructed from Sr/Ca composite. Blue line represents SST reconstructed using original equation for Fiji Porites by Linsley et al. (2004). Red line represents SST reconstructed using modified Linsley et al. (2004) equation to account for differences in mean Sr/Ca. B) SST reconstructed from Li/Mg composite. Blue line represents SST reconstructed using universal aragonite equation by Stewart et al. (2020) Red line represents SST reconstructed using modified Stewart et al. (2020) equation to account for differences in mean Sr/Ca.